THE UNIVERSITY of ADELAIDE

Analysing Ancient Focused Fluid Flow Systems in Offshore Sedimentary Basins of Australia

Tayallen Velayatham

Petroleum Geoscience

Australian School of Petroleum, University of Adelaide

July 2019

This thesis is submitted in fulfilment of the requirements for the degree of Doctor of Philosophy

Table of Contents

Abstract

There has been growing recognition of the value in studying focused fluid flow systems, such as the formation of fluid escape pipes or paleo-pockmarks, within the subsurface of sedimentary basins to better define petroleum system processes. While focused fluid flow features such as Hydrocarbon Related Diagenetic Zones (HRDZs) have been documented in offshore basins of Australia, there is little systematic assessment of their genesis nor their impact on petroleum systems. This study utilizes 3D seismic data to pioneer documentation of focused fluid flow features in offshore basins of Australia and develop geological models for the genesis of these focused fluid flow systems.

Fault associated focused fluid flows were identified in the Exmouth Plateau of the Northern Carnarvon Basin and the Ceduna Sub-basin of the Great Australian Bight. In the Exmouth Plateau, 315 crater-like depressions along a paleo-surface, referred to as paleo-pockmarks, with underlying fluid escape pipes were identified within Jurassic and Triassic sequences using three 3D seismic surveys. These focused fluid flow features occur in linear trends parallel to but laterally offset from normal faults cutting these sequences. Amongst the identified linear trends of focused fluid flow features is the longest known pockmark chain yet documented (~72 km). The normal faults are interpreted to have intersected overpressured units in the Triassic Mungaroo Formation which then triggered vertical fluid migration. The nature of the fluids themselves however (i.e. whether they were hydrocarbons), could not be determined.

In the Ceduna Sub-Basin of the Great Australian Bight along Australia's southern margin, fluid escape pipes were identified on the Ceduna 3D seismic survey within Cenozoic sedimentary rocks and the shallowest 400 m of Upper Cretaceous Hammerhead Supersequence. Each fluid escape pipe overlies the upper tip of a normal fault that displaces strata within the Hammerhead Supersequence. The spatial distribution of fluid escape pipes across the study area varies with predominant fault type; occurring in random distributions with polygonal faults to the north-west, and in linear clusters with listric faults to the south-east. The spatial link between the fluid escape pipes and faults suggest that these faults have acted as migration pathways forfluids that were subsequently vented through the pipes. Regional thermal maturation studies suggests the migrating fluids are likely to be hydrocarbons sourced from deeper Cretaceous organic rich sequences.

A series of fluid escape features and complex faulting structures (radial concentric and conjugate faults) apparently induced by deeper intrusions were identified within Mid Cenozoic sedimentary sequences of the Bass Basin imaged by the Labatt 3D seismic survey. A total of 101 fluid escape

features were documented along a horizon interpreted within the Oligocene to Miocene Torquay Group sequence, manifesting as craterlike-depressions overlying fluid escape pipes. These craters are interpreted to be maar structures or hydrothermal vents, 42 of which have overlying volcanic vents. Three areas of radial faults and 6 areas of concentric faults were identified within the Oligocene to Miocene Torquay sequences whereas 13 pairs of conjugate faults were identified within the Eocene to Miocene Demon's Bluff and Torquay sequences. The conjugate and radial fault structures are interpreted to have formed from emplacement of underlying igneous intrusions whereas the concentric faults are interpreted to have formed as a result of subsurface sediment evacuation.

The varying mechanisms that generate focused fluid flow systems may impact petroleum systems in different ways. In the Exmouth Plateau, normal faults within the Jurassic and Triassic sequences are inferred to be poor fluid migration pathways due to focused fluid flow features forming laterally offset from the fault upper tips. Fluid escape features themselves, once established, can act as migration pathways that may compromise sealing unit integrity by providing secondary migration pathways for hydrocarbons within potential reservoirs, and thus increase exploration risk by reducing the probability of long-lived hydrocarbon accumulation. In a frontier exploration basin such as the Ceduna Sub-Basin, the presence of fluid escape features that may have formed as a result of hydrocarbon migration can improve the exploration potential. Though their occurrence in the region highlights potential trap breaches, the formation of focused fluid flow features in the region proves the presence of hydrocarbon producing source rocks and viable migration pathways. Though not directly associated with hydrocarbon generation, the fluid escape features and overburden deformation structures identified in the Bass Basin can influence petroleum exploration. They provide fluid migration pathways from deeper to shallower sequences, while the associated igneous intrusions may act to impede fluid migration.

This study highlights the importance of studying ancient focused fluid flow systems (in addition to the better documented contemporary ones) to aid in hydrocarbon exploration. Improved understanding of the impact of paleo-focused fluid flows on subsurface fluid dynamics and petroleum system elements can be utilized to de-risk exploration.

Declaration

I certify that this work contains no material which has been accepted for the award of any other degree or diploma in my name, in any university or other tertiary institution and, to the best of my knowledge and belief, contains no material previously published or written by another person, except where due reference has been made in the text. In addition, I certify that no part of this work will, in the future, be used in a submission in my name, for any other degree or diploma in any university or other tertiary institution without the prior approval of the University of Adelaide and where applicable, any partner institution responsible for the joint-award of this degree.

I acknowledge that copyright of published works contained within this thesis resides with the copyright holder(s) of those works.

I also give permission for the digital version of my thesis to be made available on the web, via the University's digital research repository, the Library Search and also through web search engines, unless permission has 177been granted by the University to restrict access for a period of time.

I acknowledge the support I have received for my research through the provision of an Australian Government Research Training Program Scholarship.

Tayallen Velayatham 12th July 2019

List of Publications

Peer Reviewed Journals:

Velayatham, T., Holford, S. P., and Bunch, M. A. 2018 Ancient fluid flow recorded by remarkably long, buried pockmark trains observed in 3D seismic data, Exmouth Plateau, Northern Carnarvon Basin, Marine and Petroleum Geology, 95, 303-313

Manuscripts written for publication:

Velayatham, T., Holford, S. P., Bunch M. A., King R. C., & Magee, C. 3D Seismic Analysis of Ancient Subsurface Fluid Flow in the Exmouth Plateau, Offshore Western Australia

Velayatham, T., Holford, S. P., Bunch M. A., and King R. C., Fault Controlled Focused Fluid Flow In the Ceduna Sub-Basin, Offshore South Australia; evidence from 3D seismic reflection data

Velayatham, T., Holford, S. P., Bunch M. A., King R. C., King & Schofield, N. 3D Seismic analysis of complex faulting patterns and fluid escape features associated with late Cenozoic magmatism in the Bass Basin, offshore southeast Australia.

Acknowledgement

As close as 5 years ago, the idea of starting, much less completing, a PhD was the furthest thing from my mind and was something I could not have seen myself accomplish. Undertaking my research and writing this thesis could not have been done without the help of a great number of people.

To my supervisors: Simon P. Holford, Mark A. Bunch and Rosalind C. King

I cannot express enough gratitude to my three supervisors, without whom none of this would have been possible. Their guidance and wisdom in helping me with designing, executing and (especially) writing up the research thesis has been invaluable. With their encouragement, I was pushed far out of my comfort zone and grew in many ways that I am thankful for. You not only helped me to complete this PhD, but also made the experience an unforgettable one that has made me grow as an individual.

To my collaborative supervisors: Craig Magee and Nick Schofield

I'd like to thank Craig Magee and Nick Schofield for their contributing their time and knowledge in providing input for my research. Sharing the knowledge you have in your respective fields of expertise helped improve the quality of my research and manuscripts.

Friends and Staff at the Australian School of Petroleum

With the amount of time I spent at the School of Petroleum, the students and staff there have become akin to a second family whose support has been a great motivation. A special thanks to Hugo Burgin and Peter Reynolds who were often sounding boards for ideas and acted as 'outside' pairs of eyes; Carmine Wainman and Melissa Jade who showed me the ropes when I was starting out; Melissa and Vasanthi who worked magic as the school admin to help me with various things. I also thank my fellow students and the lecturers at the school. I may not name everyone but you have all been no less special to me.

To my family

Last and certainly not least, I give a heartfelt thank you to my family. To my beloved wife, Denise, whom without her support and encouragement at all times, would have made this endeavour impossible. To my parents who made me the person I am today and provided me with the opportunities to pursue my goals, and my sister who cheered me on throughout my research.

Chapter 1

Introduction and Thesis Rationale

Thesis Rationale: Why Study Ancient Focused Fluid Flows in offshore basins of Australia?

Australia's oil and gas industry plays a critical role in the country's energy market. Between 2016 and 2017, fossil fuels accounted for 94% of Australia's energy consumption with oil and gas comprising 62% of that total (Ball et al., 2018). Despite having up to 70 sedimentary basins, hydrocarbon exploration and development in the country are concentrated around just a few main areas; LNG projects are focused along Australia's North West Shelf and inland Queensland while 72% of the country's crude oil production comes from the Carnarvon Basin, offshore Western Australia (Thurtell et al., 2018). This provides significant opportunities for exploration in frontier or under-developed regions.

An integral part of hydrocarbon exploration is the assessment of petroleum system elements and processes (Magoon & Dow, 1994). The elements of a petroleum system include source rock, reservoir rock, sealing rock, trapping structures and overburden (Magoon & Schmoker, 2000). The processes of a petroleum system encompass hydrocarbon generation, expulsion, migration and preservation (Demaison & Huizinga, 1991; Magoon & Schmoker, 2000). Viable secondary and tertiary migration pathways comprise additional elements integral to the proper functioning of a productive petroleum system (England, 1994). In frontier or under-developed regions, 2D seismic reflection, gravity and magnetic data are often the primary sources of information from which subsurface architecture can be determined (Christopherson, 1991; Blood, 2001; Longley et al., 2002). While these data enable geologists to assess the spatial distribution of the elements of a petroleum system, it is significantly more difficult to evaluate subsurface fluid dynamics associated with oil and gas. Geophysical methods such as those mentioned above measure variations in the physical properties of subsurface rocks but are unable to discriminate variations in fluid types (Bechtel et al., 2007).

Focused subsurface fluid flows are phenomena created where fluid migrate under a pressure gradient from deeper to shallower elevation via some kind of focusing mechanism. They have been documented in various geological settings but are typically associated with basins that have high sedimentation rates or generate hydrocarbons (Gay et al., 2006a; Hustoft et al., 2009). Rapid sediment loading, particularly when associated with low permeability sediments, can result in overpressure generation and variation in lateral pressure gradients that result in focused fluid migration (Hustoft et al., 2009). The in situ generation of fluids at depth, such as from hydrocarbon generation and expulsion, could similarly generate subsurface overpressures (Tingate et al., 2001). Focused fluid flows commonly manifest along a surface as crater-like depressions referred to as pockmarks, or

paleo-pockmarks for those that have been buried and preserved (King & MacLean, 1970). Fluid expulsion along a surface may also occur without a structural manifestation along the surface. These focused fluid flow systems are often associated with low flux fluid expulsion and are referred to as seepages (Hovland & Judd, 1988). Expulsion of fluids along a surface is often facilitated by an underlying fluid migration conduit which is referred to as fluid escape pipes.

The advent of 3D seismic imaging technology has vastly improved our ability to understand subsurface fluid dynamics by providing direct evidence of three dimensional rock and fluid interactions (Cartwright & Huuse, 2005). 3D seismic datasets have increased our understanding of subsurface fluid migration systems by enabling improved imaging and definition of geological elements that make up focused fluid flow systems. Detailed imaging of focused fluid features enables identification of stratigraphic sequences from which migrating fluids are sourced from, delineation of fluid migration pathways, and identification of geological features, such as igneous intrusions or salt diapirs, that may act as a control on the spatial distribution of focused fluid flow systems (Pilcher & Argent, 2007; Andresen et al., 2011; Maia et al., 2016).

Analysis and interpretation of focused fluid flow pathways observed in seismic data have since been used to evaluate hydrocarbon prospectivity in various settings around the world. In the Gulf of Mexico, spatial distribution analysis of seafloor vents on seismic data led to clearer delineation of underlying reservoir rocks, as well as improved understanding of the reservoir pressure regime (Reilly & Flemings, 2010). In offshore West Africa, kilometre-scale fluid escape pipes were traced down to hydrocarbon bearing reservoir rocks (Løseth et al., 2011). Identification and interpretation of fluid expulsion features along an ancient, buried surface (referred to as a paleo-surface) in the Danish North Sea led to an improved understanding of underlying hydrocarbon source rock distribution and provided insight on the timing of hydrocarbon expulsion (Andresen et al., 2008).

Focused fluid flows have been studied in various regions across the globe, however, these studies have concentrated on active fluid flow systems and active seeps (Judd & Hovland, 2007; Huuse et al., 2010). Comparatively, there is a lesser understanding of ancient focused fluid flow systems. Paleo-focused fluid flow features have been documented in several offshore basins of Australia (O'Brien & Woods, 1995; Struckmeyer et al., 2002; Logan et al., 2008; Logan et al., 2010). Despite increased understanding of focused fluid migration systems, the source of fluids and controls on the formation of paleo-fluid flow features in offshore basins of Australia remains poorly defined (Logan et al., 2010; Dirstein et al., 2013). This thesis represents a first attempt to qualitatively and quantitatively analyse focused fluid flow features and develop geological models for their formation in offshore sedimentary basins of Australia, focusing on the Northern Carnarvon (Chapters 2 and 3), Bight (Chapter 4) and Bass (Chapter 5) Basins of offshore Australia as they represent currently producing, frontier and mature hydrocarbon exploration basins respectively. The approach adopted in this study integrates

geophysical, geological and petrophysical data to develop holistic subsurface models to identify and define fluid flow features in the subsurface and propose mechanisms responsible for their formation. The potential impact of these focused fluid flow features on hydrocarbon exploration is discussed in the context of their respective sedimentary basins (Chapter 6).

Thesis Outline

Literature Review

Focused fluid flows are hydrogeological processes that pertain to the focused emission or expulsion of fluids along a surface, often along the seabed-seawater interface (Judd & Hovland, 2007). Focused fluid flow systems have been recognized by the scientific community since the 1960s and surficial expressions of focused fluid flow systems were first described in the 1970s (King & MacLean, 1970; Taniguchi et al., 2002; Judd & Hovland, 2007). Since then, there has been a growing interest in the dynamic geological processes that drive the occurrence of focused fluid flows. Chapter 1 of this thesis reviews the current understanding of focused fluid flow systems by discussing their surface and subsurface manifestations, formation mechanisms, and geologic controls on spatial distribution. With a focus on ancient focused fluid flow systems, Chapter 1 also discusses workflows for identifying and interpreting paleo-focused fluid flow features utilizing seismic data.

Chapter 2: Ancient fluid flow recorded by remarkably long, buried pockmark trains observed in 3D seismic data, Exmouth Plateau, Northern Carnarvon Basin

The North West Shelf of Australia is a passive rifted continental margin and the country's premier hydrocarbon producing region, with most of the production sourced from inboard regions of the Northern Carnarvon Basin (Longley et al., 2001). Amongst the earliest documented evidence of focused fluid flows in the North West Shelf is provided by O'Brien & Woods (1995) who identified vertical zones of disrupted and chaotic seismic reflections within Eocene sandstones in the Vulcan Sub-basin of the Bonaparte Basin. These features were termed Hydrocarbon-Related Diagenetic Zones (HRDZs) and were attributed to oxidation of migrating hydrocarbons during the Late Miocene and Early Pliocene. A more recent study by Dirstein et al. (2013) identified pockmarks along the seafloor as well as paleo-pockmarks within the Triassic Mungaroo formation across the Gorgon, Glencoe, and Bonaventure 3D seismic surveys on the Exmouth Plateau of the Northern Carnarvon Basin. Dirstein et al. (2013) also utilized waveform classification methods to quantify subtle changes in the seismic response along interpreted surfaces within Mesozoic and Cenozoic sequences and characterised varying waveform classes to identify potential focused fluid migration pathways. The source and type of potential fluids involved as well as the timing of fluid expulsion, however, were not investigated in Dirstein et al. (2013).

Despite the documentation of paleo-focused fluid flows within Cenozoic and Mesozoic sequences in the North West Shelf by Dirstein et al. (2013) and O'Brien & Woods (1995), the mechanisms that led

to their formation are still unclear and there has been little investigation into the their broader occurrence across the region (Logan et al., 2010). Chapter 2 represents the first attempt to document and map paleo-focused fluid flow features within the North West Shelf, focusing on the Exmouth Plateau of the Northern Carnarvon Basin. Using 3D seismic data from the western edge of the plateau, 275 buried and preserved crater-like depressions (referred to as paleo-pockmarks) were interpreted along an unconformable surface that represents the top of the Jurassic sequence. Underlying each paleo-pockmark are fluid escape pipes that extend downward through the Jurassic sequence and terminate within the Triassic sequence. The paleo-pockmarks occur in NW-SE trending linear trains and include the longest known pockmark train yet documented (~72 km long). The occurrence of these paleo-pockmarks in linear trends across the survey area suggests an underlying geological control on the spatial distribution of the focused fluid flow features. Utilizing spatial statistics, the spatial distribution of paleo-pockmarks are quantified and shown to correlate with the orientation of normal faults that underlie the focused fluid flow features within the Triassic sequence. A control on the spatial distribution of paleo-pockmarks by the underlying normal faults is defined and an uncommon interaction between faults and fluids is documented, whereby faults acted as a trigger for focused fluid migration in the Late Jurassic, instead of acting as fluid migration pathways themselves.

The principles of this chapter demonstrates the importance of integrating geophysical and geological data in developing a comprehensive model for the formation of focused fluid flows. By understanding the process by which the paleo-focused fluid flow features had formed, we are able to develop a geological model for the formation of the Late Jurassic focused fluid flow features within which we hypothesize the source of fluids and investigate the role of paleo-overpressure generation in focused fluid migration.

Chapter 3: 3D Seismic Analysis of Ancient Subsurface Fluid Flow in the Exmouth Plateau, Offshore Western Australia

While focused fluid flow features have been documented to occur in isolation, they typically occur in fields or clusters that can extend over a range of scales, from field-wide to basin-wide occurrences (Pilcher & Argent, 2007). Identification of paleo- focused fluid flow features along the western edge of the Exmouth Plateau of the Northern Carnarvon Basin in Chapter 2 raised the question as to whether the Late Jurassic paleo-fluid expulsion event was a localised or regional occurrence. Chapter 3 follows this line of inquiry in an effort to identify similar paleo-focused fluid flow systems in the central and eastern regions of the Exmouth Plateau.

As in in Chapter 2, this study utilizes 3D seismic data to document fault-associated Late Jurassic focused fluid flow features within Triassic and Jurassic sequences in the central and eastern regions of

the Exmouth Plateau. Linear trends of paleo-pockmarks with underlying fluid escape features are interpreted along an unconformable surface that marks the top of the Jurassic sequence within the central and eastern regions of the Exmouth Plateau respectively. The paleo-fluid escape features occur in linear trends (N-S and NE-SW linear trends in central and eastern regions of the plateau respectively) that mirror the strike orientation of normal faults that underlie the fluid escape features within the Triassic Mungaroo Formation. Chapter 3 integrates its results with the results of Chapter 2 to reveal evidence of spatially organized paleo-focused fluid flow features that are correlatable across the Exmouth Plateau and implies that the Late Jurassic fluid expulsion event was a basin-wide phenomena. This hypothesis is tested by investigating regional tectonic events coeval with formation of the focused fluid flow features. The geological model for the formation of fault-associated paleo-focused fluid flows developed in Chapter 2 is expanded on by identification of a potential link between fault development and interpreted mantle plume activity during the Late Jurassic and Early Cretaceous along the southern margin of the Exmouth Plateau at the time focused fluid flow features formed.

The findings from this study and Chapter 2 further refine the existing tectonic development history of the Exmouth Plateau by revealing a previously undocumented, basin-wide normal fault system that has a radial trend across the Exmouth Plateau (with its locus located along the southern margin of the plateau) that acts as a spatial control for the formation of focused fluid flows and associated features. An attempt is made to constrain the types of fluid that formed the Late Jurassic paleo-focused fluid flow features. This chapter discusses the potential development of preserved fluid escape features as fluid migration pathways and highlights their potential impact on hydrocarbon trap risk assessment due to the ability of these fluid escape features to compromise the integrity of a seal rock sequence.

Chapter 4: Fault Controlled Focused Fluid Flow in the Ceduna Sub-basin, Offshore South Australia; evidence from 3D seismic reflection data

Like the North West Shelf, Australia's Southern Margin is a passive continental margin that developed through a series of rifting events associated with the break-up of Gondwana (Totterdell & Bradshaw, 2004). Unlike the North West Shelf however, the Great Australian Bight is a frontier region for hydrocarbon exploration with only 10 wells having been drilled there and having comparatively limited seismic survey data coverage (Totterdell & Mitchell, 2009). Various types of geological and geophysical data have been acquired in the region to more thoroughly appraise hydrocarbon potential. Synthetic aperture radar (SAR) data identified seepage slicks in the Ceduna Sub-basin (Logan et al., 2010). Seafloor dredge samples from the western part of the Ceduna Sub-basin have recovered organic rich marine shales with up to 6.9% Total Organic Carbon (TOC)

(Totterdell & Mitchell, 2009). Finally, geochemical studies of stranded coastal bitumen samples along the Bight Basin coastline suggest they originated from slow seeping hydrocarbons in the Bight Basin (Hall et al., 2014). Interpretation of regional 2D seismic data by Struckmeyer et al. (2002) identified potential gas chimneys within the Cenozoic and Late Creatcous sequences of the basin. Despite the presence of these potential hydrocarbon indicators (seeps, organic rich shales, gas chimneys), hydrocarbon charge and seal integrity are key risks for further hydrocarbon exploration in the Bight Basin (Totterdell & Mitchell, 2009). There is at present, a lack of direct evidence for hydrocarbon prone source rocks within the outboard, distal regions of the Basin (Totterdell & Mitchell, 2009). Furthermore, a paleo-oil column identified in the Eyre Sub-basin is interpreted to have been breached by a reactivated fault in the Late Cretaceous, which leads to uncertainty in trap integrity within the Bight Basin (Ruble et al., 2001).

Chapter 4 utilizes newly acquired 3D seismic data to further investigate the occurrence focused fluid flow features within the Ceduna Sub-Basin of the Bight Basin. An extensive number of focused fluid flow features were identified within the Late Cretaceous and Cenozoic successions along the south-western edge of the survey area. The focused fluid flow features are associated with the upper tip of underlying normal faults that are interpreted to be acting as a fluid migration pathways. Localized variation in the spatial distribution of focused fluid flow features along the shelf edge is reflected by a change in underlying dominant fault type; randomly distributed focused fluid flow features with underlying polygonal faults to the northwest of the study area, and linear trends of focused fluid flow features with underlying normal faults to the south east. The growth history of the normal faults has been documented by Robson et al. (2016) and Ryan et al. (2017). This chapter builds on these two studies by correlating the timing of fault development, focused fluid flow feature formation and hypothesised hydrocarbon expulsion from underlying source rock formations.

The focused fluid flow features identified in this chapter show a contrasting interaction with underlying faults when compared to the fault associated paleo-focused fluid flow features identified in Chapters 2 and 3. While the identified faults from the Exmouth Plateau and Ceduna Sub-basin both act as controls on the spatial distribution of focused fluid flow features, the faults in the Ceduna Sub-basin did so as fluid migration pathways whereas the faults identified in Chapters 2 and 3 act as a trigger for fluid migration. Chapter 4 highlights the importance of developing holistic models of the subsurface in order to accurately interpret the mechanisms and driving forces behind the formation of focused fluid flows. Furthermore, this study also contributes to understanding of Bight Basin petroleum system elements by support the presence of hydrocarbon prone source rocks and a working petroleum system.

Chapter 5: 3D Seismic analysis of complex faulting patterns and fluid escape features associated with Late Cenozoic magmatism in the Bass Basin, offshore southeast Australia

Many rift and passive margin basins are characterised by magmatism and the occurrence of igneous activity can result in the formation of focused fluid flow features such as hydrothermal vents (Planke et al., 2005; Holford et al., 2012). The occurrence of igneous material in the subsurface can directly or indirectly influence subsurface fluid migration dynamics and affect petroleum system elements in hydrocarbon generating basins (Holford et al., 2012; Senger et al., 2017). Igneous intrusions are able to induce fluid migration by superheating host rock pore fluids to generate overpressure that may induce hydraulic fracturing of the overburden and subsequently migrate vertically to form focused fluid flows (Jamtveit et al., 2004; Sun et al., 2013). If the intrusion occurs within an organic matter rich rock unit, the superheating from the intrusion could induce hydrocarbon generation, cracking and expulsion, which could result in overpressure generation (Othman et al., 2001).Conversely, igneous intrusions themselves can act as barriers for fluid migration due to their highly impermeable nature and thus can compartmentalize fluid migration in the subsurface (Senger et al., 2017). Emplacement of igneous material in the subsurface can mechanically deform the host rock that and result in the formation structures such as radial faults, dyke-induced normal faults or domal forced folds (Stewart, 2006; Jackson et al., 2013). The igneous intrusions associated faults are able to act as fluid migration pathways whereas forced fold structures can potentially develop as structural traps for hydrocarbon accumulation (Senger et al., 2017).

Chapter 5 investigates the impact of Late Cenozoic magmatism on subsurface fluid dynamics in a hydrocarbon generating basin, focusing on the Bass Basin of Southeastern Australia. The basin has been subject to multiple phases of igneous activity throughout its geologic history and is moderately explored with 45 wells (36 exploration) drilled, though there is only one producing field in the basin (Blevin et al., 2003; Cummings et al., 2004; Watson et al., 2019). Historically, the presence of igneous material prior to-drilling has been poorly predicted with 13 of the 36 exploration unexpectedly encountered igneous rocks. Chapter 5 builds upon the methodologies developed in Chapters 2-4 to document and categorize focused fluid flow features (manifesting as surficial depressions) based on their seismic morphology to discriminate between focused fluid migration features that may have been a precursor to volcanism and true volcanic features that may have similar seismic expressions as focused fluid flows. Chapter 5 also documents overburden deformation (manifesting as radial, conjugate and concentric faults) within Cenozoic sequences that are associated with emplacement of underlying igneous intrusions in the study area.

A total of 101 surficial depressions are identified within the Eocene to Miocene Torquay group sequence. The depressions are categorized based on the morphological expression of the depressions and their infilling seismic reflectors. Correlations between the spatial distribution of surficial depressions and the occurrence underlying igneous intrusions are analysed to identify potential genetic links between them. The nucleation and growth history of the radial, conjugate and concentric faults are quantitatively and qualitatively investigated and their association with underlying igneous intrusions are interpreted. Depth-displacement analysis of 7 pairs (out of 13 pairs) of identified conjugate faults improve our understanding of normal fault nucleation during igneous dyke emplacement while quantitative analysis of downward sagging seismic reflectors within the locus of concentric faults suggest the occurrence of a subsurface sediment evacuation event. The occurrence of radial faults with localized structural highs implies at the emplacement of an underlying igneous intrusion.

The methodology and workflow developed in this chapter provides a practical framework for distinguishing and analysing focused fluid flow features in regions with igneous activity. In a region where subsurface igneous material is difficult to detect on seismic data, we also demonstrate the value in understanding the development history of overburden deformation features and utilizing their occurrence to infer the presence and morphology of underlying intrusions. Where igneous intrusions occur alongside focused fluid flow features, the ability to distinguish between the two on seismic data is critical for assessing the potential impact of igneous intrusions and focused fluid flow features on petroleum systems elements (e.g. migration, source maturity, seal integrity) in order to reduce exploration risk. The accurate identification and evaluation of fluid migration pathways provides the opportunity to prioritise particular reservoir fairways and risk assess sealing units to trapping structures along the selected reservoirs.

Chapter 6: Conclusions

Chapter 6 summarizes the key findings of Chapters 2-5 and discusses the potential implications of focused fluid flow occurrences on petroleum systems elements and hydrocarbon exploration within the Northern Carnarvon, Bight, and Bass Basins. Chapter 6 also summarizes this thesis by highlighting recommendations for future research that could be done to further improve the scientific community's understanding of ancient focused fluid flow systems in offshore basins of Australia.

Literature Review

1. Introduction

Subsurface fluids that migrate from deeper to shallower depths through a focusing mechanism, such as overpressure venting or flow driven by buoyancy drive, via permeable migration pathways are referred to as focused fluid flows (Berndt, 2005; Gay et al., 2007; Anka et al., 2012). Though the term fluid is used in association with focused migration pathways, such features can be conduits for mobilized material can consist of a variety of phases: gases (biogenic gas), liquids (brine, hydrocarbon), or even solid suspensions that behave in a fluid-like manner (overpressured sandstones, salt) (Cartwright et al., 2007; Huuse et al., 2010). This thesis however focuses on focused fluid flow systems that pertain to the migration of liquids or gasses and rather than sediment remobilization occurrences.

Awareness of focused fluid flows in offshore basins originated in the 1960s with the discovery of hydrothermal vents and pockmarks on seabed surfaces on the Scotian Shelf (King & MacLean, 1970). These morphological features were interpreted as the surficial manifestations of water or gases in subterranean coastal plain rocks that percolated and expelled through the overlying unconsolidated seafloor sediments (King & MacLean, 1970; Judd & Hovland, 2007). The discovery of pockmarks triggered an increasing interest in subsurface fluid migration. Fluid migration features such as these have the potential to impact bio-, hydro- and atmospheres on local and global scales (Judd & Hovland, 2007; Cambon-Bonavita et al., 2009). For instance, the world's oceans have been estimated to have circulated through the Earth's oceanic crust via subsurface hydrothermal systems, such as spreading ridges or back-arc rifting systems, approximately every 10 million years, bringing heat exchange, chemical properties and nutrients into the oceans (Kadko et al., 1995; Judd & Hovland, 2007). Furthermore, offshore focused fluid flows are also seen as key sources of methane into the atmosphere, globally contributing at least 10 to 30 Tg which constitutes 2 to 6% of the total atmospheric methane budget (Judd & Hovland, 2007).

The significance of focused fluid flows in hydrocarbon exploration has long been recognized by the oil and gas industry. Historically, oil and gas seeps have been used as surficial indicators of underlying petroleum systems (Link, 1952). At present, research on focused fluid flows are increasingly being utilized by the oil and gas industry across the globe to improve evaluation of petroleum system elements and hydrocarbon prospectivity (Fig. 1) (Meldahl et al., 2001; Heggland, 2005). The advent and proliferation of 3D seismic imaging technology over the past three decades has enabled us to study focused fluid flow systems in greater detail with its ability to image subsurface fluid-rock interactions in three dimensions (Cartwright & Huuse, 2005). In offshore West Africa and the North Sea, interpretation of seabed fluid seeps and focused fluid flows identified on seismic data

aided in defining the location and geometry of underlying hydrocarbon reservoirs (Heggland, 1998; Gay et al., 2003). In a more generalized study, Løseth et al. (2009) evaluated the preservation capability of hydrocarbon reservoirs by interpreting the location of fluid escape relative to an underlying reservoir.

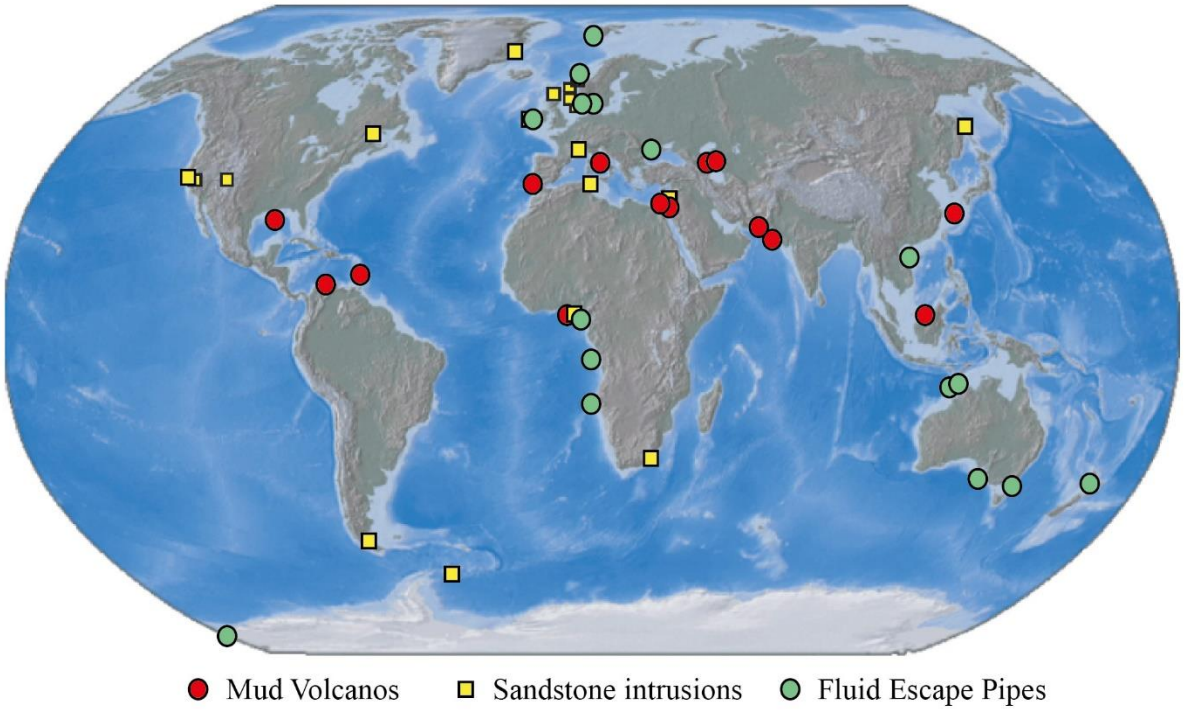

Figure 1**:** *Worldwide locations where fluid focused fluid flows have been documented and investigated (modified from Huuse et al., 2010).*

Focused fluid flows in Australian basins were first recognized by O'Brien & Woods (1995) in the Vulcan Sub-basin, offshore north-western Australia. Since then, seabed seepages and focused fluid flows have also been identified in other offshore basins around the continent such as the Gippsland and Bight basins (Fig. 1) (Struckmeyer et al., 2002; Nourollah et al., 2010). In recent years, there has been a growing interest in the potential impact of the delineation and dating of focused fluid flow features in order to aid hydrocarbon exploration (Struckmeyer et al., 2002; Logan et al., 2010). Alongside seismic reflection technology, various advanced data acquisition methods have been utilized in an effort to document fluid flow features in offshore basins of Australia. Examples of such methods include synthetic aperture radar (SAR), side-scan sonar, and seismic wavelet classification that have been utilized in the North West Shelf and the Great Australian Bight (O'Brien & Woods, 1995; Struckmeyer et al., 2001; Dirstein et al., 2013). To date however, only seafloor pockmarks and subsurface columns of attenuated acoustic signals with abrupt lateral terminations (interpreted to be hydrocarbon-related diagenetic zones) on the Yampi Shelf in north-western Australia have been linked to proven underlying hydrocarbon reservoirs associated with the Cornea oil and gas field (Rollet et al., 2006; Logan et al., 2010).

2. Surface and Subsurface Manifestations of Focused Fluid Flows

Depending on the nature of migrating fluids, focused fluid flows can manifest in a range of forms. However, this thesis is primarily focused on pockmark and fluid escape pipe features. Focused fluid flow occurrences can broadly be categorized as one of two surficial manifestations, and/or either one or both of two subsurface manifestations.

2.1. Surficial Manifestation

Focused fluid expulsion along a free stratigraphic surface (ground level, seabed) may or may not result in an observable expression such as a crater-like depression. This is primarily influenced by the type(s) of material expelled and the rate of expulsion. Expulsion of solids components such as overpressured mud can result in the formation of structural features such as mud volcanoes or submarine craters whereas low flux liquid or gas expulsions can result in seafloor seepages with no discernible structural feature. The most common surficial expression of fluid expulsion however, are pockmarks (Judd & Hovland, 2007).

2.1.1. Pockmarks

Pockmarks are circular or elliptical depressions that form in fine grained sediments and are often documented in offshore environments (Fig. 2a) (King & MacLean, 1970; Andresen et al., 2008). The term pockmark was first coined by King & MacLean (1970) to describe V-shaped notches along the sediment water interface in offshore Nova Scotia, Canada. They are interpreted to have formed through sediment removal or erosion from below as a result of ascending fluids (King & MacLean, 1970; Judd & Hovland, 2007; Cathles et al., 2010). Judd & Hovland (2007) propose a conceptual model for the formation of pockmarks whereby accumulations of fluids in near-seabed sediments produces a dome-like swelling on the seabed. As fractures develop along the domed surface, the fluids establish a migration route with the overlying water column. Establishment of this hydraulic connection leads to a fluid pressure drop in the near-seabed sediments, which results in a violent burst of escaping fluids that forms a pockmark (Judd & Hovland, 2007; Cathles et al., 2010). Pockmarks have been documented in various marine environments globally that range from estuarine through to deep marine and can form as rapidly as 20 minutes (Hovland et al., 2002; Judd & Hovland, 2007; Pilcher & Argent, 2007). In the Gulf of Mexico in 1972, a jack-up mat-supported rig ‘J. Storm II’ tilted and sank 20 minutes later (Worzel & Watkins, 1974). A seabed survey at the rig’s location revealed a flat bottomed crater 500 m across and 12 m deep. Gas plumes were observed to originate from the newly-formed pockmark, interpreted to be coming from both the rig’s broken drill stem and the crater floor. Understanding the genesis of pockmark formation can provide valuable information

on subsurface fluid dynamics; however, pockmarks do not provide information on the rate or volume of fluids that have been expelled (Cartwright et al., 2007; Andresen, 2012).

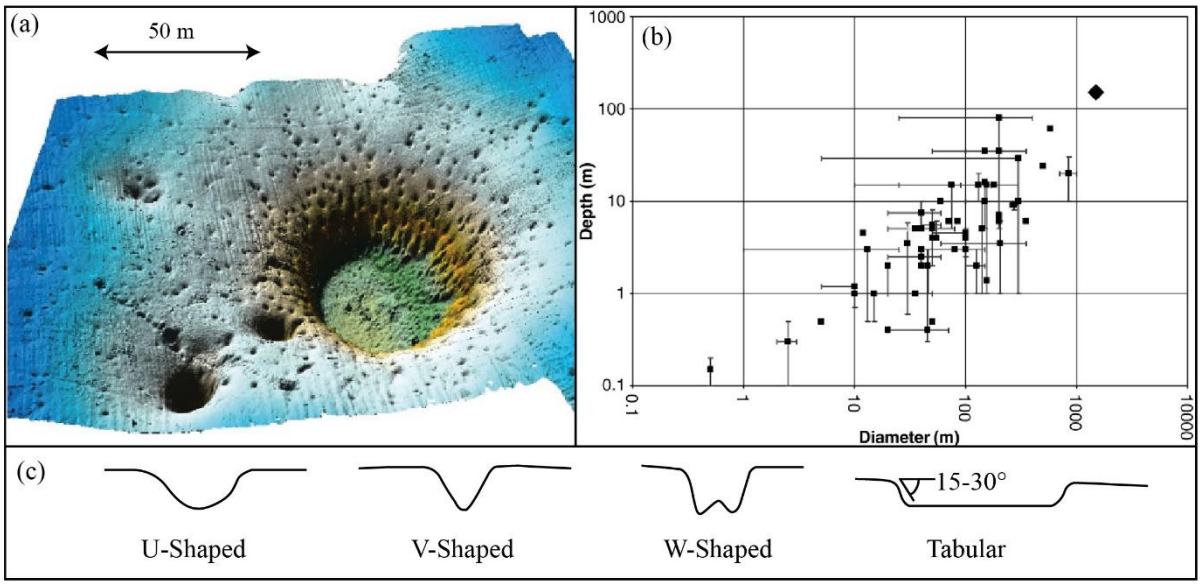

***Figure 2**: (a) Multibeam bathymetric image of a cluster of pockmarks from the Troll Field of the North Sea (modified from (Mazzini et al., 2017)). The lack of observed gas bubble or fluid seepage suggest that these pockmarks are inactive. (b) A graph illustrating the range of pockmark depth and diameter dimensions from 57 published occurrences worldwide (Pilcher & Argent, 2007). (c) Examples from the North Sea on the range of potential pockmark morphologies (Andresen et al., 2008).*

Lateral dimensions of pockmarks can vary dramatically, ranging from less than a meter up to hundreds of meters in length and width (Fig 2b). Pockmark depths can similarly range from less than 1 m up to approximately 100 m (Judd & Hovland, 2007; Pilcher & Argent, 2007). The internal structure of pockmark depressions show varying morphologies, having been described as having tabular, U-, V-, or W- shaped bases (Fig 2c) (Andresen et al., 2008). These variations in pockmark internal structures are attributed to hydrological and biological processes that take place after pockmark formation. Seafloor currents may erode downstream sides of pockmarks to result in elongated pockmark shapes such as those with tabular or V-shaped bases (Andresen et al., 2008). Continued venting of fluids that promotes development of chemosynthetic activity and biological communities, can result in hydrocarbon accumulation such as in pockets of methane gas. These hydrocarbon accumulations can promote authigenic carbonate precipitation or carbonate mound formation within the pockmark cavity to result in W-shaped pockmark bases (Hovland et al., 2002; Andresen et al., 2008).

2.1.2. Seeps

Seeps are occurrences whereby natural fluids from the subsurface are released into the overlying environment and like pockmarks, they are often identified on the seabed (Judd, 2003; Suess, 2010). While both seeps and pockmarks represent sites of subsurface fluid transport, a distinguishing feature of seeps is the absence of a surficial depressions which can be attributed to slow fluid flow rates which lack an eruptive component during fluid expulsion (Judd, 2003; Judd & Hovland, 2007). Seeps have been documented to occur in a broad range of oceanographic settings and across a wide variety of geological environment across the globe (Judd, 2003).

Though the lack of a surficial expression can make seeps difficult to detect, they can be associated with chemosynthetic biological communities and authigenic carbonate precipitation (Gay et al., 2006c; Naehr et al., 2007). Fluids that are transported through seafloor seeps are often rich in chemical elements that are the basis for organic carbon production, such as methane, hydrocarbon and hydrogen sulphide, which promote development of chemosynthetic biota (Sibuet & Roy, 2002; Cambon-Bonavita et al., 2009). Furthermore, chemical interactions between ambient seafloor water and fluids expelled at seeps can also result in authigenic carbonate precipitation (Naehr et al., 2007). Microbially driven anaerobic oxidation of methane in migrating fluids may increase fluid alkalinity through production of bicarbonate, which can then result in chemical conditions that favour precipitation of authegenic carbonate materials (Naehr et al., 2007). As such, sites of chemosynthetic biota or authigenic carbonate precipitation thus can serve as a proxy indicator for the presence of seafloor seeps.

3. Subsurface/Seismic manifestation

3.1. Buried pockmarks/Paleo-pockmarks

Seafloor pockmarks are thought to represent episodes of contemporary fluid expulsion. As such, pockmarks that have been buried and preserved, referred to as paleo-pockmarks, can be seen as evidence of ancient fluid expulsion events. Paleo-pockmarks are imaged on seismic data and can provide insight into ancient subsurface fluid dynamics (Hartwig et al., 2012). For instance, Hartwig et al. (2012) documented paleo-pockmarks within the Eocene sequence that overlie Late Cretaceous growth and listric faults in the Orange Basin, offshore South Africa. By investigating paleo-pockmark formation timing and their spatial association with the underlying Late Cretaceous faults, Hartwig et al. (2012) interpreted the paleo-pockmarks to have formed as a result of fluid expulsion from disequilibrium compaction overpressure generated during the Late Maastricthtian and Paleocene, which then utilized Late Cretaceous faults as fluid migration pathways in the Eocene.

In addition to enabling improved imaging and understanding of paleo-pockmark morphology, 3D seismic data also enables the analysis of the temporal evolution of subsurface focused fluid flow

features. For instance, continued or episodic fluid expulsion at the same location over long periods of time could result in vertical successions of pockmarks (or paleo-pockmarks) which are referred to as stacked pockmarks (Fig. 3b) (Çifçi et al., 2003). With time or age control on pockmark-bearing strata, the height of a stacked pockmark column can then be analysed to determine the time frame during which fluid expulsion occurred while the vertical spacing between paleo-pockmarks within the stacked sequence provides an indication on the frequency of fluid expulsion (Çifçi et al., 2003; Andresen et al., 2008; Moss et al., 2012b). Andresen & Huuse (2011) identified 8 stacked paleo-pockmarks in Pliocene to Pleistocene sedimentary rocks in the Lower Congo Basin. Heights of the stacked paleo pockmarks range between 50 to 600 ms two-way-time (TWT) and vertical separation of individual paleo-pockmarks are between 25 to 60 ms twt. Based on these measurements and an assumed constant sedimentation rate, initial formation of pockmarks was determined to be approximately 4 Myr ago and the recurrence interval of fluid expulsion was estimated at between 0.09–0.22 Myr.

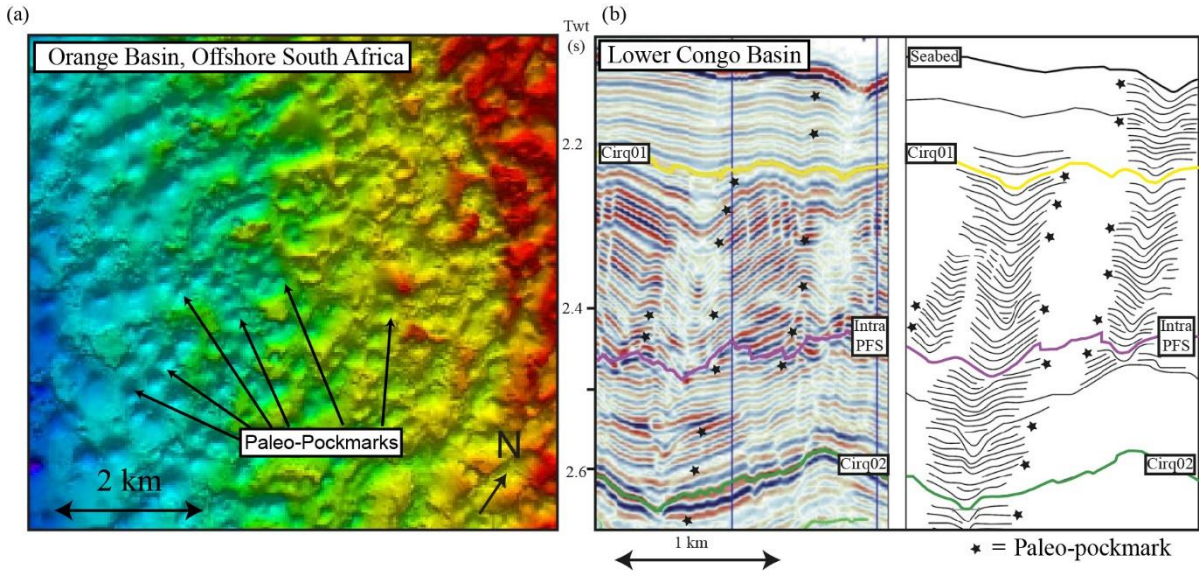

Figure 3: *(a) Paleo-pockmarks along an interpreted paleo-surface within the Eocene sequence from the Orange Basin, Offshore South Africa (Hartwig et al., 2012). (b) Seismic cross-section of three stacked pockmark successions in the Lower Congo Basin from Andresen & Huuse (2011). Stars indicate pockmarks amongst intervening draping seismic reflectors.*

3.2. Fluid escape pipes

Fluid expulsion along a surface via a pockmark is often associated with an underlying conduit that facilitates focused fluid migration. These conduits are commonly referred to as fluid escape pipes and are imaged on seismic data as vertical, pipe-like or column-like anomalies of disturbed or discontinuous seismic reflectors with enhanced or attenuated amplitudes relative to the surrounding host sequence (Fig 4) (Cartwright et al., 2007; Moss & Cartwright, 2010b). The bases of fluid escape

pipes are referred to as roots and are often linked to the fluid source regions (Cartwright & Santamarina, 2015). Vertical dimensions of fluid escape pipes commonly range between 200 to 500 m, however, they have been documented to exceed a kilometre in height (Moss & Cartwright, 2010a; Løseth et al., 2011). Though pockmarks or paleo-pockmarks are often associated with underlying fluid escape pipes, not all fluid escape pipes result in the formation of overlying pockmarks. The manifestation of fluid expulsion features along a surface overlying a fluid escape pipe is influenced by the flux rate of fluid expulsion which in turn is controlled by migrating fluid and overburden parameters, a few of which are overburden sediment density, fluid density, fluid viscosity and fluid buoyancy pressure (Cathles et al., 2010). High flux rates of fluid expulsion are likely to result in the formation of pockmarks whereas protracted, low fluid flux systems may result in stacked amplitude anomalies in overlying seismic reflectors that lack depressions along the surface of those reflectors (Gay et al., 2007; Løseth et al., 2011; Cartwright & Santamarina, 2015).

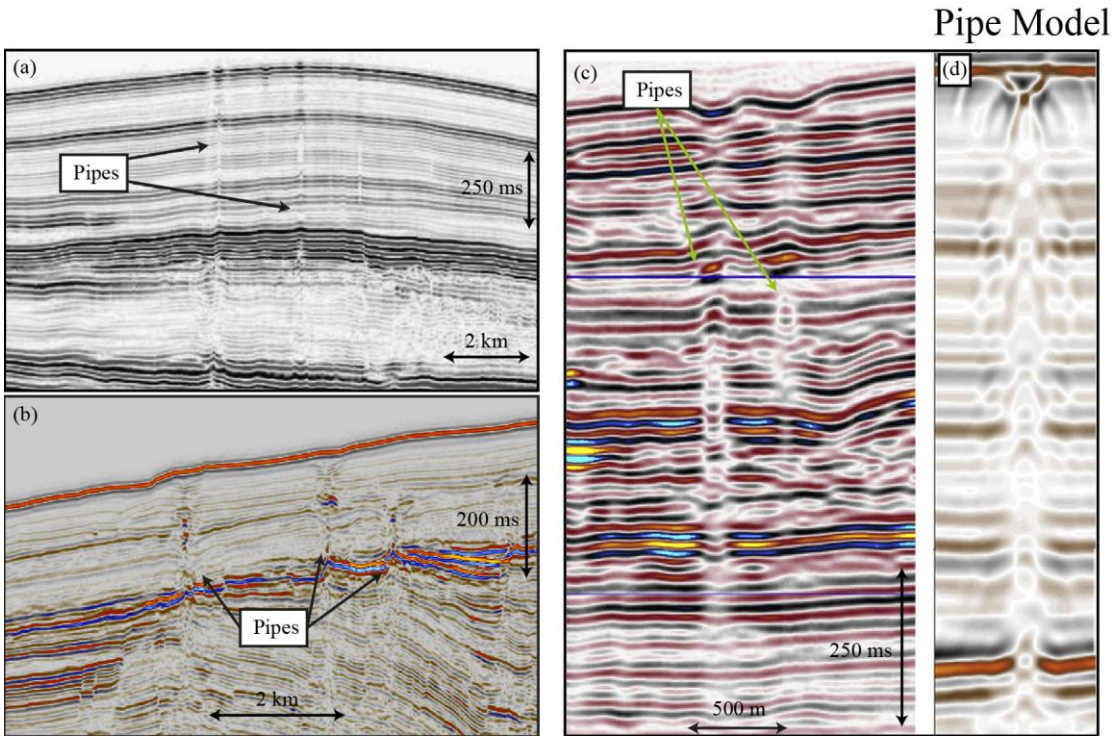

Figure 4: *Fluid escape pipes identified on seismic data from the (a) Vøring Basin, Mid Norwegian Shelf and (b) Ceduna Sub-Basin, Great Australian Bight (Cartwright et al., 2007). Similar seismic expressions are observed when (c) pipe anomalies from Offshore Nigeria are compared with (d) modelled pipe anomalies based on outcrops from Rhodes, Greece (Løseth et al., 2011).*

The mechanical interaction between fluids and rocks that form fluid escape pipes is still poorly understood. However, hydraulic fracturing from overpressure generation is widely cited as the mechanism that initiates fluid escape pipe formation and sustains their propagation (Cartwright et al., 2007; Løseth et al., 2011). As such, fluid escape pipes represent vertical conduits of enhanced

permeability through which fluids are transported faster than they normally would migrate through the undeformed rock pore network (Løseth et al., 2011; Leduc et al., 2013). The column-like shape of fluid flow pipes are indicative of a buoyant fluid drive and distortion of seismic reflectors within the pipes are often attributed to local variation introduced by the fluid to acoustic properties of the host rock (density, velocity, anisotropy) (Løseth et al., 2009; Løseth et al., 2011; Bull et al., 2018). Despite advances in seismic imaging technology, the internal structure of fluid escape pipes is poorly defined on seismic data. Seismic reflectors within fluid escape pipes have been documented with morphologies that range from continuous, concave or convex shapes to zones of chaotic reflectors with low coherence (Cartwright et al., 2007; Løseth et al., 2009; Maia et al., 2016). These differences have been attributed to varying geological processes including minor folding, hydraulic fracture networks, localized reduction in acoustic velocity and host rock diagenesis; however, they are most readily explained as being an artefact of the seismic imaging method (Cartwright et al., 2007; Løseth et al., 2009; Sun et al., 2012). Løseth et al. (2011) undertook a synthetic seismic modelling study to investigate how fluid escape pipes from outcrops in Rhodes, Greece, would be imaged on seismic data. The outcrop pipes consist of clay pipes that are up to 15 m in height and 70 cm in width that are hosted within limestone rocks, which were then scaled up to 50 m in width and 1000 m in height for seismic modelling. The pipes were modelled in four scenarios as vertical zones of varied acoustic impedance contrast relative to the background values, and with varying thicknesses. The modelling results show that the fluid escape pipes are primarily visible as a disruption of the surrounding layered sequence, and the seismic reflectors within the pipe are a result of interference from diffraction patterns on each side of the pipe (Fig. 4c). An experimental study by Bull et al. (2018) acquired high resolution, multi-component seismic reflection data over the Scanner pockmark and gas chimney complex in the North Sea to comprehensively analyse and improve understanding of the internal structure of fluid escape pipes. Interpretation of the Scanner gas chimneys on seismic data suggest that the fluid escape pipes consist of localised, connected fracture systems, which cause a local increase in anisotropy that can decrease vertical seismic velocities as well as result in complex interference patterns. This makes it difficult to accurately interpret the internal structure of fluid escape pipes. The studies of Løseth et al. (2011) and Bull et al. (2018) imply that the presence of a fluid flow pipe on seismic data is likely more a function of acoustic property variation relative to the surrounding host rock, rather than structural deformation such as folding, sagging or faulting of the affected strata. As such, a low flux fluid migration system that has significant velocity variation relative to the surrounding host rock can result in seismic imaging of a pipe on seismic data without an overlying pockmark.

4. Seismic detection workflows

As discussed in previous sections, subsurface focused fluid flows can manifest on seismic data with a range of morphologies, dimensions and varying ease of detectability. The detectability of pockmarks and fluid escape pipes is primarily constrained by size of the fluid escape features relative to the horizontal resolution of the seismic data; the smaller a fluid escape feature is, the closer the seismic line spacing and seismic receiver spacing would need to be to image it. Genuine structural manifestations such as paleo-pockmarks and either genuine or apparent structure found within fluid escape pipes can be identified on seismic amplitude cross-sections or interpreted seismic horizons, whereas non-structural expressions, such as columns of anomalous amplitudes or vertical zones with variable frequency bandwidths, can be difficult to identify with the naked eye. Imaging focused fluid flow features can be enhanced by utilizing seismic attributes that are sensitive to characteristics unique to such features (Marfurt et al., 1998; Meldahl et al., 2001). For instance, fluid escape pipes are often expressed as columns of discontinuous or chaotic seismic reflectors and can be highlighted by seismic attributes that quantify abrupt lateral changes along a seismic reflector such as "incoherence", "variance" or "similarity" (Marfurt et al., 1998). Low flux focused fluid flows can manifest as vertically stacked amplitude anomalies with no observable structural alteration to seismic reflectors. Detectability of these features can be enhanced by amplitude-associated attributes such as Root-Mean-Square (RMS), phase change, or even dominant frequency (Fig. 5 a) (Meldahl et al., 2001). Pockmarks, or paleo-pockmarks, are crater-like depression and can be highlighted by using seismic attributes that quantify localized changes in gradient or 'dip' along a seismic reflector (Fig 5b) (Meldahl & Heggland, 1999).

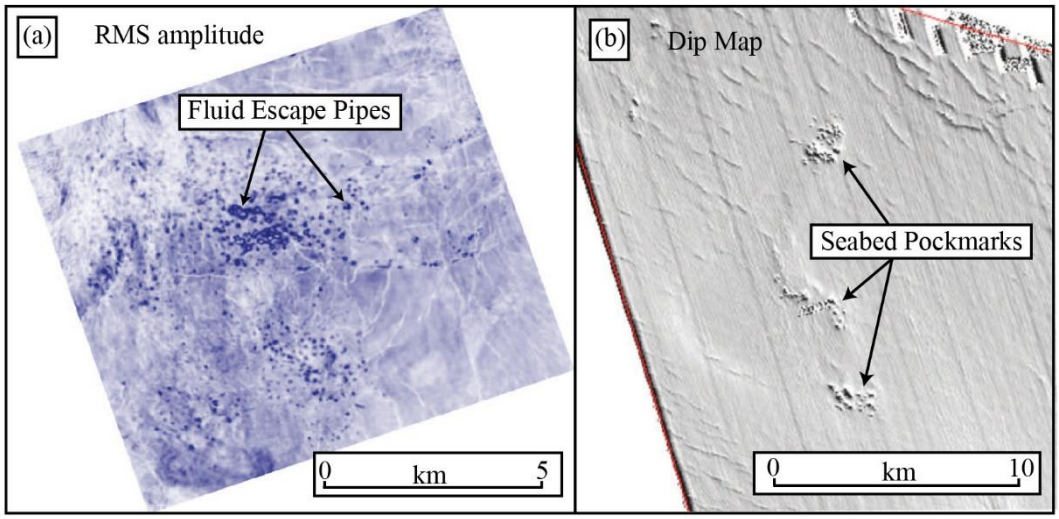

***Figure 5**: (a) RMS amplitude extracted from a 100ms interval from a Miocene succession in the Lower Congo Basin, Offshore Angola. Fluid escape pipes are imaged as having higher RMS amplitudes that the surrounding stratigraphy. (b) Map of dip attribute extracted along the seafloor in*

the Lower Congo Basin, offshore Angola. The dip attributes highlights seafloor pockmarks. (Figures modified from (Andresen et al., 2011))

A limitation of using single seismic attributes in detecting focused fluid flows is that the attributes are susceptible to highlighting structural or stratigraphic features that share similar morphologies (Marfurt & Alves, 2015). This could result in false identification or even a masking of focused fluid flows on seismic attribute maps by other features. For instance, faults, when fully resolved, are imaged on seismic data as discrete breaks in reflector coherence. The affected reflectors exhibit a relative two-way time shift either side of the (intersection trace of the) fault plane that implies a constant or steadily varying displacement along it. The discontinuity of seismic reflectors across faults can be identified by variance-type attributes (Meldahl et al., 2001; Marfurt & Alves, 2015). Similarly, fault shadow zones are sections of seismic data on the footwall of a fault that has distorted visualization due to lateral velocity gradients across the fault zone (Trinchero, 2000). These zones can appear as vertical zones of incoherent or distorted seismic reflectors, similar to the seismic expression of fluid escape pipes, and thus they can potentially be misinterpreted on a 'variance' or 'incoherence' attribute map (Marfurt & Alves, 2015).

To overcome the limitations in utilizing single attribute analysis to identify fluid escape features on seismic data, Heggland & Meldahl (1999) and Meldahl et al. (2001) introduced the 'chimney cube', a unique interpretation method that can be used to distinctly identify focused fluid flows (Fig. 6). This method relies on the interpreter recognizing seismic characteristics of targeted focused fluid flow features and making intelligent selections of seismic attributes that are able to increase their contrast or detectability (Meldahl & Heggland, 1999). The 'chimney cube' utilizes an iterative process that simultaneously analyses selected seismic attributes to generate a new attribute that is optimized for identifying focused fluid flow features. Since its inception, the 'chimney cube' has been successfully utilized in various regions to enhance imaging of focused fluid flows which have then been used to research subsurface fluid dynamics as well as evaluate hydrocarbon prospectivity (Tingdahl et al., 2001; Nourollah et al., 2010; Oyeyemi et al., 2017). For instance, the chimney cube methodology was utilized to identify potential hydrocarbon leakage along the top of two hydrocarbon reservoirs in the Gulf of Mexico (Heggland, 2005). The resulting chimney cube identified chimneys that overlie the hydrocarbon reservoir. The bases of these chimneys are associated with faults that are present along the top of the hydrocarbon reservoirs. The presence of chimneys overlying faults led to identification of non-sealing faults over the hydrocarbon reservoir, which reduced the potential for hydrocarbon accumulation within the reservoirs.

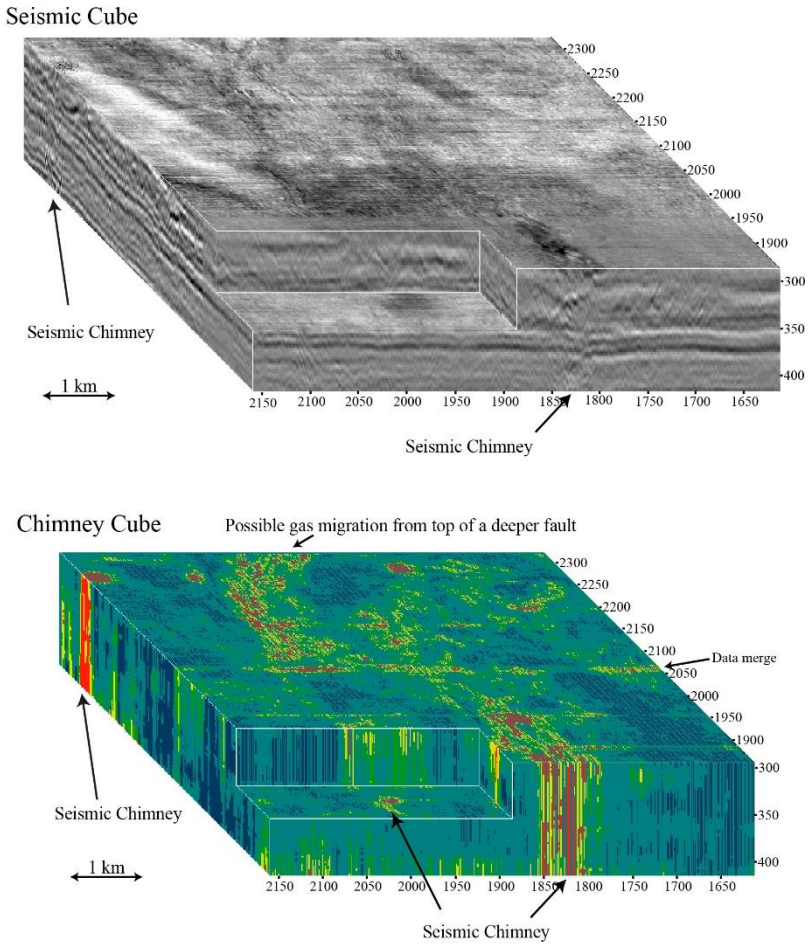

***Figure 6**: Chimney cube identifying focused fluid flow features that are not discernible on reflection amplitude cubes. (Modified from Meldahl & Heggland (1999)).*

5. Processes Responsible for Focused Fluid Flow Formation

Fluids in the subsurface commonly migrate through two mechanisms, diffusion and/or Darcy flow (Wang et al., 2010). Fluid migration through diffusion pertains to the redistribution of individual fluid molecules through random thermal motion that occurs in response to a difference in pore-fluid constituent concentrations (i.e. a concentration gradient) (Krooss & Leythaeuser, 1996). The rate of molecule diffusion is related to the magnitude of the concentration gradient (Krooss & Leythaeuser, 1996). Fluid migration through diffusion does not result in the formation of focused fluid flow features as it describes the chemical flux of fluid molecules that is independent from the flow of pore fluids (Berndt, 2005). Darcy flow, however, pertains to the volume flow of fluids through pore networks (Berndt, 2005). Fluid flow through this mechanism occurs in response to a hydraulic potential difference, or a difference in fluid pressure, and the rate of fluid migration is dependent on the pressure gradient magnitude, distance of migration and host rock permeability (Bjørlykke, 1999). In contrast with diffusion, fluid migration through Darcy flow can result in the formation of fluid

escape features as it pertains to the bulk transport of fluids across a pressure gradient (Berndt, 2005). As such focused fluid flows are seen as a key venting mechanism for sedimentary rocks that have pore fluid pressures that are higher than that of the hydrostatic gradient at a specified depth, otherwise known as overpressured sedimentary rocks (Osborne & Swarbrick, 1997). Understanding the source of overpressures or pressure gradient generation can thus provide insight into subsurface fluid dynamics that result in the formation of fluid escape features (Berndt, 2005; Cartwright et al., 2007; Løseth et al., 2011). The two most commonly cited sources of overpressure generation associated with focused fluid flows are disequilibrium compaction and fluid expansion (Law & Spencer, 1998; Ruth et al., 2004).

5.1. Disequilibrium compaction

Overpressure generation from disequilibrium compaction occurs when pore fluids in sedimentary rocks are not expelled at rapid enough rates in response to burial or sediment loading. The increase in overburden pressure would then result in a build-up of pore fluid pressure (Osborne & Swarbrick, 1997). The vertical load on a sedimentary rock at a given depth can be expressed as:

$$P = z*\rho*g$$

where P is the overburden stress, z is the thickness of the overburden, ρ is the average overburden density, and g is the gravitational constant (Osborne & Swarbrick, 1997). At a given depth, the overburden stress (P) is borne by both the rock matrix and pore fluids, as defined by Terzhagi's equation:

$$\sigma = P - P_f$$

where σ is the overburden stress borne by the rock matrix (referred to as effective stress), and P_f is the pore fluid pressure (Ruth et al., 2004). As sediments are compacted under conditions of slow burial, the overburden stress (P) increases steadily and there is a reduction of pore space which results in steady expulsion of fluids (Osborne & Swarbrick, 1997; Swarbrick & Osborne, 1998). Sandstones can compact from 39-49% porosity at deposition to 15-25% porosity at 2-3 km depth, while shales can have porosities between 65-80% at deposition that compact to 5-10% at 4-6 km depths (Osborne & Swarbrick, 1997). As long as the fluids within the pore spaces of a rock are under hydrostatic conditions, they can be expelled from the rock matrix during burial and compaction, resulting in the rock experiencing an increase in effective stress that is proportional to the increase in overburden pressure (Osborne & Swarbrick, 1997; Swarbrick & Osborne, 1998).

When sediments are rapidly buried such that fluid cannot evacuate pores uninhibited, these fluids become 'trapped' within the pore spaces, causing pore compaction to cease and resulting in the pore fluids being forced to bear the increased overburden load exerted by the encasing matrix (Swarbrick

& Osborne, 1998; Ruth et al., 2004). As burial progresses, increasing lithostatic overburden stress is borne equally by the rock matrix and pore fluid, so the pore fluid pressure trajectory now runs parallel to the lithostatic pressure trend (Swarbrick & Osborne, 1998). This results in higher than normal pore fluid pressure ("overpressure") within this sedimentary rock compartment relative to others at similar depths that underwent slower burial and orderly fluid expulsion ("hydrostatic") (Fig. 7) (Ruth et al., 2004).

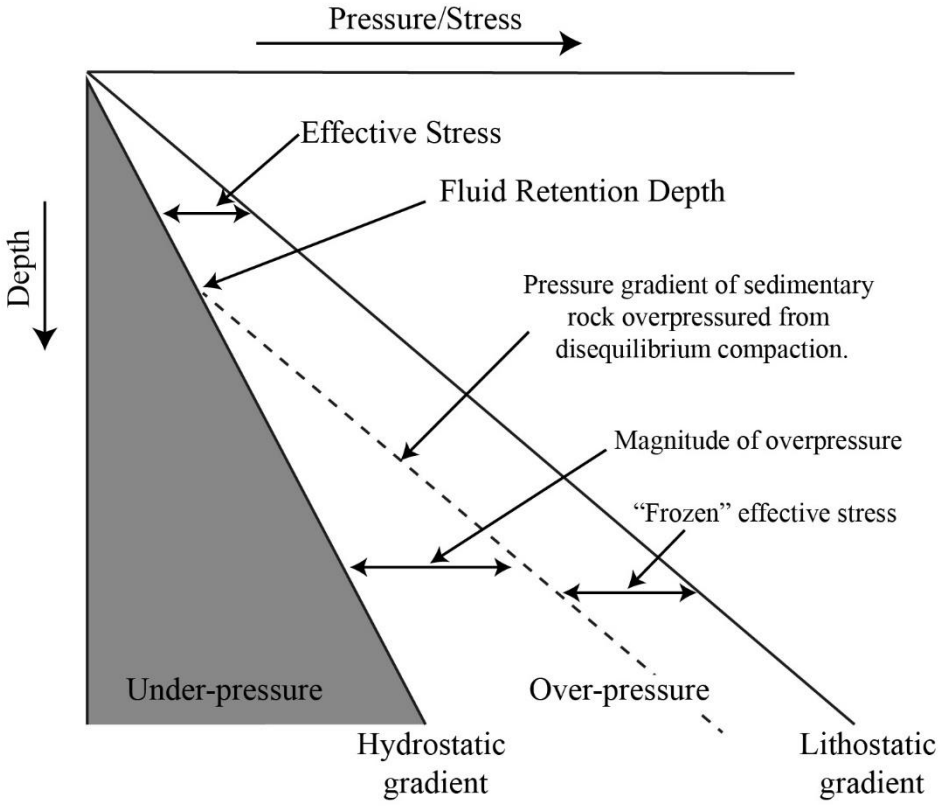

***Figure 7**: Pressure and/or stress against depth plot for overpressure generated by disequilibrium compaction. Modified from Swarbrick & Osborne (1998).*

While the overpressure generated in this manner cannot exceed the total overburden stress, it is possible for the fluid pressure to exceed the overburden fracture pressure, which would result in hydraulic fracturing, that could then lead to fluid expulsion (Osborne & Swarbrick, 1997). Hydraulic fracturing in such a manner can be catalysed by processes or mechanisms that reduce overburden stress (i.e. reduce effective stress, σ) such as tectonic faulting, sediment slumping or even glacial scouring (Pilcher & Argent, 2007).

Disequilibrium compaction is commonly documented in regions that experience rapid sedimentation, particularly with sediments that have low permeability. As such, this mechanism of overpressure generation is most likely to occur in mud or shale successions that were rapidly deposited in sedimentary basins (Swarbrick & Osborne, 1998). Approximately 400 pockmarks have been

identified on the seafloor of the Nyegga region of the Vøring Plateau, offshore Norway (Hustoft et al., 2009). The pockmarks are associated with underlying fluid escape pipes that emanate from gas-charged sediments approximately 300 – 350 meters below the seafloor. The emergence of fluid escape pipes from the same fluid source layer and the apparent development of hundreds of pockmarks more or less simultaneously, are observations that have led to the interpretation of an external mechanism that triggered focused fluid flow (Hustoft et al., 2009). Sedimentation-fluid flow modelling revealed that rapid sediment loading during the late Pleistocene (increasing from 0.5 to 35 m/ka) resulted in a rapid increase in pore pressure of the aforementioned gas charged sediments (increasing from 10 up to 400 kPa) (Hustoft et al., 2009). The development of this overpressure from disequilibrium compaction is interpreted to have resulted in the formation of the fluid escape pipes and pockmarks in the Nyegga area of the Vøring Plateau.

5.2. Fluid expansion/addition at depth

Subsurface overpressure can also be generated through the expansion or addition of fluids into pore spaces at depth. This pressure can be dissipated by fluid migration away from the area of pressure build-up; however, sedimentary rocks with low permeability, such as shales or mudstones, can impede fluid expulsion and can result in generation of overpressure (Osborne & Swarbrick, 1997).

Hydrocarbon generation is an important mechanism that can result in the addition or volumetric expansion of fluids in the subsurface. As kerogens are broken down into hydrocarbons and its by-products, they are accompanied by an expansion in volume (Fig. 8). The amount of expansion can vary depending on the ratio of solid to fluid volumetric change, which in turn, is affected by temperature and source rock parameters such as total organic content, type of hydrocarbon generated or organic matter thickness (Osborne & Swarbrick, 1997; Okiongbo, 2014). Meissner (1978) estimated that a volume expansion of up to 25% from hydrocarbon generation within the Bakken Shale of North Dakota in the United States of America, while modelling studies by Ungerer et al. (1983) indicated a volume decrease between 3-6% from kerogen maturation of Toarcian Black Shale samples that have between 0.65 to 1.3% vitrinite reflectance (Fig 8).

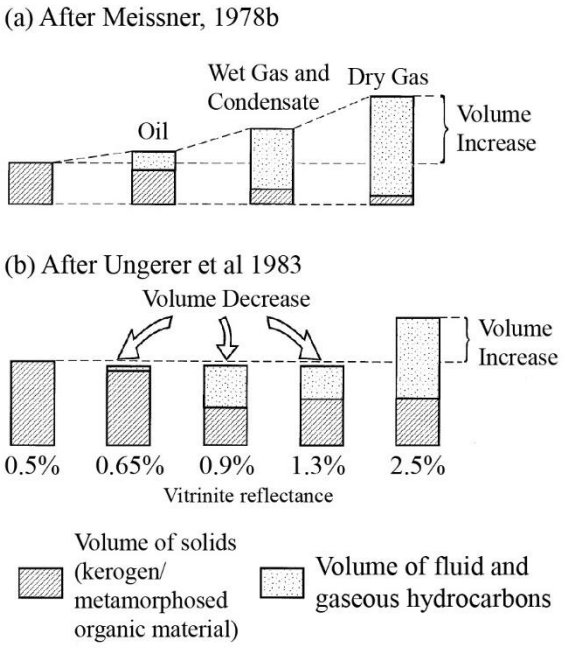

***Figure 8**: (a) Estimation of volume change when kerogen in Bakken Shale, United States of America mature to form hydrocarbons. (b) Estimation of volume change when kerogen in Toarcian Black Shale, France mature to form hydrocarbons. (Modified from Swarbrick & Osborne (1998))*

Mineral diagenesis or dehydration processes can also lead to the addition of fluids at depth. Processes such as the transformation of smectite to illite, or opal-A to opal-CT can result in the release or expulsion of fluids (Osborne & Swarbrick, 1997; Swarbrick & Osborne, 1998). Opal-A minerals can contain up to 15% weight in water, which would be expelled when the mineral undergoes dissolution and re-precipitates as Opal-CT and quartz (Hurd & Theyer, 1977; Jones & Renaut, 2004). Smectite clays are another such mineral grouping that dehydrates through diagenesis to form illite clays (Osborne & Swarbrick, 1997). Bruce (1984) estimated that the dehydration from smectite to illite transformation could increase the pore fluid volume by 6.6%. This increase in volume could be compensated for by an equal volume of compaction in the smectite clay particles; however, if clay particle compaction does not occur, the fluid volume increase could lead to overpressure generation (Osborne & Swarbrick, 1997).

Fluid expansion mechanisms are also associated with hydrothermal effects that can be caused by igneous intrusions. Fluids can be derived from the devolatilization of magma as well as from interactions between igneous intrusions and pore fluids in the host rock sequence (Cartwright et al., 2007). Localized heating or heat transfer from intrusions can superheat pore fluids, resulting in thermal expansion of fluids that can then lead to pore fluid pressure build up (Jamtveit et al., 2004). In a similar manner, igneous intrusions within source rock units have been documented to catalyse hydrocarbon generation in organic matter. The fluid volume increase from hydrocarbon generation

and expulsion could similarly result in generation of overpressure (Othman et al., 2001). Even in the absence of organic matter for hydrocarbon generation, heat transfer from igneous intrusions is able to catalyse diagenetic processes such as smectite to illite or Opal-A to Opal-CT transformations, resulting in the addition of free fluids into pore space (Cartwright et al., 2007; Aarnes et al., 2011).

5.3. Lesser documented mechanisms for focused fluid flow formation

Disequilibrium compaction and fluid expansion/addition are the most commonly cited overpressure generation mechanisms that result in focused fluid flows. To lesser extents however, focused fluid flows have also been associated with the presence of gas hydrates.

Natural gas hydrates are physical compounds that consist of water molecules forming cage-like lattice structures around natural gas molecules, commonly methane (Kvenvolden, 1993). They form in the shallow geosphere, at depths ranging between 150 to 2,000 m, and in regions of low surface temperature (~0 °C). As a result, they are often documented in polar or deep sea regions. The base of the a gas hydrate layer represents a phase boundary below which solid gas hydrates break down into gas and water (Petersen et al., 2010). These phase boundaries are often documented on seismic cross-sections as bottom simulating reflectors (BSRs). BSRs are seismic reflectors that occur within depths of several hundred meters below the surface that characteristically cross-cut seismic stratigraphy and run parallel to the sea-floor (Hyndman & Spence, 1992; Berndt et al., 2004).

Seafloor pockmarks have been documented in regions with underlying bottom-simulating reflectors (BSRs). When natural gas from the subsurface migrates to shallower depths with temperatures conducive for forming gas hydrates, they crystalize and fill up the pore space of the sedimentary rocks, effectively reducing rock permeability (Cathles et al., 2010). As natural gas migration continues, it becomes trapped at the base of the hydrate stability zone due the reduced permeability. The increasing volume of trapped natural gas can result in a pressure build up that can eventually induce hydraulic fracturing in the overlying hydrate saturated rocks and form focused fluid flow features (Fig 9) (Cathles et al., 2010; Sun et al., 2012). Examples of focused fluid flow features associated with gas hydrates can be seen in offshore China and the North Sea (Judd & Hovland, 2007).

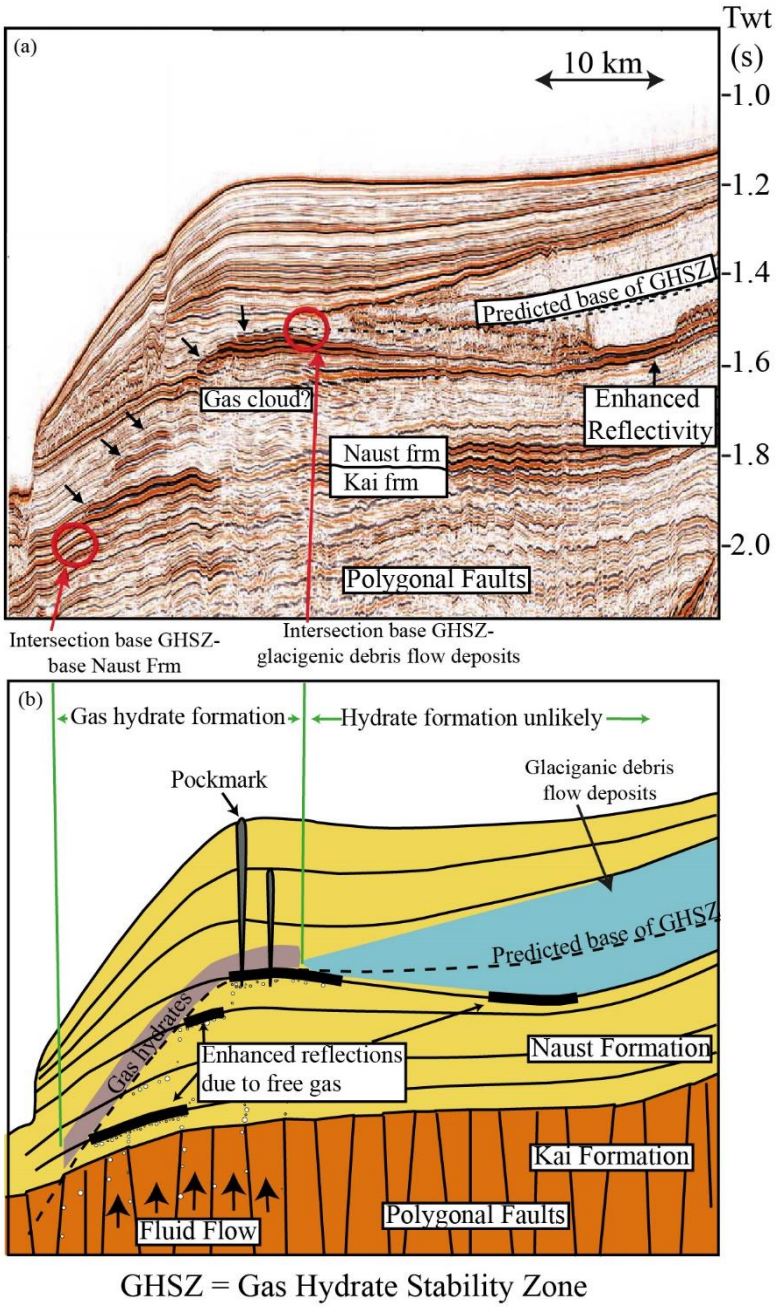

***Figure 9**: Focused fluid flow features associated with free gas accumulation below the gas hydrates in the mid-Norwegian margin. (Modified from (Bünz et al., 2003))*

6. Spatial Distribution and Geometric Arrangement of Focused Fluid Flows

Focused fluid flow features including pipes and pockmarks commonly occur with random spatial distributions i.e. they have no discernible geometric trend in their formation along a surface (Pilcher & Argent, 2007). The spatial density of randomly occurring focused fluid flow features can range from singular formations to clusters of fluid escape features (Fig. 2, 10). They have been documented to occur in spatial densities of up to 1000 per km^2 in the Chirikov Basin offshore Alaska (Gay et al., 2006b; Judd & Hovland, 2007).

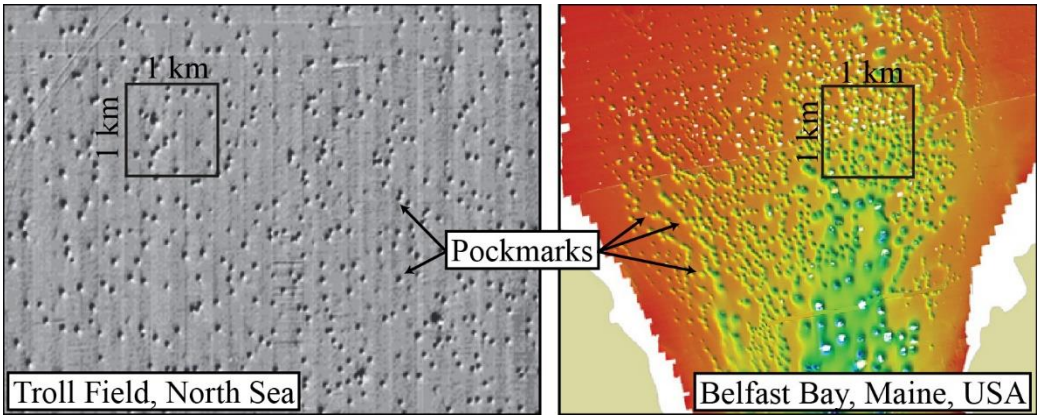

***Figure 10**: Imaged pockmarks from (a) the North Sea (Hovland, 2012) and (b) Belfast Bay (Brothers et al., 2012), United States of America. The figures show randomly distributed pockmarks with varying spatial densities across different regions.*

Structural and stratigraphic geological features such as faults, igneous intrusions or unconformity surfaces are able to act as permeable conduits for fluid migration, and thus influence fluid migration pathways. The spatial distribution of resulting focused fluid flow features should thus be influenced by the geological features that underlie them, resulting in a non-random (organised) spatial distribution (Fig 11) (Pilcher & Argent, 2007).

Faults are commonly cited structures associated with focused fluid flow features that have organized spatial distributions. They play a critical role in subsurface fluid dynamics by acting as permeable pathways for fluid migration (Cartwright et al., 2007; Pilcher & Argent, 2007). Focused fluid flow features that form to overlie upper tips of faults can result in linear spatial trends that are parallel to fault strike (Gay et al., 2007; Pilcher & Argent, 2007). Examples of such occurrences have been documented in the St. Lawrence Estuary, offshore Canada and the Eel River Basin of California, United States of America (Syvitski & Praeg, 1989; Judd & Hovland, 2007). A lesser documented relation between faults and focused fluid flow features is one where focused fluid flows develop parallel to, but laterally offset from, the upper tips of faults. In these scenarios, faults are likely to have intersected a fluid source. At the location of intersection, the fault locally reduces overburden stress, which then induces hydraulic fracturing that results in the vertical migration of fluids. This unconventional interaction between faults and fluid accumulations has been documented in the Lower Congo Basin (Maia et al., 2016).

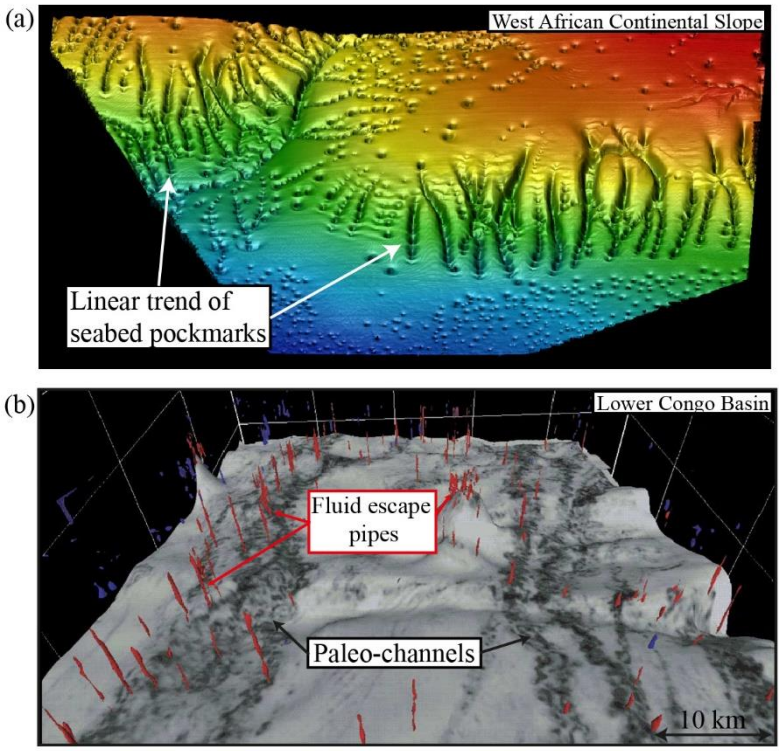

Figure 11: Organized spatial distribution of fluid flow features. (a) Linear trends of seabed pockmarks offshore Equitorial Guinea (Pilcher & Argent, 2007). (b) Sinuous belt trends of subsurface fluid escape pipes in the Lower Congo Basin (Gay et al., 2006b).

Alongside structural controls, stratigraphic features are similarly able to influence fluid migration pathways to result in organized, non-linear spatial distributions of focused fluid flow features. Stratigraphically controlled fluid migration pathways are likely to result in focused fluid flow features with spatial distributions that mirror the shape of the underlying stratigraphic feature. Sinuous trends of focused fluid flow features have been identified to correlate to the pattern or morphology of underlying submarine channels (Fig 11b) (Haskell et al., 1999; Gay et al., 2006a; Gay et al., 2007). Relative to the surrounding low permeability finer grained sediments, the coarse grained sediments of buried channel courses become preferred fluid migration pathways and reservoirs. The concentration of fluids migrating into these subsurface stratigraphic features could result in overpressure generation that is vented via focused fluid flow events (Haskell et al., 1999). In a contrasting manner, igneous intrusions are able to influence fluid migration pathways through stratigraphy by having less permeability relative to the surrounding host rock. Focused fluid flow features most commonly form along the edge of or at ridge-like junctions within sill intrusions (Davies et al., 2002; Svensen et al., 2004; Cartwright et al., 2007). As such, in igneous provinces, the lateral extent of focused fluid flow features could be a proxy indicator for the lateral extent of an underlying sill intrusions.

The interpretation of structural or stratigraphic geological features associated with focused fluid flow features can provide qualitative analysis supporting the spatial distribution of focused fluid flow

features. Utilization of spatial statistics methods, however, are able to quantify organized spatial distributions (e.g. trends) of focused fluid flows independent of associated geological features (Moss & Cartwright, 2010b; Moss et al., 2012a). Spatial and directional statistics methods have primarily been utilized in computing and mathematical fields. However, they have also been utilized in biological and geological fields to identify directional trends (Mardia & Jupp, 2000; Hammer, 2009; Moss & Cartwright, 2010b; Moss et al., 2012a; Maia et al., 2016). Spatial statistics methods, such as point alignment or nearest neighbours, predominantly utilize lateral distance measurements between fluid escape features to identify linear trends based on shortest distances and azimuthal alignments (Moss & Cartwright, 2010b; Moss et al., 2012a). Advanced spatial statistics methods, such as Voronoi polygons, divide the surface area along which fluid escape features are documented into polygons whereby each polygon contains only one fluid escape feature and any point within the polygon is of closer proximity to its associated fluid escape feature relative to fluid escape features of neighbouring polygons (Moss et al., 2012a). Quantifying spatial distributions of focused fluid flow features can be utilized to identify spatial correlations between focused fluid flows and underlying geological features. In the Lower Congo Basin offshore Angola, Maia et al. (2016) identified 3410 pockmarks along the seafloor that are underlain by polarized polygonal faults. Point alignment analysis of the pockmarks revealed that the pockmarks occur in alignments that are parallel to the underlying polarized polygonal faults. Furthermore, higher order spatial statistics revealed that the pockmarks appear to be anti-clustered over short distances (<200 m) from nearest neighbouring pockmarks. This suggests that each pockmark has an exclusion zone of ~200 m within which other pockmarks will not form (Maia et al., 2016). These results, along with the observation that the fluid escape features occur in hanging wall blocks, suggest that while the spatial distribution of pockmarks is controlled by the polarized polygonal faults, pockmark formation is not linked to the polygonal fault system. Instead, the pockmarks are interpreted to have formed as a result of gas hydrate dissociation linked to sea level changes (Maia et al., 2016). Once dissociation has occurred, gas escapes and excess pore pressure is relieved. Thus there is no driver for further dissociation to occur locally.

7. Compiled References

AARNES, I., SVENSEN, H., POLTEAU, S. & PLANKE, S., 2011, Contact metamorphic devolatilization of shales in the Karoo Basin, South Africa, and the effects of multiple sill intrusions, Chemical Geology, 281, 181-194.

ANDRESEN, K.J., HUUSE, M. & CLAUSEN, O.R., 2008, Morphology and distribution of Oligocene and Miocene pockmarks in the Danish North Sea : Implications for bottom current activity and fluid migration, Basin Research, 20, 445-466.

ANDRESEN, K.J. & HUUSE, M., 2011, 'Bulls-eye' pockmarks and polygonal faulting in the Lower Congo Basin: Relative timing and implications for fluid expulsion during shallow burial, Marine Geology, 279, 111-127.

ANDRESEN, K.J., HUUSE, M., SCHODT, N.H., CLAUSEN, L.F. & SEIDLER, L., 2011, Hydrocarbon plumbing systems of salt minibasins offshore Angola revealed by three-dimensional seismic analysis, American Association of Petroleum Geologists Bulletin, 95, 1039-1065.

ANDRESEN, K.J., 2012, Fluid flow features in hydrocarbon plumbing systems: What do they tell us about the basin evolution?, Marine Geology, 332-334, 89-108.

ANKA, Z., BERNDT, C. & GAY, A., 2012, Hydrocarbon leakage through focussed fluid flow systems in continental margins, Marine Geology, 1-3, 332-334.

BALL, A., BILLING, J., MCCLUSKEY, C., PHAM, P., PITTMAN, O., LAWSON, S., AHMAD, S., STARR, A., ROUSSEAU, J. & LAMBERT, N., 2018, Australian Energy Update, Commonwealth of Australia 2018, 39pp.

BECHTEL, T.D., BOSCH, F.P. & GURK, M., 2007, Geophysical Methods, In: Goldscheider, N. & Drew, D. (eds) Methods in karst hydrogeology. Taylor and Francis/Balkema, Netherlands, 26, 185-214.

BERNDT, C., BÜNZ, S., CLAYTON, T., MIENERT, J. & SAUNDERS, M., 2004, Seismic character of bottom simulating reflectors: examples from the mid-Norwegian margin, Marine and Petroleum Geology, 21, 723-733.

BERNDT, C., 2005, Focused Fluid Flow in Passive Continental Margins, Philosophical Transactions: Mathematical, Physical, and Engineering Sciences, 363, 2855-2871.

BJØRLYKKE, K., 1999, Principal aspects of compaction and fluid flow in mudstones, In: Aplin, A.C., Fleet, A.J. & Macquaker, J.H.S. (eds) Muds and Mudstones: Physical and Fluid Flow Properties. Geological Society of London, London, 158, 73-78.

BLEVIN, J.E. (Compiler), BOREHAM, C.J., TRIGG, K.R., CUMMINGS, A., DANIEL, R., KALDI, J., LANG, S., LEMON, N., ROOT, R., TINGATE, P. & PARTRIDGE, A.D.,2003, Petroleum Geology of the Bass Basin - Interpretation Report, An Output of the Western Tasmanian Regional Minerals Program. Geoscience Australia, Record 2013/19, 684pp.

BLOOD, M.F., 2001, Exploration for a Frontier Salt basin in Southwest Oman, GeoArabia, 6, 159-176.

BROTHERS, L.L., KELLY, J.T., BELKNAP, D.F., BARNHARDT, W.A., ANDREWS, B.D., LEGERE, C. & CLARKE, J.E.H., 2012, Shallow stratigraphic control on pockmark distribution in north temperate estuaries, Marine Geology, 329-331, 34-45.

BRUCE, C.H., 1984, Smectite Dehydration-Its Relation to Structural Development and Hydrocarbon Accumulation in Northern Gulf of Mexico Basin, AAPG Bulletin, 68, 673-683.

BULL, J.M., BERNDT, C., MINSHULL, T.A., HENSTOCK, T.J., BAYRAKCI, G., GEHRMANN, R., PROVENZANO, G., BÖTTNER, C., SCHRAMM, B., CALLOW, B., CHAPMAN, M., BIRINCI, H., YILO, N., DEWAR, M., CHEN, B., SALEEM, U., MARIN-MORENO, H., LICHTSCHLAG, A., FALCON-SUAREZ, I., ROCHE, B., JAMES, R., CONNELLY, D.P., MATTER, J., ELGER, J., KARSTENS, J. & BEST, A.I., 2018, Constraining the physical properties of chimney/pipe structures within sedimentary basins, 14th International Conference on Greenhouse Gas Control Technologies, GHGT-14, Melbourne, Australia.

BÜNZ, S., MIENERT, J. & BERNDT, C., 2003, Geological controls on the Storegga gas-hydrate system of the mid-Norwegian continental margin, Earth and Planetary Science Letters, 209, 291-307.

CAMBON-BONAVITA, M.A., NADALIG, T., ROUSSEL, E., DELAGE, E., DUPERRON, S., CAPRAIS, J.C., BOETIUS, A. & SIBUET, M., 2009, Diversity and distribution of methane-oxidizing microbial communities associated with different faunal assemblages in a giant pockmark of the Gabon continental margin, Deep-Sea Research II, 56, 2248-2258.

CARTWRIGHT, J. & HUUSE, M., 2005, 3D seismic technology: the geological 'Hubble', Basin Research, 17, 1-20.

CARTWRIGHT, J., HUUSE, M. & APLIN, A., 2007, Seal bypass systems, American Association of Petroleum Geologists Bulletin, 91, 1141-1166.

CARTWRIGHT, J. & SANTAMARINA, C., 2015, Seismic characteristics of fluid escape pipes in sedimentary basins: Implications for pipe genesis, Marine and Petroleum Geology, 65, 126-140.

CATHLES, L.M., SU, Z. & CHEN, D., 2010, The physics of gas chimney and pockmark formation, with implications for assessment of seafloor hazards and gas sequestration, Marine and Petroleum Geology, 27, 82-91.

CHRISTOPHERSON, K.R., 1991, Applications of magnetotellurics to petroleum exploration in Papua New Guinea: A model for frontier areas, The Leading Edge, 10, 21-27.

ÇIFÇI, G., DONDURUR, D. & ERGÜN, M., 2003, Deep and shallow structures of large pockmarks in the Turkish shelf, Eastern Black Sea, Geo-Marine Letters, 23, 311-322.

CUMMINGS, A.M., HILLIS, R.R. & TINGATE, P.R., 2004, New perspectives on the structural evolution of the Bass Basin: Implications for petroleum prospectivity, in: Boult, P.J., Johns, D.R., Lang, S.C. (Eds.), Eastern Australian Basins Symposium II, Petroleum Exploration Society of Australia, Adelaide, Australia, 133-149.

DAVIES, R., BELL, B.R., CARTWRIGHT, J.A. & SHOULDERS, S., 2002, Three-dimensional seismic imgagin of Paleogene dike-fed submarine volcanoes from the northeast Atlantic margin, Geology, 3, 223-226.

DEMAISON, G. & HUIZINGA, B.J., 1991, Genetic Classification of Petroleum Systems, AAPG Bulletin, 75, 1626-1643.

DIRSTEIN, J.K., HENGESH, J.V. & STANLEY, A.J., 2013, Identification of Fluid Flow Features in the Seafloor and Subsurface and their Implications for Prospect and Geohazard Assessment: Examples from the Australian Northwest Shelf, West Australian Basins Symposium 2013. Petroleum Exploration Society of Australia, Perth, WA, 1-21.

ENGLAND, W.A., 1994, Secondary Migraiton oand Accumulation of Hydrocarbons, In: Magoon, L.B. & Dow, W.G. (eds) The Petroleum System-From Source to Trap. AAPG, 60, 211-217.

GAY, A., LOPEZ, M., COCHONAT, P., SULTAN, N., CAUQUIL, E. & BRIGAUD, F., 2003, Sinuous pockmark belt as indicator of a shallow buried turbiditic channel on the lower slope of the Congo Basin, West African Margin, In: Rensenbergen, P.V., Hillis, R.R., Maltman, A.J. & Morley, C.K. (eds) Special Publication. Geological Society, London, 216, 173-189.

GAY, A., LOPEZ, M., COCHONAT, P., LEVACHE´, D., SERMONDAAZ, G. & SÈRANNE, M., 2006a, Evidences of early to late fluid migration from an upper Miocene turbiditic channel revealed by 3D seismic coupled to geochemical sampling within seafloor pockmarks, Lower Congo Basin, Marine and Petroleum Geology, 23, 387-399.

GAY, A., LOPEZ, M., COCHONAT, P., SÈRANNE, M., LEVACHÈ, D. & SERMONDADAZ, G., 2006b, Isolated seafloor pockmarks linked to BSRs, fluid chimneys, polygonal faults and stacked

Oligocene–Miocene turbiditic palaeochannels in the Lower Congo Basin, Marine Geology, 226, 25-40.

GAY, A., LOPEZ, M., ONDREAS, H., SERMONDADAZ, J.L.C. & COCHONAT, P., 2006c, Seafloor facies related to upward methane flux within a Giant Pockmark of the Lower Congo Basin, Marine Geology, 226, 81-95.

GAY, A., LOPEZ, M., BERNDT, C. & SERANNE, M., 2007, Geological controls on focused fluid flow associated with seafloor seeps in the Lower Congo Basin, Marine Geology, 244, 68-92.

HALL, P.A., MCKIRDY, D.M., GRICE, K. & EDWARDS, D.S., 2014, Australasian asphaltite strandings: Their origin reviewed in light of the effects of weathering and biodegradation on their biomarker and isotopic profiles, Marine and Petroleum Geology, 57, 572-593.

HAMMER, Ø., 2009, New statistical methods for detecting point alignments, Computers and Geosciences, 35, 659-666.

HARTWIG, A., ANKA, Z. & PRIMIO, R.D., 2012, Evidence of a widespread paleo-pockmarked field in the Orange Basin: An indication of an early Eocene massive fluid escape event offshore South Africa, Marine Geology, 332-334, 222-234.

HASKELL, N., NISSEN, S., HUGHES, M., GRINDHAUG, J., DHANANI, S., HEATH, R., KANTOROWICZ, J., ANTRIM, L., CUBANSKI, M., NATARAJ, R., SCHILLY, M. & WIGGER, S., 1999, Delineation of geologic drilling hazards using 3-D seismic attributes, The Leading Edge, 18, 373-382.

HEGGLAND, R., 1998, Gas seepage as an indicator of deper prospective reservoirs. A study based on exploration 3D seismic data, Marine and Petroleum Geology, 15, 1-9.

HEGGLAND, R. & MELDAHL, P., 1999, The chimney cube, an example of semi-automated detection of seismic objects by directive attributes and neural networks: Part II; interpretation, SEG Technical Program Expanded Abstracts, 935-940.

HEGGLAND, R., 2005, Using Gas Chimneys in Seal Integrity Analysis: A Discussion Based on Case Histories, In: Boult, P. & Kaldi, J. (eds) Evaluating fault and cap rock seals: AAPG Hedberg Series. American Association of Petroleum Geologists, 2, 237-245.

HOLFORD, S., SCHOFIELD, N., MACDONALD, J.D., DUDDY, I.R. & GREEN, P.F., 2012, Seismic analysis of igneous systems in sedimentary basins and their impacts on hydrocarbon prospectivity: Examples from the soutern Australian Margin, The APPEA Journal 52, 229-252.

HOVLAND, M. & JUDD, A.G.,1988, Seabed Pockmarks and Seepages : Impact on Geology, Biology and the Marine Environment. Graham and Trotman, London, 293 pp.

HOVLAND, M., GARDNER, J.V. & JUDD, A.G., 2002, The significance of pockmarks to understanding fluid flow processes and geohazards, Geofluids, 2, 127-136.

HOVLAND, M., 2012, The Geomorphology and Nature of Seabed Seepage Processes, In: Blondel, P. (ed) Bathymetry and Its Applications. United Kingdoms, 79-104.

HURD, D.C. & THEYER, F., 1977, Changes in the Physical and Chemical Properties of Biogenic Silica from the Central Equatorial Pacific: Part II. Refractive Index, Density and Water Content of Acid Cleaned Samples, American Journal of Science, 277, 1168-1202.

HUSTOFT, S., DUGAN, B. & MIENERT, J., 2009, Effects of rapid sedimentation on developing the Nyegga pockmark field: Constraints from hydrological modeling and 3-D seismic data, offshore mid-Norway, Geochemistry, Geophysics, Geosystems, 10, 17 pp.

HUUSE, M., JACKSON, C.A., RENSBERGEN, P.V., DAVIES, R.J., FLEMINGS, P.B. & DIXON, R.J., 2010, Subsurface sediment remobilization and fluid flow in sedimentary basins: an overview, Basin Research, 22, 342-360.

HYNDMAN, R.D. & SPENCE, G.D., 1992, A seismic study of methane hydrate marine bottom simulating reflectors, Journal of Geophysical Research: Solid Earth, 97, 6683-6698.

JACKSON, C.A., SCHOFIELD, N. & GOLENKOV, B., 2013, Geometry and controls on the development of igneous sill–related forced folds: a 2-D seismic reflection case study from offshore southern Australia, GSA Bulletin, 125, 1874-1890.

JAMTVEIT, B., SVENSEN, H., PODLADCHIKOV, Y.Y. & PLANKE, S., 2004, Hydrothermal vent complexes associated with sill intrusions in sedimentary basins, In: Brietkreuz, C. & Petford, N. (eds) Physical Geology of High-Level Magmatic Systems. Geological Society, London Special Publications, London, 234, 233-241.

JONES, B. & RENAUT, R.W., 2004, Water Content of Opal-A: Implications for the Origin of t the Laminae in Geyserite and Sinter, Journal of Sedimentary Research, 74, 117-128.

JUDD, A.G., 2003, The global importance and context of methane escape from the seabed, Geo-Marine Letters, 23, 147-154.

JUDD, A. & HOVLAND, M.,2007, Seabed Fluid Flow: The Impact on Geology, Biology and the Marine Environment. Cambridge University Press, United Kingdom, 408 pp.

KADKO, D., BAROSS, J. & ALT, J., 1995, The Magnitude and Global Impact of Hydrothermal Flux, In: Humphris, S.E., Zierenberg, R.A., Mullineaux, L.S. & Thompson, R.E. (eds) Seafloor Hydrothermal Systems: Physical, Chemical, Biiological and Geological Interactions. American Geophysical Union, 91, 446-465.

KING, L.H. & MACLEAN, B., 1970, Pockmarks on the Scotian Shelf, Geological society of America Bulletin, 81, 3141-3148.

KROOSS, B.M. & LEYTHAEUSER, D., 1996, Molecular Diffusion of Light Hydrocarbons in Sedimentary Rocks and Its Role in Migration and Dissipation of Natural Gas, In: Schumacher, D. & Abrams, M.A. (eds) Hydrocarbon migration and its near-surface expression. AAPG, 66, 173-183.

KVENVOLDEN, K.A., 1993, Gas Hydrates - Geological Perspective and Global Change, Reviews of Geophysics, 31, 173-187.

LAW, B.E. & SPENCER, C.W., 1998, Abnormal Pressure in Hydrocarbon Environments, In: Ulmishek, G.F. & Slavin, V.I. (eds) Abnormal pressures in hydrocarbon environments: AAPG Memoir. American Association of Petroleum Geologists, 70, 1-11.

LEDUC, A.M., DAVIES, R.J., SWARBRICK, R.E. & IMBER, J., 2013, Fluid flow pipes triggered by lateral pressure transfer in the deepwater western Niger Delta, Marine and Petroleum Geology, 43, 423-433.

LINK, W.K., 1952, Significance of Oil and Gas Seeps in World Oil Exploration, Bulletin of American Association of Petroleum Geologists, 36, 1505-1540.

LOGAN, G., JONES, A., RYAN, G., WETTLE, M., THANKAPPAN, M., GROSJEAN, E., ROLLET, N. & KENNARD, J., 2008, Review of Australian Offshore Natural Hydrocarbon Seepage Studies, Geoscience Australia Record: 2008/17, 235 pp.

LOGAN, G.A., JONES, A.T., KENNARD, J.M., RYAN, G.J. & ROLLET, N., 2010, Australian offshore natural hydrocarbon seepage studies, a review and re-evaluation, Marine and Petroleum Geology, 27, 26-45.

LONGLEY, I.M., BRADSHAW, M.T. & HEBBERGER, J., 2001, Australian Petroleum Provinces of the Twenty-First Century, In: Downey, M.W., Threet, J.C. & Morgan, W.A. (eds) Petroleum provinces of the twenty-first century: AAPG Memoir 74, 287-317.

LONGLEY, I.M., BUESSENSCHUETT, C., CLYDSDALE, L., CUBITT, C.J., DAVIS, R.C., JOHNSON, M.K., MARSHALL, N.M., MURRAY, A.P., SOMERVILLE, R., SPRY, T.B. & THOMPSON, N.B., 2002, The North West Shelf of Australia - A Woodside Perspective, In: Keep, M. & Moss, S. (eds) The Sedimentary Basins of Western Australia 3: Proceedings of the Petroleum Exploration Society of Australia Symposium, Perth, Western Australia, 27-88.

LØSETH, H., GADING, M. & WENSAAS, L., 2009, Hydrocarbon leakage interpreted on seismic data, Marine and Petroleum Geology, 26, 1304-1319.

LØSETH, H., WENSAAS, L., ARNSTEN, B., HANKEN, N.-M., BASIRE, C. & GRAUE, K., 2011, 1000 m long gas blow-out pipes, Marine and Petroleum Geology, 28, 1047-1060.

MAGOON, L.B. & DOW, W.G., 1994, The petroleum system: chapter 1: Part 1. Introduction, In: Magoon, L.B. & Dow, W.G. (eds) The Petroleum System-From Source to Trap. AAPG, 60, 3-24.

MAGOON, L.B. & SCHMOKER, J.W., 2000, The Total Petroleum System-The Natural Fluid Network that Constrains the Assessment Unit, Chapter PS, In: US Geological Survey World Petroleum Assessment 2000 - Description and results: U.S. Geological Survey Digital Data Series DDS-60, version 1.0, CD-ROM, disk 1, 31 pp.

MAIA, A.R., CARTWRIGHT, J. & ANDERSEN, E., 2016, Shallow plumbing systems inferred from spatial analysis of pockmark arrays, Marine and Petroleum Geology, 77, 865-881.

MARDIA, K.V. & JUPP, P.E.,2000, Directional Statistics Vol. 494, John Wiley & Sons, 441 pp.

MARFURT, K.J., KIRLIN, R.L., FARMER, S.L. & BAHORICH, M.S., 1998, 3-D seismic attributes using a semblance-based coherency algorithm, Geophysics, 63, 1150-1165.

MARFURT, K.J. & ALVES, T.M., 2015, Pitfalls and limitations in seismic attribute interpretation of tectonic features, Interpretation, 3, SB5-SB15.

MAZZINI, A., SVENSEN, H.H., FORSBERG, C.F., LINGE, H., LAURITZEN, S.-E., HAFLIDASON, H., HAMMER, Ø., PLANKE, S. & TJELTA, T.I., 2017, A climatic trigger for the giant Troll pockmark field in the northern North Sea., Earth and Planetary Science Letters, 464, 24-34.

MEISSNER, F.F., 1978, Petroleum Geology of the Bakken formation Williston Basin, North Dakota and Montana, Montana Geological Society Guidebook: Economic Geology of the Williston Basin, 19-42.

MELDAHL, P. & HEGGLAND, R., 1999, The chimney cube, an example of semi-automated detection of seismic objects by directive attributes and neural networks: Part I; methodology, SEG Technical Program Expanded Abstracts, 931-934.

MELDAHL, P., HEGGLAND, R., BRIL, B. & GROOT, P.D., 2001, Identifying faults and gas chimneys using multiattributes and neural networks, The Leading Edge, 474-482.

MOSS, J.L. & CARTWRIGHT, J., 2010a, 3D seismic expression of km-scale fluid escape pipes from offshore Namibia, Basin Research, 22, 481-501.

MOSS, J.L. & CARTWRIGHT, J., 2010b, The spatial and temporal distribution of pipe formation, offshore Namibia, Marine and Petroleum Geology, 27, 1216-1234.

MOSS, J.L., CARTWRIGHT, J., CARTWRIGHT, A. & MOORE, R., 2012a, The spatial pattern and drainage cell characteristics of a pockmark field, Nile Deep Sea Fan, Marine and Petroleum Geology, 35, 321-336.

MOSS, J.L., CARTWRIGHT, J. & MOORE, R., 2012b, Evidence for fluid migration following pockmark formation: Examples from the Nile Deep Sea Fan, Marine Geology, 303-306, 1-13.

NAEHR, T.H., EICHHUBL, P., ORPHAN, V.J., MARTIN HOVLAND, PAULL, C.K., USSLER III, W., LORENSON, T.D. & GREENE, H.G., 2007, Authigenic carbonate formation at hydrocarbon seeps in continental margin sediments: A comparative study, Deep Sea Research Part II: Topical Studies in Oceanography, 54, 1268-1291.

NOUROLLAH, H., KEETLEY, J. & O'BRIEN, G., 2010, Gas Chimney identification through seismic attribute analysis in the Gippsland Basin, Australia, The Leading Edge, 29, 896-901.

O'BRIEN, G.W. & WOODS, E.P., 1995, Hydrocarbon-Related Diagenetic Zones (HRDZs) in the Vulcan Sub-basin, Timor Sea: Recognition and Exploration Implications, The APPEA Journal, 35(1), 220-252.

OKIONGBO, K.S., 2014, Volumetrics of Petroleum Generation: Implications for Expulsion and Overpressure, Petroleum Science and Technology, 32, 1257-1263.

OSBORNE, M.J. & SWARBRICK, R.E., 1997, Mechanisms for Generating Overpressure in Sedimentary Basins: A Reevaluation, AAPG Bulletin, 81, 1023-1041.

OTHMAN, R., AROURI, K.R., WARD, C.R. & MCKIRDY, D.M., 2001, Oil generation by igneous intrusions in the northern Gunnedah Basin, Australia, Organic Geochemistry, 32, 1219-1232.

OYEYEMI, K.D., OLOWOKERE, M.T. & AIZEBEOKHAI, A.P., 2017, Hydrocarbon resource evaluation using combined petrophysical analysis and seismically derived reservoir characterization, offshore Niger Delta, Journal of Petroleum Exploration and Production Technology, 8, 17 pp.

PETERSEN, C.J., BÜNZ, S., HUSTOFT, S., MIENERT, J. & KLAESCHEN, D., 2010, High-resolution P-Cable 3D seismic imaging of gas chimney structures in gas hydrated sediments of an Arctic sediment drift, Marine and Petroleum Geology, 27, 1981-1994.

PILCHER, R. & ARGENT, J., 2007, Mega-pockmarks and linear pockmark trains on the West African continental margin, Marine Geology, 244, 15-32.

PLANKE, S., RASMUSSEN, T., REY, S.S. & MYKLEBUST, R., 2005, Seismic characteristics and distribution of volcanic intrusions and hydrothermal vent complexes in the Vøring and Møre basins, In: Doré, A.G. & Vining, B.A. (eds) Petroleum Geology: North-West Europe and Global

Perspectives—Proceedings of the 6th Petroleum Geology Conference. Geological Society of London, London, 833-844.

REILLY, M.J. & FLEMINGS, P.B., 2010, Deep pore pressures and seafloor venting in the Auger Basin,Gulf ofMexico, Basin Research, 22, 380-397.

ROBSON, A.G., KING, R.C. & HOLFORD, S.P., 2016, Structural evolution of a gravitationally detached normal fault array: analysis of 3Dseismic data from the CedunaSub-Basin,Great Australian Bight, Basin Research, 29, 605-624.

ROLLET, N., LOGAN, G.A., KENNARD, J.M., O'BRIEN, P.E., JONES, A.T. & SEXTON, M., 2006, Characterisation and correlation of active hydrocarbon seepage using geophysical data sets: An example from the tropical, carbonate Yampi Shelf, Northwest Australia, Marine and Petroleum Geology, 23, 145-164.

RUBLE, T.E., LOGAN, G.A., BLEVIN, J.E., STRUCKMEYER, H.I.M., LIU, K., AHMED, M., EADINGTON, P.J. & QUEZADA, R.A., 2001, Geochemistry and Charge History of a Palaeo-Oil Column : Jerboa-1, Eyre Sub-Basin, Great Australian Bight, In: Hill, K.C. & Bernecker, T. (eds.) Eastern Australian Basins Symposium: a refocused energy perspective for the future. Petroleum Exploration Society of Australia, Melbourne, Australia, 521-529.

RUTH, P.V., HILLIS, R. & TINGATE, P., 2004, The origin of overpressure in the Carnarvon Basin, Western Australia: Implications for pore pressure prediction, Petroleum Geoscience, 10, 247-257.

RYAN, L., MAGEE, C. & JACKSON, C.A.L., 2017, The kinematics of normal faults in the Ceduna Subbasin, offshore southern Australia: Implications for hydrocarbon trapping in a frontier basin, American Association of Petroleum Geologists Bulletin, 101, 321-341.

SENGER, K., MILLETT, J., PLANKE, S., OGATA, K., EIDE, C.H., FESTØY, M., GALLAND, O. & JERRAM, D.A., 2017, Effects of igneous intrusions on the petroleum system: a review, First Break, 35, 47-56.

SIBUET, M. & ROY, K.O.L., 2002, Cold Seep Communities on Continental Margins: Structure and Quantitative Distribution Relative to Geological and Fluid Venting Patterns, In: Wefer, G., Billett, D., Hebbeln, D., Jørgensen, B.B., Schlüter, M. & Weering, T.C.E.v. (eds) Ocean Margin Systems. Springer, Berlin, Heidelberg, 235-251.

STEWART, S.A., 2006, Implications of passive salt diapir kinematics for reservoir segmentation by radial and concentric faults, Marine and Petroleum Geology, 23, 843-853.

STRUCKMEYER, H.I.M., WILLIAMS, A., COWLEY, R., TOTTERDELL, J., LAWRENCE, G. & O'BRIEN, G., 2002, Evaluation of Hydrocarbon Seepage in the Great Australian Bight, The APPEA Journal, 42.1, 371-385.

STRUCKMEYER, H.I.M., TOTTERDELL, J.M., BLEVIN, J.E., LOGAN, G.A., BOREHAM, C.J., DEIGHTON, I., KRASSAY, A.A. & BRADSHAW, M.T., 2001, Charactor, Maturity and Distribution of Potential Cretaceous Oil Source Rocks in the Ceduna Sub-Basin, Bight Basin, Great Australian Bight, In: Hill, K.C. & Bernecker, T. (eds.) Eastern Australasian Basins Symposium. Petroleum Exploration Society of Australia, Melbourne, Victoria, 543-552.

SUESS, E., 2010, Marine Cold Seeps, In: Timmis, K.N. (ed) Handbook of hydrocarbon and lipid microbiology. Springer, Berlin, 185-203.

SUN, Q., WU, S., CARTWRIGHT, J., LÜDMANN, T. & YAO, G., 2013, Focused fluid flow systems of the Zhongjiannan Basin and Guangle Uplift, South China Sea, Basin Research, 25, 97-111.

SUN, Y., WU, S., DONG, D., LÜDMANN, T. & GONG, Y., 2012, Gas hydrates associated with gas chimneys in fine-grained sediments of the northern South China Sea, Marine Geology, 311-314, 32-40.

SVENSEN, H., PLANKE, S., MALTHE-SØRENSSEN, A., JAMTVEIT, B., MYKLEBUST, R., EIDEM, T.R. & REY, S.S., 2004, Release of methane from a volcanic basin as a mechanism for initial Eocene global warming, Nature, 429, 542-545.

SWARBRICK, R.E. & OSBORNE, M.J., 1998, Mechanisms That Generate Overpressures: An Overview, In: Law, B.E., Ulmishek, G.F. & Slavin, V.I. (eds) Abnormal pressures in hydrocarbon environments : AAPG Memoir. AAPG, 13-34.

SYVITSKI, J.P.M. & PRAEG, D.B., 1989, Quaternary Sedimentation in the St. Lawrence Estuary and Adjoining Areas, Eastern Canada: An Overview Based on High-Resolution Seismo-Stratigraphy, Géographie physique et Quaternaire, 43, 291-310.

TANIGUCHI, M., BURNETT, W.C., CABLE, J.E. & TURNER, J.V., 2002, Investigation of submarine groundwater discharge, Hydrological Processes, 16, 2115-2129.

THURTELL, D., NGUYEN, T., MOLONEY, J., PHILALAY, M., DRAHOS, N., MARTIN, K., BATH, A. & GIBBONS, M., 2018, Resources and Energy Quarterly, Commonwealth of Australia, 125 pp.

TINGATE, P.R., KHAKSAR, A., RUTH, P.V., DEWHURST, D., RAVEN, M., YOUNG, H., HILLIS, R. & DODDS, K., 2001, Geological controls on overpressure in the Northern Carnarvon Basin, The APPEA Journal, 41(1), 573-594.

TINGDAHL, K.M., BRIL, A.H. & GROOT, P.F.D., 2001, Imrpoving seismic chimney detection using directional attributes, Journal of Petroleum Science and Engineering, 29, 205-211.

TOTTERDELL, J. M & BRADSHAW, B.E., 2004, The structural framework and tectonic evolution of the Bight Basin, in: Boult, P.J., Johns, D.R., S.C.Lang (Eds.), Eastern Australasian Basins Symposium II. Petroleum Exploration Society of Australia, Adelaide, Australia, 41-61.

TOTTERDELL, J. & MITCHELL, C. (Editors), 2009, Bight basin Geological Sampling and Seepage Survey: RV Southern Surveyor Survey: RV Southern Surveyor SS01/2007, Geoscience Australia Record 2009/24, 128 pp.

TRINCHERO, E., 2000, The fault shadow problem as an interpretation pitfall, The Leading Edge, 19, 132-135.

UNGERER, P., BEHAR, E. & DISCAMPS, D., 1983, Tentative calculation of the overall volume expansion of organic matter during hydrocarbon genesis from geochemistry data. Implications for primary migration, Advances in Organic Geochemistry, 129-135.

WANG, X., WU, S., YUAN, S., WANG, D., MA, Y., YAO, G., GONG, Y. & ZHANG, G., 2010, Geophysical signatures associated with fluid flow and gas hydrate occurrence in a tectonically quiescent sequence, Qiongdongnan Basin, South China Sea, Geofluids, 10, 351-368.

WATSON, D., HOLFORD, S., SCHOFIELD, N. & MARK, N., 2019, Failure to predict igneous rocks encountered during exploration of sedimentary basins: A case study of the Bass Basin, Southeastern Australia, Marine and Petroleum Geology, 9, 526-547.

WORZEL, J.L. & WATKINS, J.S., 1974, Location of a Lost Drilling Platform, Offshore Technology Conference, Texas, 2 pp.

Chapter 2

Ancient fluid flow recorded by remarkably long, buried pockmark trains observed in 3D seismic data, Exmouth Plateau, Northern Carnarvon Basin

(Published as Velayatham, T., Holford, S. &Bunch, M., 2018, Ancient fluid flow recorded by remarkably long, buried pockmark trains observed in 3D seismic data, Exmouth Plateau, Northern Carnarvon Basin, Marine and Petroleum Geology, 95, 303–313.)

Statement of Authorship

Title of Paper	Ancient fluid flow recorded by remarkably long, buried pockmark trains observed in 3D seismic data, Exmouth Plateau, Northern Carnarvon Basin
Publication Status	☑ Published ☐ Accepted for Publication ☐ Submitted for Publication ☐ Unpublished and Unsubmitted w ork w ritten in manuscript style
Publication Details	Velayatham, T., Holford, S., Bunch, M., 2018. Ancient fluid flow recorded by remarkably long, buried pockmark trains observed in 3D seismic data, Exmouth Plateau, Northern Carnarvon Basin. Marine and Petroleum Geology 95, 303-313.

Principal Author

Name of Principal Author (Candidate)	Tayallen Velayatham		
Contribution to the Paper	Performed seismic data interpretation and spatial statistics analysis described in the study, wrote manuscript and is corresponding author.		
Overall percentage (%)	70		
Certification:	This paper reports on original research I conducted during the period of my Higher Degree by Research candidature and is not subject to any obligations or contractual agreements with a third party that would constrain its inclusion in this thesis. I am the primary author of this paper.		
Signature		Date	27/5/2019

Co-Author Contributions

By signing the Statement of Authorship, each author certifies that:

i. the candidate's stated contribution to the publication is accurate (as detailed above);

ii. permission is granted for the candidate in include the publication in the thesis; and

iii. the sum of all co-author contributions is equal to 100% less the candidate's stated contribution.

Name of Co-Author	Simon P. Holford		
Contribution to the Paper	Supervised development of work, helped with data interpretation, provided feedback and edited manuscript.		
Signature		Date	27/5/19

Name of Co-Author	Mark Bunch		
Contribution to the Paper	Supervised development of work, helped with data interpretation, provided feedback and edited manuscript.		
Signature		Date	27/05/2019

Please cut and paste additional co-author panels here as required.

Ancient fluid flow recorded by remarkably long, buried pockmark trains observed in 3D seismic data, Exmouth Plateau, Northern Carnarvon Basin

Tayallen Velayatham*[1], Simon P. Holford[1] and Mark A. Bunch[1]

[1]Australian School of Petroleum, University of Adelaide, Adelaide, Australia

***** Corresponding author

Email: tayallen.velayatham@adelaide.edu.au

Keywords: fluid flow; pockmarks, fluid escape pipes, overpressure;

Abstract

We present 3D seismic data from the Exmouth Plateau, offshore northwest Australia shows 275 paleo-pockmarks of latest Jurassic age, organised into three linear NNW-SSE oriented pockmark trains, the longest exceeding 72 km. Spatial statistics indicate a high probability that these linear pockmark arrangements are not random. The trains are parallel to an array of linked normal faults with similar NNW-SSE strikes, with pockmarks underlain by feeder pipes that nucleate along or close to the fault planes. We interpret the faults to have intersected an overpressured unit and acted as a spatial control on the development of the feeder pipes and pockmarks. Our results reveal an important role of faults in controlling laterally extensive pockmark trains, and highlight the value of 3D seismic data in identifying large-scale ancient fluid flow within sedimentary basins.

1. Introduction

Pockmarks are crater-like depressions that develop in fine grained marine or lacustrine sediments across a diverse range of geological settings (Hovland and Judd, 1988; King and MacLean, 1970). They represent surficial expressions of the focussed expulsion of (typically overpressured) subsurface fluids, and can provide insight into fluid migration dynamics and overpressure in the shallow subsurface (Cartwright and Santamarina, 2015; O'Brien and Woods, 1995). Expelled fluid composition can vary from biogenic gases and hydrocarbons to brine, potentially impacting the bio-, hydro- and atmospheres on both local and global scales (Cambon-Bonavita et al., 2009; Hovland and Judd, 1988). Judd and Hovland (2007) suggest that active seabed sources of methane (seeps, vents, mud volcanoes) globally contribute at least 10 to 30 Tg per year into the atmosphere, contributing 2 to 6 % of the total atmospheric methane budget.

Pockmarks commonly occur in isolation or patches with random spatial distributions; however, underlying geological or stratigraphic structures can act as preferred fluid migration pathways that result in organised spatial distributions (Cartwright et al., 2007; Pilcher and Argent, 2007). Haskell et al. (1999) suggest that faults acted as fluid migration pathways to form overlying linear pockmark trends in offshore Nigeria. Gay et al. (2003) document sinuous pockmark trains in the Congo Basin that reflect the stratigraphy of a buried, overpressured turbiditic channel. Although geologically recent pockmarks have been studied extensively (Gay et al., 2003; Huuse et al., 2010), there has been less focus on ancient pockmarks. We define paleo-pockmarks as pockmarks that have been buried and preserved within the subsurface rock record. Though difficult to observe due to decreasing spatial resolution in seismic data with increasing depth, the identification and study of

paleo-pockmarks may provide insights into ancient fluid migration and expulsion events (Andresen et al., 2008; Ho et al., 2012).

Here we use marine 3D seismic data to document a system of paleo-pockmark trains of extraordinary length and linearity along an ancient, buried surface that marks the top of the Jurassic sedimentary rock sequence in the Exmouth Plateau, offshore Northwest Australia. We quantify the linearity of the pockmark trains using spatial statistics and identify the structural controls that led to their distinctive spatial and temporal distribution. We further assess sources and fluid types that formed these pockmarks and discuss their implications for how the subsurface fluid flow system has operated within the study area.

2. Regional Geology

2.1. Geological Setting of the Exmouth Plateau

The Exmouth Plateau is a thinned, subsided continental block within the Northern Carnarvon basin, offshore Northwest Australia (Fig. 1a) (Exon and Buffler, 1992). The basin is a passive margin filled with 15 km of mostly Mesozoic-age sediments (Hocking, 1988). Deltaic and fluvial-lacustrine sedimentary rocks of the Mungaroo, Brigadier and Athol formations were deposited across the plateau from the Triassic through to the early Jurassic (Fig. 1b, c) (Hocking, 1988; Veevers, 1988). Isolated carbonate reef build-ups were deposited in restricted areas along the outboard regions of the Exmouth Plateau during the Rhaetian at the end of the Triassic (Fig. 2e, f) (Grain et al., 2013). Growth of the reefs are attributed to a lack of siliclastic inputs and prevailing ocean currents (Grain et al., 2013). Rifting in the Pliensbachian resulted in northeast to southwest (NE-SW) striking faults across the Exmouth Plateau as well as the formation of Jurassic sub-basins along the plateau's south-eastern margin (Barber, 1982; Haq et al., 1992; Longley et al., 2002). These sub-basins became Jurassic sediment depocentres which deprived the plateau of sediment supply and resulted in a thin Mid to Late Jurassic sequence (Tindale et al., 1998). Between the Callovian and Valanginian, the northern, western and southern margins of the Exmouth Plateau underwent seafloor spreading, the initiation of which uplifted the plateau and exposed it to erosion (Boyd et al., 1992; Karner and Driscoll, 1999; Tindale et al., 1998). The orientation of extension at this time was oblique to the pre-existing northwest to southeast (NW-SE) trend of Permian fault blocks underlying the plateau, causing these blocks to rotate and form NNW-SSE striking extensional faults that cross-cut existing NE-SW faults in the Jurassic and Triassic sequences (Haq et al., 1992; Karner and Driscoll, 1999; Pryer et al., 2002). As rifting ceased by the end of the Valanginian, the basin underwent post-rift subsidence and developed as a passive margin, interrupted only by an episode of compression in the Miocene (Chongzhi et al., 2013). Deltaic and marine sediments were deposited across the plateau throughout

the Cretaceous; carbonate sedimentation was predominant by end-Cretaceous (Fig. 1b, c) (Chongzhi et al., 2013; Karner and Driscoll, 1999).

2.2. Current Exploration Status of Exmouth Plateau

Though the Northern Carnarvon Basin is one of Australia's biggest hydrocarbon producing regions, exploration in the basin has been primarily focused on the Jurassic sub-basins to the south-east of the Exmouth Plateau. However, exploration interest related to the Exmouth Plateau increased after the discovery of the Io-Jansz gas field in 2000, resulting in one of Australia's largest gas accumulations (GeoscienceAustralia and BREE, 2014). Drilling results across the plateau over the past 5 years have shifted the extent of proven gas discoveries out to the western edge of the plateau, leading to increasing interest in the exploration potential in the distal parts of the plateau (GeoscienceAustralia and BREE, 2014). Hydrocarbon charge across the Exmouth Plateau is interpreted to be sourced from organic-rich shales of the Triassic Mungaroo formation. Late Jurassic and Early Cretaceous deltaic to shallow marine sediments are the primary reservoirs on the plateau with a thick Cretaceous marine shale sequence acting as a regional seal and Jurassic to Cretaceous rift-related normal faults being the migration (Bradshaw, 1993; Bradshaw et al., 1994; Longley et al., 2002).

The aforementioned Rhaetian carbonate reefs have also been an exploration interest in recent years, as demonstrated by the Tiberius-1 which was drilled into a reef to test a carbonate reservoir play type, though no hydrocarbons were encountered (Grain et al., 2013).

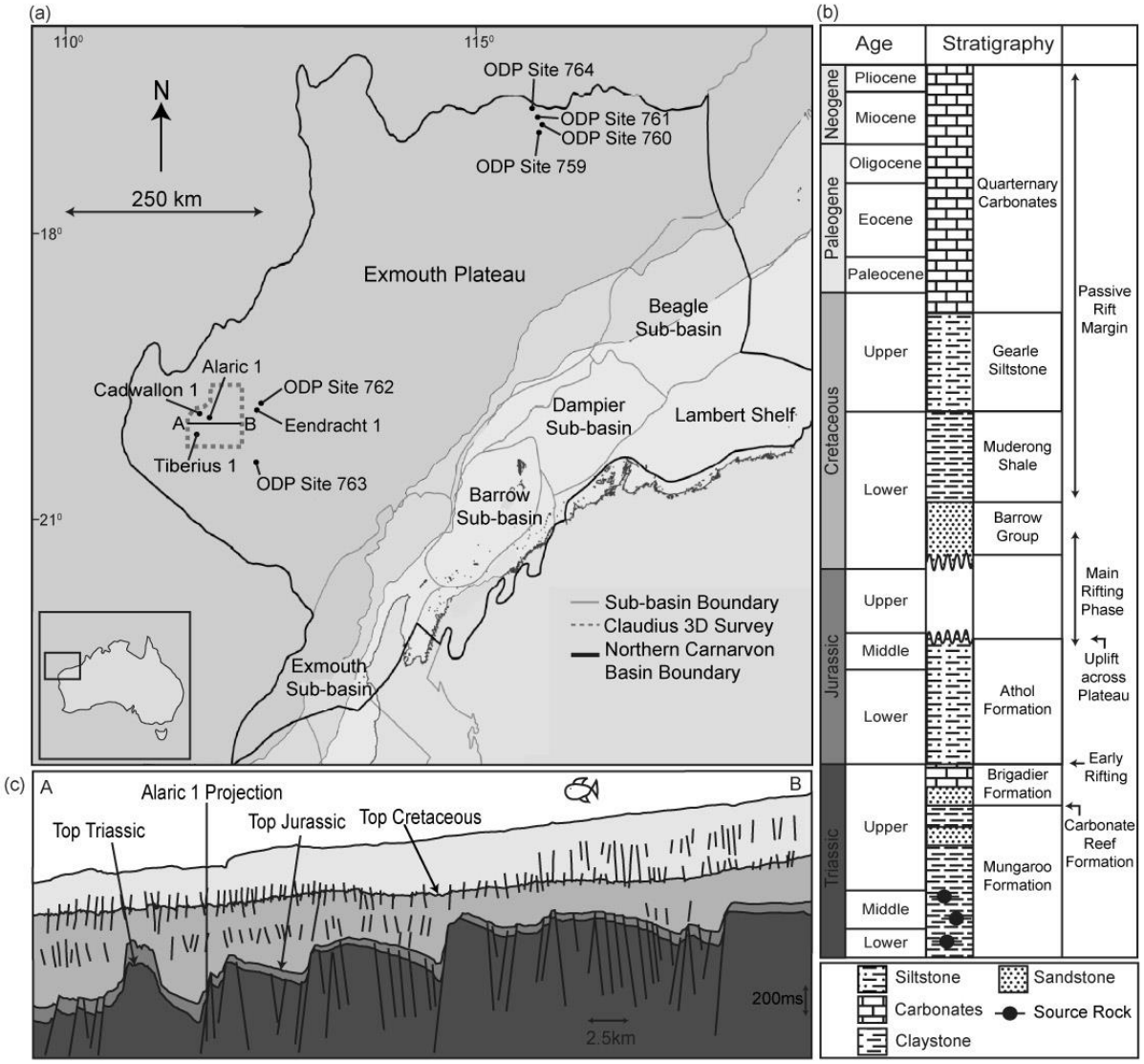

Figure 1*: (a) Location of study area in the Northern Carnarvon Basin, offshore northwest Australia (Modified from Northern Carnarvon Basin Biozonation and Stratigraphy Map, Geoscience Australia). (b) Generalized stratigraphic column and major tectonic events in the study area since the Triassic. (c) Representative cross-section of the study area.*

3. Data and Methodology

3.1. 3D Seismic Data

The focus of this study is the Claudius 3D seismic survey, a 3,700 km^2 time-migrated data set, located on the western edge of the Exmouth Plateau. The data is zero-phase processed with SEG reverse polarity, i.e. an increase in acoustic impedance is represented by a trough. The survey inline and crossline spacings are 12.5 m and 18.75 m, respectively. At the two-way time interval of interest (2.8–3.4 s), the dominant frequency is ~50 Hz and the velocity is ~2400 ms^{-1} based on sonic log

measurements from the Alaric-1 well, giving a vertical resolution of ~15 m, estimated as a quarter of the dominant wavelength. Full stack seismic data was used for seismic attribute analysis while angle-stacks were used to identify amplitude versus offset (AVO) effects that are potentially indicative of hydrocarbon occurrence (Avseth et al., 2008).

3.2. Interpreted Horizons and Seismic Stratigraphy

Of the interpreted surfaces, two that relate to the mapping and statistical analysis of paleo-pockmarks are discussed in this paper; the Top Mungaroo and Top Jurassic surfaces. These are regionally correlatable surfaces based on the regional tectonostratigraphic model described by Marshall and Lang (2013). The Top Mungaroo surface, equivalent to the TR30.1 in Marshall and Lang (2013), is of latest Norian age (~209.5 Ma) and marks the top of the Mungaroo Formation, a regional hydrocarbon source and reservoir unit, consisting primarily of deltaic siliclastics (Adamson et al., 2013; Grain et al., 2013). In the seismic data, the Top Mungaroo surface is a peak and the underlying sequence is expressed as laterally continuous, parallel reflections of low amplitude, with interspersed high amplitude reflections. The Top Jurassic surface, equivalent to the J47.0 in Marshall and Lang (2013), is an unconformable surface that is approximately of early Kimmeridgian age (~157.3 Ma) (Longley et al., 2002). The interval bound by the Top Jurassic and Top Mungaroo surfaces consists of a thin, early Jurassic calcareous claystone that is mostly absent in the outboard Exmouth Plateau, and Late Triassic carbonates assigned to the Brigadier Formation (Adamson et al., 2013; Exon et al., 1992; Haq et al., 1992). This combined sequence is interpreted to be approximately of Callovian to early Rhaetian age (163.5 – 208.5 Ma). In seismic data, the Top Jurassic surface is a trough and the sequence bound by the Top Jurassic and Top Mungaroo is expressed by continuous parallel reflections with low to moderate amplitudes. Overlying the Top Jurassic surface is the Valanginian to Berriasian (~139 – 145 Ma) aged Barrow Group sequence.

3.3. Spatial Statistics

Statistical analysis was undertaken to quantify the linearity of the distribution of paleo-pockmarks. Three methods for point alignment analysis (Hammer, 2009) were compared; the multiple blade, multinomial sector and continuous sector methods. The continuous sector method was used in this study as it was found to be the most robust of them. This method analyses azimuths between a central point, representing a pockmark, and other points within a defined circular radius from the central point to detect linear alignments (Hammer, 2009). The length of the radius in this study was defined based on the observed distances between documented paleo-pockmarks. The significance of the measured orientations was then tested using Rayleigh's test for circular distributions (Hammer, 2009). This test produces a 'p-value' that quantifies the likeliness of a spatial distribution as being random;

the smaller the p-value, the less likely the spatial distribution is one that is random (Mardia and Jupp, 2000).

4. Results

4.1. Paleo-pockmark Morphology and Spatial Distribution

The survey area is divided into two sections based on the presence of Triassic carbonate reef mounds; the western section with reef mounds, and the eastern section without (Fig. 2a). A total of 275 elliptical crater-like depressions, interpreted to be buried pockmarks, were identified and mapped along the Top Jurassic horizon. The majority (n = 251) of the paleo-pockmarks are in the eastern section of the study area and with the remaining 24 identified in the western section, where they occur in close proximity to the carbonate reef mounds. The lateral dimensions of the paleo-pockmarks are measured using the approach shown in Figure 2(d). The length of the long axis varies between 76–1,082 m (average = 343 m) and the short axis between 65-726 m (average = 264 m). In cross-section, the paleo-pockmarks have an upward concave shape, with either a curved or flat base (Fig. 2c). The depths of the paleo-pockmarks (D in Figure 2(d)) vary from 20 to 95 m, a large number of which (n = 83) have seismic reflections within them.

Underlying each paleo-pockmark are near vertical, pipe-like features, that are characterised by either laterally interrupted or continuous seismic reflections that sag-downwards, and have low acoustic impedance contrast in comparison to adjacent reflectors (Fig 2c). The lateral dimensions of the pipes are similar to those of the associated paleo-pockmarks. The pipes extend from the base of the paleo-pockmarks, into the underlying Triassic sequence with heights (H in Figure 2(d)) ranging between 110 and 740 m (average = 430m).

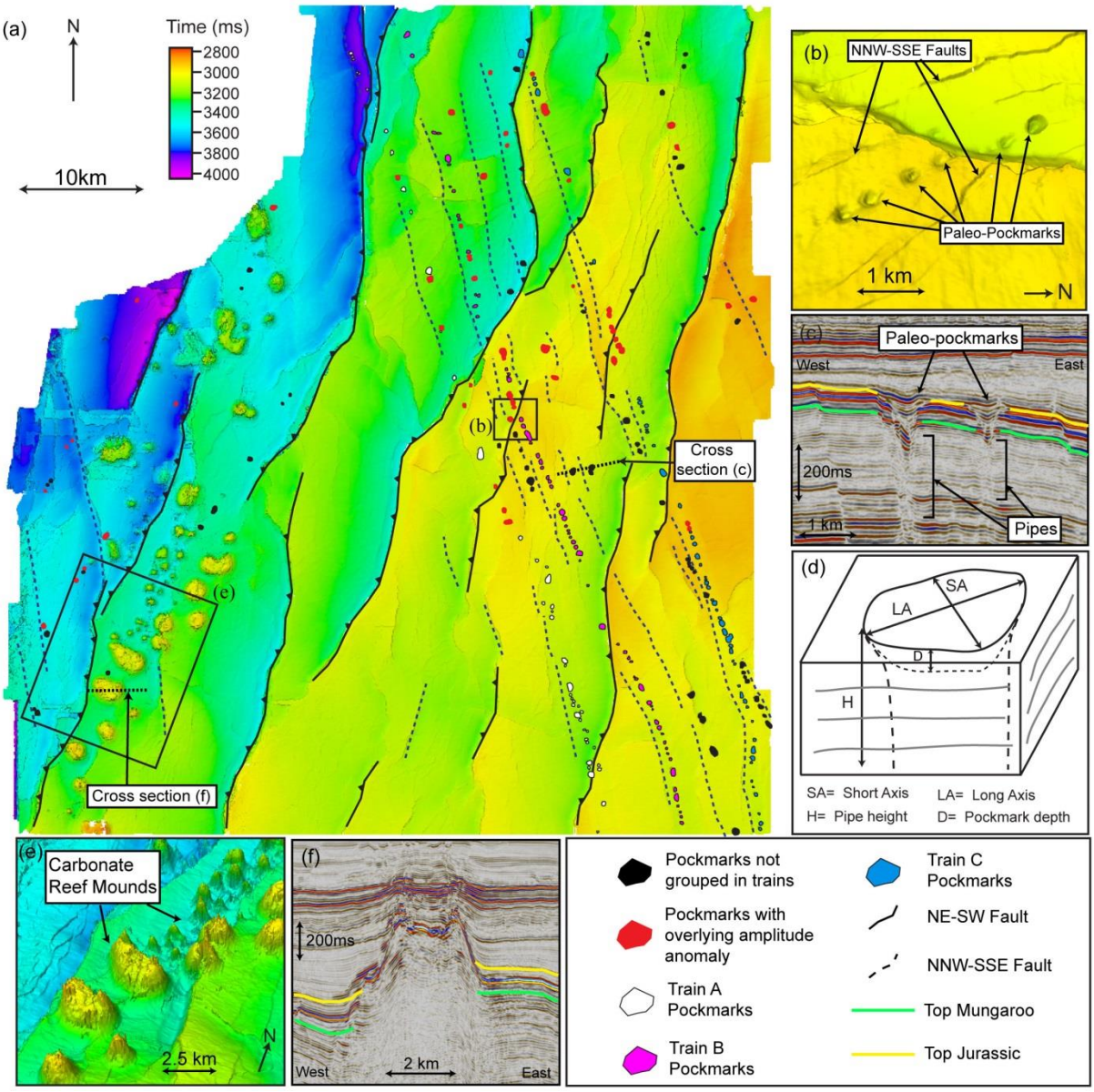

***Figure 2**: (a) Top Jurassic horizon with 275 identified paleo-pockmarks; 251 in the eastern region and 24 in the western region. (b) Enlarged images of the paleo-pockmarks parallel to NNW-SSE striking faults along the Top Jurassic horizon. (c) Seismic cross-section that shows the paleo-pockmarks and pipes. (d) Schematic of how the paleo-pockmark and pipe dimensions were measured. (e) Rhaetian carbonate mounds mapped along the Top Jurassic. (f) Seismic cross section of the Rhaetian carbonate reef.*

The paleo-pockmarks in the eastern section occur in sub-parallel, NNW-SSE trends, from which three extraordinarily long, sub-linear pockmark trains are identified (trains A, B and C) (Fig. 2a). The longest of these trains (train B) consists of at least 73 individual paleo-pockmarks and is approximately 72 km long within the limits of the Claudius 3D survey. Train A, measuring approximately 70 km, consists of 52 paleo-pockmarks while train C, measuring approximately 62 km, consists of 66 paleo-pockmarks. Though 61 paleo-pockmarks in the eastern region were not grouped

into trains, they show spatial alignments that are sub parallel to the three main trains. The linearity of the 251 paleo-pockmarks within the eastern section was quantified utilizing the continuous sector method (Hammer, 2009).

The largest distances between paleo-pockmarks in adjacent pockmark trains reach up to approximately 10 km, whereas the distances of paleo-pockmarks within a pockmark train reach up to approximately 4.3 km. We define three search radii, 3.6 km, 9.2 km and 13 km, that sufficiently sample the paleo-pockmarks at different scales. The continuous sector method for point alignment detection was then applied on the western and eastern regions of the study area.

In the eastern part of the study area where the pockmark trains are most prominent, the continuous sector method identified 100 alignments with a mean orientation of 162^0 with a 3.6 km search radius (Fig. 3c), 145 alignments with a mean orientation of 162^0 with a 9.2 km search radius (Fig. 3e), and 180 alignments with a mean orientation of 154^0 with a 13 km search radius (Fig. 3g). While the mean orientation is the same when using 3.6 km and 9.2km search radii, the different mean orientation for a 13 km search radius is likely due to the large search radius that led to detection of linear trends in a WSW-ENE orientation across paleo-pockmarks from different trains. The varying search radii also show how linear trends within each train are better identified with a smaller search radius, while the larger search radii detect larger scale linear trends of the pockmark trains. From Rayleigh's test for all three search radii, a p-value $<< 0.001$ was calculated. These results strongly support the inference that the linear orientations of the pockmark trains are not a random occurrence.

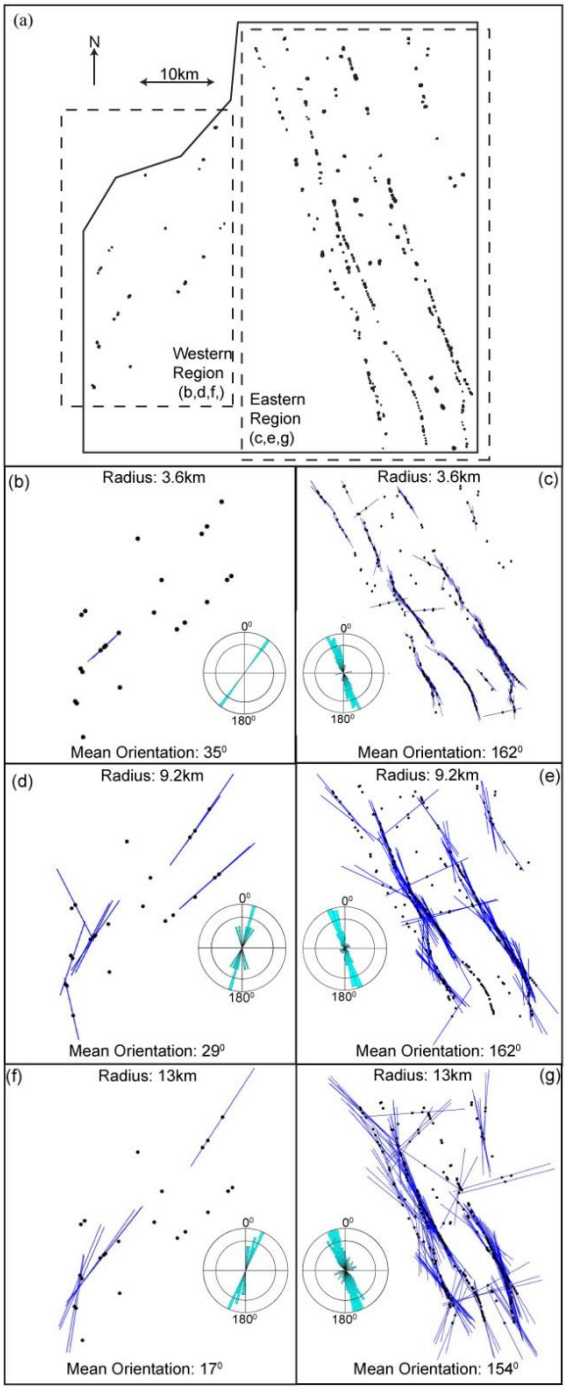

***Figure 3**: Point alignment detection using the continuous sector method by Hammer (2009) for paleo-pockmarks in the western (b,d,f,) and eastern regions (c,e,g).Three ranges of search radii were used based on distances between paleo-pockmarks; 3.6 km (a,b,), 9.2 km (c,d), and 13 km (e,f).*

Quantification of linear orientation for paleo-pockmarks in the western region was done using the same statistical method and with the similar search radii. Three alignments with a mean orientation of 35^0 were detected with the 3.6 km search radius (Fig. 3b), while 10 alignments with a mean orientation of 29^0 were detected with 9.2 km (Fig. 3d), and 8 alignments with a mean orientation of 17^0 were detected with 13 km (Fig. 3f). The fewer number of alignment detections

could be due to the overall larger spacings between paleo-pockmarks in this region. The Rayleigh test produced a p-value < 0.02 for the 3.6km search radius, though there were only 3 samples. For the 9.6 km and 13 km radii, a p value < 0.001 was obtained, suggesting that the spatial distribution of the paleo-pockmarks in the western region are not random. However, the paleo-pockmarks in this region are located amidst Triassic carbonate reef mounds and it is unclear if the presence of the mounds had prevented or masked underlying fluid escape features, thus interfering with the spatial alignment of the paleo-pockmarks (Fig. 2a).

4.2. Amplitude Anomalies Overlying the Paleo-pockmarks

Localized high amplitude anomalies associated with paleo-pockmarks were identified within the overlying Cretaceous sequence, above 49 pockmarks (Fig. 2a; 4a). The anomalies in the western region (n = 9) are along the same stratigraphic horizon within the Barrow Group at 49 to 167 m above the paleo-pockmarks (Fig. 4f), whilst the anomalies in the eastern region (n = 42) are located within the Muderong Shale formation at 27 to 219 m above the paleo-pockmarks (Fig. 4d, e). The anomalies are expressed as peak reflections, representing a decrease of acoustic impedance, with higher amplitudes than the adjacent seismic reflections (Fig. 4b, c). When examined on seismic angle stacks, the amplitudes of the anomalies increase with angle of reflection, potentially indicating the presence of hydrocarbons (Avseth et al., 2008).

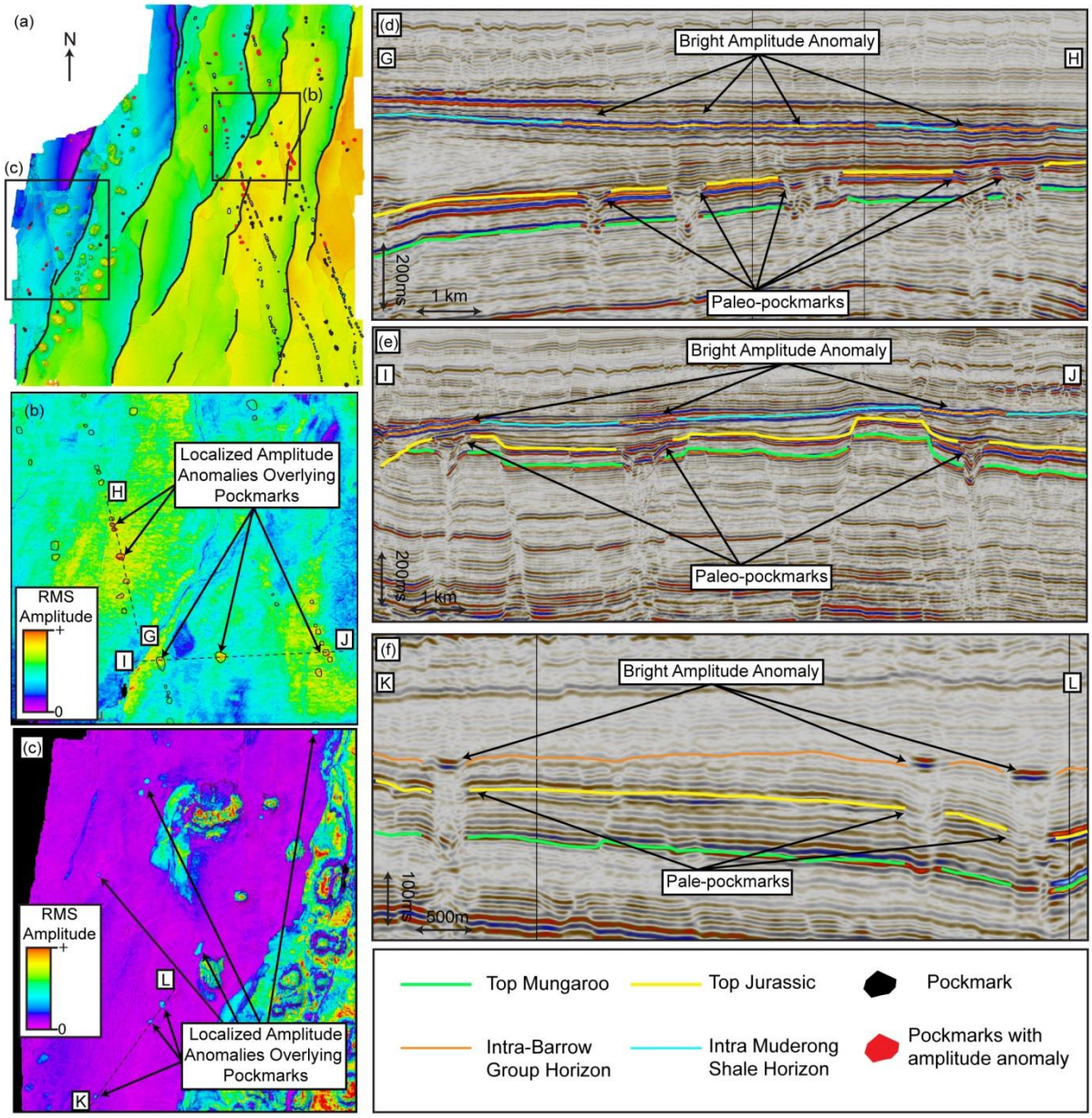

Figure 4: *(a) Top Jurassic horizon with documented paleo-pockmarks. (b) RMS amplitude map of reflector within the Muderong Shale formation in the eastern region with localized bright amplitude anomalies. (c) RMS amplitude map of reflector within the Barrow Group formation in the western region with localized bright amplitude anomalies. (d,e,f,) Seismic cross-sections that image the localized bright amplitude anomalies overlying the paleo-pockmarks.*

5. Discussion

5.1. Evidence for Structural Control on Paleo-pockmark Train Length and Alignment

We have documented three extraordinarily long pockmark trains at the top of the Jurassic sedimentary succession in the western Exmouth Plateau. Though pockmark trains have been identified in various regions (Brothers et al., 2012; Pilcher and Argent, 2007; Rise et al., 1999), the length of the longest pockmark train from this study (train B at 72 km) is more than double that of the previously documented longest pockmark train that measures 30 km in the Congo Basin of West Africa (Gay et al., 2003). The spatial alignment of the pockmark trains in this study is remarkably consistent with the orientation of NNW-SSE striking normal fault arrays that occur throughout the eastern section. These arrays comprise of linked normal faults whose upper tips terminate at the Top Jurassic horizon and extend down into the Triassic Mungaroo formation within the limits of seismic resolution. The fault planes have dip angles that range from 40^0 to 60^0. The strike orientations of 34 NNW-SSE faults were measured, giving an average orientation of 162^0. Though resolvable in the eastern region, the NNW-SSE striking faults are less prevalent in the western region. Furthermore, lower seismic resolution, due to the interval of interest being up to 700 ms deeper than the eastern region, and presence of the carbonate reef mounds make it difficult to identify and interpret NNW-SSE striking faults in the western region.

The paleo-pockmarks overlie the planes of the NNW-SSE striking fault arrays and are thus located within hanging wall blocks. The paleo-pockmarks do not overlie the tips of the faults, but are laterally offset by 81 to 1,685 m measured along the Top Jurassic horizon with 90% of the paleo-pockmarks in the eastern section offset within 400 to 1,000 m of fault traces (Fig. 2a). Though these ranges of offsets are measured for all paleo-pockmarks, the same variations in offset values are measured for paleo-pockmarks within each pockmark train. The number of faults within the arrays varies from 8 (associated with train A) to 12 (associated with train B), with individual fault lengths ranging from 2.5 to 12 km and maximum resolvable throws varying between 45 to 75 m. Fault displacement analysis was undertaken to investigate a possible correlation between the magnitude of fault displacement and paleo-pockmark occurrence. Fault throw for seven NNW-SSE faults from the eastern region were measure and graphed with locations where paleo-pockmarks were identified, and no relationship between throw and paleo-pockmark location was observed (Fig. 5). Nevertheless, based on the observations between the NNW-SSE faults and fluid escape features, it is likely that there is a spatial relationship between fault strike and paleo-pockmark location. Spatial statistics to test the similarity of the fault strike orientations (mean = 162^0) and pockmark train orientations (mean = 162^0) were calculated. Based on the results, the probability of the pockmark train and NNW-SSE

fault strike orientations being correlated (p[similar]) was 0.7, supporting the likelihood of a spatial correlation between them.

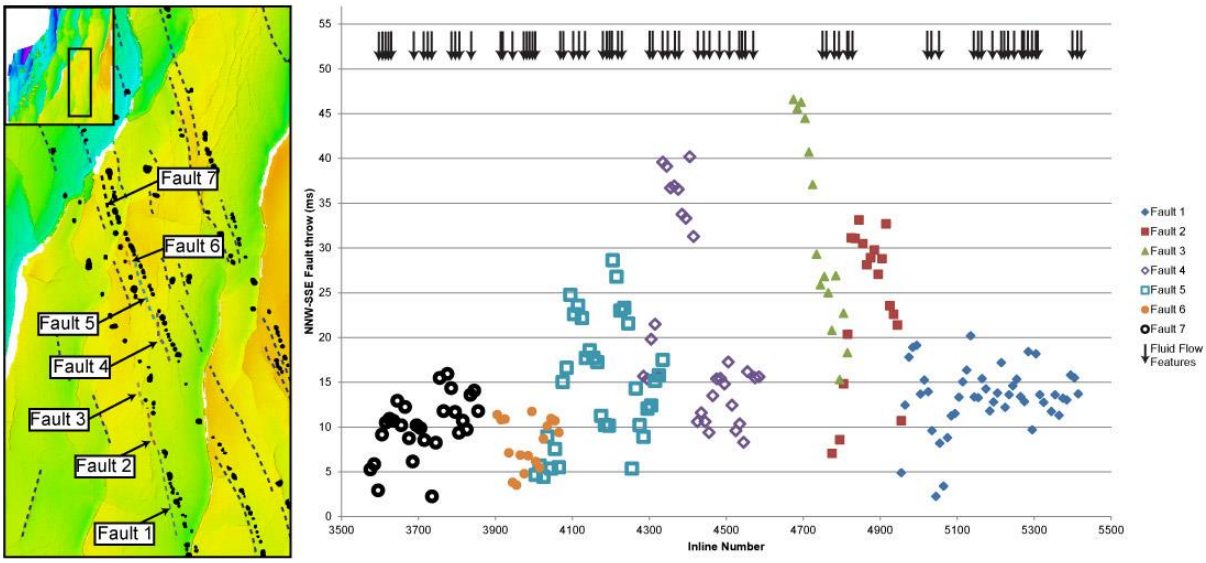

Figure 5: *The graph plots the amount of fault throw (ms) for seven mapped NNW-SSE faults against survey inline number that act as a proxy for distance along fault strike. The black arrows atop the graph indicate locations where fluid escape features associated with those faults were identified. No correlation between the amount of fault throw and presence of fluid flow features are identified.*

To determine the timing of faulting relative to paleo-pockmark formation, we conducted detailed isochron mapping of the early Jurassic and latest Triassic sequence, which is the interval bound by the Top Jurassic and Top Mungaroo horizons. Our mapping reveals little to no variation in isochron thickness across the NNW-SSE striking faults in contrast with variations in isochron thickness up to 130 ms (~156 m) across NE-SW striking normal faults (Fig. 6a). This indicates that the NE-SW faults were active during the deposition of the Jurassic sequence, while the NNW-SSE faults had formed after deposition of the Jurassic sequence. Deposition of Jurassic sediments on the Exmouth Plateau ceased by the Oxfordian (163.5 Ma) when the plateau was uplifted (Hocking, 1988). The Jurassic sequence underwent erosion until the early to mid Kimmeridgian, after which sedimentation across the plateau resumed in the Berriasian (145 Ma) with deposition of the Barrow Group sequence (Exon and Buffler, 1992; Longley et al., 2002). Isochron mapping, combined with the observation that the NNW-SSE faults do not extend into the Cretaceous sequence, constrains the timing of faulting to be between the Oxfordian and Berriasian (163.5 Ma – 145 Ma), coeval with propagation of seafloor spreading from the northern margin of the plateau, to its western and southern margins. The orientation of extension from sea-floor spreading is inferred to be oblique to Permian NW-SE striking faults that underlie the plateau, causing the rotation of basement blocks which formed

the NNW-SSE striking faults in the overlying sedimentary rocks (Haq et al., 1992; Karner and Driscoll, 1999; Pryer et al., 2002).

The timing of paleo-pockmark formation is inferred from the consistent presence of paleo-pockmarks along the Top Jurassic horizon and the lack of fluid escape features in the overlying Cretaceous sequence. The Top Jurassic horizon is an unconformable surface that represents erosion as the plateau was uplifted between the Oxfordian and the Kimmeridgian (Longley et al., 2002). Had the paleo-pockmarks and feeder pipes formed prior to uplift of the plateau, we would expect to observe feeder pipes that terminate along the Top Jurassic horizon, without variable preservation of paleo-pockmarks. Furthermore, no paleo-pockmarks or feeder pipes are observed in the overlying Berriasian to Valanginian age Barrow Group sequence. This lead us to interpret that the paleo-pockmarks formed subsequent to erosion and development of the Top Jurassic unconformity, but prior to the deposition of the Cretaceous sequence, roughly constraining the timing of formation to be between the late Kimmeridgian and Berriasian (152-145 Ma).

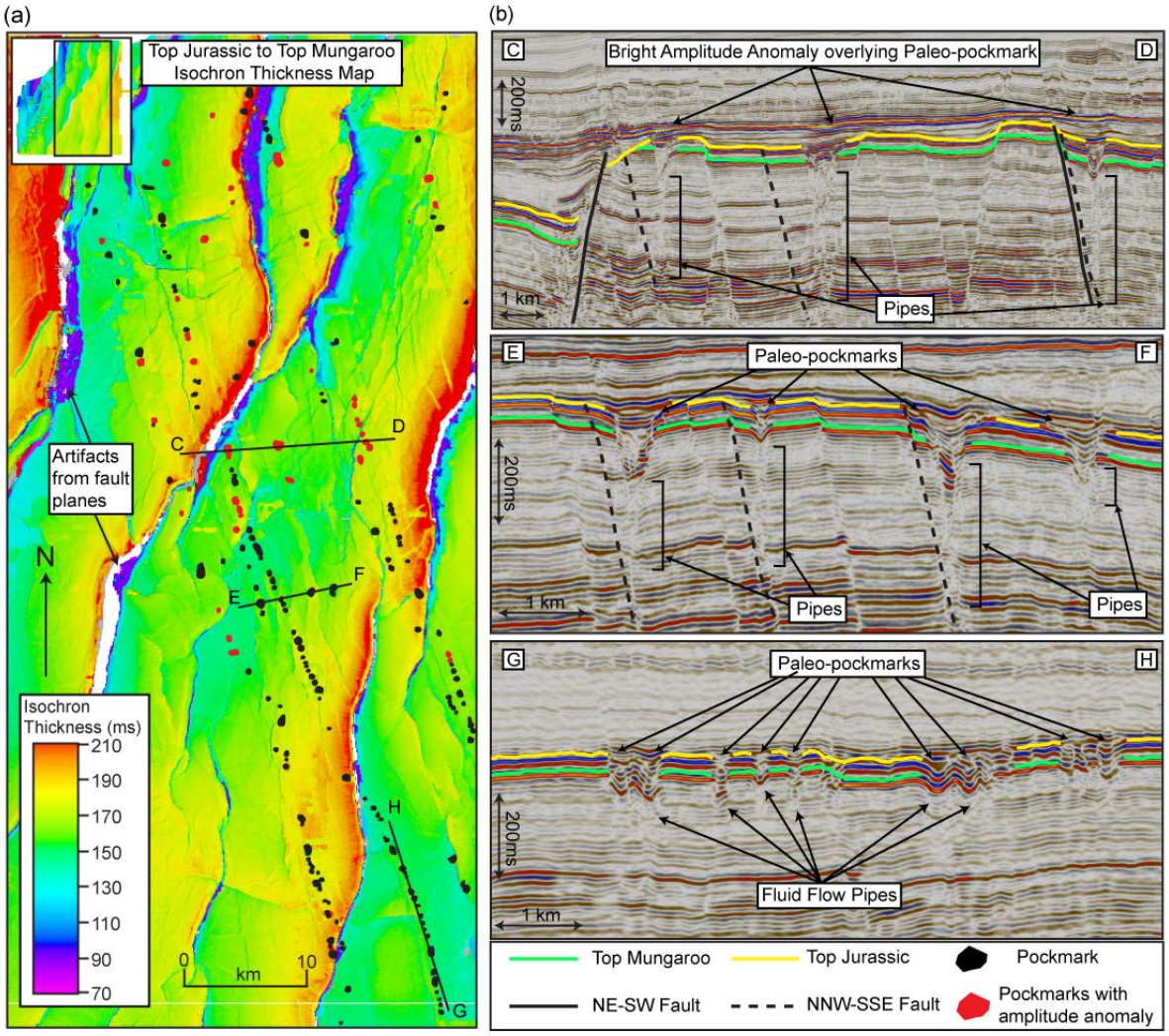

***Figure 6**: (a) Isochron thickness map of the Early Jurassic and Late Triassic sequence (Top Jurassic to Top Mungaroo interval) in the eastern region with the identified paleo-pockmarks. (b) Seismic*

cross sections showing the morphology of paleo-pockmarks and pipes with overlying amplitude anomalies. Only NNW-SSE faults that are interpreted to intersect the base of pipe formations have been highlighted.

5.2. Model for Paleo-pockmark Formation

We have identified 275 buried pockmarks developed on a latest Jurassic unconformity on the Exmouth Plateau, with the majority of these features organised into three extraordinarily long and linear trains. These trains are strongly aligned with a series of low-displacement, NNW-SSE striking normal fault arrays, which appear to have formed between the Oxfordian and Berriasian (163.5 Ma to 145 Ma). Faults often provide conduits for fluid flow and paleo-pockmark formation (Haskell et al., 1999; O'Brien and Woods, 1995), though in the data presented here, paleo-pockmarks are laterally offset from fault traces, by up to 1,700 m, instead of overlying them. All identified paleo-pockmarks are underlain by pipe-like features that are inferred to represent fluid escape pipes, through which overpressured fluids migrated vertically (Andresen et al., 2011; Moss and Cartwright, 2010). Of the identified pipes, 39 have seismically-resolvable bases that originate at or within 70 ms of the NNW-SSE fault planes in the Mungaroo Formation (Fig. 6b). It is plausible that the bases of the remaining pipes also nucleate at the NNW-SSE striking faults, but are below the seismic resolution threshold.

We propose that the NNW-SSE faults intersected an overpressured unit within the Mungaroo Formation, a regional hydrocarbon source and reservoir-bearing sequence, known to contain present-day overpressures (Tingate et al., 2001). The point of intersection between the fault and overpressured unit may have focused the drainage of overpressured fluids, which subsequently migrated vertically and were expelled at the exposed Late Jurassic unconformity, thereby forming the paleo-pockmarks (Fig. 7). Studies have shown that when overburden pressure is reduced locally, such as by faulting or sediment slumping, overpressured fluids are able to hydraulically fracture overlying sediments and migrate vertically (Løseth et al., 2011; Reilly and Flemings, 2010). Furthermore, the timing of the formation of these fluid escape features is constrained to be coeval with regions of the Exmouth Plateau being uplifted and exposed to erosion, which is suggested to have been caused by the initiation of rifting along the plateau margins (Longley et al., 2002). The reduction in confining pressure may have contributed to overpressure generation that led to the formation of the fluid escape features (Andresen and Huuse, 2011).

The variation in offset distances between the paleo-pockmarks and the upper tips of the NNW-SSE faults is interpreted to be due to the heterogeneity of the Triassic sequence along with the varying dip angles of the NNW-SSE faults. The Triassic Mungaroo formation is a consisting of interbedded sandstones and claystones, and this could have resulted in varying burial depths for the overpressured unit or even multiple source intervals of the overpressured fluids (Adamson et al., 2013).

Though the nature of the expelled fluids cannot be constrained, the implication of overpressure dissipation via focused fluid flow has implications for hydrocarbon prospectivity in the poorly explored Exmouth Plateau. The Mungaroo Formation contains deltaic source rocks that are thought to have charged gas accumulations in reservoirs at the Alaric 1 and Cadwollon 1 wells (Grain et al., 2013). If the paleo-pockmarks represent the focused escape of hydrocarbons sourced from the Mungaroo Formation during the Late Jurassic (157.3 to 145 Ma), this has important ramifications for the generative potential and charge history of Mungaroo Formation source rocks.

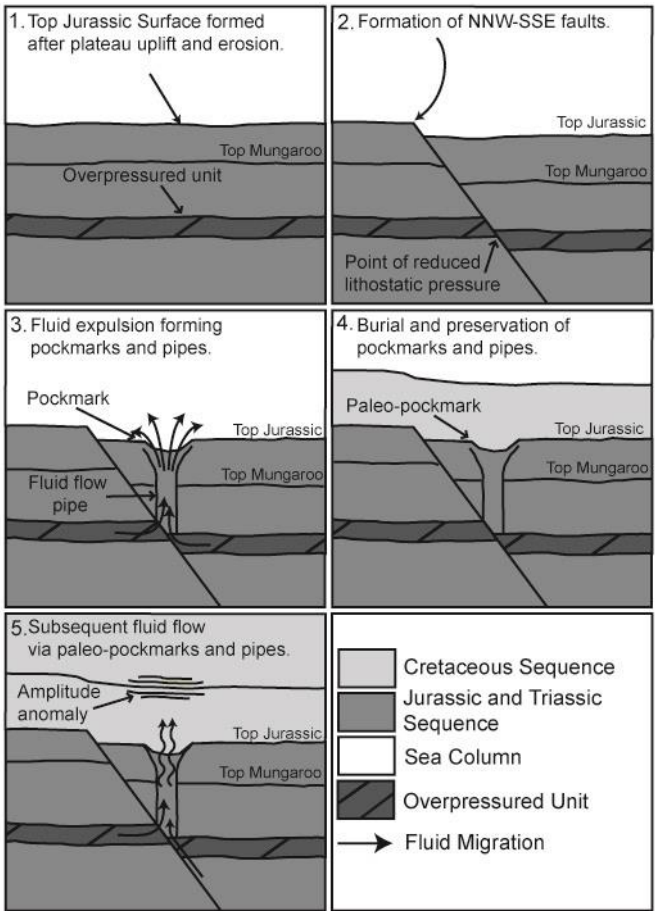

Figure 7*: Schematic illustration of the proposed model for the formation of paleo-pockmarks, pipes and potential fluid migration subsequent to their formation.*

Our model for pockmark train genesis is analogous to that of Maia et al. (2016), who proposed a model of faults intersecting an overpressured fluid source interval to explain the linear alignment of pockmarks overlying a polygonal fault system in the Lower Congo Basin. Pilcher and Argent (2007) invoked a similar model to explain the formation of curvi-linear "pockmark gullies" in offshore Angola, with localisation of the gullies controlled by listric slump faults intersecting an overpressured interval, similarly to Maia et al. (2016). Our study represents an advance on this previous work, demonstrating that laterally-extensive, low-displacement normal fault arrays that

intersect primed fluid source horizons can control the spatial distribution of fluid escape features to result in highly elongate pockmark trains, whilst also implying that faults can profoundly influence shallow plumbing systems without necessarily providing primary conduits (i.e. fluid migration along the fault planes) for fluid migration and escape. While our proposed model is reflected by the pockmark trains in the eastern region, it is further supported by the more sporadic spatial distribution of paleo-pockmarks in the western region, where NNW-SSE striking faults do not occur.

The NE-SW faults in this survey are observed to have no association with the formation of the paleo-pockmarks and fluid escape pipes. The linear trends of the fluid escape features are not parallel with the strike of these faults. The NE-SW faults have a complex growth history as they had been active in the Late Triassic and reactivated through the Jurassic (Exon et al., 1992; Hocking, 1988). We interpret the formation of these faults to predate the overpressure generation within the Triassic sequence; otherwise we would expect to observe paleo-pockmarks within the Triassic sequence since the NE-SW faults were active by the Late Triassic. There are similarly no observations of fluid escape features overlying the upper tips of the NE-SW faults that might suggest they acted as fluid migration pathways. This may be attributed to the clay rich nature of the Mungaroo formation, which resulted in sealing faults that prevent fluid migration. Though we cannot confirm the sealing properties of the NE-SW faults, this hypothesis is supported by data from the Alaric-1 well. The well drilled into a hydrocarbon reservoir on a tilted fault block edge with the adjacent fault acting as a seal, and no indications of hydrocarbon leakage.

The observation of amplitude anomalies suggestive of hydrocarbon accumulations, above a large number of the buried pockmarks indicates that these features, and their underlying feeder pipes, have influenced subsequent fluid migration. Studies by Ho et al. (2012) and Andresen et al. (2011) similarly document examples in offshore Angola where fluid escape pipes and paleo-pockmarks were reutilized as fluid migration conduits by thermogenic hydrocarbons and methane subsequent to their formation. While the origin of this phase of fluid migration is unclear, it is interpreted to be due to further maturation of Triassic source rocks, a result of continuous burial after the paleo-pockmarks and fluid escape pies had formed. The amplitude anomalies in the western and eastern regions occurring at different stratigraphic levels are attributed to variations in burial depths of hydrocarbon source rocks, as inferred from the variation in depths to the Top Jurassic horizon. This inference, however, cannot be confirmed as the Triassic source rocks in this region have not been drilled into.

6. Conclusions

We have identified and mapped 275 paleo-pockmarks of latest Jurassic age evident in Claudius 3D seismic survey data on the Exmouth Plateau of the Northern Carnarvon basin. The majority (n=251) of these paleo-pockmarks and their underlying pipes are aligned within three highly linear NNW-SSE oriented pockmark trains, with the longest train measuring up to 72 km in length. Spatial

statistical analysis of the pockmark trains indicates that their extraordinary linearity is highly unlikely to be a random occurrence. The pockmark trains are parallel to a series of NNW-SSE-striking linked extensional faults with maximum displacements ranging from 45 to 75 m. These faults are interpreted to have breached one, or multiple, overpressured units within the Triassic Mungaroo formation, leading to vertical fluid migration, and fluid expulsion along the Top Jurassic surface. The faults are interpreted to have formed between the Oxfordian and Berriasian (~163.5 – 145 Ma), while the paleo-pockmarks are approximated to have formed between the late Kimmeridgian and Berriasian (~152 M – 145 Ma). Amplitude anomalies observed in overlying Cretaceous sedimentary rocks suggests that, subsequent to their formation, the feeder pipes and paleo-pockmarks were utilized as hydrocarbon migration pathways. The model of paleo-pockmark generation proposed in this study builds on existing models for interaction of faults and fluid escape pipes by suggesting that the faults act as spatial controls for fluid migration as opposed to providing primary fluid migration pathways themselves.

7. Acknowledgments

We would like to thank the reviewers and editor for constructive comments for this paper, as well as Schlumberger for the use of Petrel software.

8. References

Adamson, K.R., Lang, S.C., Marshall, N.G., Seggie, R.J., Adamson, N.J., Bann, K.L., 2013. Understanding the Late Triassic Mungaroo and Brigadier Deltas of the Northern Carnarvon Basin, North West Shelf, Australia, West Australian Basins Symposium 2013 Proceedings. Petroleum Exploration Society of Australia, Perth, Western Australia, 29 pp.

Andresen, K.J., Huuse, M., 2011. 'Bulls-eye' pockmarks and polygonal faulting in the Lower Congo Basin: Relative timing and implications for fluid expulsion during shallow burial. Marine Geology, 111-127.

Andresen, K.J., Huuse, M., Clausen, O.R., 2008. Morphology and distribution of Oligocene and Miocene pockmarks in the Danish North Sea : Implications for bottom current activity and fluid migration. Basin Research 20, 445-466.

Andresen, K.J., Huuse, M., Schodt, N.H., Clausen, L.F., Seidler, L., 2011. Hydrocarbon plumbing systems of salt minibasins offshore Angola revealed by three-dimensional seismic analysis. American Association of Petroleum Geologists Bulletin 95, 1039-1065.

Avseth, P., Dræge, A., Wijingaarden, A.-J.v., Johansen, T.A., Jørstad, A., 2008. Shale rock physics and implications for AVO analysis: A North Sea demonstration. The Leading Edge 27, 788-797.

Barber, P.M., 1982. Palaeotectonic evolution and hydrocarbon genesis of the central Exmouth Plateau. The APPEA Journal 22(1), 131-144.

Boyd, R., Williamson, P., Haq, B., 1992. Seismic stratigraphy and passive margin evolution of the southern Exmouth Plateau, in: Rad, U.v., Haq, B.U. (Eds.), Proceedings of the Ocean Drilling Program. Scientific Results. College Station, TX (Ocean Drilling Program), pp. 39-59.

Bradshaw, M., 1993. Australian petroleum Systems. Petroleum Exploration Society of Australia Journal 21.

Bradshaw, M., Bradshaw, J., Murray, A., Needham, J., Spencer, L., Summons, R., Wilmot, J., Winn, S., 1994. Petroleum Systems in West Australian Basins, in: Purcell, P.G., Purcell, R.R. (Eds.), The Sedimentary Basins of Western Australia. Petroleum Exploration Society of Australia, Perth, Western Australia.

Brothers, L.L., Kelly, J.T., Belknap, D.F., Barnhardt, W.A., Andrews, B.D., Legere, C., Clarke, J.E.H., 2012. Shallow stratigraphic control on pockmark distribution in north temperate estuaries. Marine Geology 329-331, 34-45.

Cambon-Bonavita, M.A., Nadalig, T., Roussel, E., Delage, E., Duperron, S., Caprais, J.C., Boetius, A., Sibuet, M., 2009. Diversity and distribution of methane-oxidizing microbial communities associated with different faunal assemblages in a giant pockmark of the Gabon continental margin. Deep-Sea Research II 56, 2248-2258.

Cartwright, J., Huuse, M., Aplin, A., 2007. Seal bypass systems. American Association of Petroleum Geologists Bulletin 91, 1141-1166.

Cartwright, J., Santamarina, C., 2015. Seismic characteristics of fluid escape pipes in sedimentary basins: Implications for pipe genesis. Marine and Petroleum Geology 65, 126-140.

Chongzhi, T., Guoping, B., Junlan, L., Chao, D., Xiaoxin, L., Houwu, L., Dapeng, W., 2013. Mesozoic lithofacies palaeogeography and petroleum prospectivity in North Carnarvon Basin, Australia. Journal of Paleogeography 2, 81-92.

Exon, N.F., Buffler, R.T., 1992. Mesozoic seismic stratigraphy and tectonic evolution of the western Exmouth Plateau, in: Rad, U.v., Haq, B.U. (Eds.), Proceedings of the Ocean Drilling Program. Scientific Results. College Station, TX (Ocean Drilling Program), pp. 61-81.

Exon, N.F., Haq, B.U., Rad, U.v., 1992. Exmouth Plateau revisited: Scientific drilloing and geological framework, in: Rad, U.v., Haq, B.U. (Eds.), Proceedings of the Ocean Drilling Program. Scientific Results. College Station, TX (Ocean Drilling Program), pp. 3-20.

Gay, A., Lopez, M., Cochonat, P., Sultan, N., Cauquil, E., Brigaud, F., 2003. Sinuous pockmark belt as indicator of a shallow buried turbiditic channel on the lower slope of the Congo Basin, West African Margin, in: Rensenbergen, P.V., Hillis, R.R., Maltman, A.J., Morley, C.K. (Eds.), Special Publication. Geological Society, London, pp. 173-189.

GeoscienceAustralia, BREE, 2014. Australian Energy Resource Assessment, 2nd Edition ed. Geoscience Australia, Canberra.

Grain, S.L., Peace, W.M., Hooper, E.C.D., McCartain, E., Massara, P.J., Marshall, N.G., Lang, S.C., 2013. in: Beyond the Deltas: Late Triassic Isolated Carbonate Build-ups on the Exmouth Plateau, Carnarvon Basin, Western Australia, West Australian Basins Symposium 2013 Proceedings. Petroleum Exploration Society of Australia, Perth, Western Australia, 32 pp.

Hammer, Ø., 2009. New statistical methods for detecting point alignments. Computers and Geosciences 35, 659-666.

Hammer, Ø., Harper, D.A.T., Ryan, P.D., 2001. Past: Paleontological statistics software package for education and data analysis. Palaeontologia Electronica 4.

Haq, B.U., Boyd, R.L., Exon, N.F., Rad, U.v., 1992. Evolution of the Central Exmouth Plateau: A post-drilling perspective, in: Rad, U.v., Haq, B.U. (Eds.), Proceedings of the Ocean Drilling Program. Scientific Results. College Station, TX (Ocean Drilling Program), pp. 801-816.

Haskell, N., Nissen, S., Hughes, M., Grindhaug, J., Dhanani, S., Heath, R., Kantorowicz, J., Antrim, L., Cubanski, M., Nataraj, R., Schilly, M., Wigger, S., 1999. Delineation of geologic drilling hazards using 3-D seismic attributes. The Leading Edge 18, 373-382.

Ho, S., Cartwright, J.A., Imbert, P., 2012. Vertical evolution of fluid venting structures in relation to gas flux, in the Neogene-Quaternary of the Lower Congo Basin, Offshore Angola. Marine Geology 332-334, 40-55.

Hocking, R.M., 1988. Regional Geology of the Northern Carnarvon Basin, in: Purcell, P.G., Purcell, R.R. (Eds.), The North West Shelf Australia: Proceedings of the Petroleum Exploration Society of Australia, Perth, 1988.

Hovland, M., Judd, A.G., 1988. Seabed Pockmarks and Seepages. Graham and Trotman, London.
Huuse, M., Jackson, C.A., Rensbergen, P.V., Davies, R.J., Flemings, P.B., Dixon, R.J., 2010. Subsurface sediment remobilization and fluid flow in sedimentary basins: an overview. Basin Research 22, 342-360.

Judd, A., Hovland, M., 2007. Seabed Fluid Flow: The Impact on Geology, Biology and the Marine Environment. Cambridge University Press, Cambridge, U.K.

Karner, G.D., Driscoll, N.W., 1999. Style, timing and distribution of tectonic deformation across the Exmouth Plateau, northwest Australia, determined from stratal architecture and quantitative basin modelling, in: Niocaill, C.M., Ryan, P.D. (Eds.), Special Publications. Geological Society London, pp. 271-311.

King, L.H., MacLean, B., 1970. Pockmarks on the Scotian Shelf. Geological society of America Bulletin 81, 3141-3148.

Longley, I.M., Buessenschuett, C., Clydsdale, L., Cubitt, C.J., Davis, R.C., Johnson, M.K., Marshall, N.M., Murray, A.P., Somerville, R., Spry, T.B., Thompson, N.B., 2002. The North West Shelf of Australia - A Woodside Perspective, in: Keep, M., Moss, S. (Eds.), The Sedimentary Basins of Western Australia 3: Proceedings of the Petroleum Exploration Society of Australia Symposium, Perth, Western Australia, pp. 27-88.

Løseth, H., Wensaas, L., Arnsten, B., Hanken, N.-M., Basire, C., Graue, K., 2011. 1000 m long gas blow-out pipes. Marine and Petroleum Geology 28, 1047-1060.

Maia, A.R., Cartwright, J., Andersen, E., 2016. Shallow plumbing systems inferred from spatial analysis of pockmark arrays. Marine and Petroleum Geology 77, 865-881.

Mardia, K.V., Jupp, P.E., 2000, Directional Statistics Vol. 494, John Wiley & Sons, 441 pp.

Marshall, N.G., Lang, S.C., 2013. A New Sequence Stratigraphic Framework for the North West Shelf, Australia, West Australian Basins Symposium 2013 Proceedings. Petroleum Exploration Society of Australia, Perth, Western Australia, 32 pp.

Moss, J.L., Cartwright, J., 2010. 3D seismic expression of km-scale fluid escape pipes from offshore Namibia. Basin Research 22, 481-501.

O'Brien, G.W., Woods, E.P., 1995. Hydrocarbon-Related Diagenetic Zones (HRDZs) in the Vulcan Sub-basin, Timor Sea: Recognition and Exploration Implications. The APPEA Journal 35(1), 220-252.

Pilcher, R., Argent, J., 2007. Mega-pockmarks and linear pockmark trains on the West African continental margin. Marine Geology 244, 15-32.

Pryer, L.L., Romine, K.K., Loutit, T.S., Barnes, R.G., 2002. Carnarvon Basin architecture and structure defined by the integration of mineral and petroleum exploration tools and techniques. The APPEA Journal 42(1), 287-309.

Reilly, M.J., Flemings, P.B., 2010. Deep pore pressures and seafloor venting in the Auger Basin,Gulf ofMexico. Basin Research 22, 380-397.

Rise, L., Sættem, J., Fanavoll, S., Thorsnes, T., Ottesen, D., Bøe, R., 1999. Sea-bed pockmarks related to fluid migration from Mesozoic bedrock strata in the Skagerrak offshore Norway. Marine and Petroleum Geology 16, 619-631.

Tindale, K., Newell, N., Keall, J., Smith, N., 1998. Structural Evolution and Charge History of the Exmouth Sub-basin, Northern Carnarvon Basin, Western Australia., in: Purcell, P.G., Purcell, R.R. (Eds.), The Sedimentary Basins of Western Australia 2: Proceedings of the Petroleum Exploration Society of Australia Symposium, Perth, Western Australia, pp. 447-472.

Tingate, P.R., Khaksar, A., Ruth, P.v., Dewhurst, D., Raven, M., Young, H., Hillis, R., Dodds, K., 2001. Geological controls on overpressure in the Northern Carnarvon Basin. The APPEA Journal 41(1), 573-594.

Veevers, J.J., 1988. Morphotectonics of Australia's Northwestern Margin - A Review, in: Purcell, P.G., Purcell, R.R. (Eds.), The North West Shelf Australia: Proceedings of the Petroleum Exploration Society of Australia, Perth, 1988.

Chapter 3

3D Seismic Analysis of Ancient Subsurface Fluid Flow in the Exmouth Plateau, Offshore Western Australia

Statement of Authorship

Title of Paper	3D Seismic Analysis of Ancient Subsurface Fluid Flow In the Exmouth Plateau, Offshore Western Australia
Publication Status	☐ Published ☑ Accepted for Publication ☐ Submitted for Publication ☐ Unpublished and Unsubmitted w ork w ritten in manuscript style
Publication Details	Velayatham, T., Holford, S.P., Bunch, M., King, R.C., Magee, C., 2019, 3D Seismic Analysis of Ancient Subsurface Fluid Flow in the Exmouth Plateau. Offshore Western Australia, In: Keep, M. and Moss, S., West Australian Basin Symposium

Principal Author

Name of Principal Author (Candidate)	Tayallen Velayatham
Contribution to the Paper	Performed seismic data interpretation and spatial statistics analysis described in the study, wrote manuscript and is corresponding author.
Overall percentage (%)	75
Certification:	This paper reports on original research I conducted during the period of my Higher Degree by Research candidature and is not subject to any obligations or contractual agreements with a third party that would constrain its inclusion in this thesis. I am the primary author of this paper.
Signature	Date 27/5/2019

Co-Author Contributions

By signing the Statement of Authorship, each author certifies that:

i. the candidate's stated contribution to the publication is accurate (as detailed above);

ii. permission is granted for the candidate in include the publication in the thesis; and

iii. the sum of all co-author contributions is equal to 100% less the candidate's stated contribution

Name of Co-Author	Simon P. Holford
Contribution to the Paper	Supervised development of work, helped with data interpretation, provided feedback and edited manuscript.
Signature	Date 27/5/19

Name of Co-Author	Mark Bunch
Contribution to the Paper	Supervised development of work, helped with data interpretation, provided feedback and edited manuscript.
Signature	Date 27/05/2019

Please cut and paste additional co-author panels here as required.

Name of Co-Author	Rosalind King		
Contribution to the Paper	Supervised development of work, helped with data interpretation, provided feedback and edited manuscript.		
Signature		Date	24/06/2019

Name of Co-Author	Craig Magee		
Contribution to the Paper	Provided feedback and edited manuscript.		
Signature		Date	30/05/2019

3D Seismic Analysis of Ancient Subsurface Fluid Flow in the Exmouth Plateau, Offshore Western Australia

T. Velayatham[a]*, S. P. Holford[a], M. Bunch[a], R. C. King[b] & C. Magee[c]

[a] Australian School of Petroleum, University of Adelaide, SA 5005, Australia

[b] School of Physical Sciences, University of Adelaide, SA 5005, Australia

[c] Institute of Geophysics and Tectonics, School of Earth Science and Environment, University of Leeds, Leeds, United Kingdom

* Corresponding author email: tayallen.velayatham@adelaide.edu.au

Abbreviated Title: Focused Fluid Flow, Exmouth Plateau

Keywords: focused fluid flow, seismic interpretation, pockmarks, Exmouth plateau, fluid escape pipes

1. Abstract

This paper investigates ancient focused fluid flow events in the Exmouth Plateau of the Northern Carnarvon Basin of Australia. A total of 40 paleo-pockmarks and accompanying feeder pipes were identified within the Triassic and Jurassic sequences imaged in the Io-Jansz and Thebe 3D surveys. We also document pertinent features relevant to focused fluid flow, including polygonal faults within Cretaceous to Paleogene-age sequences and 81 present day sea-floor pockmarks within the Thebe 3D survey. The feeder pipes identified within the Triassic and Jurassic sequences appear to originate from the Triassic Mungaroo Formation and terminate along an unconformity surface that marks the top of the Jurassic sequence. The fluid flow features occur in linear trends that are parallel to the strikes of normal faults within the Triassic and Jurassic sequences. Our model for the origin of these fluid flow features suggests that they formed when faults intersected overpressured strata within the Mungaroo Formation, locally reducing the overburden pressure, enabling focused vertical migration of the fluids. While the reasons for fault nucleation and growth is uncertain, the faults may have formed in response to igneous dyke intrusions in the underlying Mungaroo Formation. The source of fluids vented through the escape features could not be definitively identified in this study. The results of this study could introduce a previously under-investigated fluid migration pathway into Jurassic sequences in the Exmouth Plateau.

2. Introduction

Focused fluid flows occur when subsurface fluids are channelled to shallower depths along a localised pathway. Though the term ‘fluid’ is used, the remobilized material can consist of liquids, gas, or even solids that behave in a fluid-like manner (Cartwright et al., 2007; Huuse et al., 2010). Focused fluid flows provide insight into geological processes such as hydrocarbon generation and migration (Baristeas et al., 2012; Cartwright & Santamarina, 2015), fluid release from overpressured sediments (Aminzadeh et al., 2002; Reilly & Flemings, 2010; Leduc et al., 2013), or enhanced biogenic activity (Hovland et al., 1993; Langhi et al., 2016). Advances in seismic reflection technology have improved detection and imaging of focused fluid flow features in the subsurface (Cartwright & Huuse, 2005; Løseth et al., 2009). Focused fluid flows in seismic data are commonly expressed as vertical zones of disrupted seismic reflections; however, structural surfaces such as faults and salt diapir flanks can also act as fluid migration pathways that minimize the seismic expression of fluid migration (Hansen et al., 2005; Leduc et al., 2013). The expulsion of subsurface fluids at the Earth’s surface are commonly expressed as pockmarks (Gay et al., 2004; Andresen et al., 2008) but can also manifest as deep sea vents (Chen et al., 2005), mud volcanoes (Loncke et al., 2004), and mud diapirs (Barber et al., 1986).

Focused fluid flow events are typically observed around margins or basins with high sedimentation rates (Hustoft et al., 2009; Huuse et al., 2010), contemporary hydrocarbon generation (Gay et al., 2006; Anka et al., 2012) and/or sequences of overpressured sedimentary rocks (Reilly & Flemings, 2010). Studies have also documented focused fluid flow in active convergent margins (Christodoulou et al., 2003) and subduction zones (Wallmann et al., 1997). In this paper, we present evidence for ancient focused fluid flow events in the Exmouth Plateau, Northern Carnarvon Basin (Fig. 1). The Northern Carnarvon Basin, a sedimentary basin in offshore northwest Australia, formed in the Late Carboniferous rift and developed through episodes of rifting between the mid-Jurassic and Early Cretaceous before transitioning into a passive margin basin from the mid-Cretaceous to the present (Longley et al., 2002). The Northern Carnarvon Basin is an established hydrocarbon generation province and is documented to have contemporary overpressure in the Cretaceous- to Triassic-aged sediments, particularly in the Muderong Shale, Dingo Claystone, Barrow Group and Mungaroo formations (Tingate et al., 2001; Van Ruth et al., 2004) (Fig. 1). Despite the potential for focused fluid flow occurrence, there is little documentation of them in the basin (Dirstein et al., 2013; Hengesh et al., 2013).

This study uses 3D seismic data to document paleo-focused fluid flow events in two study areas within the Exmouth Plateau (Fig. 1). The primary expressions of the paleo-fluid flow events are elliptical crater-like depressions with underlying feeder pipes in the Triassic and Jurassic sequences. We also document tiered polygonal fault systems that have the potential to influence subsurface fluid migration dynamics. We propose a model for the formation of the ‘crater-like’ depressions and discuss the ramifications of their presence for working petroleum. Though the focus of this study is the ‘crater-like’ depressions, we also describe under-documented polygonal faults within the Cretaceous and Cenozoic sediments, and present-day seafloor depressions that were identified in the study areas.

3. Geological Setting

The Northern Carnarvon Basin (Fig. 1), situated on Australia’s North West Shelf, is a passive margin basin that formed in the Late Carboniferous and developed through rifting events associated with the break-up of Gondwana through the Jurassic and Early Cretaceous (Hocking, 1988). The offshore portion of the basin covers an area of approximately 535,000 km^2 and is filled with a succession of Mesozoic to Cenozoic sediments up to 15 km thick (Stagg et al., 2004). The primary tectonic elements of the Northern Carnarvon Basin are four NE-SW trending Jurassic sub-basins (Beagle, Barrow, Exmouth and Dampier), Peedamullah and Lambert Shelves to the southeast, the Rankin Platform along the northwestern margin of the Barrow and Dampier sub-basins, and the Exmouth Plateau that extends northwest to the outboard portion of the basin (Fig 1; Stagg & Colwell, 1994;

Stein, 1994; Longley et al., 2002). Bounding the Northern Carnarvon Basin are the Southern Carnarvon Basin to the south, Western Australia to the southeast, the Roebuck and Canning basins to the northeast, and the Argo, Gascoyne, and Cuvier Abyssal plains to the north, west and southwest respectively (Longley et al., 2002).

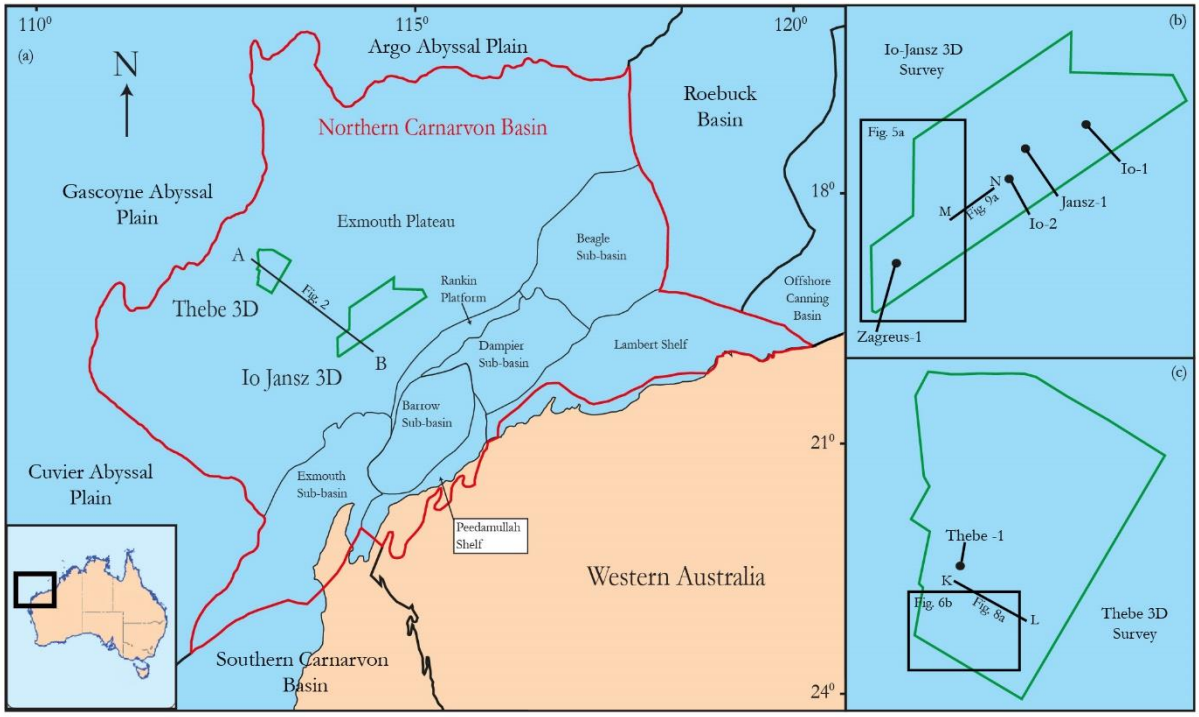

***Figure 1**. (a)Location of the Northern Carnarvon Basin (outlined in red) along with tectonic elements that define and border the basin. The study areas, Thebe 3D and Io-Jansz 3D surveys, are highlighted in green polygons. A zoom-in of the (b) Io-Jansz 3D and (c) Thebe 3D survey areas from (a) with petroleum wells within each survey and location references for figures in later sections of this paper.*

The Northern Carnarvon Basin formed and developed through episodic rifting events between the Carboniferous and the Cretaceous (Haq et al., 1992). Rifting in the Late Carboniferous initiated the basin, followed by a period of minimal tectonic activity throughout the Permian and Triassic (Hocking, 1988; Veevers, 1988; Longley et al., 2002). Rifting within the basin reinitiated during the Pliensbachian, forming the Jurassic sub-basins (Exmouth, Dampier, Barrow and Beagle) and the Exmouth Plateau (Hocking, 1988; Tindale et al., 1998). This episode of rifting also developed NE-SW striking extensional faults across the Exmouth Plateau, forming horsts and grabens that define many of the structural features in the Jurassic and Triassic sediments (Barber, 1982; Haq et al., 1992). In the Callovian, seafloor spreading initiated to the north of the basin, subsequently forming the Argo Abyssal Plain, and uplifted the Exmouth Plateau (Tindale et al., 1998; Stagg et al., 2004). Seafloor spreading geographically progressed from the north to the west and southwest of the Exmouth Plateau in the Berriasian and Valanginian, resulting in the formation of the Gascoyne and Cuvier abyssal plains (Haq et al., 1992; Longley et al., 2002), with the Northern Carnarvon Basin thereafter situated

on a passive margin, with little tectonic activity in the mid- and Late Cretaceous (Barber, 1982; Exon & Buffler, 1992; Tindale et al., 1998). Throughout the Cenozoic, the basin continued to develop as a passive margin basin, dominated by thermal subsidence but with an episode of compression during the Miocene (Longley et al., 2002).

The stratigraphy of the Exmouth Plateau comprises a sedimentary sequence composed primarily of Mesozoic sedimentary rocks (Fig. 2). Following Late Carboniferous rifting, up to nine kilometres of Triassic sediments were deposited in the newly formed Northern Carnarvon Basin, including the marine Locker Shale and the fluvio-deltaic Mungaroo Formation (Exon & Buffler, 1992; AGSO North West Shelf Study Group, 1994). The Exmouth Plateau was deprived of sediment supply in the Early Jurassic due to the Jurassic sub-basins to the east acting as the primary sediment depocentres, resulting in a thin Jurassic sequence across the plateau consisting of siltstones and claystones of the Murat Siltstone, Athol and Brigadier formations (Hocking, 1988). The plateau was uplifted in the Callovian, coinciding with seafloor spreading to the north and exposed the thin Jurassic sequence to erosion (Barber, 1982; AGSO North West Shelf Study Group, 1994). As seafloor spreading geographically progressed to the west and southwest of the Exmouth Plateau in the Berriasian and Valanginian, igneous material was intruded into the Triassic and Jurassic successions of the Exmouth Plateau (Longley et al., 2002; Holford et al., 2013). The intrusions manifest primarily as dykes and sills that are predominant in the southern region of the plateau (Frey et al., 1998; Rohrman, 2013). Marine transgressions coinciding with the Berriasian and Valanginian seafloor spreading led to deposition of the deltaic Barrow Group and marine Muderong Shale formations across the plateau (Hocking, 1988; Haq et al., 1992). Detrital input to the Exmouth Plateau began to decline after deposition of the Muderong Shale as the basin began to develop as a passive margin (Exon et al., 1992; Tindale et al., 1998). Transformation of the basin into a passive margin basin in the mid-Cretaceous saw deposition of claystones and siltstones of the Windalia Radiolarite and Gearle Siltstones (Stagg et al., 2004). By the end of the Cretaceous, sediment deposition in the Northern Carnarvon Basin had changed from siliciclastics to carbonates (Hocking, 1988). Carbonate deposition continued through the Cenozoic, resulting in a 500–1000m thick succession of carbonates across the Exmouth Plateau (Boyd et al., 1992; Cathro et al., 2003).

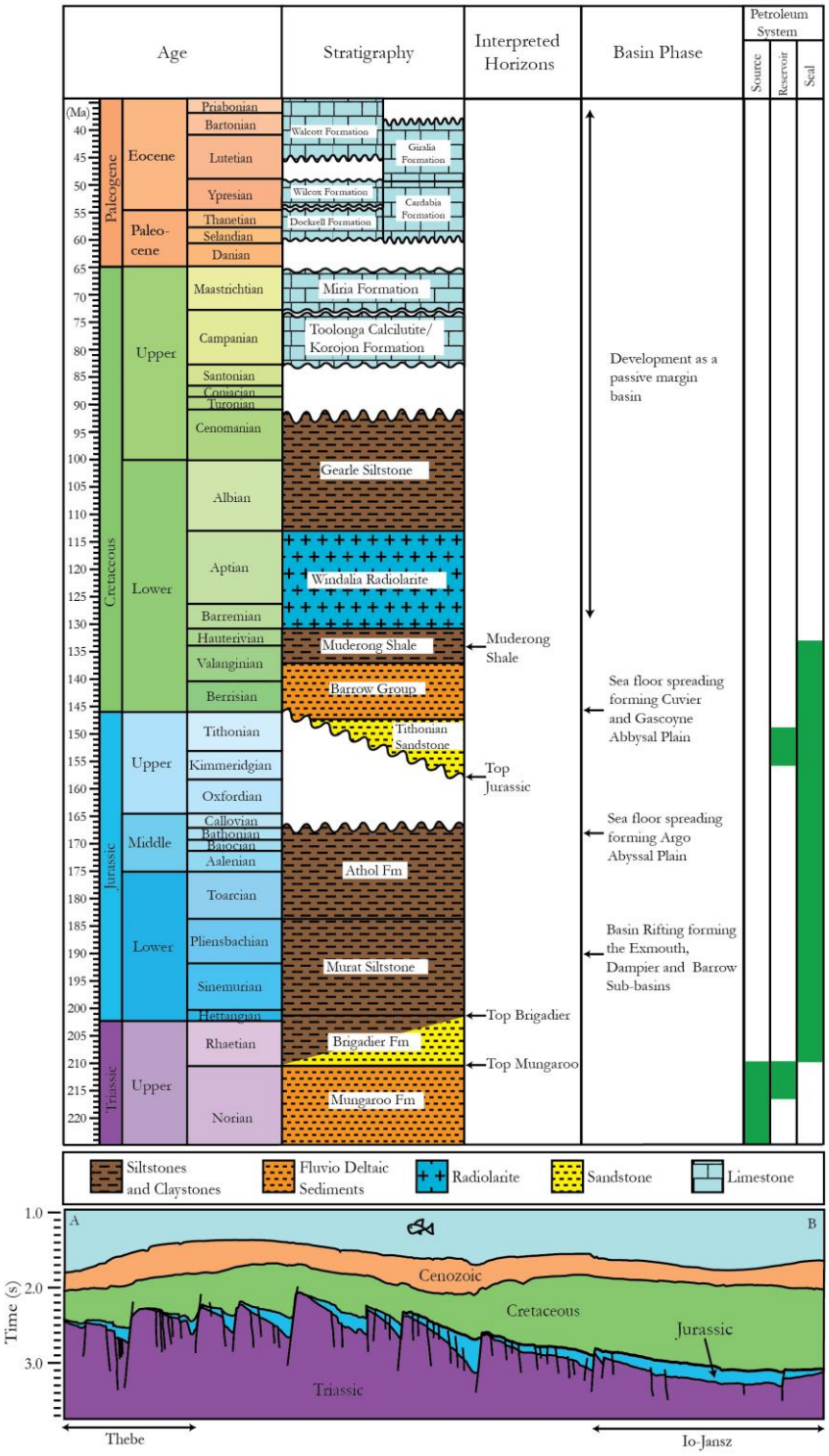

Figure 2: Generalized chronostratigraphic chart of the Exmouth Plateau. (modified from Northern Carnarvon Basin Biozonation and Stratigraphy Chart 36, 2010, Geoscience Australia). Underlying the chronostratigraphic chart is a schematic cross-section along A –B (from Fig 1a) that illustrates the general structural elements in a seismic cross-section on the Exmouth Plateau.

4. Data and Methodology

Two time-migrated, full-stack seismic datasets from the Exmouth Plateau were interpreted in this study: the Io-Jansz and HEX07B (referred to henceforth as Thebe) 3D seismic surveys (Fig. 1). The Io-Jansz 3D survey covers an area of ~2900 km2 and has water depths that range from 1200-1400 m. It has inline and crossline bin spacing of 18.75 x 12.5 m, and a record length of 6 seconds. Data from this survey was processed to have SEG normal polarity, i.e. a peak represents an increase in acoustic impedance. The Thebe 3D survey covers an area of ~1200 km2 and has water depths that range from 900–1200 m. It has inline and crossline bin spacing of 25 x 12.5 m and a record length of 4.5 seconds. Data from this survey was processed to have SEG reverse polarity, i.e. a peak represents a decrease in acoustic impedance.

Stratigraphic units in the seismic data are calibrated to five wells; Thebe-1, Io-1, Io-2, Zagreus-1 and Jansz-1 (Figs 2b and 2c). Thebe-1 is located in the Thebe 3D survey while Io-1, Io-2, Jansz-1, and Zagreus-1 are within the Io-Jansz 3D survey. The well depths are tied to seismic two-way time (TWT) using available VSP and sonic log data. Seismic horizons are interpreted based on well stratigraphic markers.

Interval velocity data is available in a 450 km2 region of the Io-Jansz survey centred around Io-1 well. A conservative velocity estimate for the Triassic and Jurassic sequences that contain the main features of interest to this study is approximated to be 3400 ms-1. This value was used to convert TWT measurements in seconds to depth in metres in the Jurassic and Triassic sequences in the Io-Jansz 3D. In the Thebe 3D, a conservative velocity estimate of 2500 ms-1 was used for TWT to depth conversion, based on sonic measurements of the Jurassic and Triassic sequences from Thebe-1 well. The variation in velocities used for TWT to depth conversion is attributed to two factors; (1) the inherent difference in measurement resolution and operational frequency bandwidth between surface reflection and wireline measurement methods (Stewart et al., 1984); and (2) Jurassic and Triassic sequences in Io-Jansz 3D are ~1s TWT deeper than in Thebe 3D, possibly resulting in them having a higher degree of compaction, and thus higher velocities, in Io-Jansz 3D than in Thebe 3D. In the two survey areas, the dominant frequencies of the Jurassic and Triassic sequences are 40–50 Hz, giving a vertical resolution of 16–20 m.

Four subsurface horizons (Top Mungaroo, Top Brigadier, Top Jurassic, and Top Muderong Shale) and the seafloor were interpreted based on their relevance to mapping paleo-pockmarks and other fluid flow features (Fig. 2). The seafloor was interpreted as a peak in the Io-Jansz 3D, and a trough in the Thebe 3D. The Top Muderong Shale is a polygonally faulted horizon and is interpreted as a trough in the Io-Jansz 3D and a peak in the Thebe 3D. The Top Jurassic horizon represents the regional Callovian–Oxfordian unconformity surface. The thin Jurassic sequence is imaged as

continuous parallel reflectors in the surveys with more prominent syn-rift depositional features in the Thebe 3D. It is interpreted as a trough in the Io-Jansz 3D and a peak in the Thebe 3D. The Top Brigadier horizon is an intra-Jurassic horizon, interpreted as a trough, that was only interpreted in the Io-Jansz 3D as it has mostly been eroded in the Thebe survey area. The deepest horizon interpreted is the Triassic Top Mungaroo Formation. The seismic reflections within the underlying Triassic sequence form a stack of continuous parallel reflectors that mimic the shape of the Top Mungaroo horizon. This horizon is interpreted as a trough in the Io-Jansz 3D and a peak in the Thebe 3D.

Fluid flow features are commonly expressed in seismic data as vertical zones of degraded imaging and these characteristics can be used to highlight fluid flow features using seismic attributes such as variance and consistent dip (Marfurt et al., 1998). Variance is an attribute that detects abrupt lateral variation along seismic reflections while consistent dip measures lateral changes in the gradient of a seismic reflector. Consistent dip is an attribute enhances variation in gradient along a seismic reflector in the inline or crossline directions. Lateral amplitude variations were imaged using Root Mean Square (RMS) amplitude calculations within a 20 ms window centred along the interpreted horizons.

5. Fluid Flow Features in Io-Jansz and Thebe 3D survey areas

5.1. Vertically Disrupted Zones (VDZs) and ‘Crater-like’ Depressions

Columns of disrupted seismic reflections, referred to as vertically disrupted zones (VDZs) are identified within the Triassic and Jurassic sequences of the two seismic surveys. Furthermore, each VDZs underlies elliptical, ‘crater-like’ depressions that are identified along the Top Jurassic horizon of both surveys. The VDZs across the two surveys share similarities in their dimensions but exhibit variation in their seismic expression. The VDZs are categorized into four types (Fig. 3). Type A VDZs are defined as having discontinuous seismic reflections overlying columns of concave-down seismic reflections (Fig. 3a). Type B VDZs have continuous seismic reflections that have lower amplitudes relative to the surrounding reflections. Furthermore, the depressions that overlie type B VDZs have seismic reflections within them (Fig. 3b). Type C VDZs have either discontinuous or continuous downward sagging reflectors within its column. There is no variation in seismic amplitudes within type C VDZs relative to the hosting stratigraphy (Fig. 3c). Type D VDZs are characterized by minimal or no disruption of seismic reflections within the columns compared to type A, B and C VDZs. Finally, type D VDZs have concave down reflectors within its column though the defining characteristic of this VDZ type is the upward deflection of seismic reflectors above the VDZs and their associated depressions (Fig. 3d).

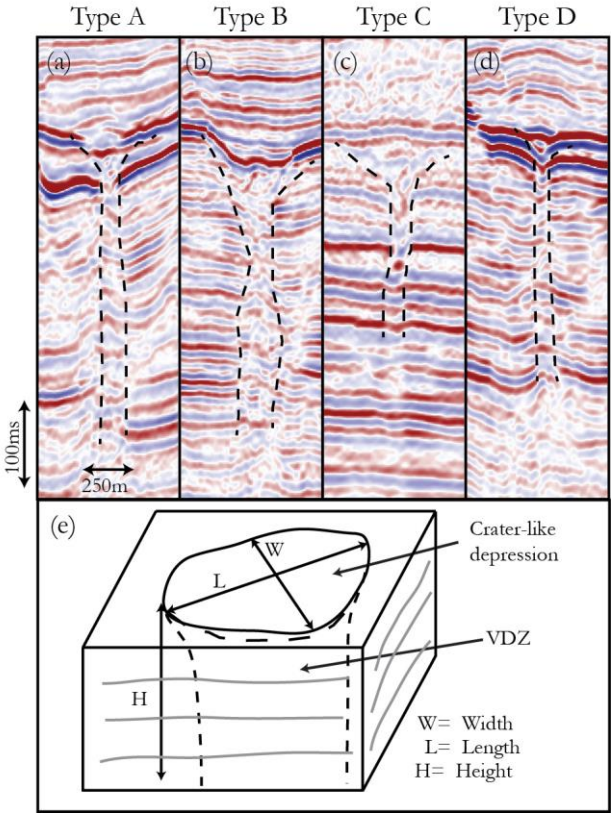

Figure 3: *Categories of Vertically Disrupted Zones (VDZs): a) Type A (VDZ T15 from Fig. 4). b) Type B (VDZ T9 in Fig. 4). c) Type C (VDZ IJ10 in Fig. 5). d) Type D (VDZ T6 in Fig. 4). e) Generalized schematic of a crater-like depression and underlying VDZ illustrating how the length, width and heights of the features were defined and measured.*

The dimensions of the 'crater-like' depressions and VDZs are measured in this study as per the schematic in Figure 3. The length is defined as the depression's longest axis along the Top Jurassic horizon while the width is defined as its shortest axis. The heights of the VDZs are measured from the top of the feature to as deep as the seismic disruption can be recognized on a seismic cross-section.

5.1.1. Crater-like depressions and VDZ's in Thebe 3D

A total of 17 VDZs (labelled T1-T17) with overlying 'crater-like' depressions are identified in NNW-SSE linear trends along the eastern edge of the Thebe 3D survey, comprising five Type A, four Type B and eight Type D VDZs (Fig. 4b). Along the Top Jurassic horizon, the depressions have low RMS amplitudes relative to their surroundings (Fig. 4c). Bases of the VDZs, referred to as roots, extend into and terminate within the Triassic Mungaroo Formation. The roots show no common surface of origin within the formation, though it is possible that the true roots are below seismic resolution and extend deeper.

Average dimensions of the long and short axes of the depressions are 310 m and 240 m while the average height of the VDZs is 220 m. A detailed summary on the range of dimensions for the depressions and VDZs are presented in Table 1. No correlation is identified between the planform dimensions of the 'crater-like' depressions with the height of VDZs. When imaged using the variance attribute, VDZs manifest as ellipses on time slice planes and as columns on cross sections. Their variance values range from 0.4 - 0.7 while the background variance values range from 0.05 to 0.15 (Figs 4d and 4e).

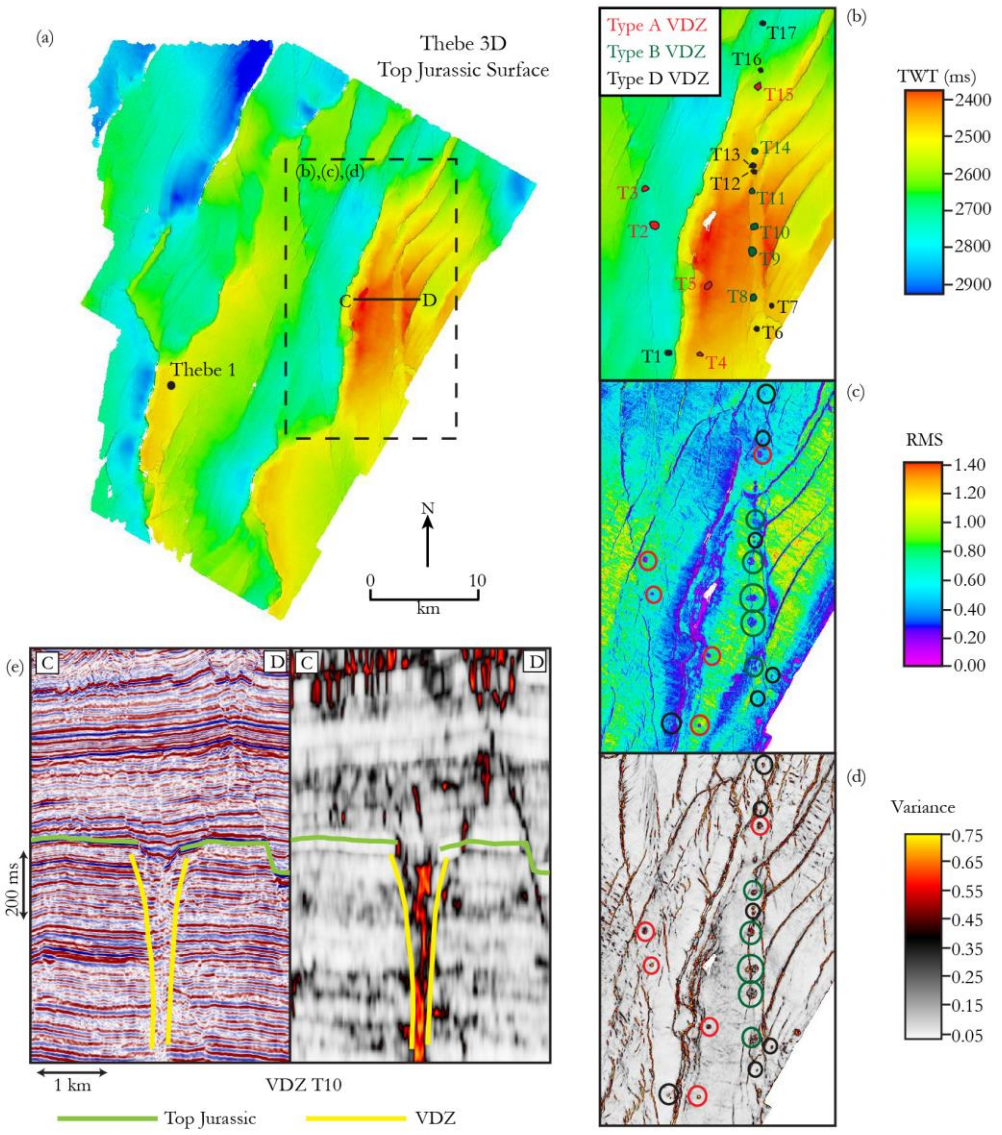

Figure 4: *a) Interpreted TWT horizon of the Top Jurassic surface in the Thebe 3D survey. b) A zoomed in location of the Top Jurassic TWT horizon from (a) along which locations of VDZs are overlayed. The number and polygon colors correspond to the VDZ type as described in the legend. Expression of these VDZs with c) RMS and d) variance attributes extracted along the Top Jurassic horizon. e) Imaging of VDZ T10 on seismic and variance cross-sections along line C-D from (a).*

5.1.2.Crater-like depressions and VDZ's in Io Jansz 3D

Along the south-western and western regions of the Io-Jansz 3D seismic survey, 23 Type C VDZs (labelled IJ1-IJ23)are identified in the Triassic and Jurassic sequences (Fig. 5a). They occur in linear NNE-SSW trends. The roots of the VDZs originate within the Triassic Mungaroo Formation with no common surface of origin and terminate at the Top Jurassic horizon where they are overlain by 'crater-like' depressions (Fig. 5c).

Average dimensions of the depression's long and short axes are 313 m and 246 m while the average height of the VDZs is 307 m. Seismic reflections within the VDZs are either discontinuous, or have a downward sag of up to 55 m (Figs 5d). A detailed summary on the range of dimensions for depressions and VDZs are presented in Table 1. When imaged with the variance attribute, VDZs appear as ellipses in time-slice planes and columns on cross sections. Their variance values range from 0.3-0.7 while the hosting background variance values range from 0.02-0.1 (Figs 5b and 5e). The VDZs and paleo-pockmarks within this 3D survey are not uniquely distinguishable using RMS amplitude measurements due to the lack of variation in seismic reflection amplitudes between the VDZs and surrounding reflectors.

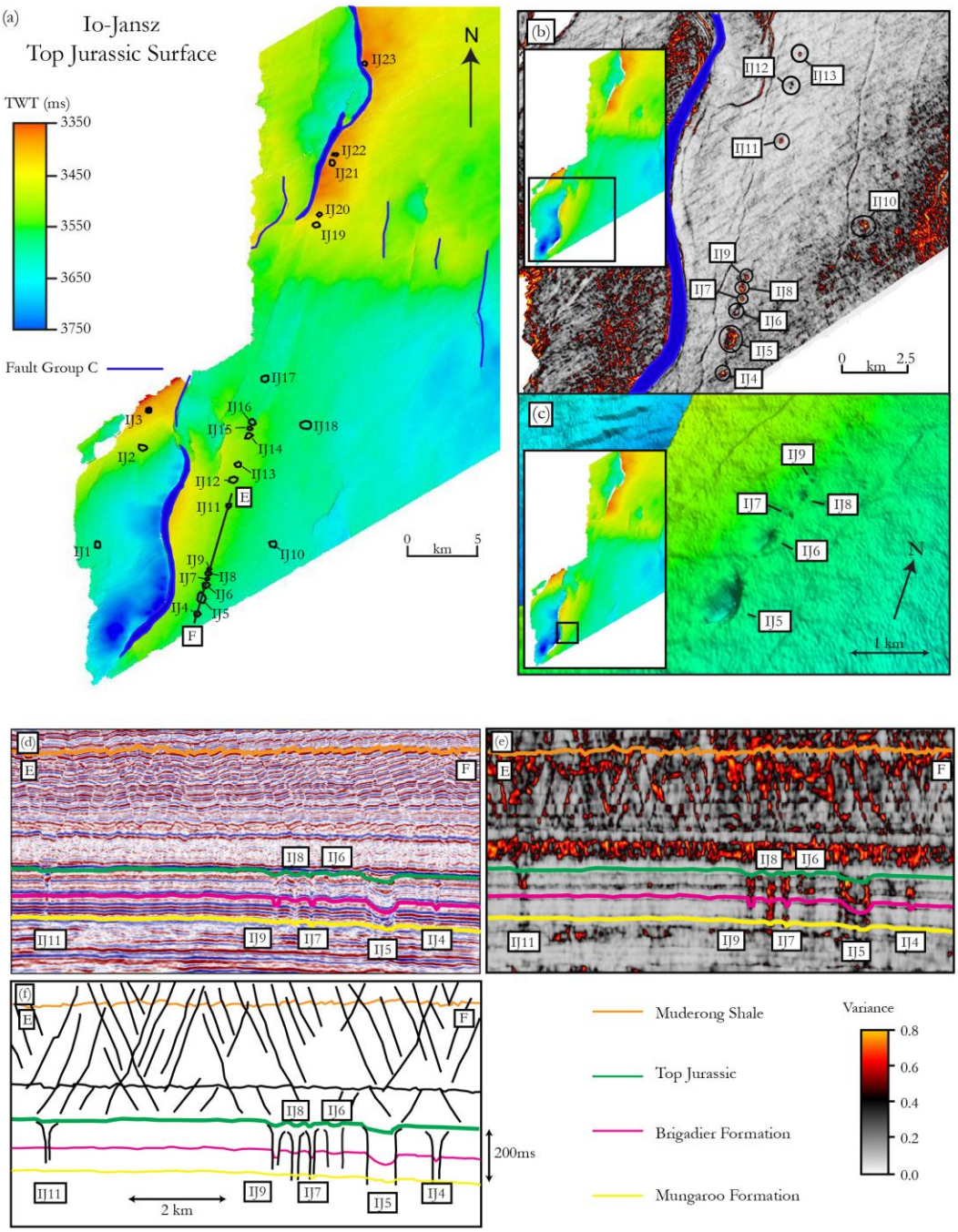

Figure 5: *a) Interpreted TWT horizon of the Top Jurassic surface in the Io-Jansz survey (from Fig. 1b), with an overlay of the VDZ locations and numbers. b) Sub-section of (a) that images expressions of VDZs with the variance attribute extracted along the Top Jurassic horizon. c) A zoomed-in 3D view of the Top Jurassic horizon from (a) illustrating craterlike-depressions with vertical exaggeration. A cross-section along line E-F in (a) is imaged using d) seismic data, e) variance attribute, and (f) schematic illustration. These cross-sections highlight the expressions of VDZs and other structural features.*

	Io-Jansz 3D			Thebe 3D		
	Maximum	Minimum	Average	Maximum	Minimum	Average
Long Axis (m)	800	140	350	616	148	310
Short Axis (m)	590	125	270	472	115	240
Surface Area (km^2)	0.316	0.007	0.076	0.250	0.014	0.075
VDZ Height (m)	640	102	363	433	47	177

Table 1: *Collective measurements of VDZs and paleo-pockmarks dimensions in the two surveys.*

5.2. Seafloor Depressions in Thebe 3D

In the Thebe 3D seismic survey, 81 circular depressions are identified along the seafloor in the southern region of the survey, of which 5 are identified within seafloor troughs or gullies (Fig. 6). The average length and width of the depressions are 392 m and 241 m, while their average depths are 10 m. Unlike the buried Jurassic 'crater-like' depressions, the seafloor depressions do not have underlying VDZs or feeder pipes, nor do they have linear spatial distributions. Instead, underlying 33 of the seafloor depressions are vertically stacked depressions that extend as far down as 67m (using 1680 ms-1 for time to depth conversion) (Fig. 6c).

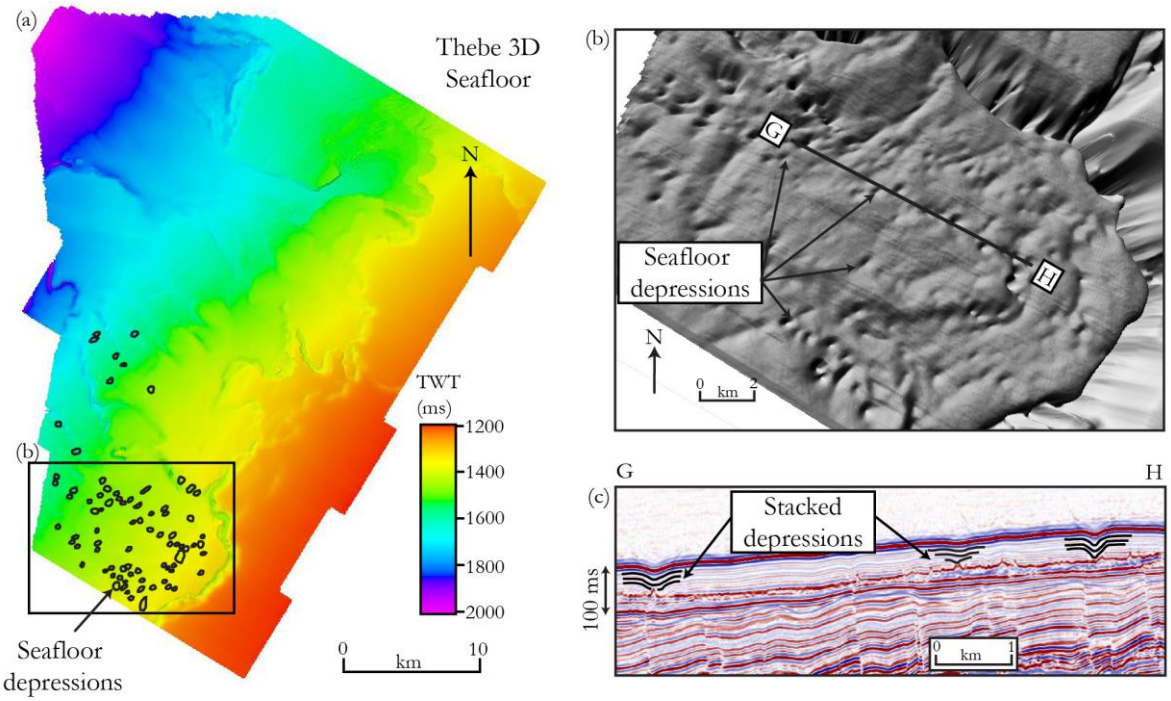

Figure 6: *a) Interpreted TWT seafloor horizon at Thebe 3D with seafloor depressions depicted by polygons. b) A sub-section of the TWT seafloor horizon (From Fig 1c and 6a) with a monochrome color scheme and vertical exaggeration that highlights seismic imaging of seafloor depressions. c)*

Seismic cross-section along G-H from (b) showing the seafloor depressions with underlying and stacked depressions.

5.3. Normal Faults

Normal faulting is prevalent within the Triassic and Jurassic sequences of both 3D surveys (Fig 7). The interpreted Top Jurassic and Top Mungaroo horizons from the Thebe 3D and Io-Jansz 3D surveys highlight the predominant fault trends in the two areas. Consistent dip attributes extracted within a 50 ms time window along the Top Mungaroo horizon of both surveys reveal a series of linear features within the Triassic sequences (Figs 7b and 7d). On seismic cross-sections, these features were identified to be a series of low-throw (~20 m) normal faults that form a series of horsts and graben. These faults are henceforth referred to as 'minor faults' (Figs 7e and 7f). In both study areas, the upper tips of the minor faults terminate along the Top Jurassic horizon. The minor faults extend down into the Triassic Mungaroo Formation, where their termination depths can't be accurately determined due to the deterioration of seismic data quality and decreasing seismic resolution (~20 m threshold).

5.3.1. Thebe 3D

Two predominant trends of faults are identified with in the Jurassic and Triassic sequences; NE-SW (Fault Group A) and NNW-SSE to N-S trends (Fault Group B) (Fig. 7a). The fault planes of Group A dip to the NW and SE with throws up to 800 m while fault planes of Group B dip towards the SW and NE with fault throws up to 100 m. Minor faults are identified in the eastern region of the survey area where the VDZs are identified. The minor faults strike NNW-SSE, sub-parallel to fault group B, and the minor fault planes dip NNE and SSW (Fig. 7b).

5.3.2. Io-Jansz 3D

Normal faults within the Io-Jansz 3D survey are predominantly oriented NE-SW with fault planes dip NW and have throws up to 650m (Fault group C; Figs 7c). Within the Io-Jansz 3D, minor faults are identified predominantly at the western and south-western regions of the survey where the VDZs are documented. The minor faults in Io-Jansz 3D strike NE-SW, and the fault planes dip to the NW and SE (Fig 7d).

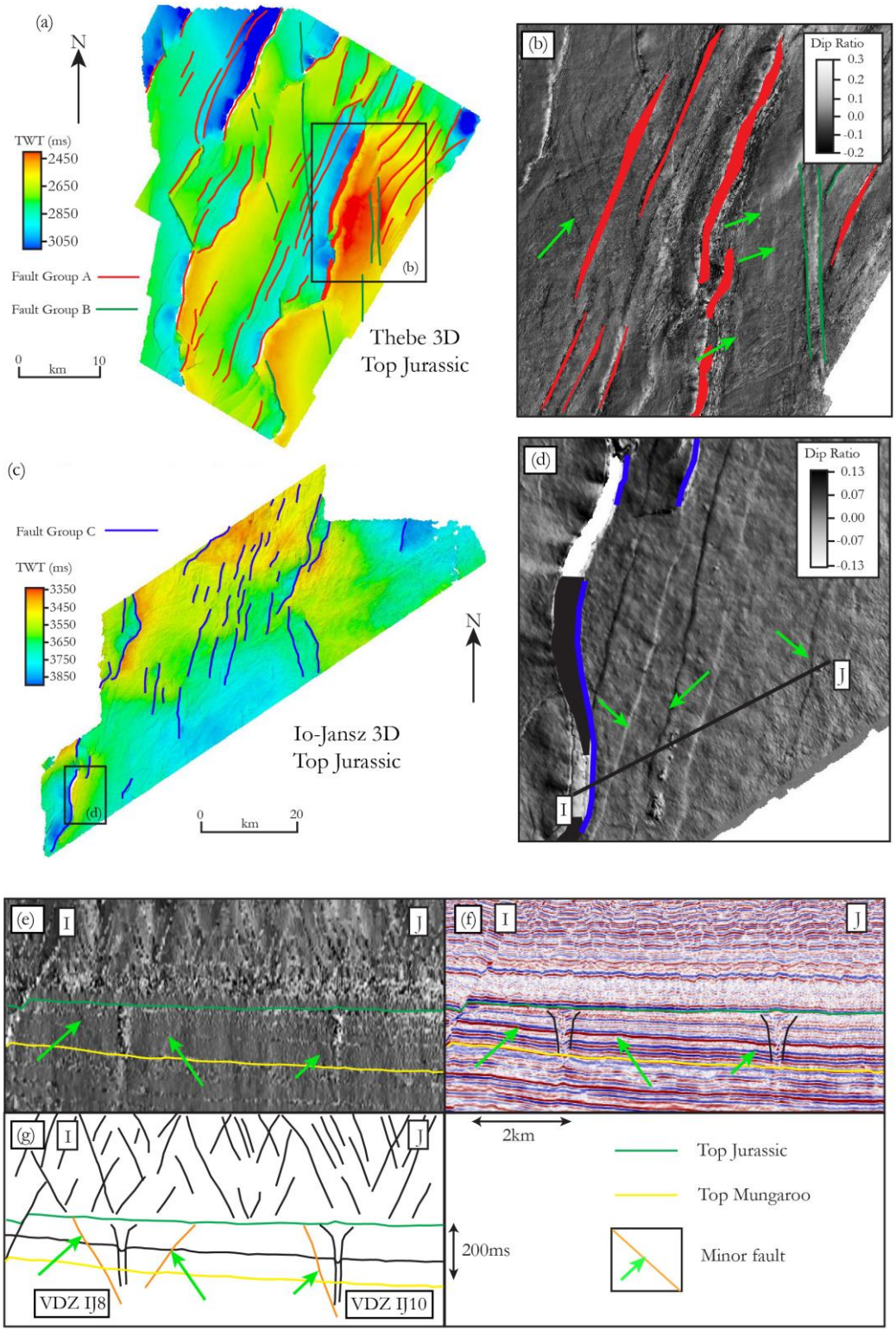

Figure 7: *Fault groups displayed on TWT maps of the Top Mungaroo horizons (a, b) and the Io-Jansz survey (c and d). a). Top Mungaroo time-structure map in the Thebe survey, b) linear features highlighted by the extracted consistent dip attribute. c). Top Mungaroo time-structure map of the Io-Jansz survey, d) linear features highlighted by the extracted consistent dip attribute. e) consistent dip*

and f) seismic cross sections along line I-J, show the linear features to be low-throw faults (highlighted by green arrows).

5.4. Polygonal faults

Polygonal faults are characterised by strike planes that intersect at various angles to form polygonal patterns (Cartwright et al., 2003). The faults develop through multiple layers, referred to as tiers by Cartwright (1994), where some faults are isolated to individual tiers while others extend across multiple tiers. Faults are categorized by their 'order' which refer to the number of tiers a fault extends across. The highest order of faults refers to faults that extend across all tiers and the lowest order refers to those that occur within an individual tier. For instance, in a polygonal fault system with three tiers, first order faults are defined as those that extend across all tiers, while second order faults extend across two consecutive tiers and third order faults are isolated to individual tiers (Gay et al., 2004). While polygonal faults have been identified on seismic data in the Exmouth Plateau of the Northern Carnarvon Basin, there is a lack of documentation on the tiers and orders of these faults.

In both the Io-Jansz and Thebe 3D surveys, multiple systems of polygonal faults are identified over several chronostratigraphic sequences that are vertically separated from one another by lithologic sequences that contain no polygonal faults. The faulted chronostratigraphic sequences are the Lower Cretaceous (LC), Upper Cretaceous (UC) and Cenozoic (CZ) sequences. The LC and UC sequences comprise of lithologic formations that can be correlated across the two seismic surveys. The LC sequence consists of the Barrow Group and Muderong Shale formations, while the UC sequence consists of the Gearle Siltstone, Toolonga Calcilutite, Miria and Korojon formations. The CZ sequence consists of the Girilia and Cardabia formations in the Thebe 3D and the Walcott, Wilcox and Dockrell Formations in the Io-Jansz 3D. Though the formations that compose the CZ sequence cannot be correlated across the two survey areas, they represent chronostratigraphic equivalents of each other.

5.4.1. Thebe 3D

Two systems of polygonal faults are identified in Thebe 3D (Fig. 8a), an older system within the LC sequence (LC system) and a younger system that spans both the UC and CZ sequences (UC-CZ system). These polygonal fault systems extend laterally throughout the survey area.

Two fault tiers are identified within the LC system where the lower tier consists of the Barrow Group Formation and the upper tier consists of the Muderong Shale Formation (Figs 8a and 8c). First order faults propagate across both the Barrow Group and Muderong Shale formations while second order faults are isolated within the individual tiers. First order faults have a maximum throw of 30 m and second order faults have and maximum throw of 18 m.

The UC-CZ system consists of three tiers and is separated from the LC system by the Windalia Radiolarite Formation. The lowest tier consists of Late Cretaceous Gearle Siltstone, Toolonga, Miria and Korojon formations, while the middle and upper tiers consist of the Girilia and Cardabia formations of the Paleogene (Figs 8a and 8b). Three orders of faults are identified; first order faults extend across all three tiers, second order faults extend across either the younger or older two tiers, and third order faults are isolated to individual tiers. The maximum fault throw measurements are 38 ms for first order faults, 18 ms for second order faults and 8 ms for third order faults.

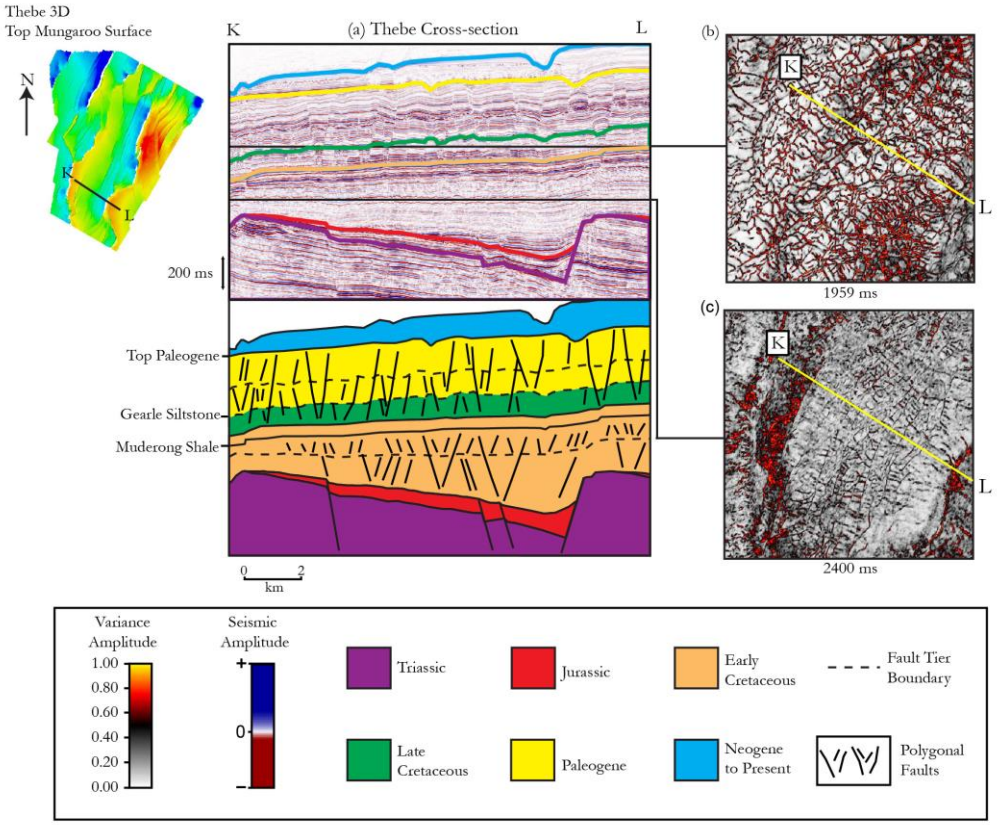

***Figure 8**: Polygonal fault system in Thebe 3D. (a) shows cross-section K-L with major horizons interpreted, and a schematic illustrating the sets and tiers of polygonal faults. b) Time slices of the variance attribute show the polygonal patterns of fault intersections within the Gearle Siltstone formation, whereas c) shows the Muderong Shale and Barrow Group formations.*

5.4.2.Io-Jansz 3D

Three systems of polygonal faults are identified in the Io-Jansz 3D survey. The oldest system is identified within the LC sequence (LC system), with a younger system identified in the UC sequence (UC system) and the youngest system is identified within the CZ sequence (CZ system) (Fig. 9a). Due to erosion of the LC, UC and CZ sequences in the north-eastern parts of the survey area, mapping of

the polygonally faulted sequences is constrained to the south-western and central regions of Io-Jansz 3D.

Two tiers are identified within the LC polygonal fault system. The lower tier consists of the Barrow Group Formation while the upper tier consists of the Muderong Shale Formation (Figs 9a and 9d). First order faults extend from the base of the Barrow Group to the top of the Muderong Shale Formation while second order faults are identified within each tier. We observe a higher fault density in the lower tier as compared to the upper tier. The maximum fault throws are 20 ms for first order faults and 12ms for second order faults.

The UC polygonal fault system is also comprised of two fault tiers, both occurring within the Gearle Siltstone Formation. This system is separated from the LC system by the Windalia Radiolarite Formation (Figs 9a and 9c). Similar to the LC system, first order and second order faults were identified, however; where the Windalia Radiolarite Formation is thin, some first order faults from the UC system are documented to dip-link with first order faults from the LC system. The maximum throw of first order faults is 30 ms while the maximum throw of second order faults is 10 ms. Polygonal fault density is observed to vary with the UC sequence thickness. From the southwest towards the central area, over a distance of 47 km, the UC sequence thickness decreases from 1100 m to 450 m (before being completely eroded further northeast) while polygonal fault density increases from 2.5 to 5.5 faults per km2.

The CZ system of polygonal faults is limited to a narrow region of the Io-Jansz 3D survey area. This is due to the Walcott, Wilcox, and Dockrell formations having been eroded in the southwest and northeast of the survey area (Figs 9a and 9b). Where identified, the CZ and UC systems are vertically separated from each other by a layer of undifferentiated, erosional deposits that are not polygonally faulted. Two tiers of faults are identified with the lower tier consisting of the Dockrell Formation, while the Wilcox and Walcott formations make up the upper tier. We observe a higher density of second order faults in the lower tier than in the upper tier. The maximum throw of first order faults is 26 ms and 12 ms for second order faults.

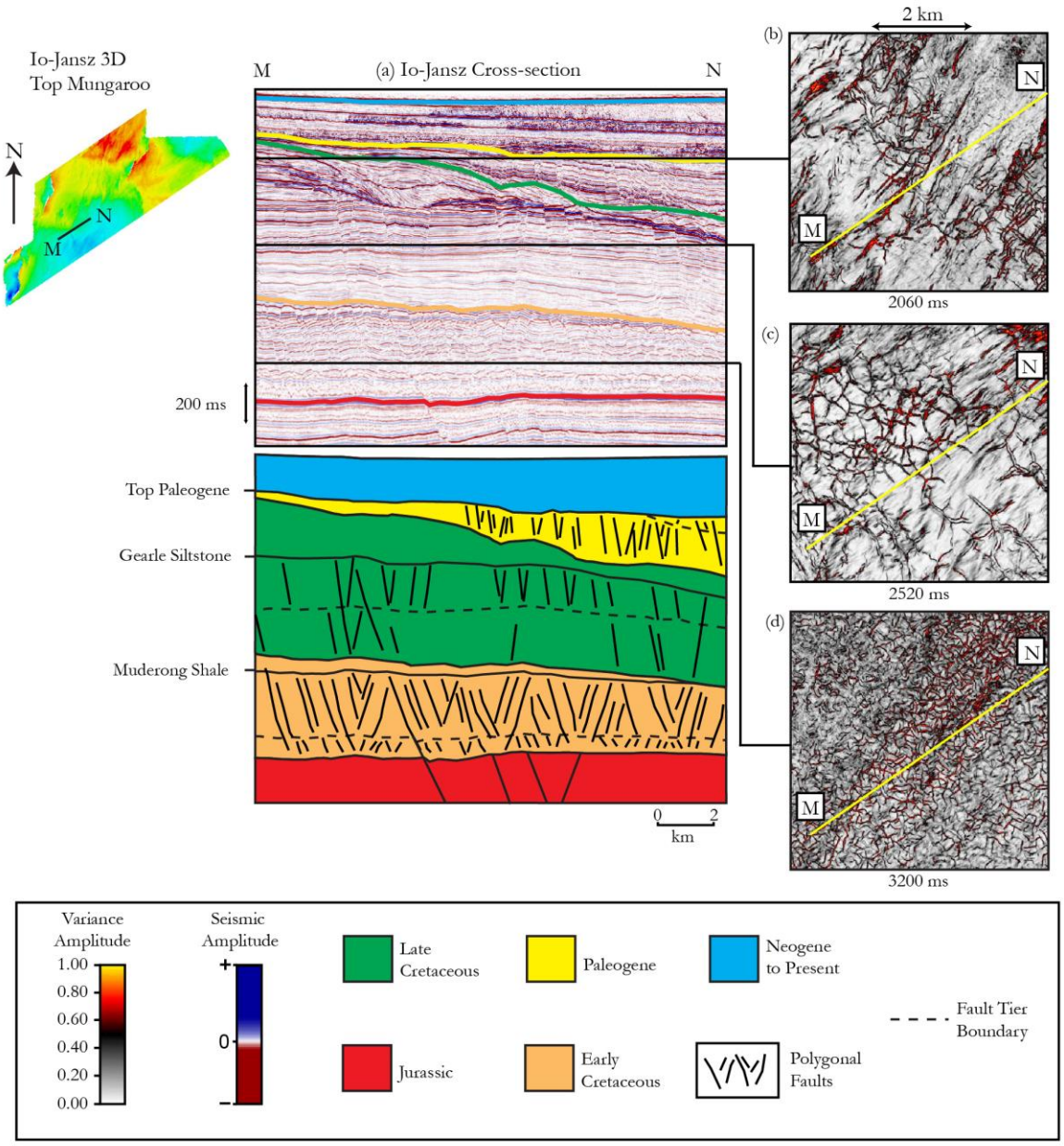

***Figure 9**: Polygonal fault system in the Io-Jansz 3D. a) shows cross-section M-N with major horizons interpreted, and a schematic illustrating the sets and tiers of polygonal faults. b) Time slices of the variance attribute show the polygonal patterns of fault intersections within the Paleogene sequence, whereas c) shows the Gearle Siltstone formation and d) shows the Muderong Shale and Barrow Group formations.*

6. Discussion

Focused fluid flows are phenomena associated with fluid migration from deeper to shallower depths through a focusing mechanism. They provide valuable information of subsurface fluid dynamics, as

well as insights into fluid migration pathways. In this study we document ancient focused fluid flow features, expressed on seismic data as 'crater-like' depressions along the Top Jurassic surface with underlying VDZs within the Jurassic and Triassic sequences of the two seismic surveys. We also document tiered polygonal fault systems that are often associated with focused fluid expulsion and have the potential to influence subsurface fluid dynamics as migration pathways. We discuss the mechanisms that form the 'crater-like' depressions, VDZs, and polygonal faults, along with the implication of their presence on hydrocarbon migration.

6.1. Interpretation of 'crater-like' depressions and VDZs

The VDZs are interpreted to represent conduits for vertical fluid migration while their overlying elliptical, crater-like depressions are interpreted to be paleo-pockmarks (Cartwright et al., 2007; Løseth et al., 2009; Moss & Cartwright, 2010). The distortion or downward sag of seismic reflectors within the VDZs can be attributed primarily to velocity variations or seismic processing artefacts as opposed to disruption or deformation of the strata (Cartwright et al., 2007; Gay et al., 2007; Løseth et al., 2011). Experimental work by Bull et al. (2018) suggests that fluid escape pipes consist of localized connected fracture systems which are then exploited by fluids to migrate through to shallower depths. The increased anisotropy from the fracture sets within the fluid escape pipe, relative to the surrounding stratigraphy, could then result in a decrease seismic velocity, which then results in a localized 'pull-down' effect on seismic reflectors.

Seismic processing of the Io-Jansz 3D and Thebe 3D surveys were optimized to image hydrocarbon reservoirs at depth intervals similar to those of where the VDZs are identified, making it unlikely that the VDZs are data processing artefacts. In the Io-Jansz 3D, the imaging target is at approximately 3.0s TWT while the VDZs are identified within 3.3–3.7s TWT. In the Thebe 3D, the imaging target of interest is at approximately 2.5s TWT while the VDZs are identified within 2.4–2.8s TWT. There are also no geological structures or seismic anomalies that overly the VDZs to suggest that the VDZs are residual artefacts of imaging the overburden.

Løseth et al. (2011) modelled the seismic expression of a vertical fluid migration conduit by a representing the conduit as a column of low velocity. In their model, a pipe, representing VDZs, was embedded in a sequence of horizontal stratigraphic layers that represent the background. The material within the pipe was varied with different acoustic impedance contrasts between the pipe and the background. Synthetic seismic data was then generated and processed. The results of their study describe the seismic expression of low velocity columns as a "vertical disruption of the seismic reflectors abruptly terminating against the column". VDZs in this study show similar characteristics to the modelling results described by Løseth et al. (2011) supporting our interpretation that the VDZs are fluid migration conduits.

Variation in the sizes and seismic expressions between the four types of VDZs and their paleo-pockmarks are influenced by factors such as volume and rate of fluid flow, the mechanical properties of host sediments and fluid types (Hovland & Judd, 1988; Judd & Hovland, 2007; Andresen, 2012). While the genesis of the VDZs as a whole is discussed in later sections of this paper, information on the aforementioned parameters are not known for this study. As a result, we are not able to constrain the cause of variation in the seismic expressions between the four types of VDZs.

6.2. Genesis of Fluid Flow Features in Relation to Faults

The VDZs in both 3D surveys formed in linear trends that occur parallel to the minor faults and lie within graben bounded by the minor faults. These two observations suggest that the minor faults have exerted a structural control on the genesis of VDZs. Studies have documented pockmarks with underlying pipes on seismic data, similar to the VDZs, whose roots that originate at the upper tips of fault planes, indicating the faults were functioning as conduits or fluid migration pathways (Cartwright et al., 2007; Gay et al., 2007; Løseth et al., 2009; Huuse et al., 2010). In this study however, upper tips of the minor faults terminate along the Top Jurassic horizon and the pockmarks are laterally offset from them along the surface. The shortest distances between pockmarks and the nearest minor fault along the Top Jurassic horizon range from 170 to 450 m in the Thebe 3D and 450 to770 m in the Io-Jansz 3D. No VDZs or pipes were observed within the Cretaceous sediments that overlie the Top Jurassic horizon. Upon closer analysis of the minor faults and VDZs on seismic cross-sections, we observe the roots of several VDZs (7 in Io-Jansz 3D and 7 in Thebe 3D) intersecting planes of the minor faults within the Triassic Mungaroo Formation. Though this intersection is poorly resolved, it is better imaged with the consistent dip attribute. (Figs 7e and 7f). This intersection between VDZs and minor faults is not observed for all VDZs, however it is plausible that a similar relation exits for the remaining VDZs but are below the seismic resolution threshold. The relation between the faults and VDZs, along with the absence of fluid flow features in the sediments overlying the Top Jurassic horizon, suggests that the faults are not acting as fluid migration pathways. The vertical morphology of the fluid flow pipes, which cross-cut the background stratigraphy, suggests that the driving force of fluid migration was high enough to overcome the overburden pressure.

Based on these relations between the VDZs and minor faults, along with the VDZ's morphology, we propose that the minor faults intersected a layer of overpressured fluids that then initiated vertical fluid migration at the point of intersection (Fig. 10). A similar mechanism for fluid migration was used by Maia et al. (2016) and Pilcher & Argent (2007) to explain the occurrence of pockmarks identified in offshore Angola and offshore Gabon. Faults are able to locally alter the stress field and reduce formation permeability, thus inducing hydraulic fracturing of overlying sediments and triggering vertical fluid migration (Pilcher & Argent, 2007; Cartwright & Santamarina, 2015).

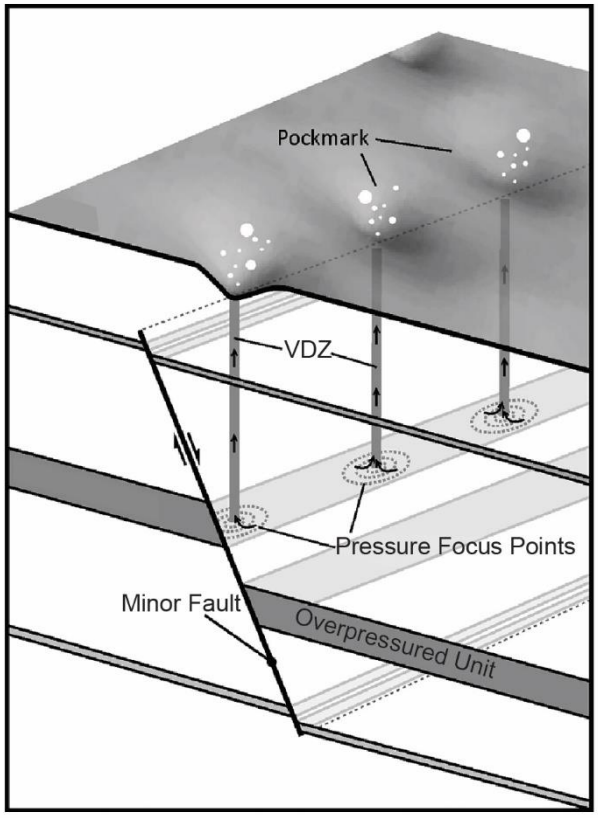

***Figure 10**: Proposed model for the formation of VDZs and paleo-pockmarks in this study (modified after from Maia et al., 2016).*

6.3. Timing of VDZ and Paleo-Pockmark Formation

In both the Thebe 3D and Io-Jansz 3D surveys, the shallowest termination of VDZs and minor faults are along the Top Jurassic horizon. No VDZs or paleo-pockmarks were identified in the overlying Cretaceous sequence, indicating that the VDZs had formed prior to its deposition. The fluid expulsion event that formed the paleo-pockmarks are interpreted to have occurred as a solitary event as opposed to being an episodic or interrupted release of fluids. Moss & Cartwright (2010) and Andresen & Huuse (2011) document vertically stacked successions of pockmarks that indicate episodic fluid expulsion where the expulsion rates are up to 10 Ma and 1.8 Ma respectively. The absence of vertically stacked paleo-pockmarks in our study area agrees with our interpretation of a solitary fluid expulsion event. These observations suggest that the paleo-pockmarks and VDZs had formed during the Late Jurassic and Early Cretaceous, i.e. after deposition of the Jurassic sediments but prior to deposition of the Early Cretaceous Barrow Group sequence.

Timing of the formation of minor faults was constrained using isochron thickness maps that were generated for the Thebe 3D and Io-Jansz 3D surveys. Abrupt lateral variation of time thickness values in orientations parallel to fault strike on isochron maps can be used as indicators of fault growth within a time interval, i.e. the larger the time thickness variation, the larger the fault displacement. In

the Thebe 3D survey, isochron maps of the Jurassic and Lower Cretaceous sediments were generated using the Top Mungaroo, Top Jurassic and Top Muderong Shale horizons (Figs 11a and 11b). The Jurassic isochron map shows lateral variation in time thickness of up to 280 ms (450 m) across Group A faults, while there is no change in time thickness values across Group B faults. On the Early Cretaceous isochron map, variations in time thickness of up to 200 ms (320 m) is observed across Group A faults and 100 ms (160 m) across Group B faults. The observation that minor fault displacement was absent in the Jurassic isochron map but is present in the Cretaceous isochron map constrains the timing of minor fault growth to be approximately between the Kimmeridgian (early Late Jurassic) and the Berriasian (Early Cretaceous).

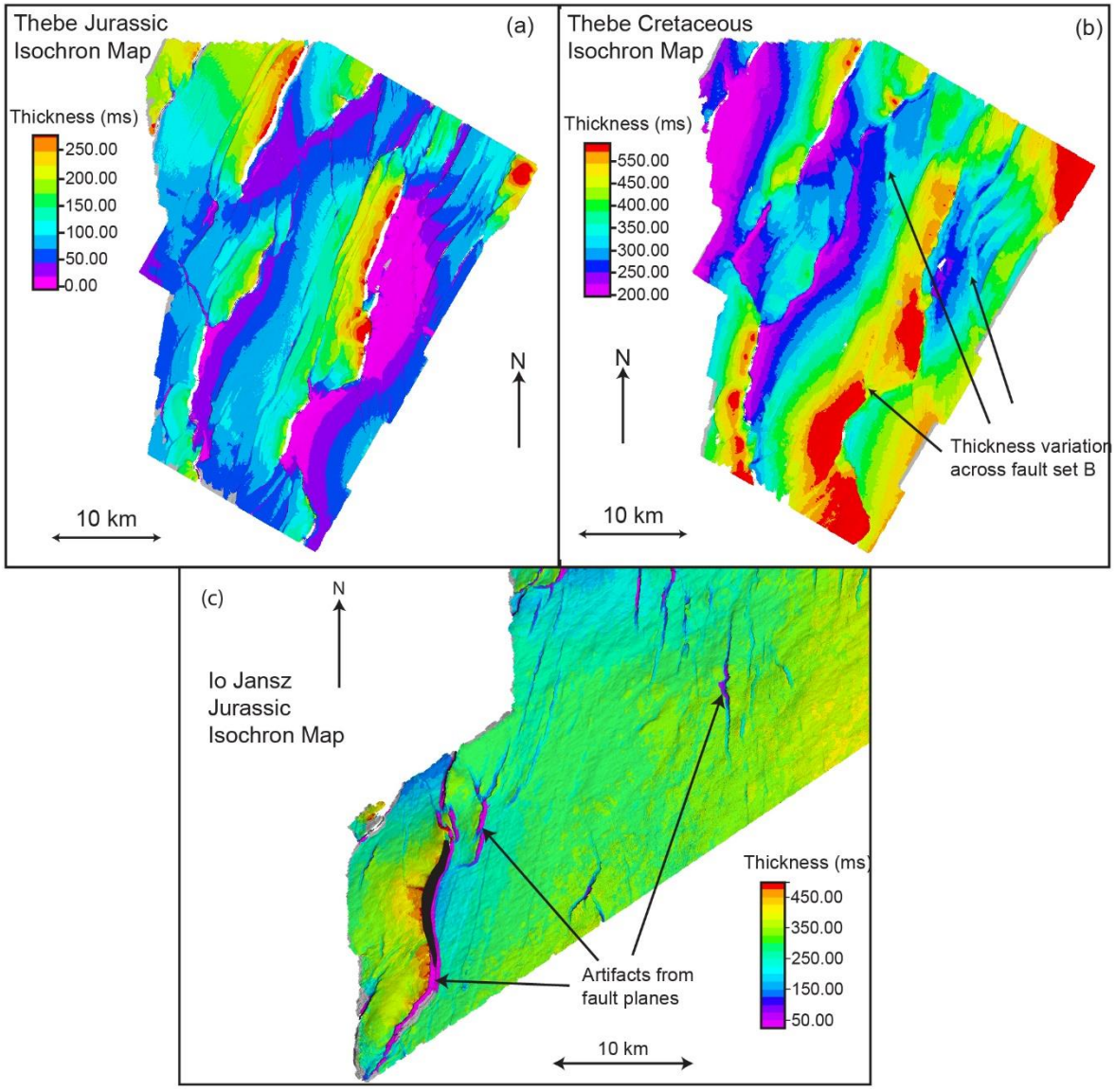

Figure 11: *Isochron thickness maps of the Thebe 3D a) Jurassic and b) Cretaceous sequences and Io-Jansz 3D c) Jurassic sequence.*

In the Io-Jansz 3D survey, an isochron map of the Jurassic sediments was generated with the Top Jurassic and Top Muderong Shale. The isochron map shows variation in time thickness of up to 350 ms (560 m) across Group C faults and little to no time thickness variation across the minor faults (Fig. 11c). An isochron map was generated for the Cretaceous sequence, using the Top Muderong Shale and Top Jurassic; however, time thickness variation due to the minor faults were overprinted by thickness variations from polygonal faults (up to 50 ms) in the Early Cretaceous sediments overlying the Jurassic sediments. As such variations in time thickness associated with the minor faults could not be accurately determined through isochron mapping. The timing of minor fault displacement in the Io-Jansz 3D was instead determined from interpretation of seismic cross-sections. Minor fault interpretations show that the faults intersect and displace the Top Brigadier and Top Jurassic horizons, however; they do not extend into the overlying Cretaceous sediments (Fig. 7f). Furthermore, there is no observed variation in stratal thickness within the Jurassic sequence adjacent to the minor faults to suggest syn-depositional fault development. These observations on stratigraphic extent of minor faults, as well as Jurassic sequence stratal thicknesses, suggests that the faults had formed after the deposition of the Jurassic sedimentary rocks and prior to the deposition of the Cretaceous sediments. We thus constrain the timing of minor fault formation in the Io-Jansz 3D to be between the Kimmeridgian and the Berriasian, similar to those of the Thebe 3D. The timing of minor fault formation in both surveys can be related to the regional tectonic activity of the Northern Carnarvon Basin. During the Late Jurassic and Early Cretaceous, sea-floor spreading had initiated to the west and southwest of the Exmouth Plateau (Haq et al., 1992; Longley et al., 2002).

Similar minor faults located along the western edge of the Exmouth Plateau were documented by Velayatham et al. (2018) with the Claudius 3D seismic survey. The strike orientations of the minor faults from these three surveys are observed to have an approximate radial trend when plotted onto a map (Fig. 12e). Across a distance of approximately 305 km between the Claudius 3D and Io-Jansz 3D, (160 km between Claudius 3D and Thebe 3D, 145 km between Thebe 3D and Io-Jansz 3D), the bearing of minor fault strikes changes from 347° in the Claudius 3D, to 356° in the Thebe 3D and to 15° in Io-Jansz 3D. An extrapolation of these strike indicates that the “locus” of the radial trend is situated along the southern margin of the Exmouth Plateau. The southern margin of the Exmouth Plateau contains a well-documented Late Jurassic-Early Cretaceous igneous province (Holford et al., 2013; Rohrman, 2013, 2015; Magee et al., 2016). Rohrman (2013) and Rohrman (2015) suggest that this magmatism could be linked to mantle plume activity that was active between the Callovian and Valanginian. Reeve et al. (2016) suggest, however, that the mantle plume model is not plausible due to the lack of evidence for voluminous magmatism onshore during the Early Cretaceous and the absence of a present-day plume whose path could be reconstructed to the southern margin of the Exmouth Plateau. Nevertheless, the time frame of inferred mantle plume activity is coeval with the formation of minor faults, and suggests a possible genetic link between the two.

Variance slices within the Triassic sequence that underlie the minor faults (3.4 s in Thebe and 4.5 s in the Io-Jansz 3D) reveals linear features that are parallel to the strike of minor faults within each survey area (Figs 12a and 12c). The strikes of these linear features also have a regional scale radial trend across the two survey areas, with orientations that change from 356° in the Thebe 3D to 15° in the Io-Jansz 3D over a distance of 145 km. On seismic cross-sections, these linear features are imaged as vertical zones of low seismic amplitudes in Io-Jansz 3D and vertical zones of incoherent seismic reflectors in Thebe 3D. The cross-section expressions of the linear features are similar to those of igneous dykes identified in the Bass Basin, offshore southeast Australia (Holford et al., 2017). These observations suggest that the linear features may be igneous dykes, potentially sourced from the proposed mantle plume along the Exmouth Plateau's southern margin.

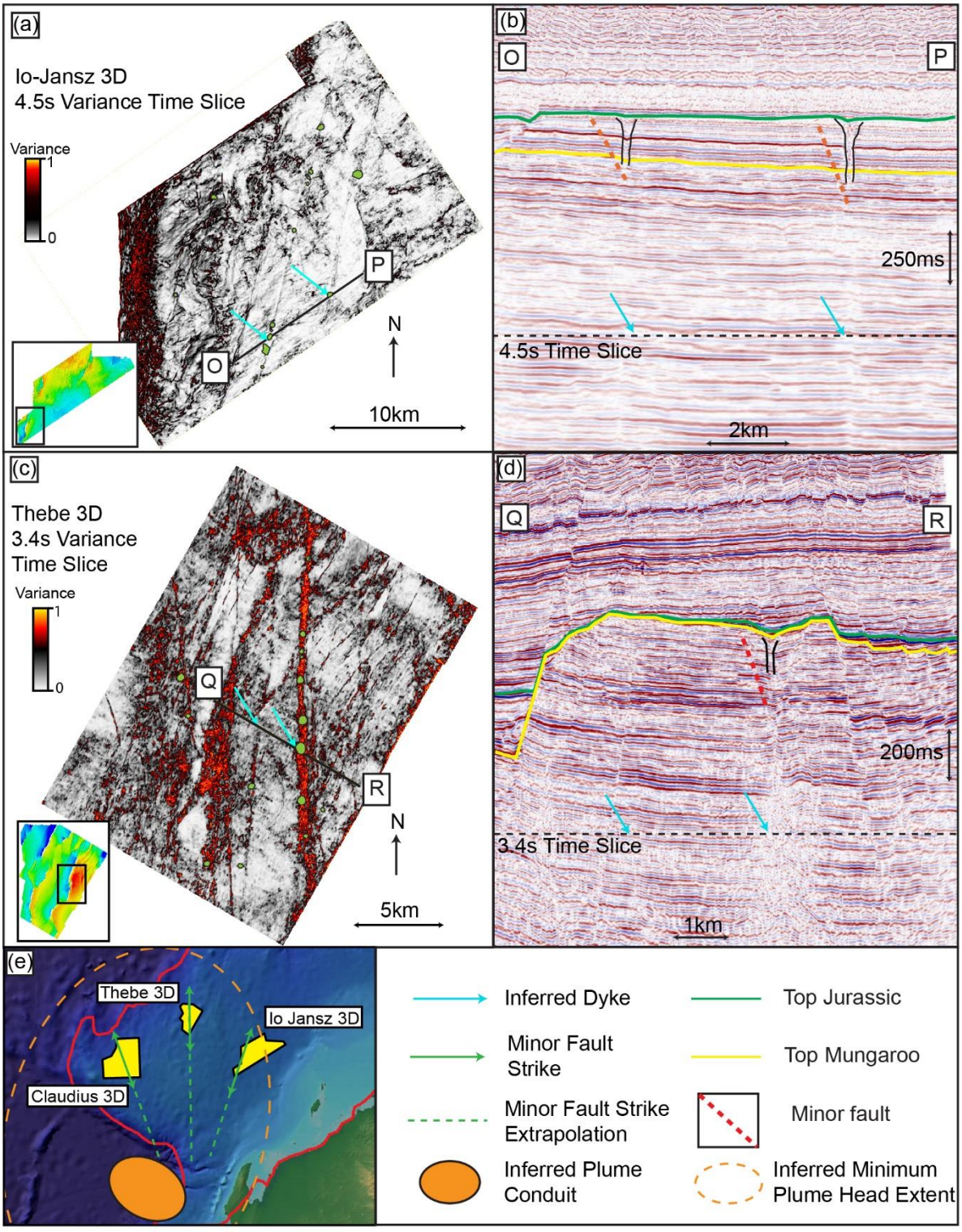

Figure 12: *Variance time slices and seismic cross sections of Io-Jansz 3D (a and b) and Thebe 3D (c and d) that show inferred dykes in the Triassic sequences. e) Radial trend of minor fault strikes can be extrapolated to a locus along the southern Exmouth Plateau margin where Rohrman (2015) suggests a mantle plume was active in the Late Jurassic.*

6.4. Overpressure Mechanism and Fluid Source

The intersection of the VDZ roots and minor fault planes in the Triassic Mungaroo Formation suggest that the fluids which formed the VDZs were sourced from the Mungaroo Formation itself. The Mungaroo Formation is evidenced to have present day overpressured sequences in parts of the Northern Carnarvon Basin, however; these pressures do not reflect the paleo-pressure regime. Overpressures often occur in sediments with low permeabilities; however, these sediments are not absolutely impermeable and overpressure compartments can leak (Luo & Vasseur, 2016). Over geological time, the physical properties of an overpressured sequence may evolve and result in an increase or decrease of overpressure dissipation rates (Luo & Vasseur, 2016). Thus present day pressure magnitudes within a sequence may not be the same as paleo-pressure magnitudes (Tingate et al., 2001; Luo & Vasseur, 2016). Studies of overpressure within the Mungaroo Formation in the Northern Carnarvon Basin propose two potential sources of contemporary overpressure; disequilibrium compaction and fluid expansion from hydrocarbon generation (Tingate et al., 2001; Van Ruth et al., 2004). We note that these studies are focused on the Jurassic sub-basins (Exmouth, Barrow and Dampier) as there are a limited number of pressure measurements from the Mungaroo Formation on the Exmouth Plateau.

Overpressure generation from disequilibrium compaction is often associated with sedimentary basins that have high sedimentation rates (>100 m / Ma) such as the Gulf of Mexico (Mudford & Best, 1989). Modelling results by Yu & Lerche (1996) however suggest that the host rock lithology can be a key factor of overpressure generation in regions with lower sedimentation rates. For instance, a shale dominated section with sedimentation rates of 50 m/Ma can develop overpressures at approximately 2000 m below mudline. The Mungaroo Formation is documented to be up to 6 km thick on the Exmouth Plateau having had sedimentation rates of up to 50 m/Ma (Powell et al., 1982; Adamson et al., 2013). Based on lithological descriptions of ditch cutting and rotary side-wall core data from Thebe-1, Thebe-2 and Zagreus-1, sediments of the Mungaroo Formation are interpreted to consist of deltaic to marginal marine sequences that predominantly consist of claystone or sandstones with interbedded claystones. The documented sedimentation rate and fine-grained sediment composition, suggests that disequilibrium compaction is a plausible mechanism for local overpressure generation within the Mungaroo Formation on the Exmouth Plateau.

Alongside disequilibrium compaction, overpressure generation from hydrocarbon generation is another potential source of overpressure generation within the Mungaroo Formation (Tingate et al., 2001). The Triassic Mungaroo Formation is a regionally recognized hydrocarbon source unit and has been documented to be overpressured in parts of the Northern Carnarvon Basin (Tingate et al., 2001; Ruth et al., 2004). This suggests that overpressure development within the Mungaroo Formation

through hydrocarbon generation is a plausible hypothesis to explain the formation of paleo-focused fluid flows identified in this study. We test the hypothesis of hydrocarbon generation as a fluid source and fluid expansion as a contributor to the paleo-overpressure generation with burial history modelling based on the geology of Io-Jansz 3D survey (Fig. 13). The 1D model consists of the Jurassic and Triassic sequences represented by the Athol, Brigadier and Mungaroo formations. Total organic carbon content of 2.0% was used for the Mungaroo Formation, based on a study by He & Middleton (2002) that averaged 1043 Mungaroo Formation samples from the Northern Carnarvon Basin. Assigned heat flow values are 70mW/m2 for the mid-Jurassic, and 55 W/m2 for the base of the model, with a smooth gradient in between, based on heat flow modelling by He & Middleton (2002).

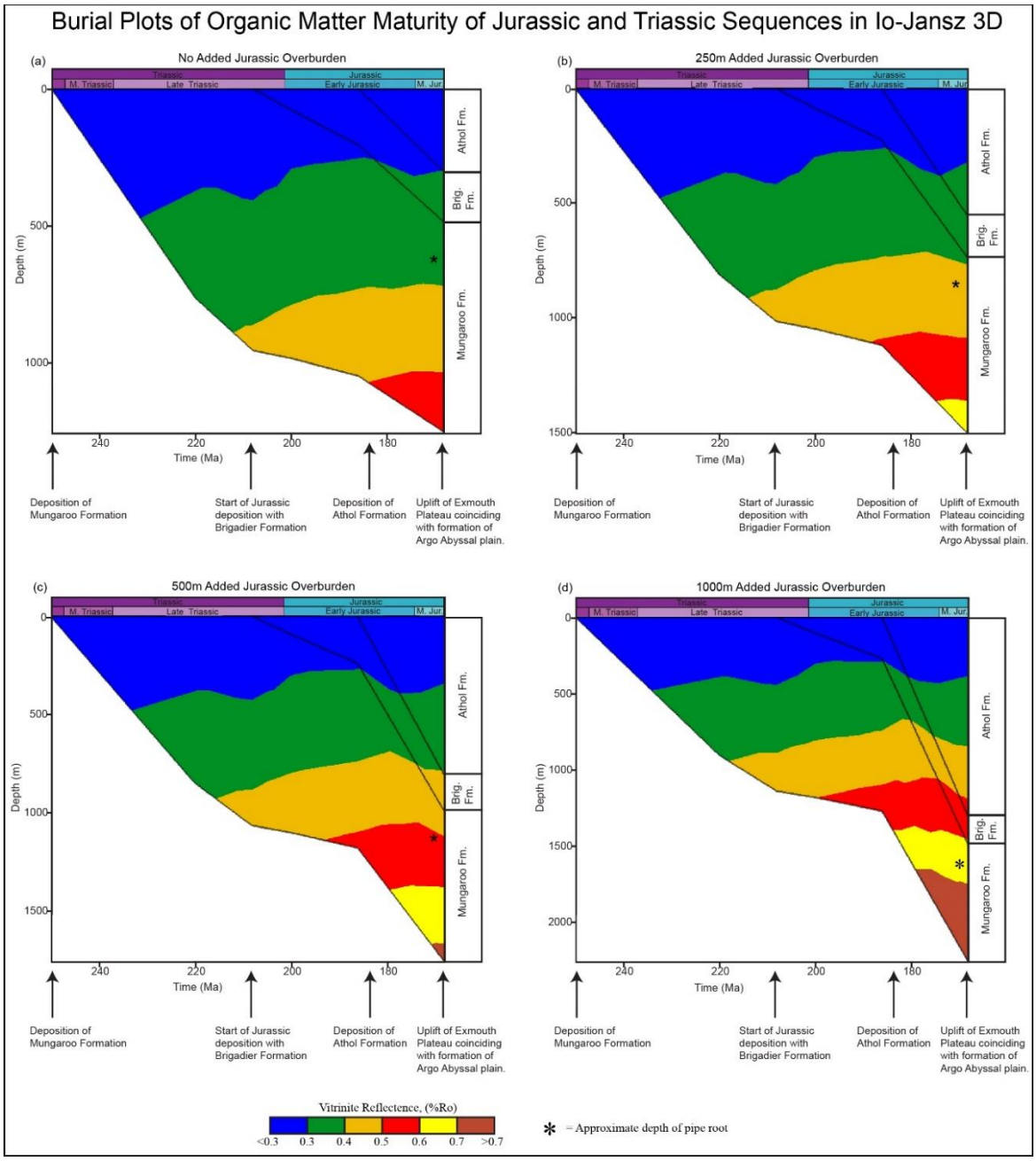

Figure 13: *Burial plot from 1D modelling of organic maturity within the Mungaroo Formation.*

The modelling results show that at depths corresponding to the roots of the VDZs in Io-Jansz 3D, the vitrinite reflectance is between 0.3-0.4 % (Fig. 13a). While these values suggest that the organic matter is immature for hydrocarbon generation (Fig 13; Burnham & Sweeney, 1989; Carr, 2000), it should be noted that this model uses the eroded Top Jurassic for the top of the model, not accounting for the Jurassic sediments that would have been eroded during the uplift of the Exmouth Plateau. Though the extent of erosion is uncertain, we test the effect of a hypothetically thicker Jurassic overburden on organic matter maturity within the Triassic sequence. Upon adding 250m, 500m, and 1000m to the Jurassic sequence thickness, modelled vitrinite reflectance values at depths corresponding to the roots of VDZs are approximately 0.45, 0.52 and 0.68% respectively (Figs 13b, 13 c and 13d). Burnham & Sweeney (1989) suggest that oil generation for typical marine source rocks starts at vitrinite reflectance values of 0.5-0.65%, thus it is plausible that the presence of a thicker Jurassic sequence would have further promoted hydrocarbon generation and potentially contributed to overpressure generation.

Regional uplift of the plateau and overburden erosion can induce the generation of overpressures by altering effective stress conditions with sedimentary rock sequences. Corcoran & Dore (2002) suggest that the removal of overburden during uplift, without re-equilibration of pore-pressures could lower the effective stresses and induce hydraulic fracturing. Furthermore, Katahara & Corrigan (2002) indicate that the presence of gas in a rock unit that is experiencing erosional unloading tends to induce overpressures.

The burial history modelling results presented here, together with results from studies by Corcoran & Dore (2002) and Katahara & Corrigan (2002), suggest that the hypothesis of hydrocarbon generation being a fluid source as well as contributor to overpressure generation is plausible. The modelling study of Yu & Lerche (1996) along with the documented sedimentation rates and lithologic composition of the Mungaroo Formation also indicate that overpressure generation within the sequence through disequilibrium compaction is also a viable hypothesis. Without sufficient direct measurements of the Triassic formation in the Exmouth Plateau however, the exact overpressure mechanism and fluid content of the VDZs cannot be determined in this study.

7. Implications for Hydrocarbon Exploration on the Exmouth Plateau

The Northern Carnarvon Basin is a well-developed hydrocarbon exploration region with exploration focused on the Barrow, Dampier, Exmouth and Beagle sub-basins. In recent years, exploration over the Exmouth Plateau has increased, focusing on plays associated with the Triassic Mungaroo Formation. The primary play type across the Exmouth Plateau revolves around hydrocarbon migration

from Mungaroo Formation source rocks to shallower reservoirs via faults that are able to access the deeper source rocks (Longley et al., 2002). In this study, we expand on this play type by developing an improved understanding of fluid migration events whereby the faults act as a trigger for fluid migration. It its plausible that the faults had also acted as fluid migration pathways, however, we find no evidence to support this hypothesis within the two seismic surveys.

The findings of this study have both positive and negative ramifications for hydrocarbon exploration. If the VDZs were formed by hydrocarbons, they may be indicative of regions with working petroleum systems. In addition to this, once the VDZs and paleo-pockmarks have been buried and preserved, they can act as potential fluid migration pathways for deeper sourced fluids. If the VDZs occur within a seal unit however, they could compromise the seal integrity by functioning as conduits from which hydrocarbons in an underlying reservoir could leak out from.

The potential presence of igneous dykes within the Mungaroo Formation (Rohrman, 2013) could increase exploration risk within the area, by acting as impermeable barriers to hydrocarbon migration within the Mungaroo Formation. Dykes have been documented as causing compartmentalization of source and reservoir sequences in the Bass Basin, offshore south-east Australia and the Faroe-Shetland Basin in the NE Atlantic Margin (Holford et al., 2013; Holford et al., 2017).

Polygonal faults within the Northern Carnarvon Basin have previously been documented at the Gorgon Platform to the south of the Rankin Trend (McCormack & McClay, 2013); however, there is limited systematic documentation of polygonal fault systems on the Exmouth Plateau. The polygonal faults identified in this study occur within similar or chronostratigraphically equivalent sequences to those identified in McCormack & McClay (2013). Tier 1 and Tier 2 polygonal faults of McCormack & McClay (2013) occur within the equivalent Lower Cretaceous sequence of this study that consists of the Barrow Group and Muderong Shale formations, while Tier 3 polygonal faults of McCormack & McClay (2013) occur within the equivalent Upper Cretaceous sequence of this study that consists of the Gearle Siltstone, Tooloonga Calcilutite, Korojon Calcilutite and Miria formations. Unlike in this study however, McCormack & McClay (2013) did not document polygonal faults within the Girilia and Cardabia formations of the Cenozoic sequence. Polygonal fault throws observed in this study (8-38ms TWT) also show a similar range of offsets with those of MCMC (10 – 25ms TWT).

8. Potential Impact of Tiered Polygonal Fault Systems on Subsurface Fluid Dynamics

Several models have been proposed for the origins of polygonal faults, and the most widely used model is of sediment dewatering due to compaction or dissolution of water bearing minerals (Cartwright & Dewhurst, 1998; Cartwright et al., 2003; Seebeck, 2015). Berndt et al. (2003)

document fluid escape features, similar to the VDZs of this study, overlying polygonal faults along the mid-Norwegian margin. The study concluded that the source of fluids was expulsion from the host rock due to dewatering during the formation of polygonal faults. In this study however, we observe no indication of focused either fluid migration within or overlying polygonal fault systems identified in the Io-Jansz 3D and Thebe 3D surveys.

Though not implicitly associated with fluid expulsion, the polygonal faults identified in this study have the potential to play a critical role in influencing subsurface fluid dynamics and hydrocarbon exploration as fluid migration pathways. This has been argued by Seebeck et al. (2015) who investigated the impact of polygonal faulting on seal integrity in the Petrel Sub-basin of the Bonaparte Basin of the North West Shelf. In their study, Seebeck et al. (2015) identified polygonal faults within the Early to Late Cretaceous Bathurst Island Group (BIG), which predominantly consists of marine mudstones. The BIG sequence acts a regional seal within the Petrel Sub-basin for underlying Jurassic to Early Cretaceous reservoirs. Though predominantly constrained to occur within the BIG group, polygonal faults were also observed to extend into underlying Jurassic reservoir formations by Seebeck et al. (2015). Their study also identified columnar seismic anomalies, interpreted to be gas chimneys, that rise along normal faults within the Jurassic sequences and through the BIG sequence up to the seabed (Seebeck et al., 2015). Their study suggests that there is potential connectivity between polygonal faults and the Jurassic normal faults to facilitate fluid migration from the Jurassic sequences into the BIG formation, and then through the sequence via polygonal faults (Seebeck et al., 2015).

The seal, reservoir and fluid migration petroleum systems elements described by Seebeck et al. (2015) in the Petrel Sub-Basin are somewhat analogous to those of the Jansz-Io field within this study area. Though hydrocarbons in Thebe are reservoired within the Triassic Mungaroo Formation, hydrocarbons in Jansz-Io are reservoired within Jurassic-age sandstones that are overlain by polygonally faulted Early Cretaceous Barrow Group and Muderong Shale formations that act as a regional seal (Kovack et al., 2004; Jenkins et al., 2017). Fault mapping in our study shows that there is a potential for vertical connectivity between normal faults within the Jurassic sequence and the polygonal faults of the Barrow Group and Muderong Shale Formation (Fig 7, Fig 8, Fig 9). Such fault connectivity could act as fluid migration pathways that hydraulically connect Mungaroo Formation sourced hydrocarbons with shallower formations that overlie the Muderong shale. Seal integrity for the Jansz-Io field does not seem to have been compromised by polygonal faults within the Barrow Group and Muderong Shale formations, as no focused fluid flows have been documented to be associated with polygonal faults overlying the reservoir (Jenkins et al., 2017). Nevertheless, the occurrence of polygonal faults within the regional seal formation could imply an increase seal risk associated with hydrocarbon plays across the Exmouth Plateau that are similar to Jansz-Io

9. Summary and Conclusions

In this study, we document previously undescribed focused fluid flow features in the Triassic and Jurassic sequences in the Exmouth Plateau of the Northern Carnarvon Basin. Also documented are tiered polygonal fault systems within the Cretaceous and Cenozoic sequences of the Exmouth Plateau. A total of 40 paleo-pockmarks are identified along the top of the Jurassic sequence with underlying fluid flow conduits that extend into the Triassic sequence. The focused fluid flow features form linear trends that are parallel to low-displacement normal faults in each survey; a NE-SW trend in Io-Jansz 3D and a NNW-SSE trend in Thebe 3D. The faults extend from the top of the Jurassic sequence into the Mungaroo Formation with the paleo-pockmarks laterally offset from the faults along the Top Jurassic horizon. The low throw faults are interpreted to have intersected an overpressured sequence within the Mungaroo Formation. The intersection with the overpressured sequence locally reduced the lithostatic overburden pressure, which then focussed the fluids to migrate vertically. Neither the mechanism that generated the overpressure or the nature of the fluids could be determined in this study. Overpressure studies in the Northern Carnarvon Basin narrow down the likely mechanisms to either fluid expansion of hydrocarbon, or undercompaction. The strikes of the minor faults exhibit a radial trend on regional scales, and are potentially linked to underlying dyke intrusions. The proposed model of paleo-fluid migration improves our understanding of subsurface fluid dynamics and can be utilized in evaluating petroleum system elements in the area. Though no fluid escape features were identified to be associated with the polygonal fault systems, they nevertheless have the potential to influence fluid migration as migration pathways and impact risk assessment in hydrocarbon exploration.

10. Acknowledgements

The authors would like to thank Geoscience Australia for providing the open file 3D seismic and well data that was used in this study. We also acknowledge Schlumberger (Petrel and PetroMod), Ikon Science (RokDoc), and CGG GeoSoftware (Jason Workbench) of provision of the software necessary for the data analysis. This research is supported by ARC Discovery Project DP1601158.

11. References

ADAMSON, K.R., LANG, S.C., MARSHALL, N.G., SEGGIE, R.J., ADAMSON, N.J. & BANN, K.L., 2013, Understanding the Late Triassic Mungaroo and Brigadier Deltas of the Northern Carnarvon Basin, North West Shelf, Australia, in KEEP, M. & MOSS, S.J. (Eds), The Sedimentary Basins of Western Australia IV, Proceedings of the Petroleum Exploration Society of Australia Symposium, Perth, 2013, 29 pp.

AGSO North West Shelf Study Group 1994, Deep Reflections on the North West Shelf: Changing perceptions of Basin Formation, in PURCELL, P.G. & PURCELL, R.R. (Eds), The Sedimentary Basins of Western Australia, Proceedings of the Petroleum Exploration Society of Australia Symposium, Perth, 1994, 63–76

AMINZADEH, F., CONNOLLY, D., HEGGLAND, R., MELDAHL, P. & DE GROOT, P., 2002, Geohazard detection and other applications of chimney cubes, The Leading Edge, 21, 681–685.

ANDRESEN, K.J., HUUSE, M. & CLAUSEN, O.R., 2008, Morphology and distribution of Oligocene and Miocene pockmarks in the Danish North Sea : Implications for bottom current activity and fluid migration, Basin Research, 20, 445–466.

ANDRESEN, K.J. & HUUSE, M., 2011, 'Bulls-eye' pockmarks and polygonal faulting in the Lower Congo Basin: Relative timing and implications for fluid expulsion during shallow burial, Marine Geology, 279, 111–127.

ANDRESEN, K.J., 2012, Fluid flow features in hydrocarbon plumbing systems: What do they tell us about the basin evolution? Marine Geology, 332–334, 89–108.

ANKA, Z., BERNDT, C. & GAY, A., 2012, Hydrocarbon leakage through focussed fluid flow systems in continental margins, Marine Geology, 1–3, 332–334.

BARBER, A.J., TJOKROSAPOETRO, S. & CHARLTON, T.R., 1986, Mud volcanoes, shale diapirs, wrench faults, and melanges in accretionary complexes, Eastern Indonesia, AAPG Bulletin, 70, 1729–1741.

BARBER, P.M., 1982, Palaeotectonic evolution and hydrocarbon genesis of the central Exmouth Plateau, The APPEA Journal, 2, 131–144.

BARISTEAS, N., ANKA, Z., DE PRIMIO, R., RODRIGUEZ, J.F., MARCHAL, D. & DOMINGUEZ, F., 2012, Distribution of hydrocarbon leakage indicators in the Malvinas Basin, offshore Argentine continental margin, Marine Geology, 332, 56–74.

BERNDT, C., BÜNZ, S. & MIENERT, J., 2003, Polygonal fault systems on the mid-Norwegian margin: a long-term source for fluid flow, in VAN RENSBERGEN, P., R.H., MALTMAN, A. & MORLEY, C. (Eds), Subsurface Sediment Mobilization, Geological Society of London Special Publication, London, 216, 283–290.

BOYD, R., WILLIAMSON, P. & HAQ, B., 1992, Seismic stratigraphy and passive margin evolution of the southern Exmouth Plateau, in VON RAD, U. & HAQ, B.U. (Eds), Proceedings of the Ocean Drilling Program, Scientific Results, College Station, TX, 122, 39–59.

BULL, J.M., BERNDT, C., MINSHULL, T.A., HENSTOCK, T.J., BAYRAKCI, G., GEHRMANN, R., PROVENZANO, G., BÖTTNER, C., SCHRAMM, B., CALLOW, B., CHAPMAN, M., BIRINCI, H., YILO, N., DEWAR, M., CHEN, B., SALEEM, U., MARIN-MORENO, H., LICHTSCHLAG, A., FALCON-SUAREZ, I., ROCHE, B., JAMES, R., CONNELLY, D.P., MATTER, J., ELGER, J., KARSTENS, J. & BEST, A.I., 2018, Constraining the physical properties of chimney/pipe structures within sedimentary basins, 14th International Conference on Greenhouse Gas Control Technologies, GHGT-14, Melbourne, Australia.

BURNHAM, A.K. & SWEENEY, J.J., 1989, A chemical kinetic model of vitrinite maturation and reflectance, Geochimica et Cosmochimica Acta, 53, 2649–2657.

CARR, A.D., 2000, Suppression and retardation of vitrinite reflectance, Part 1. Formation and significance for hydrocarbon generation, Journal of Petroleum Geology, 23, 313–343.

CARTWRIGHT, J., 1994, Episodic basin-wide hydrofracturing of overpressured Early Cenozoic mudrock sequences in the North Sea Basin, Marine and Petroleum Geology, 11, 587–607.

CARTWRIGHT, J. & DEWHURST, D.N., 1998, Layer-bound compaction faults in fine-grained sediments, Geological Society of America Bulletin, 110, 1242–1257.

CARTWRIGHT, J., JAMES, D. & BOLTON, A., 2003, The genesis of polygonal fault systems: a review, in VAN RENSBERGEN, P., R, R.H., Maltman, A. & MORLEY, C. (Eds), Subsurface Sediment Mobilization. Geological Society of London Special Publication, London, 216, 223–243.

CARTWRIGHT, J. & HUUSE, M., 2005, 3D seismic technology: the geological 'Hubble', Basin Research, 17, 1–20.

CARTWRIGHT, J., HUUSE, M. & APLIN, A., 2007, Seal bypass systems, AAPG Bulletin, 91, 1141–1166.

CARTWRIGHT, J. & SANTAMARINA, C., 2015, Seismic characteristics of fluid escape pipes in sedimentary basins: Implications for pipe genesis, Marine and Petroleum Geology, 65, 126–140.

CATHRO, D.L., AUSTIN, J.A. & MOSS, G.D., 2003, Progradation along a deeply submerged Oligocene–Miocene heterozoan carbonate shelf: How sensitive are clinoforms to sea level variations?, AAPG Bulletin, 87, 1547–1574.

CHEN, D.F., HUANG, Y.Y., YUAN, X.L. & CATHLES, L.M.C., III, 2005, Seep carbonates and preserved methane oxidizing archaea and sulfate reducing bacteria fossils suggest recent gas venting on the seafloor in the Northeastern South China Sea, Marine and Petroleum Geology, 22, 613–621.

CHRISTODOULOU, D., PAPATHEODOROU, G., FERENTINOS, G. & MASSON, M., 2003, Active seepage in two contrasting pockmark fields in the Patras and Corinth gulfs, Greece, Geo-Marine Letters, 23, 194–199.

CORCORAN, D.V. & DORÉ, A.G., 2002, Depressurization of hydrocarbon-bearing reservoirs in exhumed basin settings: evidence from Atlantic margin and borderland basins, Geological Society of London, Special Publications, 196, 457–483.

DIRSTEIN, J.K., HENGESH, J.V. & STANLEY, A.J., 2013, Identification of fluid flow features in the seafloor and subsurface and their Implications for prospect and geohazard Assessment: examples from the Australian Northwest Shelf, in KEEP, M. & MOSS, S.J. (Eds), The Sedimentary Basins of Western Australia IV, Proceedings of the Petroleum Exploration Society of Australia Symposium, Perth, 2013, 21 pp

EXON, N.F. & BUFFLER, R.T., 1992, Mesozoic seismic stratigraphy and tectonic evolution of the western Exmouth Plateau, in von RAD, U. & HAQ, B.U. (Eds), Proceedings of the Ocean Drilling Program, Scientific Results, College Station, 122, 61–81.

EXON, N.F., HAQ, B.U. & von RAD, U., 1992, Exmouth Plateau revisited: scientific drilloing and geological framework, in von RAD, U. & HAQ, B.U. (Eds), Proceedings of the Ocean Drilling Program, Scientific Results, College Station, 122, 3–20.

FREY, Ø., PLANKE, S., SYMONDS, P.A. & HEEREMANS, M., 1998, Deep crustal structure and rheology of the Gascoyne volcanic margin, western Australia, Marine Geophysical Researches, 20, 293–311.

GAY, A., LOPEZ, M., COCHONAT, P. & SERMONDADAZ, G., 2004, Polygonal faults-furrows systemrelated to early stages of compaction – upper Miocene to recent sediments of the Lower Congo Basin, Basin Research, 16, 101–116.

GAY, A., LOPEZ, M., COCHONAT, P., LEVACHE´, D., SERMONDAAZ, G. & SERANNE, M., 2006, Evidence of early to late fluid migration from an upper Miocene turbiditic channel revealed by 3D seismic coupled to geochemical sampling within seafloor pockmarks, Lower Congo Basin, Marine and Petroleum Geology, 23, 387–399.

GAY, A., LOPEZ, M., BERNDT, C. & SERANNE, M., 2007, Geological controls on focused fluid flow associated with seafloor seeps in the Lower Congo Basin, Marine Geology, 244, 68–92.

GEOSCIENCE AUSTRALIA, 2010, Northern Carnarvon Basin Biozonation and Stratigraphy Chart 36.

HANSEN, J.P.V., CARTWRIGHT, J.A., HUUSE, M. & CLAUSEN, O.R., 2005, 3D seismic expression of fluid migration and mud remobilization on the Gjallar Ridge, offshore mid-Norway, Basin Research, 17, 123–139.

HAQ, B.U., BOYD, R.L., EXON, N.F. & von RAD, U., 1992, Evolution of the Central Exmouth Plateau: A post-drilling perspective, in von RAD, U. & HAQ, B.U. (Eds), Proceedings of the Ocean Drilling Program, Scientific Results, College Station, 122, 801–816.

HE, S. & MIDDLETON, M., 2002, Pressure seal and deep overpressure modelling in the Barrow Sub-basin, North West Shelf, Australia, in KEEP, M. & MOSS, S.J. (Eds), The Sedimentary Basins of Western Australia 3, Proceedings of the Petroleum Exploration Society of Australia Symposium, Perth, 2002, 19 pp.

HENGESH, J.V., DIRSTEIN, J.K. & STANLEY, A.J., 2013, Landslide Geomorphology Along the Exmouth Plateau Continental Margin, North West Shelf, Australia, Australian Geomechanics, 48, 71–92.

HOCKING, R.M., 1988, Regional Geology of the Northern Carnarvon Basin, in PURCELL, P.G. & PURCELL, R.R. (Eds), The North West Shelf Australia, Proceedings of the Petroleum Exploration Society of Australia Symposium, Perth, 1988, 97–114.

HOLFORD, S., SCHOFIELD, N., JACKSON, C.A., MAGEE, C., GREEN, P.F. & DUDDY, I.R., 2013, Impacts of igneous intrusions on source and reservoir potential in prospective sedimentary basins along the Western Australian continental margin, in KEEP, M. & MOSS, S. J. (Eds), The Sedimentary Basins of Western Australia IV, Proceedings of the Petroleum Exploration Society of Australia Symposium, Perth, 2013, 12 pp.

HOLFORD, S., SCHOFIELD, N. & REYNOLDS, P., 2017, Subsurface fluid flow focused by buried volcanoes in sedimentary basins: evidence from 3D seismic data, Bass Basin, offshore southeastern Australia, Interpretation, 5, SK39–SK50.

HOVLAND, M. & JUDD, A.G.,1988, Seabed Pockmarks and Seepages : Impact on Geology, Biology and the Marine Environment. Graham and Trotman, London, 293 pp.

HOVLAND, M., CROKER, P.F. & MARTIN, M., 1993, Fault-associated seabed mounds (carbonate knolls?) off western Ireland and north-west Australia, Marine and Petroleum Geology, 11, 232–246.

HUSTOFT, S., DUGAN, B. & MIENERT, J., 2009, Effects of rapid sedimentation on developing the Nyegga pockmark field: constraints from hydrological modeling and 3-D seismic data, offshore mid-Norway, Geochemistry, Geophysics, Geosystems, 10, https://doi.org/10.1029/2009GC002409.

HUUSE, M., JACKSON, C.A., VAN RENSBERGEN, P., DAVIES, R.J., FLEMINGS, P.B. & DIXON, R.J., 2010, Subsurface sediment remobilization and fluid flow in sedimentary basins: an overview, Basin Research, 22, 342–360.

JENKINS, C.C., DUCKETT, A., BOYETT, B.A., GLENTON, P.N., MILLS, A.A., SCHAPPER, M.C. & WILLIAMS, M.A., 2017, The Jansz-Io Gas Field, Northwest Shelf Australia: a giant stratigraphic trap, in MERRIL, R.K. & STERNBACH, C.A. (Eds), Giant fields of the decade 2000–2010: AAPG Memoir, 113, 305–326.

JUDD, A. & HOVLAND, M.,2007, Seabed Fluid Flow: The Impact on Geology, Biology and the Marine Environment. Cambridge University Press, Cambridge, U.K., 475 pp.

KATAHARA, K.W. & CORRIGAN, J.D., 2002, Effect of gas on poroelastic response to burial or erosion, :in HUFFMAN, A.R. & BOWERS, G.L. (Eds), Pressure regimes in sedimentary basins and their prediction: AAPG Memoir, 76, 6 pp.

KOVACK, G.E., DEWHURST, D.N., RAVEN, M.D. & KALDI, J.G., 2004, The influence of composition, diagenesis and compaction on seal capacity in the Muderong Shale, Carnarvon Basin, The APPEA Journal, 44, 201–222.

LANGHI, L., STRAND, J. & ROSS, A.S., 2016, Fault-related biogenic mounds in the Ceduna Sub-basin, Australia: Implications for hydrocarbon migration, Marine and Petroleum Geology, 74, 47–58.

LEDUC, A.M., DAVIES, R.J., SWARBRICK, R.E. & IMBER, J., 2013, Fluid flow pipes triggered by lateral pressure transfer in the deepwater western Niger Delta, Marine and Petroleum Geology, 43, 423–433.

LONCKE, L., MASCLE, J. & PARTIES, F.S., 2004, Mud volcanoes, gas chimneys, pockmarks and mounds in the Nile deep-sea fan (Eastern Mediterranean): geophysical evidences, Marine and Petroleum Geology, 21, 669–689.

LONGLEY, I.M., BUESSENSCHUETT, C., CLYDSDALE, L., CUBITT, C.J., DAVIS, R.C., JOHNSON, M.K., MARSHALL, N.M., MURRAY, A.P., SOMERVILLE, R., SPRY. T.B., & THOMPSON, N.B., 2002, The North West Shelf of Australia – A Woodside perspective, in KEEP, M. & MOSS, S. J. (Eds), The Sedimentary Basins of Western Australia 3, Proceedings of the Petroleum Exploration Society of Australia Symposium, Perth, 2002, 27–88.

LØSETH, H., GADING, M. & WENSAAS, L., 2009, Hydrocarbon leakage interpreted on seismic data, Marine and Petroleum Geology, 26, 1304–1319.

LØSETH, H., WENSAAS, L., ARNSTEN, B., HANKEN, N.-M., BASIRE, C. & GRAUE, K., 2011, 1000 m long gas blow-out pipes, Marine and Petroleum Geology, 28, 1047–1060.

LUO, X. & VASSEUR, G., 2016, Overpressure dissipation mechanisms in sedimentary sections consisting of alternating mud-sand layers, Marine and Petroleum Geology, 78, 883–894.

MAGEE, C., DUFFY, O.B., PURNELL, K., BELL, R.E., JACKSON, C.A. & REEVE, M.T., 2016, Fault-controlled fluid flowinferred from hydrothermal vents imaged in 3Dseismic reflection data, offshore NW Australia, Basin Research, 28, 299–318.

MAIA, A.R., CARTWRIGHT, J. & ANDERSEN, E., 2016, Shallow plumbing systems inferred from spatial analysis of pockmark arrays, Marine and Petroleum Geology, 77, 865–881.

MARFURT, K.J., KIRLIN, R.L., FARMER, S.L. & BAHORICH, M.S., 1998, 3-D seismic attributes using a semblance-based coherency algorithm, Geophysics, 63, 1150–1165.

McCORMACK, K.D. & McCLAY, K., 2013, Structural architecture of the Gorgon Platform, North West Shelf, Australia, in KEEP, M. & MOSS, S. J. (Eds), The Sedimentary Basins of Western Australia IV, Proceedings of the Petroleum Exploration Society of Australia Symposium, Perth, 2013, 23 pp.

MOSS, J.L. & CARTWRIGHT, J., 2010, 3D seismic expression of km-scale fluid escape pipes from offshore Namibia, Basin Research, 22, 481–501.

MUDFORD, B.S. & BEST, M.E., 1989, Venture Gas Field, offshore Nova Scotia: case study of overpressuring in region of low sedimentation rate, AAPG Bulletin, 73, 1383–1396.

PILCHER, R. & ARGENT, J., 2007, Mega-pockmarks and linear pockmark trains on the West African continental margin, Marine Geology, 244, 15–32.

POWELL, D.E., KENT, P., DUNHAM, K., KARNER, G., OSMASTON, M.F. & KENZIE, A.S., 1982, The northwest Australian continental margin, Philosophical Transactions of the Royal Society of London. A305, 45–62.

REEVE, M.T., JACKSON, C.A., BELL, R.E., MAGEE, C. & BASTOW, I.D., 2016, The stratigraphic record of prebreakup geodynamics: evidence from the Barrow Delta, offshore Northwest Australia, Tectonics, 35, 1935–1968.

REILLY, M.J. & FLEMINGS, P.B., 2010, Deep pore pressures and seafloor venting in the Auger Basin,Gulf ofMexico, Basin Research, 22, 380–397.

ROHRMAN, M., 2013, Intrusive large igneous provinces below sedimentary basins: an example from the Exmouth Plateau (NW Australia), Journal of Geophysical Research, 118, 4477–4487.

ROHRMAN, M., 2015, Delineating the Exmouth mantle plume (NW Australia) from denudation and magmatic addition estimates, Lithosphere, 7, 589–600.

SEEBECK, H., 2015, Polygonal faulting and seal integrity in the Bonaparte Basin, Australia, Marine and Petroleum Geology, 60, 120–135.

SEEBECK, H., TENTHOREY, E., CONSOLI, C. & NICOL, A., 2015, Polygonal faulting and seal integrity in the Bonaparte Basin, Australia, Marine and Petroleum Geology, 60, 120–135.

STAGG, H.M.J. & COLWELL, J.B., 1994, The structural foundations of the Northern Carnarvon Basin, in Purcell, P.G. & Purcell, R.R. (Eds), The Sedimentary Basins of Western Australia. Petroleum Exploration Society of Australia, Perth, Western Australia, 349–364.

STAGG, H.M.J., ALCOCK, M.B., BERNARDEL, G., MOORE, A.M.G., SYMONDS, P.A. & EXON, N.F., 2004, Geological framework of the Outer Exmouth Plateau and Adjacent Ocean Basins, Geoscience Australia Record 2004/13.

STEIN, A., 1994, Rankin Platform, Western Australia: structural development and exploration potential, in PURCELL, P.G. & PURCELL, R.R. (Eds), The Sedimentary Basins of Western Australia, Proceedings of the Petroleum Exploration Society of Australia Symposium, Perth, 1994, 509–524.

STEWART, R.R., HUDDLESTON, P.D. & KAN, T.K., 1984, Seismic versus sonic velocities: A vertical seismic profiling study, Geophysics, 49, 1153–1168.

TINDALE, K., NEWELL, N., KEALL, J. & SMITH, N., 1998, Structural evolution and charge history of the Exmouth Sub-basin, Northern Carnarvon Basin, Western Australia, in PURCELL, P.G. & PURCELL, R.R. (Eds), The Sedimentary Basins of Western Australia 2, Proceedings of the Petroleum Exploration Society of Australia Symposium, Perth, 1998, 447–472.

TINGATE, P.R., KHAKSAR, A., van RUTH, P., DEWHURST, D., RAVEN, M., YOUNG, H., HILLIS, R. R. & DODDS, K., 2001, Geological controls on overpressure in the Northern Carnarvon Basin, The APPEA Journal, 41, 573–594.

VAN RUTH, P., HILLIS, R. & TINGATE, P., 2004, The origin of overpressure in the Carnarvon Basin, Western Australia: Implications for pore pressure prediction, Petroleum Geoscience, 10, 247–257.

VEEVERS, J.J., 1988, Morphotectonics of Australia's Northwestern Margin – a review, in PURCELL, P.G. & PURCELL, R.R. (Eds), The North West Shelf Australia, Proceedings of the Petroleum Exploration Society of Australia Symposium, Perth, 1988, 19–28.

VELAYATHAM, T., HOLFORD, S. & BUNCH, M., 2018, Ancient fluid flow recorded by remarkably long, buried pockmark trains observed in 3D seismic data, Exmouth Plateau, Northern Carnarvon Basin, Marine and Petroleum Geology, 95, 303–313.

WALLMANN, K., LINKE, P., SUESS, E., BOHRMANN, G., SAHLING, H., SCHLÜTER, M., DÄHLMANN, A., LAMMERS, S., GREINERT, J. & von MIRBACH, N., 1997, Quantifying fluid flow, solute mixing, and biogeochemical turnover at cold vents of the eastern Aleutian subduction zone, Geochimica et Cosmochimica Acta, 61, 5209–5219.

YU, Z. & LERCHE, I., 1996, Modelling abnormal pressure development in sandstone/shale basins. Marine and Petroleum Geology, 13, 179–193.

Chapter 4

Fault Controlled Focused Fluid Flow In the Ceduna Sub-Basin, Offshore South Australia; evidence from 3D seismic reflection data

Statement of Authorship

Title of Paper	Fault Controlled Focused Fluid Flows In the Ceduna Sub-Basin, Offshore South Australia
Publication Status	☐ Published ☐ Accepted for Publication ☐ Submitted for Publication ☑ Unpublished and Unsubmitted w ork w ritten in manuscript style
Publication Details	Velayatham, T., Holford, S.P., Bunch, M., King, R.,

Principal Author

Name of Principal Author (Candidate)	Tayallen Velayatham
Contribution to the Paper	Performed seismic data interpretation and spatial statistics analysis described in the study, wrote manuscript and is corresponding author.
Overall percentage (%)	75
Certification:	This paper reports on original research I conducted during the period of my Higher Degree by Research candidature and is not subject to any obligations or contractual agreements with a third party that would constrain its inclusion in this thesis. I am the primary author of this paper.
Signature	Date 27/5/2019

Co-Author Contributions

By signing the Statement of Authorship, each author certifies that:

i. the candidate's stated contribution to the publication is accurate (as detailed above);

ii. permission is granted for the candidate in include the publication in the thesis; and

iii. the sum of all co-author contributions is equal to 100% less the candidate's stated contribution.

Name of Co-Author	Simon P. Holford
Contribution to the Paper	Supervised development of work, helped with data interpretation, provided feedback and edited manuscript.
Signature	Date 27/5/19

Name of Co-Author	Mark Bunch
Contribution to the Paper	Supervised development of work, helped with data interpretation, provided feedback and edited manuscript.
Signature	Date 27/05/2019

Name of Co-Author	Rosalind King		
Contribution to the Paper	Supervised development of work, helped with data interpretation, provided feedback and edited manuscript.		
Signature		Date	24/06/2019

Please cut and paste additional co-author panels here as required.

Fault Controlled Focused Fluid Flow In the Ceduna Sub-Basin, Offshore South Australia; evidence from 3D seismic reflection data

Tayallen Velayatham, Simon P. Holford, Mark A. Bunch & Rosalind C. King

Abstract

Fluid escape features (e.g. pipes) are observable manifestations of fluid migration processes and can provide information on subsurface fluid dynamics. This paper investigates the spatial link between fluid escape features and underlying faults in the Ceduna Sub-basin of the Bight Basin along Australia's southern margin. The Ceduna Sub-basin is the largest depocenter of the Mesozoic Bight Basin that formed as a result of rifting between Australia and Antarctica in the Mid Jurassic. The study area is located in the northwest of the Ceduna Sub-basin within which three sets of fluid escape pipes were identified along the study area's south-western edge. The first set (set 1) is observed within the siliclastic Wobbegong and carbonitic Dugong Supersequences of Paleocene to Pleistocene age, while the second set (set 2) is observed within the top 400 ms (~485 m) of Santonian to Maastrichtian deltaic Hammerhead Supersequence and the third set (set 3) within the top 450 ms (~600 m) of the Turonian to Santonian Tiger Supersequence that predominantly consists of mudstones. We focus this study on analysing the first two sets of fluid escape features due to the poor seismic imaging quality of set 3 fluid escape pipes which makes accurate interpretations difficult. Dimensions of set 1 and set 2 fluid escape pipes range from 50 ms (60 m) to 400 ms (485 m) in height and 70 to 180 m in width. Bases, or roots, of the fluid escape features overlie the upper tips of normal faults within the Hammerhead Supersequence. The spatial distribution of fluid escape features and predominant underlying faulting style within the Hammerhead Supersequence vary along the study area; distributed fluid escape features overly polygonal faults to the northeast while linear clusters of fluid escape features overlie normal faults in the southwest of the study area. The spatial link between the fluid escape features and underlying faults was quantified using spatial statistics and the results support the interpretation that the faults had acted as fluid migration pathways. The polygonal and

normal faults developed in the Late Cretaceous and are interpreted to have transmitted fluids from the Lower Cretaceous Blue Whale, White Pointer and Tiger Supersequences. These supersequences have been identified as containing potential source rocks, thus the fluids that formed the fluid escape features are potentially hydrocarbons. Geochemical analysis of potential source rocks from the Bight Basin, combined with regional basin modelling results suggest that hydrocarbon generation and expulsion from the Mid Cretaceous sequences initiated as early as the Mid Cretaceous (~95 Ma) and continued through to the Cenozoic (~15 Ma). Hydrocarbon presence is seen as a key risk for exploration in the Ceduna Sub-basin. This study highlights potential fluid migration pathways in a distal region of the Ceduna Sub-basin, and if the fluids that formed the fluid escape features identified in this study are indeed hydrocarbons, it could increase confidence in the presence of a working petroleum system.

1. Introduction

Focused fluid flows in sedimentary basins are common yet complex expressions of subsurface fluid dynamics that are typically driven by processes including sediment compaction, hydrocarbon buoyancy or differential pressures (Berndt, 2005; Davies et al., 2008). Fluids migrate from deeper to shallower depths by means of hydraulic fracturing or via permeable geological and stratigraphic pathways such as faults, fractures, buried channels or along igneous intrusions (Cartwright et al., 2007; Davies et al., 2012; Schofield et al., 2019). While studies of focused fluid flows are primarily utilized in environmental, biological and geohazard-related fields, they can play a critical role in hydrocarbon exploration, particularly when assessing the petroleum systems of frontier basins (Judd and Hovland, 2007; Andresen et al., 2011). Recognition of subsurface fluid escape features on seismic data can provide information on the presence of mature source rocks, hydrocarbon reservoirs, and highlight fluid migration pathways (Abrams, 2005). Heggland (1998) identified sustained gas seepages that manifested as clusters of seismic chimneys and buried craters on the seabed in the North Sea. Analysis on the spatial distribution and vertical extent of these chimneys led to the identification of an underlying hydrocarbon reservoir. Fluid escape features can also be utilized to assess the hydrocarbon preservation capability of reservoirs (Abrams, 2005). Løseth et al. (2009) documented the seismic expression of fluid escape features associated with leakage processes above hydrocarbon filled traps. Depending on the location of the fluid escape features relative to the seal or reservoir structure, seal integrity or reservoir spill capacity could can be assessed, and the risk of hydrocarbon presence within the reservoir could be evaluated. Interpretation of focused fluid flow features to understand subsurface fluid dynamics can be particularly valuable in frontier exploration basins, where direct evidence of petroleum system elements and processes is often limited.

The Bight Basin, located offshore along the Australia's southern continental margin, is a frontier hydrocarbon exploration basin and the Ceduna Sub-basin is the largest depocenter within it (Struckmeyer et al., 2001). Over the past two decades, the Bight Basin has become a growing focus for exploration interest, with prospective petroleum systems associated with thick Mid to Late Cretaceous deltaic and marine sedimentary rocks (Bradshaw et al., 2002; Totterdell et al., 2008). These Mid to Late Cretaceous sedimentary rocks are interpreted to provide a wide range of hydrocarbon play types with structural and stratigraphic traps that have the potential to contain substantive liquid hydrocarbon accumulations (Bradshaw et al., 2002; Struckmeyer et al., 2001; Totterdell et al., 2008). Nevertheless, hydrocarbon charge is a key exploration risk within the basin. To address this risk, various data acquisition surveys have been conducted within the basin to evaluate its petroleum potential, including seafloor sampling, dredge sampling, synthetic aperture radar (SAR) and seismic reflection surveys (Figure 1) (Logan et al., 2008; Struckmeyer et al., 2002; Totterdell and Mitchell, 2009). A dredging survey by Geoscience Australia in 2009 recovered Mid Cretaceous organic-rich marine shales from the western edge of the Ceduna Sub-basin that indicate the potential presence of hydrocarbon source rocks in the distal regions of the sub-basin (Totterdell and Mitchell, 2009; Totterdell et al., 2008). Regional 2D seismic lines have revealed indications of fluid escape features, imaged as anomalous seismic chimneys that are interpreted to be associated with migrating hydrocarbons (Struckmeyer et al., 2002). Furthermore, Langhi et al. (2016) identified Paleocene to Eocene aged biogenic mounds within the Central Ceduna Sub-basin that are closely associated with underlying faults which intersect potential Mid Cretaceous source rocks (Figure 1). A proposed model for the genesis of these mounds is fault-associated hydrocarbon seepage, whereby episodic fluid migration occurred between the Late Cretaceous and Early Cenozoic (Langhi et al., 2016; Struckmeyer et al., 2001). Seal integrity is also seen as an exploration risk. Fluid history analysis from Jerboa-1 well of the Eyre Sub-basin, located to the west of the Ceduna Sub-basin, revealed an interpreted paleo-oil column with hydrocarbons sourced from Late Jurassic to Early Cretaceous source rocks, which has since been breached due to fault reactivation during the Late Cretaceous (Ruble et al., 2001). The main phase of hydrocarbon generation from the aforementioned source rocks is interpreted to be between the Late Cretaceous and Early Cenozoic (Struckmeyer et al., 2001). Given that the timing of fault reactivation is thought to be coeval with hydrocarbon generation, it is particularly important to constrain the timing of fluid migration within the basin to evaluate its hydrocarbon potential (Struckmeyer et al., 2002; Totterdell et al., 2008).

In this study, we use recently acquired 3D seismic reflection data to document evidence of Late to post-Cretaceous focused fluid flow events in the Ceduna Sub-basin of the Bight Basin, offshore South Australia. In particular, we analyse the spatial variability of inferred fluid flow features and the potential role of basin structures, specifically faults, in dictating the underlying fluid migration pathways. We also attempt to constrain the timing of fluid flow, and the potential geological sources

of the fluids, with the aim of contributing to improved assessments of petroleum charge as well as seal risks within the Ceduna Sub-basin.

2. Geological Setting

The Ceduna Sub-basin is the largest depocenter of the Bight Basin, offshore South Australia (Totterdell and Bradshaw, 2004; Willcox and Stagg, 1990). It is an east-west trending sub-basin that covers an area of approximately 90,000 km^2 and contains up to 15 km of Mesozoic sedimentary rocks (Figure 1) (Struckmeyer et al., 2001). The sub-basin is bordered by the Eyre and Recherche sub-basins to the west, the Madura Shelf and Eucla Basins to the north, the Duntroon sub-basin to the east and the South Australian Abyssal Plain to the south (Struckmeyer et al., 2001).

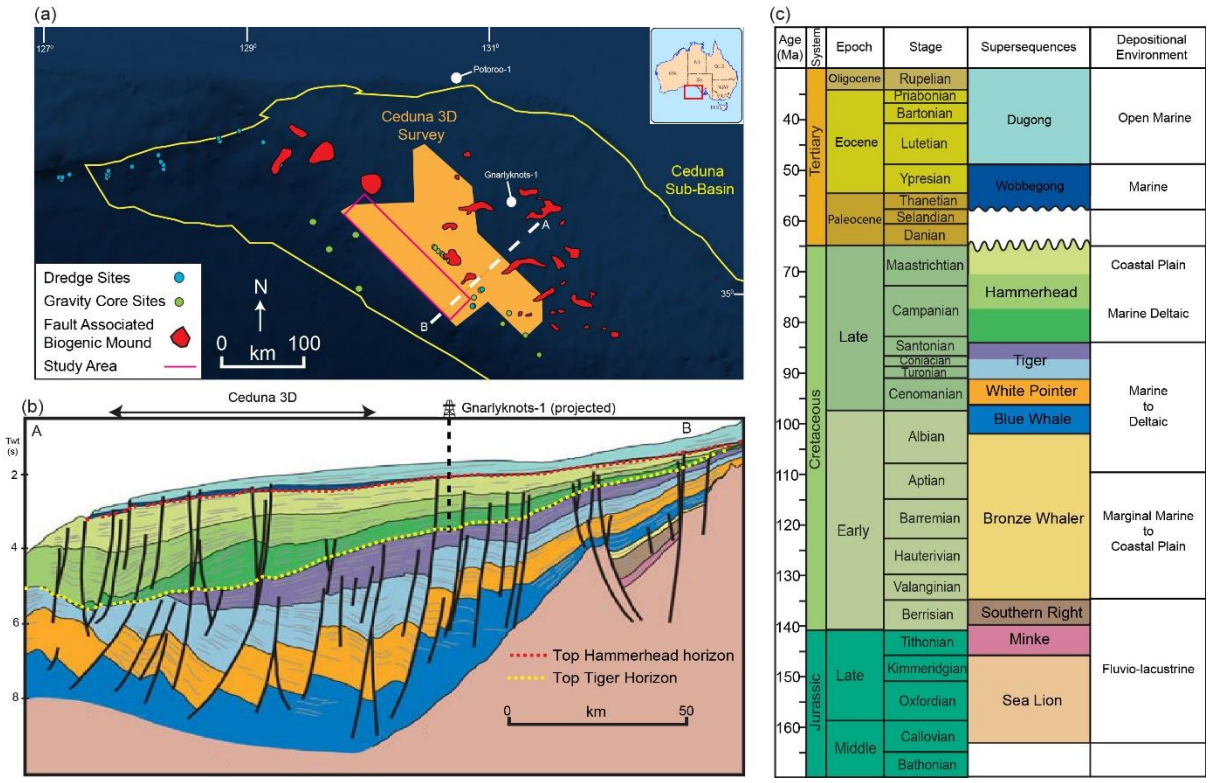

***Figure 1**: (a) Location of the Ceduna 3D seismic survey, exploration wells, sampling survey locations and biogenic mounds in the Ceduna Sub-Basin (Langhi et al., 2016; Totterdell and Mitchell, 2009). (b) Regional cross section showing the stratigraphy of the Ceduna Sub-basin. (c) Tectonostratigraphic chart of the Bight Basin, modified from Totterdell et al. (2000).*

The Bight Basin formed as a result of intracontinental rifting between Australia and Antarctica during the breakup of eastern Gondwana, after which it developed through multiple phases of subsidence (Totterdell et al., 2000; Totterdell et al., 2008; Totterdell and Bradshaw, 2004; Willcox and Stagg, 1990). A comprehensive chronostratigraphic framework detailing the evolution of the basin through these phases has been developed by Totterdell et al. (2000) and is referred to in this paper (Figure 1c).

Northwest-southeast oriented rifting commenced during the Mid-Late Jurassic, forming extensional and transtensional half-grabens throughout the eastern region of the Ceduna Sub-Basin (Krassay and Totterdell, 2003; Totterdell and Bradshaw, 2004). During this phase of mechanical extension (Basin Phase 1 of Totterdell et al. (2000)), the basin was filled with fluvio-lacustrine sedimentary rocks that comprise of the Callovian-Kimmeridgian Sea Lion and Tithonian–Early Berriasian Minke Supersequences (Totterdell et al., 2000). This period of extension was followed by a phase of slow thermal subsidence (Basin Phase 2) during which fluvio-lacustrine to deltaic and marine sedimentary rocks of the Southern Right and the Bronze Whaler Supersequences were deposited between the Valanginian and Mid Albian (Totterdell et al., 2000; Totterdell and Bradshaw, 2004).

An abrupt increase in subsidence rates during the Mid Albian marked the start of a new phase in basin development (Basin Phase 3), whereby marine mudstones of the Blue Whale Supersequence were deposited in the Ceduna Sub-Basin (Totterdell et al., 2000; Totterdell and Bradshaw, 2004). This sequence was then overlain by rapid progradational deposition of the deltaic White Pointer Supersequence in the Cenomanian (Totterdell et al., 2000; Totterdell and Bradshaw, 2004). Deposition of the White Pointer Supersequence was accompanied by the formation of listric growth faults that sole out along a decollement surface within the Blue Whale Supersequence (Totterdell and Bradshaw, 2004). These faults are characterised by growth strata in the White Pointer Supersequence and triangular-shaped shale diapirs, adjacent to the faults, sourced from the Blue Whale Supersequence (Totterdell et al., 2000; Totterdell and Bradshaw, 2004). Growth of the listric faults ceased by the Late Cenomanian when the Turonian- Santonian Tiger Supersequence, comprising marine to marginal marine mudstones, was deposited above the White Pointer Supersequence (Totterdell et al., 2000). Though there is some uncertainty regarding the timing of the onset of seafloor spreading to the south of the Bight Basin, most authors assign a late Santonian age, marking continental separation of Australia and Antarctica, and accompanied by normal reactivation of the Cenomanian listric faults (Sayers et al., 2001; Struckmeyer et al., 2001; Totterdell and Bradshaw, 2004).

Following continental separation, the Bight Basin became established as a passive margin basin and entered a period of reduced subsidence rates (Basin Phase 4) (Totterdell et al., 2000; Totterdell and Bradshaw, 2004). Between the late Santonian and Maastrichtian, deltaic sedimentary rocks of the Hammerhead Supersequence were deposited in the Ceduna Sub-basin, reaching thicknesses of up to 5 km in the central parts of the sub-basin (Krassay and Totterdell, 2003; Totterdell et al., 2000). The Hammerhead Supersequence consists of three higher order deltaic sequences with the older two having progradational stratal geometries and the youngest characterised by aggradational strata geometries (Totterdell et al., 2000). The Hammerhead Supersequence is structurally defined by high-angle (52° – 58°) planar normal faults that dip towards the southwest, and listric growth faults that are latest Maastrichtian to early Paleocene in age that similarly dip towards the southwest (Krassay and

Totterdell, 2003; Robson et al., 2017; Totterdell and Bradshaw, 2004). Both the planar extensional and listric fault sets are interpreted to have formed as a result of gravitational instability caused by the supersequence's rapid, progradational deposition; however, the listric faults are also interpreted to be associated with reactivation of underlying Cenomanian listric faults (Krassay and Totterdell, 2003; Robson et al., 2017; Ryan et al., 2017).

The Hammerhead Supersequence is overlain by marginal marine to deltaic sedimentary rocks of the Wobbegong Supersequence, deposited between the Paleocene and early Eocene (Totterdell et al., 2000). Separating the Hammerhead and Wobbegong supersequences is an unconformity surface that represents a 5 - 7 m.y. hiatus in sedimentation (Totterdell et al., 2000). The Wobbegong Supersequence is thin (~250 m), relative to the underlying stratigraphic sequences, throughout the Ceduna Sub-basin and tapers out at the sub-basin's southern margin. The Ceduna Sub-basin is also characterised by igneous intrusions within the Wobbegong, Hammerhead and Tiger supersequences, interpreted to have been emplaced during the Mid Eocene and proposed to be associated with the onset of rapid seafloor spreading along Australia's southern margin at that time (Holford et al., 2012; Reynolds et al., 2017). The intrusion morphologies have been identified primarily as sills and laccoliths with lateral dimensions ranging between 2 to 23 km and 5 to 270 m in thickness (Reynolds et al., 2017).

Overlying the Wobbegong Supersequence is the mid Eocene-Pleistocene Dugong Supersequence, which contains a basal sandstone unit that transitions up into cool water carbonates (Totterdell et al., 2000).

3. Data and Methodology

This study uses the Ceduna 3D seismic reflection survey that was acquired in 2012 and covers an area of ~12,000 km^2 (Figure 1). The data extends to 9 s two-way-time (TWT) with water depths ranging from 1.5 to 4 s TWT. Survey inlines are oriented northwest-southeast in 15 m intervals and crosslines are oriented northeast-southwest in 12.5 m intervals. The data is zero phase processed with peaks representing an increase in acoustic impedance and troughs representing decrease in acoustic impedance. The interval velocity and frequency of the 3D seismic data is approximately 2100 ms^{-1} and 45 Hz at the Cenozoic interval and approximately 3243 ms^{-1} and 25 Hz at the Turonian (Tiger Supersequence) interval. This gives a vertical resolution of 12 m and 30 m at the Cenozoic and Turonian intervals respectively.

Two petroleum wells were utilized for stratigraphic control and tied to the Ceduna 3D seismic data; Potoroo-1 and Gnarlyknots-1 (Figure 1). Potoroo-1 is located 70 km north of the survey area while Gnarlyknots-1 is located 45km northeast of the survey area. Potooroo-1 recovered samples from Mid Miocene to Mid Cretaceous sedimentary rocks, whereas Gnarlyknots-1 recovered samples from Late

to Mid Cretaceous sedimentary rocks. The two wells were tied to the 3D seismic survey using regional 2D seismic lines that intersect both wells and 3D seismic data. Regional interpretation studies by Totterdell et al. (2000) and Krassay and Totterdell (2003) were also used to constrain interpretation of stratigraphic boundaries within the study area that were not intersected at the two well locations. A power function derived using velocity survey data from Potoroo-1 and Gnarlyknots-1 were used to convert two-way-time (twt) measurements to depth (Figure 2) (Robson et al., 2017).

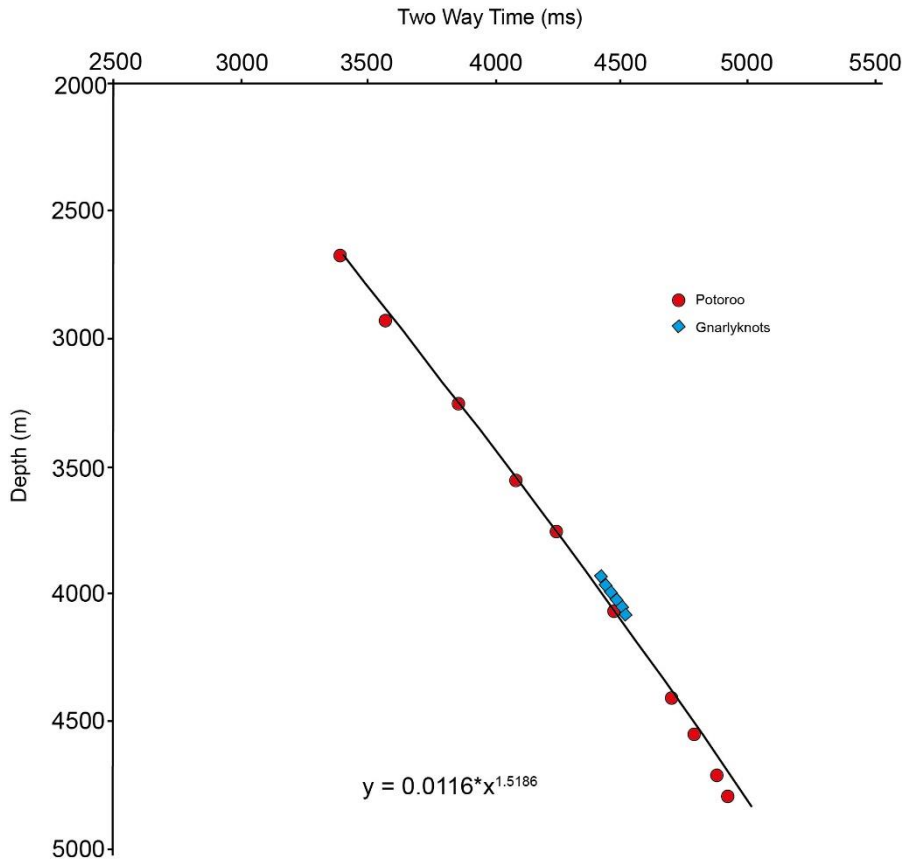

Figure 2*: A power function was derived using velocity survey data from Potoroo – 1 and Gnarlyknots -1 wells to convert time values to approximated depth measurements in this study.*

Of the horizons interpreted in this study, three are discussed in detail in this paper; the Seafloor, Top Hammerhead and Top Tiger horizons. The estimated ages of these horizons are based on the regional sequence framework developed by Totterdell et al. (2000). The Seafloor horizon is interpreted as a peak. The sequence bound by the Seafloor and Top Hammerhead horizon (referred to as the Cenozoic sequence) is expressed as parallel seismic reflectors, characterised by low to moderate seismic amplitudes. The Top Hammerhead horizon is an unconformable surface that is interpreted as a trough (Totterdell and Bradshaw, 2004). The seismic sequence underlying the Top Hammerhead horizon is characterised by clinoform geometries of moderate seismic amplitudes with interspersed high amplitudes. The Top Tiger horizon represents the top of the Tiger Supersequence and the base of the

Hammerhead Supersequence. This horizon is interpreted as a trough and the underlying seismic sequence is characterised by parallel seismic reflectors of low seismic amplitude. In addition to interpretation of seismic amplitudes, variance, a seismic attribute that detects and highlights abrupt lateral changes or discontinuities along a seismic reflector, was used to identify and map focused fluid flows and faults in this study (Meldahl and Heggland, 1999).

Statistical analysis was undertaken to identify and quantify trends in the spatial distribution of fluid flow features. After comparing three methods (multiple blade, multinominal sector, continuous sector), the continuous sector method was selected for point alignment analysis in this study as it was found to be the most robust of the methods (Hammer, 2009; Hammer et al., 2001). In this method, each fluid flow feature will act as a central point and orientations between the central and neighbouring points within a defined radial distance are analysed. The significance of the identified orientations are then tested with Rayleigh's test for circular distributions (Hammer, 2009). This test produces a p-value that quantifies the likelihood of a spatial distribution as being random; the smaller the p-value, the less likely the spatial distribution is random (Mardia and Jupp, 2000).

4. Seismic Interpretation Results

An estimated 1541 vertical zones of disrupted or discontinuous seismic reflectors (referred to as "columns") were identified along the southwestern edge of the seismic reflection survey (referred to as the "study area") (Figure 1, 3). Within the study area, three sets of 'columns' were identified based on the stratigraphic sequences in which they occur; the first and shallowest set within the Cenozoic sequence (referred to as set 1), the second within the upper Hammerhead Supersequence (referred to as set 2), and the third within the Upper Tiger Supersequence (referred to as set 3). The focus of analysis and discussion of this study will be on the first and second sets of 'columns'. The seismic data quality at depths where set 3 'columns' are identified is not sufficient for the features to be interpreted and analysed with confidence. Nevertheless, the imaging characteristics and spatial distribution of these columns are still documented in this study.

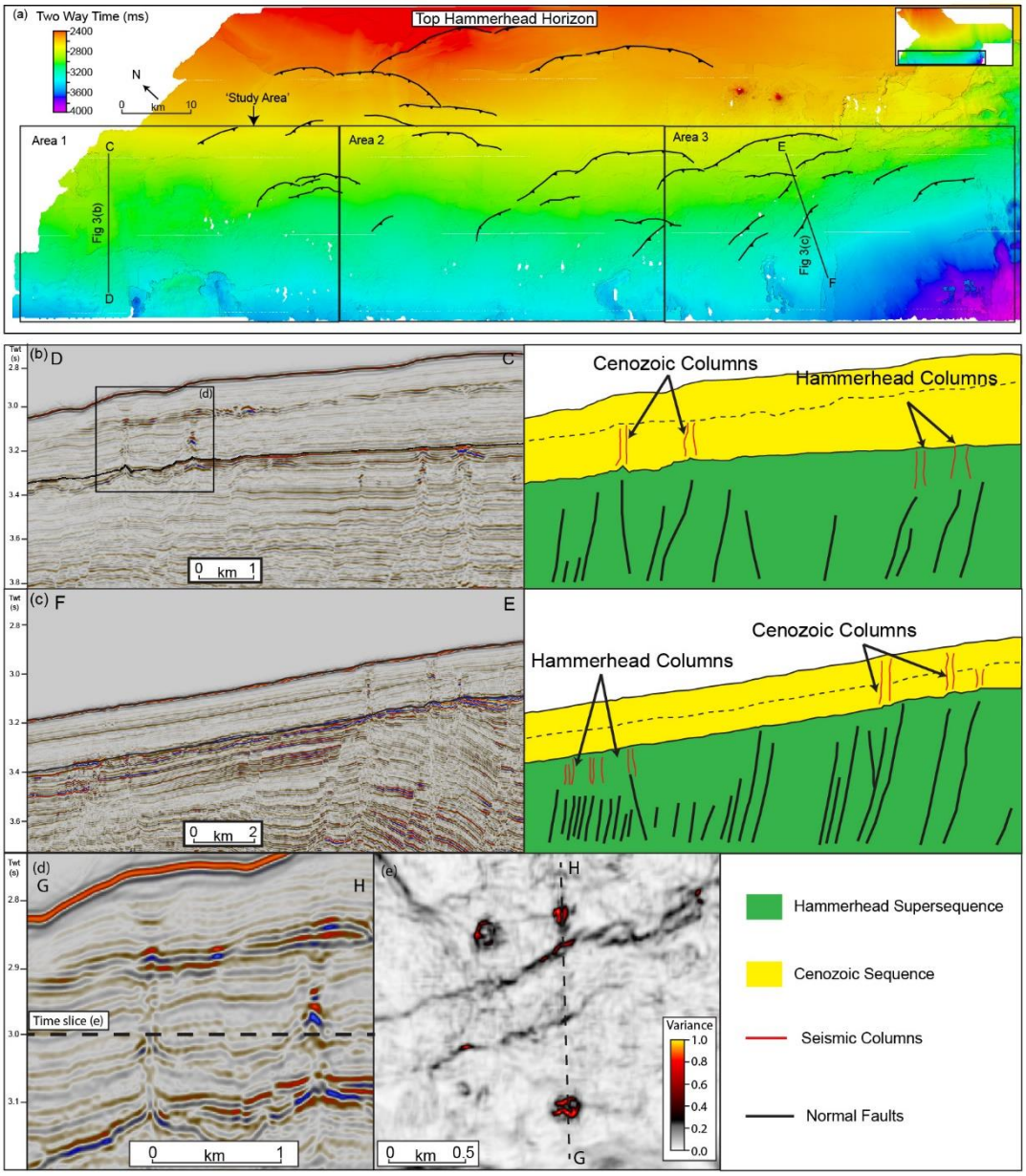

***Figure 3**: (a) Interpreted Top Hammerhead horizon showing the 'study area'. Seismic cross sections from (b) Area 1 and (c) Area 3 illustrating identified Cenozoic and Hammerhead columns. (d) A zoom in of the 'columns' and (e) a variance time slice at 3.0 s TWT highlighting the 'columns'. (Figure not oriented with North at the top.)*

4.1. Set 1 (Cenozoic) Columns

4.1.1. Seismic expressions

Of the 1541 identified columns, 703 (46%) consist of set 1 columns. The seismic expression of Cenozoic 'columns' encompasses vertical zones of convex upward seismic reflectors with amplitudes higher than the surrounding reflectors, laterally discontinuous seismic reflectors, or vertical zones of convex downward seismic reflectors (Figure 3). Imaging of these features is enhanced when using the

variance attribute, whereby the 'columns' have variance values >0.5 compared to background variance values of ~0.01. The heights of the columns range from 50 ms (~60 m) to 270 ms (~310 m) while their widths range between 70 to 180 m.

Set 1 columns occur within Cenozoic strata (Figure 3). The lower terminus of the columns, referred to as the bases or roots, terminate along the Top Hammerhead horizon whereas their upper terminus terminates at varying levels within the Cenozoic sequence, the shallowest of which terminate along the seafloor. Furthermore, out of the 703 set 1 columns, the root of 588 columns (84%) is associated with the upper tip of underlying normal faults within the Hammerhead Supersequence.

4.1.2. Spatial Distribution

The Cenozoic columns are documented along the study area, however, their occurrence is focused at the north-western (Area 1) and south-eastern (Area 3) corners of the study area. In Area 1, the columns have a random spatial distribution whereas in Area 3, they occur in linear trending clusters with orientations that range between 271-305° (Figure 5, 6). Between the two corners of the study area, referred to as Area 2, the spatial distribution of the columns is predominantly sporadic; however, column spatial distribution shows a transitioning to linear clusters towards the southeast of this area.

4.2. Set 2 (Hammerhead) Columns

4.2.1. Seismic Expression

Of the 1541 columns, 806 (54%) are identified to be set 2 columns. The occurrence of set 2 columns within the Hammerhead Supersequence is restricted to ~400 ms (485 m) beneath the Top Hammerhead horizon. Set 2 columns are predominantly manifested as vertical columns of upward deflected seismic reflectors that have higher amplitudes than the adjacent, undisturbed reflectors (Figure 3). Similar to the Cenozoic columns, the Hammerhead columns have variance values of at least 0.5 compared to background variance values of 0.01. The upper terminus of these columns is along the Top Hammerhead horizon while their roots terminate at varying depths within 400ms (~485 m) below the aforementioned horizon. Column heights range from 120 – 400 ms (140 - 485 m), and have a similar widths as those of the Cenozoic columns (70 – 180 m). Like the Cenozoic columns, upper tips of normal faults within the Hammerhead Supersequence underlie the base of 670 (83%) Hammerhead columns.

4.2.2. Spatial Distribution

The spatial distribution of Hammerhead columns along the study area is similar to those of the Cenozoic columns. The Hammerhead columns have a sporadic spatial distribution in Area 1 and cluster in linear trends with orientations between 271-305° in Area 3 (Figure 5,6). Within Area 2, the

spatial distribution of the columns transition from having a random spatial distribution in the northwest of this region to linear trending clusters to the southeast.

4.3. Set 3 (Top Tiger) Columns

4.3.1. Seismic Expressions

A total of 32 (2%) columns were identified within the Tiger Supersequence, occurring at depths restricted to ~450 ms (600 m) below the interpreted Top Tiger Horizon, which translates to between 1000 to 1450 ms (1200 – 1800 m) below the seafloor. They are imaged as vertical zones of discontinuous and or convex upward seismic reflectors (Figure 4). Heights of the columns range from 150 ms (200 m) to 450 ms (600 m) with the upper tips of the columns terminating against the Top Tiger horizon.

4.3.2. Spatial Distribution

Of the 32 columns, 23 are identified within Area 1 of the study area and 9 occur in the northern corner of the survey. No spatial distribution trends are observed with the Tiger columns.

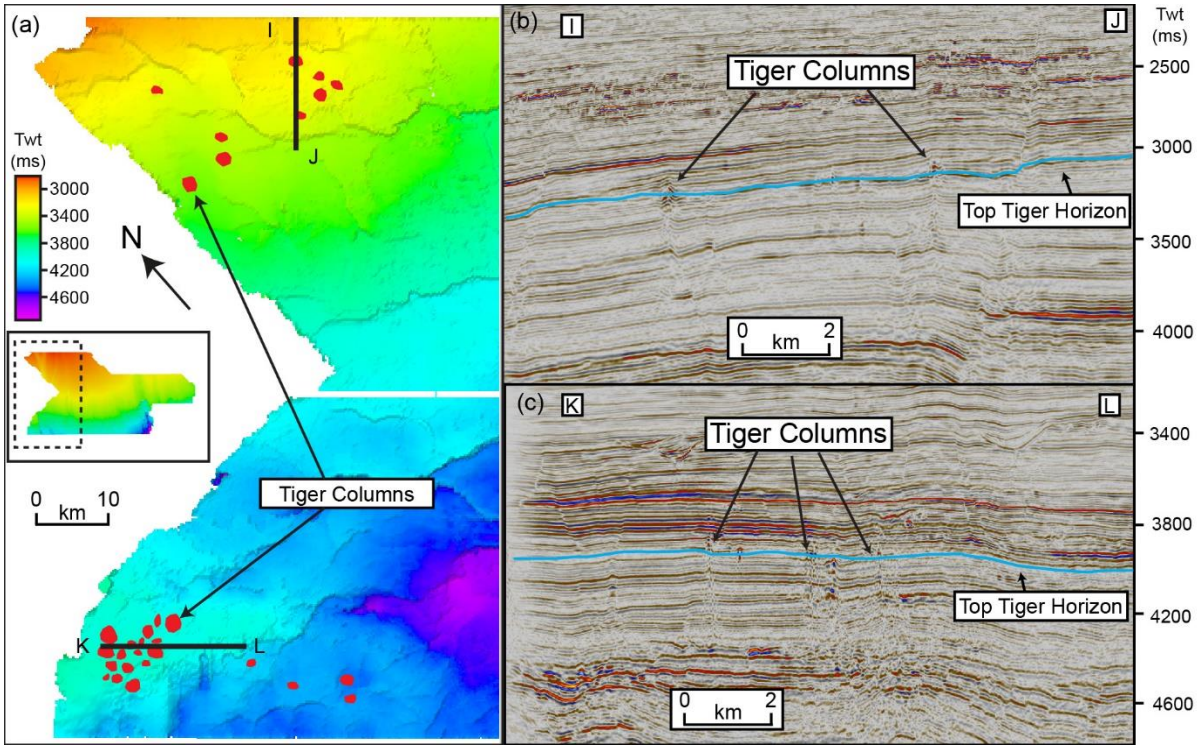

Figure 4*: Set three columns identified along the Top Tiger horizon. (Figure not oriented with North at the top.)*

4.4. Faults Underlying Set 1 and Set 2 Columns

Normal faults are observed to underlie the Cenozoic and Hammerhead columns. Like the column's spatial distribution trends, the predominant type of extensional faults within the Hammerhead Supersequence varies within the study area. Faulting in the Hammerhead Supersequence predominantly consists of polygonal faults in Area 1 and normal faults (referred to as primary faults) in Area 3. The predominant fault type in Area 2 shows a transition from polygonal faults in the northwest to primary faults in the southeast.

4.4.1. Polygonal faults in Area 1

In Area 1, faulting within the Hammerhead Supersequence is predominantly polygonal faults with interspersed primary faults (Figure 5). The polygonal faults are characterised by variable strike orientations, and their vertical extent is stratigraphically constrained within the Hammerhead Supersequence; they do not extend into the overlying Cenozoic sequence nor the underlying Tiger Supersequence (Cartwright and Dewhurst, 1998). Polygonal faults develop in layers, also known as tiers, and the individual faults can be categorized by their 'order', referring to the number of tiers the faults extend across (Cartwright, 1994). In this survey, two tiers, and two orders of polygonal faults were identified. First order faults are defined as those that are vertically constrained within individual tiers, while second order faults are those that extend across both tiers. The fault throws range between 7 and 21 ms (~9 – 25 m).

Three primary faults, along with associated synthetic and antithetic faults (referred to secondary faults), were interpreted in Area 1. These primary faults extend from the top of the Hammerhead Supersequence down through the Tiger and White Pointer Supersequences to sole out along a decollement surface within the Blue Whale Supersequence. The primary faults have an average strike orientation of 315^0 and throws that range between 31 to 87 ms (37 – 115 m) within the Hammerhead Supersequence.

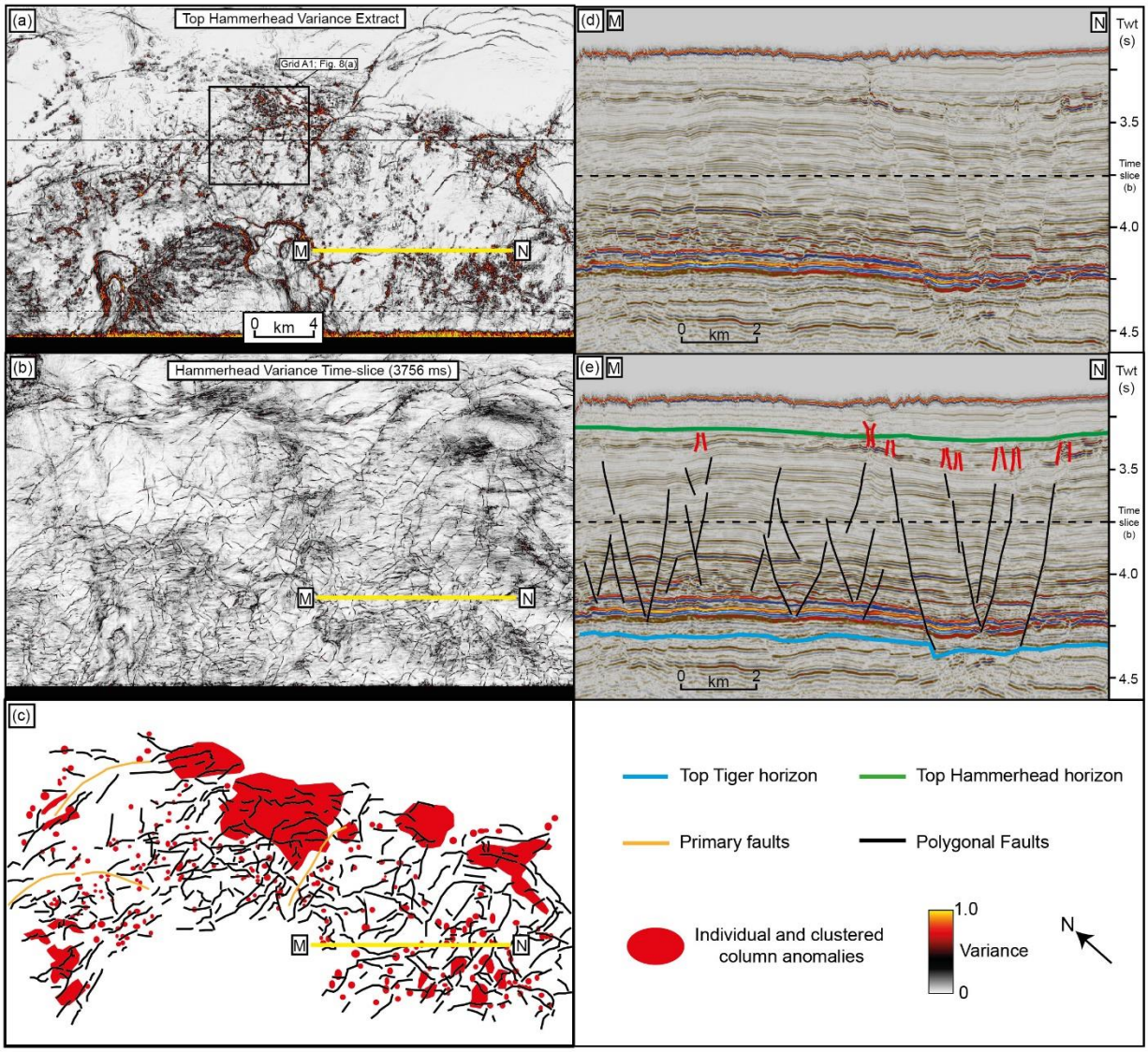

Figure 5: *From Area 1 in Fig 3. (a) Variance attribute extract along the Top Hammerhead horizon highlighting columns. (b) Variance Time slice at 3750ms highlighting polygonal faulting within the Hammerhead Supersequence. (c) Sketch that overlies the identified columns from (a) with underlying fault strikes from (b). Seismic cross section (d) with and (e) without interpretations, illustrating the polygonal faults and columns. (Figure not oriented with North at the top.)*

4.4.2. Primary Faults in Area 3

Faults in Area 3 are predominantly primary faults with associated synthetic and antithetic secondary faults; however, the primary faults in this area show prominent listric characteristics (Figure 6). A total of 27 primary faults were interpreted in this area. Seven (7) of the interpreted primary faults have similar vertical extents as those interpreted in Area 1, extending from the top of the Hammerhead Supersequence down through the Tiger and White Pointer Supersequences to sole out along a detachment surface within the Blue Whale Supersequence. The remaining 20 primary faults are

stratigraphically constrained to occur within the Hammerhead Supersequence, whereby they extend from the top of the supersequence and sole out along the top of the Tiger Supersequence. The secondary faults similarly occur within the Hammerhead Supersequence only. They do not intersect the Top Hammerhead horizon nor do they extend down to the detachment surface along the top of the Tiger Supersequence. Primary faults in this area have strike orientations that average 280° and throws that range between 63 to 280 ms (75 – 360 m) within the Hammerhead Supersequence.

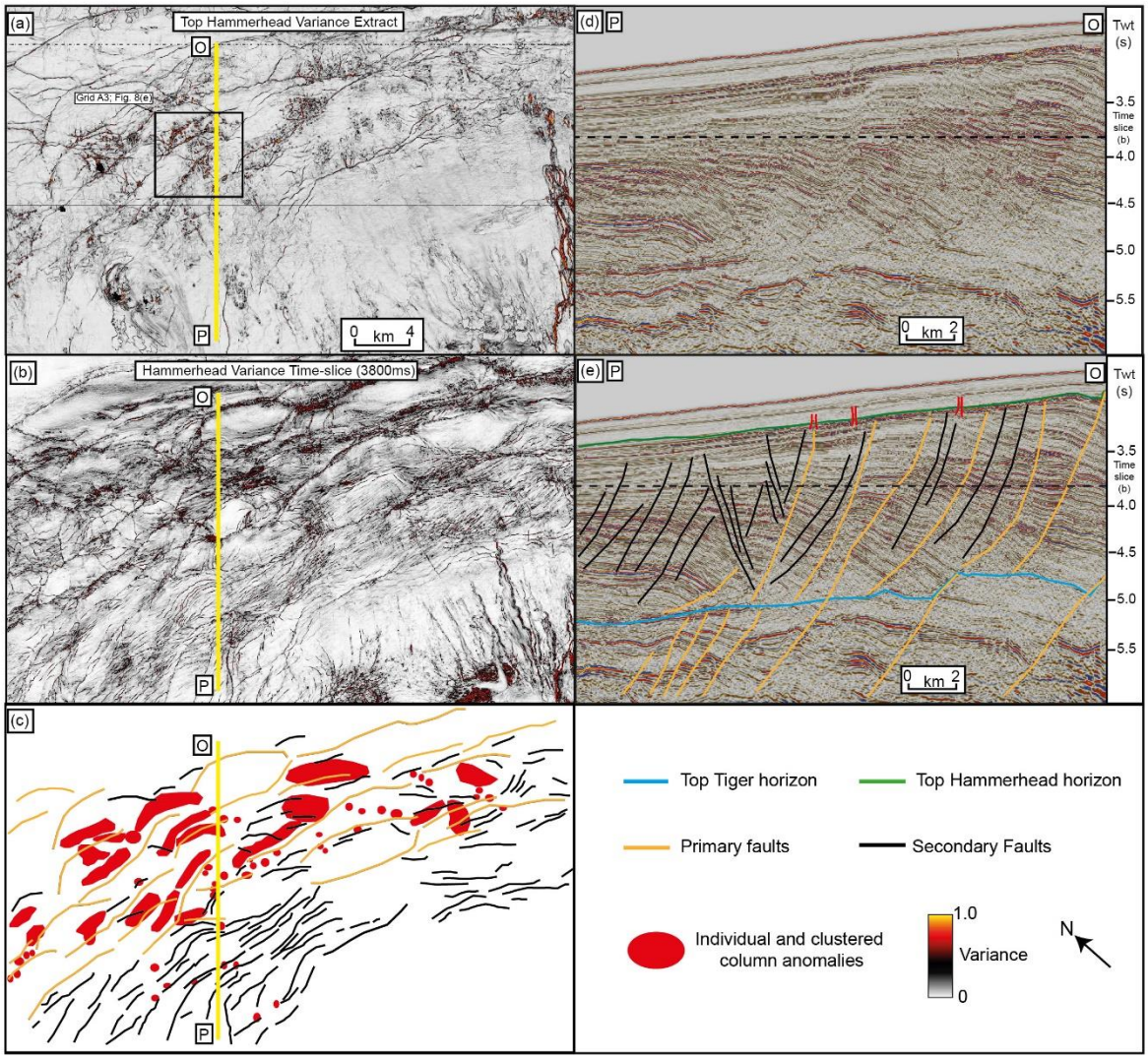

Figure 6: *From Area 3 in Fig 3. (a) Variance attribute extract along the Top Hammerhead horizon highlighting columns. (b) Variance Time slice at 3800ms highlighting primary faults with secondary faults within the Hammerhead Supersequence. (c) Sketch that overlies the identified columns from (a) with underlying fault strikes from (b). Seismic cross section (d) with and (e) without interpretations, illustrating the faults and columns. (Figure not oriented with North at the top.)*

4.4.3. Faults in Area 2

The predominant fault type within the Hammerhead Supersequence in Area 2 shows a gradual change from the northwest to the southeast (Figure 7). To the northwest, faulting consists predominantly of polygonal faults. Dimensions of the polygonal faults are similar to those described in section 4.4.1 above. We then observe an increase in the number of primary faults towards the southeast of Area 2 that show increasing listric characteristics.

A total of 6 primary faults were interpreted in this area. These faults extend from the top of the Hammerhead Supersequence, down through the Tiger and White Pointer Supersequences to sole out within the Blue Whale Supersequence. The primary faults have an average orientation of 300° and have throws that range between 45 to 145 ms (56 - 185 m) within the Hammerhead Supersequence.

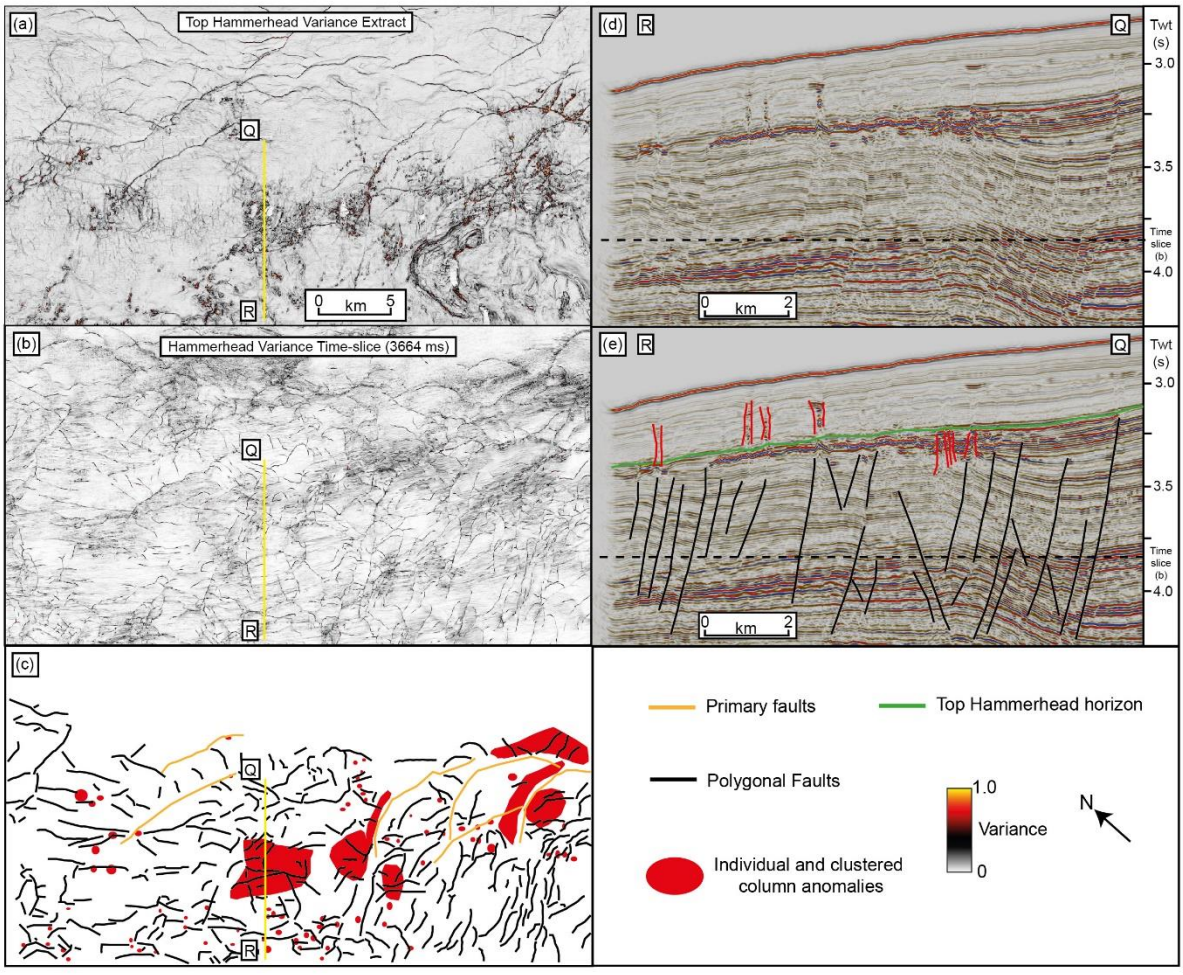

Figure 7: *From Area 2 in Fig 3. (a) Variance attribute extract along the Top Hammerhead horizon highlighting 'columns'. (b) Variance Time slice at 3664 ms highlighting polygonal, primary and secondary faults within the Hammerhead Supersequence. (c) Sketch that overlies the identified*

columns from (a) with underlying fault strikes from (b). Seismic cross section (d) with and (e) without interpretations, illustrating the faults and column. (Figure not oriented with North at the top.)

5. Discussion

We document columnar seismic anomalies along the top 400 ms (485 m) of the Hammerhead Supersequence and within the Cenozoic sequence along the southwestern edge of the Ceduna 3D survey area. Based on the column-like morphology of these features, they could be interpreted to be either dissolution pipes or fluid escape pipes. Dissolution pipes form by dissolution of rocks at depth to form subsurface cavities that subsequently result in a collapse pipe, whereas fluid escape pipes are conduits of vertically migrating fluids that are commonly associated with naturally seeping or overpressured fluid sources (Cartwright et al., 2007). Dissolution pipes are likely to occur within host-rocks that can undergo karstification or are dissolvable, such as evaporates and carbonates (Cartwright et al., 2007). While the Cenozoic Dugong Supersequence consists of carbontes, the underlying Wobbegong and Hammerhead Supersequences are predominantly siliclastic, within which dissolution pipes are not able to form. Given that 54% of the identified columns occur within the Hammerhead Supersequence, it is unlikely that the columns are dissolution pipes. We thus interpret them to be fluid escape pipes. Fluid escape pipes represent the manifestation of focused fluid flows on seismic data. They are often described as zones of increased permeability through which fluids are transported at faster rates than they would have through the undeformed host rock (Leduc et al., 2013; Løseth et al., 2011). The chaotic or distorted nature of the seismic reflectors within the fluid escape pipes can be attributed to variations in velocity between them and the surrounding sedimentary rocks (Cartwright et al., 2007; Løseth et al., 2011).

The increased seismic amplitudes of the fluid escape pipes relative to the surrounding host rock indicates a contrast in acoustic impedance between them. Amplitude anomalies within fluid escape pipes are often associated with the presence of low velocity fluids such as hydrocarbons, or zones of cementation that resulted from localized diagenesis during fluid migration (Moss and Cartwright, 2010).

Fluid escape pipes are recognized as pathways of focused fluid venting from underlying source regions (Cartwright and Santamarina, 2015). Judd and Hovland (2007) indicate that the occurrence of focused fluid flows can range from high energy, explosive events to low energy, gentle events which may or may not result in a surficial expression of fluid expulsion. Fluid expulsion along a surface often results in crater-like depressions known as pockmarks, or paleo-pockmarks if they have been buried and preserved; however, they do not provide information on the rate or amount of fluids that have been expelled (Andresen, 2012; Cartwright et al., 2007). No pockmarks were identified to

overlie the fluid escape pipes documented in this study, suggesting that fluid expulsion which formed the fluid escape pipes was of low energy.

5.1. Evidence for Fault Controlled Focused Fluid Flow

The spatial distribution of Cenozoic and Hammerhead fluid escape pipes documented in this study changes within the study area, from having a random spatial distribution in Area 1 (in the northwest) to occurring in linear clusters in Area 3 (in the southeast)(Figure 5a, 6a). We also observe a change in the pre-dominant fault type within the Hammerhead Supersequence along the study area; varying from polygonal faults in the Area 1 to primary faults in Area 3 (Figure 5b, 6b). The apparent correlation between the spatial distribution of fluid escape features and pre-dominant fault type along the study area, together with the observation that each fluid escape pipe overlies the upper tip of an extensional fault within the Hammerhead Supersequence, suggests that the faults and fluid escape pipes are spatially linked. A variance attribute extract from a 100 ms time window below the Top Hammerhead horizon shows the spatial overlap between Hammerhead fault strikes and locations of fluid escape pipes (Figure 5c, 6c). This observation supports our interpretation that the faults and fluid escape pipes are spatially linked.

To further demonstrate the spatial link between fluid escape pipes and underlying faults, we utilize spatial statistics to quantify the change in spatial distribution trends of fluid escape pipes between Area 1 and Area 3 (Figure 8). Two 7 by 7 km areas (referred to as ‘grid A1’ and ‘grid A3’) with spatial distributions of fluid escape features that are representative of those in Area 1 and Area 3 were identified and used for spatial statistics analysis (Figure 5a, 6a). We define three search radii (r) of 1.5, 2.5 and 3.5 km that sufficiently sample fluid escape pipes within each grid. At grid A1, 74 alignments were identified when r is 3.5 km, 15 alignments when r is 2.5 km and 11 alignments when r is 1.5 km (Figure 8b, c, d). From Rayleigh’s test, p values of 0.8, $3x10^{-5}$ and 0.2 were calculated when r is 3.5, 2.5 and 1.5 km respectively. The varying orientations of the alignments identified and relatively high p-value when r is 3.5 km show that the spatial distribution of the fluid escape features is random. While relatively low p-values were obtained when r is 2.5 and 1.5 km, it is based on a limited number of identified alignments that are focused around a smaller cluster of fluid escape pipes. These p-values are thus not representative of the overall spatial distribution.

At grid A3, 88, 99, and 56 alignments were identified when r is 3.5, 2.5 and 1.5 km respectively (Figure 8e, f, g). From Rayleighs test, p values significantly lower than 0.01 were obtained for all search radii. Furthermore, the mean orientation of the alignments are 296°, 297° and 276°, which is similar to the average primary fault strike orientation of 280°. The low p values and consistency in the alignment orientations show that it is highly unlikely for the spatial distribution of fluid escape pipes in Area 3 to be random.

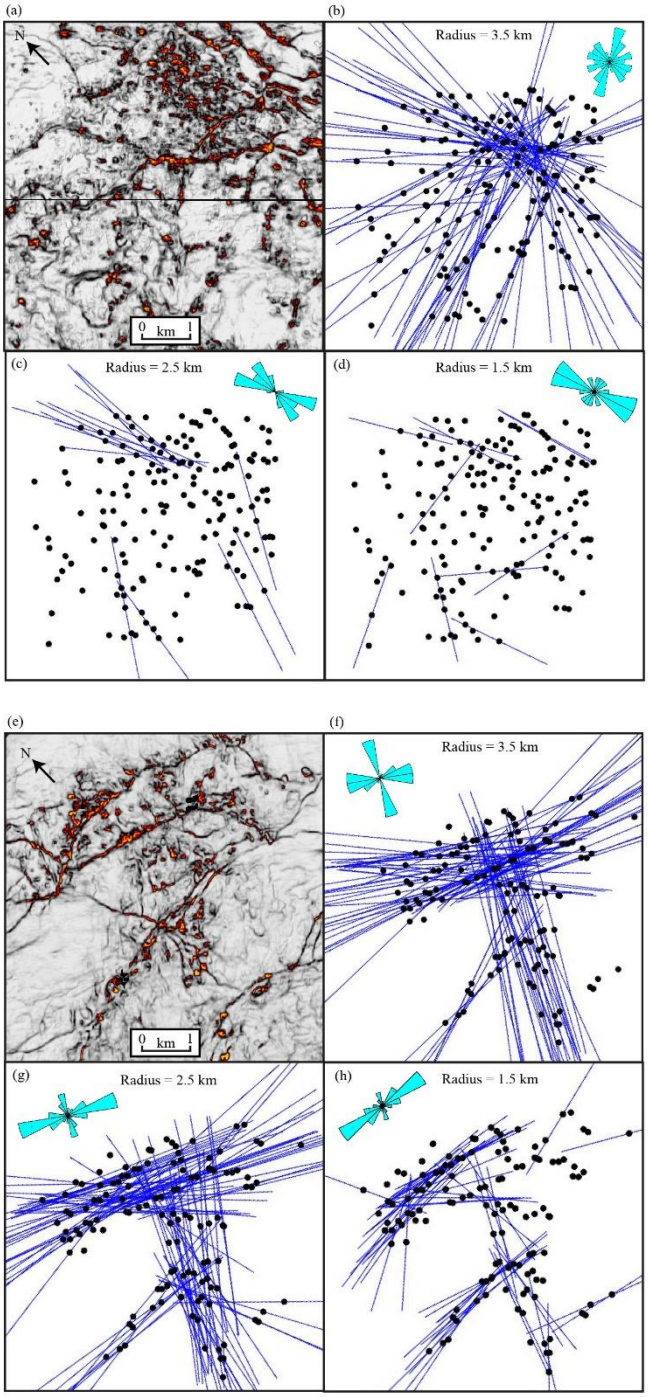

***Figure 8**: Spatial statistics analysis for fluid escape pipe distribution in (a) grid A1 and (e) grid A3. Alignments identified for search radii of (b, f) 3.5 km, (c, g) 2.5 km, and (d, h) 1.5 km are displayed.*

The results of spatial statistics analysis reinforce our interpretation of a spatial link between the fluid escape pipes and underlying faults. The random spatial distribution in Area 1 can be attributed to the variable strike orientations of the underlying polygonal faults whereas the linear trends in Area 3 can be attributed to the underlying primary faults.

The spatial link between the fluid escape features and the Hammerhead faults that underlie them suggest that the faults had acted as fluid migration pathways. Similar interactions between faults and fluids have been documented in various regions across the globe. In the Lower Congo basin, Gay et al. (2007) documented fluid escape features within elongated fault depressions along the seabed. The faults are interpreted to have acted as migration pathways for fluids from reservoirs at least 800 m below the seafloor. In the Hammerfest Basin of the Barrents Sea, regional subsurface faults were identified to act as migration avenues for thermogenic fluids from Jurassic hydrocarbon reservoirs to shallower Paleocene strata (Ostanin et al., 2013).

Establishing the timing of fluid escape pipe formation would provide information on the periods of fluid migration, which could then be used to identify a potential source of fluids (Andresen, 2012). Given the spatial link between fluid escape pipes and Hammerhead faults, it is critical to understand the fault growth history and its development as fluid migration conduits in order to determine the timing of fluid escape pipe formation.

5.2. Fault Development as Migration Pathways

5.2.1. Primary Faults

The primary faults are documented within the Hammerhead Supersequence along the ‘south-western edge of the study area and are the predominant fault type in Area 3 (Figure 3). The upper tips of these faults terminate along the unconformity surface that marks the top of the Hammerhead Supersequence, and their bases sole out along either of two identified detachment surfaces; one within the Blue Whale Supersequence (referred to as Type A faults), and the other along the top of the Tiger Supersequence (referred to as Type B faults). A third set of normal faults were identified in the stratigraphic sequences that underlie the Hammerhead Supersequence (referred to as Type C faults). The upper tips of these faults terminate along the top of the Tiger Supersequence and they extend down through the Tiger and White Pointer Supersequences to sole out along a detachment surface within the Blue Whale Supersequence. Several studies have indicated that the Type A and Type B faults identified in this study formed during the Late Cretaceous, between the Santonian and Maastrichtian, whereas Type C faults developed during the Mid Cretaceous, between the Cenomanian to Santonian (Totterdell and Bradshaw, 2004; Krassay and Totterdell, 2003; Kovacevic et al., 2015; Macdonald et al., 2012).

Detailed studies on primary fault nucleation and development within the Ceduna Sub-Basin have recently been undertaken by Robson et al. (2017) and Ryan et al. (2017). These faults were studied using displacement-distance, displacement-depth and expansion index analysis to develop fault growth profiles. Results of their studies identified three types of growth histories for Type A faults; (a) continuous propagation of Type C faults from their nucleation in the Cenomanian through to the

Maastrichtian; (b) reactivation and propagation of Type C faults during the Maastrichtian with a period of halted development between the Turonian and early Campanian; (c) nucleation and growth of Type B faults within the Hammerhead Supersequence that dip-linked with Type C faults by the late Maastrichtian. Ryan et al. (2017) suggested that Type A faults within the study area predominantly developed through dip-linking between Type B and Type C faults (Figure 9). Based on the results of these studies, we also interpret that although Type B and Type C faults are not observed to be dip-linked on seismic data within this study, it is possible that there is a connection between the upper tips of Type C faults and the bases of the Type B faults that is below the seismic resolution threshold.

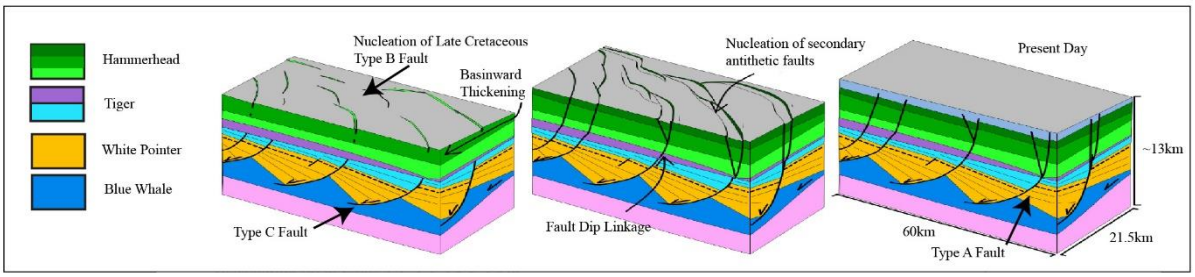

Figure 9. *Illustrated growth history and fault plane interaction between the Cenomanian-Santonian Type C faults and the Santonian-Maastrichtian Type B faults. Modified from (Robson et al., 2017).*

5.2.2. Polygonal Faults

Polygonal faults are defined as arrays of layer-bound extensional faults with varying fault strike orientations that form within fine-grained stratigraphic intervals (Cartwright et al., 2003). The mechanisms by which polygonal faults form are poorly understood and a topic of ongoing debate. Studies have proposed several models for their formation including gravity collapse, density inversion, syneresis and dehydration of water bearing minerals (Cartwright and Dewhurst, 1998; Cartwright et al., 2003; Seebeck, 2015).

In this study, we document a polygonal fault system that consists of two tiers and with two ‘orders’ of faults within the Hammerhead Supersequence. The polygonal faults occur predominantly in Areas 1 and 2 of the ‘study area’ (Figure 3). Their locality along the distal most part of the survey is interpreted to be due to the basin-ward increase in clay content within the Hammerhead Supersequence (King and Mee, 2004; Krassay and Totterdell, 2003). These faults do not propagate into the overlying Cenozoic sequence nor the underlying Tiger Supersequence and are interpreted to have formed at the end of the Cretaceous. As was discussed with Type B and Type C listric faults, it is possible that the lower tips of the polygonal faults are linked with the upper tips of the Type C faults and that the linkage between them is below seismic resolution.

5.3. Migration Pathways

Primary and polygonal faults within the Hammerhead Supersequence are interpreted to have developed during the Campanian and Maastrichtian of the Late Cretaceous. The fluid escape pipes documented in this study occur within the Cenozoic sequence and the top 400 ms (485 m) of the Hammerhead Supersequence. This observation leads us to interpret that the faults had developed as fluid migration pathways by the end of the Cretaceous. This is supported by the lack of fluid escape features identified within the Hammerhead Supersequence at depths deeper than 400 ms (485 m) below the Top Hammerhead horizon. The primary faults and polygonal faults had nucleated and developed within the Hammerhead Supersequence between the Santonian and Maastrichtian. Had there been fluid migration during their initial development, we would expect to observe fluid escape pipes at varying depths within the Hammerhead Supersequence.

5.4. Fluid Source

As previously discussed, primary and polygonal faults within the study area are interpreted to have developed as fluid migration pathways by the end of the Cretaceous. The formation of fluid escape pipes overlying the upper tips of the faults indicates that they formed after fault development. Furthermore, we also observe that the upper tips of the fluid escape pipes terminate at varying depths within the Cenozoic sequence. This suggests that fluid expulsion and fluid escape pipe formation persisted from the Late Cretaceous through to the Cenozoic, though poor age control within the Cenozoic sequence precludes more precise constraints on their age. Similar deductions for continuous or episodic fluid expulsion events were made in offshore Namibia where fluid escape pipes with upper tips that terminate at varying stratigraphic levels were observed (Moss and Cartwright, 2010).

Type B faults and polygonal faults had nucleated within the Hammerhead Supersequence between the Campanian and Maastrichtian. Type B faults then dip linked with underlying Type C faults to form Type A faults. Although not observable on seismic data within this study, the lower tips of Type B faults and polygonal faults are interpreted to be connected with the upper tips of Type C faults based on fault growth patterns identified by Robson et al. (2017) and Ryan et al. (2017). Based on these fault development observations, the fluids that formed the fluid escape pipes are hypothesized to be sourced from two potential source groups; the Hammerhead Supersequence, or the ‘pre-Hammerhead’ sequences (Mid Cretaceous Tiger, White Pointer and Blue Whale Supersequences).

Samples of the Hammerhead Supersequence that were recovered from Gnarlyknots -1 indicate that the sequence is sand rich. It could be argued that samples taken at the well are from proximal parts of the basin and that in the distal parts of the basin, the sedimentary rocks would have higher clay content, evidenced by the presence polygonal faults. Clay minerals such as smectite may be altered to

illite through diagenesis and will release water in this processes, thus making it a possible source of fluids for fluid escape pipe formation (Hall et al., 1986).

Alongside the primary faults within Area 3, secondary synthetic and antithetic faults are also identified within the Hammerhead Supersequence. These secondary faults are contained within the Hammerhead Supersequence and do not intersect the Top Hammerhead horizon nor do they extend down to the detachment surface along the top of the Tiger. If the Hammerhead Supersequence was a source of fluids, we would expect to observe a higher degree of association between the fluid escape features and the secondary faults. The fluid escape features are instead predominantly associated with Type A and Type B primary faults which are linked to deeper stratigraphic sequences (Figure 6).

In Area 1, faults within the Hammerhead Supersequence are predominantly polygonal faults. While mechanisms that forms polygonal faults are still poorly understood, these faults are often associated with fluid expulsion during their formation due to the dewatering of clay minerals (Cartwright, 1994; Cartwright and Dewhurst, 1998; Gay et al., 2004). It could be then be argued that the fluid escape pipes that overlie the polygonal faults were a result of fluid expulsion during fault formation; however, the fluids expelled during polygonal fault formation generally migrate through diffusive flow mechanisms as opposed to focused fluid migration (Berndt et al., 2003; Cartwright and Lonergan, 1996). Diffusive fluid flow is a low flux fluid migration process that does not form fluid escape features such as fluid escape pipes or pockmarks (Berndt, 2005; Judd and Hovland, 2007). Wang et al. (2010) further indicate that the low permeability and strong capillary forces of fine grained sediments make are it unlikely for fluids to be expelled are rates sufficient to form fluid escape features.

Based on the observations and analysis made in this section, we rule out the hypothesis that the fluids which formed the fluid escape pipes are sourced from the Hammerhead Supersequence and are instead interpreted to be sourced from the Tiger, White Pointer or Blue Whale Supersequences.

5.5. Fluid Composition

Whilst we hypothesise that the observed fluid escape pipes had formed from fluids sourced from the Albian to Coniacian Blue Whale, White Pointer, or Tiger Supersequences, we are unable however, to determine the fluid composition based on the seismic data observations. Direct measurements or sample analysis from sedimentary rocks within the fluid escape pipes would be needed to accurately determine fluid composition. Increased amplitudes of seismic reflectors within fluid escape pipes, relative to the surrounding reflectors, can be attributed to the presence of hydrocarbons or host rock alteration by thermogenic fluids (Forrest et al., 2010; Løseth et al., 2009).

Numerous studies and surveys conducted within the Ceduna Sub-basin have provided evidence that favors the interpretation of the fluids sourced from the Blue Whale, White Pointer and basal Tiger supersequences being hydrocarbons (King and Mee, 2004; Longley et al., 2001). These stratigraphic sequences have been identified as potentially containing hydrocarbon source rocks within the main depocenter of the sub-basin (Struckmeyer et al., 2001). Petroleum modelling studies have been undertaken to determine the timing of generation and expulsion of hydrocarbons from the Blue Whale, White Pointer, Tiger and Hammerhead Supersequences in the Ceduna Sub-basin (Struckmeyer et al., 2001; Totterdell et al., 2008). Results from the modelling studies constrained the timing of hydrocarbon expulsion to be between 95 to 55 Ma for the Blue Whale Supersequence, 80 and 15 Ma for the White Pointer, and 80 to 25 Ma for the basal Tiger Supersequences (Figure 10). Struckmeyer et al (2001) further suggests that hydrocarbons from phases of expulsions during the Mid Cretaceous, prior to deposition of the Hammerhead Supersequence, may have been reservoired within the White Pointer and Tiger Supersequences. The results from the modelling studies are in agreement with our interpreted timing of fluid migration and fluid escape pipe formation. Type A and type B faults, along with the polygonal faults, are interpreted to have developed as fluid migration pathways by the Late Cretaceous, coeval with the hydrocarbon expulsion phases of source rocks within the Blue Whale, White Pointer and Tiger Supersequences.

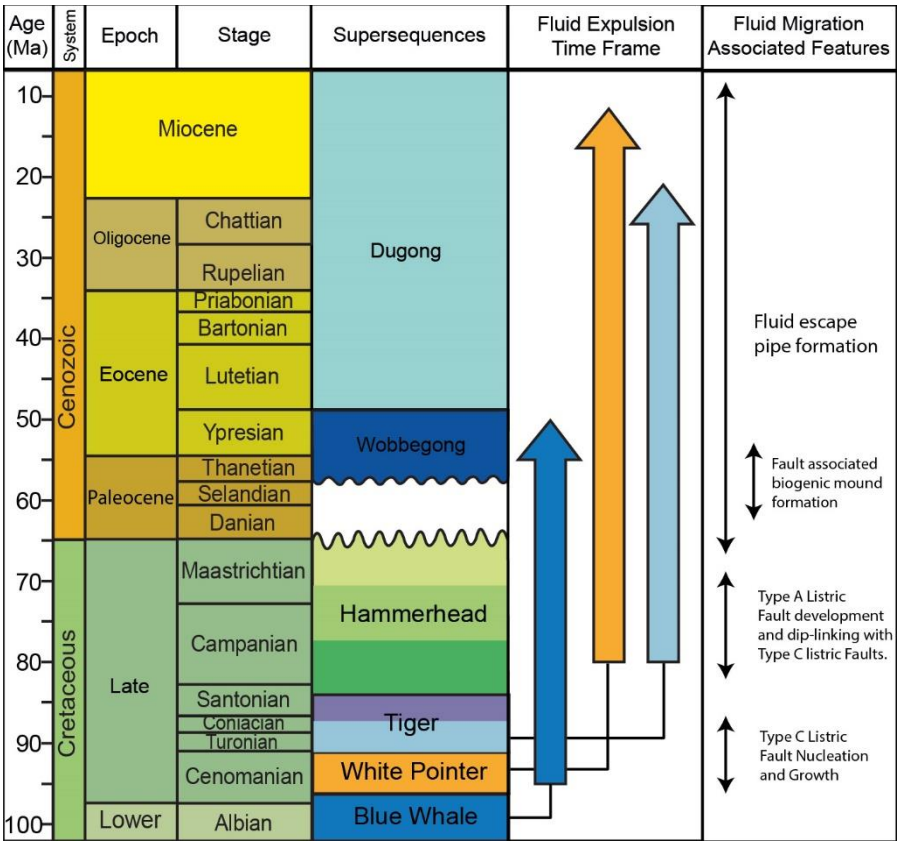

***Figure 10**: Timing of hydrocarbon expulsion from Mid Cretaceous source rocks. Edited from Struckmeyer et al. (2001).*

A study by Langhi et al. (2016) documented Cenozoic biogenic mounds that were observed to have spatial links with Hammerhead Supersequence faults that underlie them, similar to the spatial links observed between fluid escape pipes and Hammerhead Supersequence faults in this study (Figure 1). These biogenic mounds overlie the Top Hammerhead horizon and are interpreted to have formed during the Paleocene to Eocene (Langhi et al., 2016). These mounds do not show any relationship to paleo-bathymetric highs, and thus Langhi et al. (2016) propose a model whereby the biogenic mound growth is attributed to hydrocarbon seepage sourced from the Tiger and White Pointer supersequences that had utilized normal faults, similar to Type A faults of this study, as migration pathways. The proposed model for biogenic mound growth in Langhi et al. (2016) agrees with our interpretation that the primary and polygonal faults identified in our study are facilitating migration for fluids sourced from the Blue Whale, White Pointer and Tiger Supersequences.

A regional model of source rock distribution within the Bight Basin was developed by Struckmeyer et al. (2001) to assess the source rock potential of the Ceduna Sub-Basin. Geochemical data from 13 wells across the Ceduna, Sub-Basin, Eyre Sub-Basin, Duntroon and Polda Basins were utilized in developing this model. Analysis of the samples show total organic content (TOC) vales of up to 22%, with even higher values measured in coals from the samples. Though these samples were taken from wells along proximal parts of the sub-basin, similar organic rich rocks are suggested to be present within the main depocenter along the distal region of the Ceduna Sub-basin (King and Mee, 2004; Struckmeyer et al., 2001).

6. Implications of this study for Hydrocarbon Exploration in the Ceduna Sub-Basin

The Ceduna Sub-Basin is a frontier exploration region in Australia. Despite undergoing multiple phases of petroleum exploration since the 1970s, to date, only 5 exploration wells having been drilled in the sub-basin – four of which are in the proximal margins of the sub-basin (Somerville, 2001; Strand et al., 2017). Hydrocarbon charge is perceived to be the major exploration risk in the sub basin (Somerville, 2001). A lack of direct evidence for oil-prone source rocks in the distal regions of the sub-basin has resulted in exploration focussed along the proximal regions of the sub-basin. Of the five exploration wells in the sub-basin, two have shown indications of a working petroleum system. Oil and gas shows were reported from Greenly-1 and low abundance oil filled fluid inclusions were documented at Gnarlyknots-1 (Strand et al., 2017; Totterdell and Mitchell, 2009).

The results of this study contributes to the existing body of evidence which indicates the presence of a working petroleum system in the distal regions of the Ceduna Sub-Basin. Our findings show that the faults along the shelf edge were functional fluid migration pathways that had facilitated the migration

of potential hydrocarbons from the Mid Cretaceous Blue Whale, White Pointer and basal Tiger Supersequences to shallower late Cretaceous and Cenozoic intervals. Documentation of fluid escape pipes with upper terminuses that terminate along the seafloor indicate that it is plausible that the faults are active fluid migration pathways at present. Although the analysis of this study was based on a survey that covers only a part of the Ceduna Sub-Basin, the observations and results can be applied to other regions of the sub-basin to infer the presence of a working petroleum system.

7. Conclusion

We document fluid escape features within the Cenozoic and top 400 ms of the Maastrichtian Hammerhead supersequence along the southwestern edge of the survey area in the Ceduna Sub-basin. The fluid escape features overlie the upper tips of normal faults within the Hammerhead Supersequence and have varying spatial distributions between the north-western and south-eastern corners of the study area; a sporadic arrangement in the north-western corner and linear trends in the south-eastern corner. This variation in spatial distribution is reflected in the change of predominant fault type within the Hammerhead Supersequence that underlie the fluid escape features within the study area; polygonal faulting to the northwest and listric faults to the southeast. Both the polygonal and listric faults are interpreted to have facilitated fluid migration and based on their fault growth histories, they developed as migration pathways by the end of the Cretaceous. The fluids are interpreted to be hydrocarbons sourced from the Early Cretaceous Blue Whale, White Pointer, and Tiger Supersequences. Petroleum systems modelling suggests that hydrocarbon expulsion from these sequences was between 95 Ma to 15 Ma, between the Mid Cretaceous and Mid Cenozoic. The findings of this study contribute to existing research on better understanding the sub-basins petroleum prospectivity by identifying potential hydrocarbon migration pathways and potentially reducing exploration risk in distal parts of the sub-basin.

8. References

Abrams, M.A., 2005. Significance of hydrocarbon seepage relative to petroleum generation and entrapment. Marine and Petroleum Geology, 22, 457-477.

Andresen, K.J., 2012. Fluid flow features in hydrocarbon plumbing systems: What do they tell us about the basin evolution? Marine Geology, 332-334, 89-108.

Andresen, K. J., Huuse, M., Schodt N. H., Clausen, L. F., Seidler L., 2011. Hydrocarbon plumbing systems of salt minibasins offshore Angola revealed by three-dimensional seismic analysis, 95, 1039-1065.

Berndt, C., 2005. Focused Fluid Flow in Passive Continental Margins. Philosophical Transactions: Mathematical, Physical, and Engineering Sciences, 363, 2855-2871.

Berndt, C., Bünz, S., Mienert, J., 2003. Polygonal fault systems on the mid-Norwegian margin: a long-term source for fluid flow, in: Rensbergen, P.v., R, R.H., Maltman, A., Morley, C. (Eds.), Subsurface Sediment Mobilization. Geological Society of London Special Publication, London, 283-290.

Bradshaw, M., Foster, C., Wilcox, B., Struckmeyer, H., 2002. Australia's Frontier Basins and Prospects for New Petroleum Provinces, In: 17th World Petroleum Congress, world Petroleum Congress, 10 pp.

Cartwright, J., 1994. Episodic basin-wide hydrofracturing of overpressured Early Cenozoic mudrock sequences in the North Sea Basin. Marine and Petroleum Geology, 11, 587-607.

Cartwright, J., Dewhurst, D.N., 1998. Layer-bound compaction faults in fine-grained sediments. GSA Bulletin, 110, 1242-1257.

Cartwright, J., Huuse, M., Aplin, A., 2007. Seal bypass systems. American Association of Petroleum Geologists Bulletin, 91, 1141-1166.

Cartwright, J., James, D., Bolton, A., 2003. The Genesis of polygonal fault systems: a review, in: Rensbergen, P.v., R, R.H., Maltman, A., Morley, C. (Eds.), Subsurface Sediment Mobilization. Geological Society of London Special Publication, London, 223-243.

Cartwright, J., Lonergan, L., 1996. Volumetric contraction during the compaction of mudrocks: a mechanism for the development of regional-scale polygonal fault systems. Basin Research, 8, 183-193.

Cartwright, J., Santamarina, C., 2015. Seismic characteristics of fluid escape pipes in sedimentary basins: Implications for pipe genesis. Marine and Petroleum Geology, 65, 126-140.

Davies, R.J., Goulty, N.R., Meadows, D., 2008. Fluid flow due to the advance of basin-scale silica reaction zones. GSA Bulletin, 120, 195-206.

Davies, R.J., Mathias, S.A., Moss, J., Hustoft, S., Newport, L., 2012. Hydraulic fractures: How far can the go? Marine and Petroleum Geology, 37, 1-6.

Forrest, M., Roden, R., Holeywell, R., 2010. Risking seismic amplitude anomaly prospects based on database trends. The Leading Edge, 29, 936-940.

Gay, A., Lopez, M., Berndt, C., Seranne, M., 2007. Geological controls on focused fluid flow associated with seafloor seeps in the Lower Congo Basin. Marine Geology, 244, 68-92.

Gay, A., Lopez, M., Cochonat, P., Sermondadaz, G., 2004. Polygonal faults-furrows systemrelated to early stages of compaction - upper Miocene to recent sediments of the Lower Congo Basin. Basin Research, 16, 101-116.

Hall, P.L., Astill, D.M., Mcconnell, J.D.C., 1986. Thermodynamic and structural aspects of the dehydration of smectites in sedimentary rocks. Clay Minerals, 21, 633-648.

Hammer, Ø., 2009. New statistical methods for detecting point alignments. Computers and Geosciences, 35, 659-666.

Hammer, Ø., Harper, D.A.T., Ryan, P.D., 2001. Past: Paleontological statistics software package for education and data analysis. Palaeontologia Electronica, 4, 9 pp.

Heggland, R., 1998. Gas seepage as an indicator of deper prospective reservoirs. A study based on exploration 3D seismic data. Marine and Petroleum Geology, 15, 1-9.

Holford, S., Schofield, N., MacDonald, J.D., Duddy, I.R., Green, P.F., 2012. Seismic analysis of igneous systems in sedimentary basins and their impacts on hydrocarbon prospectivity: Examples from the soutern Australian Margin, The APPEA Journal 52, 229-252.

Judd, A., Hovland, M., 2007. Seabed Fluid Flow: The Impact on Geology, Biology and the Marine Environment. Cambridge University Press, United Kingdom, 408 pp.

King, S.J., Mee, B.C., 2004. The seismic stratigraphy and petroleum potential of the Late Cretaceous Ceduna Delta, Ceduna Sub-Basin Great Australian Bight, in: Boult, P.J., Johns, D.R., S.C.Lang

(Eds.), Eastern Australian Basins Symposium II. Petroleum Exploration Society of Australia, Adelaide, Australia, 63-73.

Krassay, A.A., Totterdell, J.M., 2003. Seismic stratigraphy of a large, Cretaceous shelf-margon delta complex, offshore southern Australia. American Association of Petroleum Geologists Bulletin, 87, 935-963.

Kovacevic, J., Cuneen, J., Elders, C., 2015. Evolution of detached listric fault systems in the Ceduna Delta, Bight basin: Insights from 3D seismic data. ASEG Extended Abstracts, 2015(1), 1-4.

Langhi, L., Strand, J., Ross, A.S., 2016. Fault-related biogenic mounds in the Ceduna Sub-basin, Australia: Implications for hydrocarbon migration. Marine and Petroleum Geology, 74, 47-58.

Leduc, A.M., Davies, R.J., Swarbrick, R.E., Imber, J., 2013. Fluid flow pipes triggered by lateral pressure transfer in the deepwater western Niger Delta. Marine and Petroleum Geology, 43, 423-433.

Logan, G., Jones, A., Ryan, G., Wettle, M., Thankappan, M., Grosjean, E., Rollet, N., Kennard, J., 2008. Review of Australian Offshore Natural Hydrocarbon Seepage Studies, Geoscience Australia Record: 2008/17, 235 pp.

Longley, I.M., Bradshaw, M.T., Hebberger, J., 2001. Australian Petroleum Provinces of the Twenty-First Century, in: Downey, M.W., Threet, J.C., Morgan, W.A. (Eds.), Petroleum provinces of the twenty-first century: AAPG Memoir 74, pp. 287-317.

Løseth, H., Gading, M., Wensaas, L., 2009. Hydrocarbon leakage interpreted on seismic data. Marine and Petroleum Geology, 26, 1304-1319.

Løseth, H., Wensaas, L., Arnsten, B., Hanken, N.-M., Basire, C., Graue, K., 2011. 1000 m long gas blow-out pipes. Marine and Petroleum Geology, 28, 1047-1060.

Macdonald, J., Backé, G., King, R., Holford, S., Hillis, R., 2012. Geomechanical modelling of fault reactivation in the Ceduna Sub-basin, Bight Basin, Australia. Geological Society , London, Special Publications 367, 71-89.

Mardia, K.V., Jupp, P.E., 2000, Directional Statistics Vol. 494, John Wiley & Sons, 441 pp.

Meldahl, P., Heggland, R., 1999. The chimney cube, an example of semi-automated detection of seismic objects by directive attributes and neural networks: Part I; methodology. SEG Technical Program Expanded Abstracts, 931-934.

Moss, J.L., Cartwright, J., 2010. 3D seismic expression of km-scale fluid escape pipes from offshore Namibia. Basin Research, 22, 481-501.

Ostanin, I., Anka, Z., Primio, R.d., Bernal, A., 2013. Hydrocarbon plumbing systems above the Snøhvit gas field: Structural control and implications for thermogenic methane leakage in the Hammerfest Basin, SW Barents Sea. Marine and Petroleum Geology, 43, 127-146.

Reynolds, P., Holford, S., Schofield, N., Ross, A., 2017. The shallow depth emplacement of mafic intrusions on a magma-poor rifted margin: An example from the Bight Basin, southern Australia. Marine and Petroleum Geology, 88, 605-616.

Robson, A., King, R., Holford, S., 2017. Structural evolution of a gravitationally detached normal fault array: analysis of 3D seismic data from the Ceduna Sub-Basin, Great Australian Bight, Basin Research, 29, 605-624.

Ruble, T.E., Logan, G.A., Blevin, J.E., Struckmeyer, H.I.M., Liu, K., Ahmed, M., Eadington, P.J., Quezada, R.A., 2001. Geochemistry and Charge History of a Palaeo-Oil Column : Jerboa-1, Eyre Sub-Basin, Great Australian Bight, In: Hill, K.C. & Bernecker, T. (eds.) Eastern Australian Basins Symposium: a refocused energy perspective for the future. Petroleum Exploration Society of Australia, Melbourne, Australia, 521-529.

Ryan, L., Magee, C., Jackson, C.A.L., 2017. The kinematics of normal faults in the Ceduna Subbasin, offshore southern Australia: Implications for hydrocarbon trapping in a frontier basin. American Association of Petroleum Geologists Bulletin, 101, 321-341.

Sayers, J., Symonds, P.A., Direen, N.G., Bernardel, G., 2001. Nature of the continent-ocean transition on the non-volcanic rifted margin of the central Great Australian Bight. Geological Society , London, Specail Publications, 187, 51-76.

Schofield, N., Holford, S., Edwards, A., Mark, N., Pugliese, S., 2019. Overpressure Transmission through Interconnected Igneous Intrusions. AAPG Bulletin, 36 pp.

Seebeck, H., 2015. Polygonal faulting and seal integrity in the Bonaparte Basin, Australia. Marine and Petroleum Geology, 60, 120-135.

Somerville, R., 2001. The Ceduna Sub-basin: A Snapshot of Prospectivity. The APPEA Journal 41(1), 321-346.

Strand, J., Langhi, L., Ross, A.S., Dyt, C., 2017. Coupled stratigraphic and fault seal modelling used to describe trap integrity in the frontier Bight Basin, Australia. Marine and Petroleum Geology, 86, 474-485.

Struckmeyer, H.I.M., Totterdell, J.M., Blevin, J.E., Logan, G.A., Boreham, C.J., Deighton, I., Krassay, A.A., Bradshaw, M.T., 2001. Charactor, Maturity and Distribution of Potential Cretaceous Oil Source Rocks in the Ceduna Sub-Basin, Bight Basin, Great Australian Bight, In: Hill, K.C. & Bernecker, T. (eds.) Eastern Australasian Basins Symposium. Petroleum Exploration Society of Australia, Melbourne, Victoria, 543-552.

Struckmeyer, H.I.M., Williams, A., Cowley, R., Totterdell, J., Lawrence, G., O'Brien, G., 2002. Evaluation of Hydrocarbon Seepage in the Great Australian Bight. The APPEA Journal 42.1, 371-385.

Totterdell, J.M., Blevin, J.E., Struckmeyer, H.I.M., Bradshaw, B.E., Colwell, J.B., Kennard, J.M., 2000. A new sequence framework for the Great Australian Bight: starting with a clean slate. APPEA Journal 40(1), 95-120.

Totterdell, J.M., Bradshaw, B.E., 2004. The structural framework and tectonic evolution of the Bight Basin, in: Boult, P.J., Johns, D.R., S.C.Lang (Eds.), Eastern Australasian Basins Symposium II. Petroleum Exploration Society of Australia, Adelaide, Australia, 41-61.

Totterdell, J.M., Mitchell, C., 2009. Bight basin Geological Sampling and Seepage Survey: RV Southern Surveyor Survey: RV Southern Surveyor SS01/2007, Geoscience Australia Record 2009/24, 128 pp.

Totterdell, J.M., Struckmeyer, H., Boreham, C.J., Monteil, E., Bradshaw, B.E., 2008. Mid-Late Cretaceous organic-rich rocks from the eastern Bight Basin: implications for prospectivity. In: J.E. Blevin, B.E. Bradshaw and C. Uruski (eds), Eastern Australian Basins Symposium III. Petroleum Exploration Society of Australia, Special Publication, 137-158.

Wang, X., Wu, S., Yuan, S., Wang, D., Ma, Y., Yao, G., Gong, Y., Zhang, G., 2010. Geophysical signatures associated with fluid flow and gas hydrate occurrence in a tectonically quiescent sequence, Qiongdongnan Basin, South China Sea. Geofluids, 10, 351-368.

Willcox, J.B., Stagg, H.M.J., 1990. Australia' southern margin: A product of oblique extension. Tectonophysics, 173, 269-281.

Chapter 5

3D Seismic analysis of complex faulting patterns and fluid escape features associated with late Cenozoic magmatism in the Bass Basin, offshore southeast Australia.

Statement of Authorship

Title of Paper	Seismic analysis of complex faulting patterns and fluid escape features in the Igneous province of the Bass Basin, Offshore Southeast Australia
Publication Status	☐ Published ☐ Accepted for Publication ☐ Submitted for Publication ☑ Unpublished and Unsubmitted w ork w ritten in manuscript style
Publication Details	Velayatham, T., Holford, S.P., Bunch, M., King, R., Schofield, N.

Principal Author

Name of Principal Author (Candidate)	Tayallen Velayatham
Contribution to the Paper	Performed seismic data interpretation and spatial statistics analysis described in the study, wrote manuscript and is corresponding author.
Overall percentage (%)	75
Certification:	This paper reports on original research I conducted during the period of my Higher Degree by Research candidature and is not subject to any obligations or contractual agreements with a third party that would constrain its inclusion in this thesis. I am the primary author of this paper.
Signature	Date 27/5/2019

Co-Author Contributions

By signing the Statement of Authorship, each author certifies that:

i. the candidate's stated contribution to the publication is accurate (as detailed above);

ii. permission is granted for the candidate in include the publication in the thesis; and

iii. the sum of all co-author contributions is equal to 100% less the candidate's stated contribution.

Name of Co-Author	Simon P. Holford
Contribution to the Paper	Supervised development of work, helped with data interpretation, provided feedback and edited manuscript.
Signature	Date 27/5/19

Name of Co-Author	Mark Bunch
Contribution to the Paper	Supervised development of work, helped with data interpretation, provided feedback and edited manuscript.
Signature	Date 24/05/2019

Name of Co-Author	Rosalind King		
Contribution to the Paper	Supervised development of work, helped with data interpretation, provided feedback and edited manuscript.		
Signature		Date	24/06/2019

Please cut and paste additional co-author panels here as required.

Name of Co-Author	Nick Schofield		
Contribution to the Paper	Provided feedback and edited manuscript.		
Signature		Date	18/06/2019

Please cut and paste additional co-author panels here as required.

3D Seismic analysis of complex faulting patterns and fluid escape features associated with late Cenozoic magmatism in the Bass Basin, offshore southeast Australia.

Tayallen Velayatham, Simon Holford, Mark Bunch, Rosalind King, Nick Schofield

1. Abstract

Igneous intrusions in sedimentary petroleum basins are often regarded as having a negative impact on the elements of the petroleum system, though the impact of intrusion-related deformation features on petroleum systems is not well understood. In this study, we use 3D seismic reflection data to document a variety of deformation styles associated with igneous intrusions that were emplacement during late Cenozoic magmatic activity in the Bass Basin, offshore southeastern Australia; three intrusion associated normal fault systems (conjugate faults, concentric faults, radial faults) and fluid escape pipes. These deformation features occur within approximately 600 m of the associated with underlying igneous intrusions and occur within the Late Eocene to Miocene Demons Bluff and Torquay formations. The conjugate faults bound grabens and are interpreted to have formed in response to underlying dyke intrusions, whilst the radial faults are interpreted to have formed in response to overburden uplift from an emplaced, underlying intrusion that could not be identified in this study. We identify 101 fluid escape features that show variation in both the morphology of their surficial depressions and of the seismic reflection characteristics of their infilling deposits. These features are interpreted to be hydrothermal or volcanic vents with underlying pipe-like feeders, depending on their spatial association with adjacent or underlying igneous intrusions. The concentric fault systems are associated with surficial depressions, and quantitative analysis of reflector sags within these depressions suggest that they are a result of subsurface subsidence in response to

formation of maar-craters. The magmatic-related deformation features documented in this study may have multiple effects on working petroleum systems, such as providing secondary fluid flow pathways that can either reduce seal integrity, or enable migration into shallower reservoirs.

2. Introduction

The emplacement of magma within a sedimentary basin can present multiple challenges to hydrocarbon exploration and production (Schutter, 2003; Senger et al., 2017). For example, igneous intrusions such as dykes and sills can act as conduits for hydrocarbon fluids if they are fractured and permeable, though if impermeable, they can act as fluid migration barriers and can cause compartmentalization of the source or reservoir units (Cartwright et al., 2007; Holford et al., 2012; Senger et al., 2017). A more well-known impact is conductive and convective heat transfer from igneous intrusions within a source rock unit could induce hydrocarbon generation to result in source rock maturation or even over-maturation (Othman et al., 2001; Schofield and Totterdell, 2008). Igneous intrusions can also indirectly degrade the quality of potential hydrocarbon reservoir rocks. High temperature (>200° C)hydrothermal fluids that are derived from igneous intrusions or generated from heat transfer between igneous intrusions and subsurface fluids can be highly mineralizing and precipitate as cement when mobilizing through sedimentary rocks, thus reducing reservoir porosity and permeability of reservoir rocks (Holford et al., 2012; Parnell et al., 2005). In addition to the impacts on fluid flow properties of host rocks, magma intrusions can also have deleterious effects on the quality of seismic reflection data. For example, velocities of igneous intrusions (5.5 – 6.5 km/s) are often high relative to velocities of the surrounding host sedimentary rock (~3 km/s) (Senger et al 2017). These high velocity contrasts can result in distortions of underlying seismic reflectors, making it difficult to interpret both the intrusions and underlying strata (Jackson et al., 2013; Reynolds et al., 2018).

Subsurface magma transport and emplacement often results in deformation of the surrounding and overlying host rock, with the spectrum of deformation features encompassing calderas, fluid escape pipes, maar-diatremes, or forced folding of overburden. Deformation associated with the emplacement of igneous intrusions can have an array of impacts on the elements of a petroleum system (Holford et al., 2012). For example, igneous intrusions can be associated with the superheating of pore fluids within adjacent host rocks, resulting in overpressure generation, sediment fluidization or even sediment dissolution. These processes can result in subsurface focused fluid migration and expulsion (Jamtveit et al., 2004; Sun et al., 2013). Interaction of igneous intrusions with water in the near surface can also result in phreatomagmatic explosions, which in turn can lead to the formation of collapse structures such as calderas and maar-diatremes (Boyce, 2013; Schulz et al., 2005). These igneous intrusion associated collapse structures can form with complex fault systems that are

potentially able to influence subsurface fluid dynamics by providing fluid migration pathways (Reynolds et al., 2018; Schulz et al., 2005). Emplacement of igneous intrusions such as sills in the subsurface can result in structural deformation of the overburden to form forced fold structures that have the potential to act as hydrocarbon traps (Jackson et al., 2013; Schmiedel et al., 2017; Schutter, 2003). For instance, the Benbecula South well in the Rockall Basin of the United Kingdom discovered gas in a domal structure that was interpreted to have formed as a result of an underlying igneous emplacement (Schofield et al., 2018). As an igneous intrusion is emplaced into the host rock, the overburden can be uplifted in response to elastic bending to form domes with geometries that are similar to the underlying intrusion (Jackson et al., 2013; Schmiedel et al., 2017). While the impact of magmatic emplacements on petroleum systems have been the focus of numerous studies, there is less understanding of the impact of intrusion associated structural deformation features on petroleum systems.

The Bass Basin is a Cretaceous-Cenozoic failed rift basin located offshore south-eastern Australia. The basin contains a rich record of Cenozoic magmatism, manifested by synrift Paleocene lava flows and igneous sills, as well as post-rift Oligocene to Miocene submarine monogenetic volcanoes (Blevin et al., 2003; Reynolds et al., 2018; Watson et al., 2019). The basin is moderately explored with 45 wells drilled, 36 of which are exploration wells (Blevin et al., 2005) . Of the 36 exploration wells, 25 (55%) have encountered igneous lithologies in the subsurface (Watson et al., 2019). Extensive studies have been undertaken to understand the spatial distribution, emplacement mechanisms, seismic expressions and impact on petroleum systems of igneous intrusions within the Bass Basin (Blevin et al., 2003; Holford et al., 2012; Holford et al., 2017; Reynolds et al., 2018; Watson et al., 2019). Whilst the extrusive and intrusive components of this magmatism have been studied in relation to their impacts on petroleum systems, there has been comparatively little investigation of the potential impacts of deformation associated with igneous intrusions on hydrocarbon exploration and development. In this study, we document a broad array of intrusion induced overburden deformation features in the Bass Basin using 3D seismic data. We investigate the genesis and evolution of the overburden deformation features by analysing the variations in their morphology and spatial associations with interpreted underlying igneous intrusions within the study area. We also discuss the potential impact of these intrusion induced overburden deformation features on petroleum systems and hydrocarbon exploration in the region.

3. Geological Setting

The Bass Basin is located in the Bass Strait between Victoria and Tasmania, in the eastern part of Australia's rioted southern continental margin (Fig 1). It represents the failed arm of a rift system that developed primarily through three phases. The first phase occurred during the Late Jurassic to Early

Cretaceous as a part of the Southern Margin Rift System which initiated the separation between Australia and Antarctica (Cummings et al., 2004; Stagg et al., 1999). The second phase of rifting occurred during the Late Cretaceous to Early Paleocene, when rift systems developed along Australia's eastern margin, culminating in the formation of the Tasman Sea (Cummings et al., 2004; Hill et al., 1995). The third phase of rifting initiated in the Late Cretaceous, coeval with initiation of the second phase, along the Tasman Fracture Zone to the west (Blevin et al., 2003; Cummings et al., 2004). Structurally, the Bass Basin is characterized by a system of NW-SE trending half grabens, three of which have been defined as the deepest depocenters in the basin. These are the Cormorant, Yolla and Pelican troughs (Blevin et al., 2003; Holford et al., 2012).

The ages of sedimentary rocks in the Bass Basin ranges from Early Cretaceous to recent (Fig 1) (Blevin et al., 2003). We use formation nomenclature developed by Lennon et al. (1999) to describe the stratigraphic succession in the basin. Synchronous with the first phase of extension, Early Cretaceous sediments of the Otway Group were deposited during a period of slow subsidence (Blevin et al., 2003). This unit unconformably overlies the basement, and consists primarily of fluvial channel sands and volcanogenic sediments with minor deposits of coaly floodplain shales (Blevin et al., 2005; Lennon et al., 1999). The Otway Group is overlain by a thick sequence of interbedded sandstones, siltstone and coals that were deposited in fluvio-deltaic and lacustrine environments (Lennon et al., 1999). This sequence is known as the Eastern View Coal Measures (EVCM) and can further sub-divided into three sub-sequences, the Upper, Middle and Lower EVCM, based on intra-formational unconformities (Lennon et al., 1999). The Demon's Bluff Formation overlies the EVCM sequence, and comprises carbonaceous shales and siltstones. Deposition of these finer grained sediments reflects a change in depositional environment to increasingly marine conditions following a regional marine transgression (Lennon et al., 1999). Subsequent rise in sea level during the Late Oligocene led to deposition of the Torquay Group in an open marine setting. This unit comprises calcareous shales at its base that grade upward into bioclastic limestones (Blevin et al., 2005; Lennon et al., 1999).

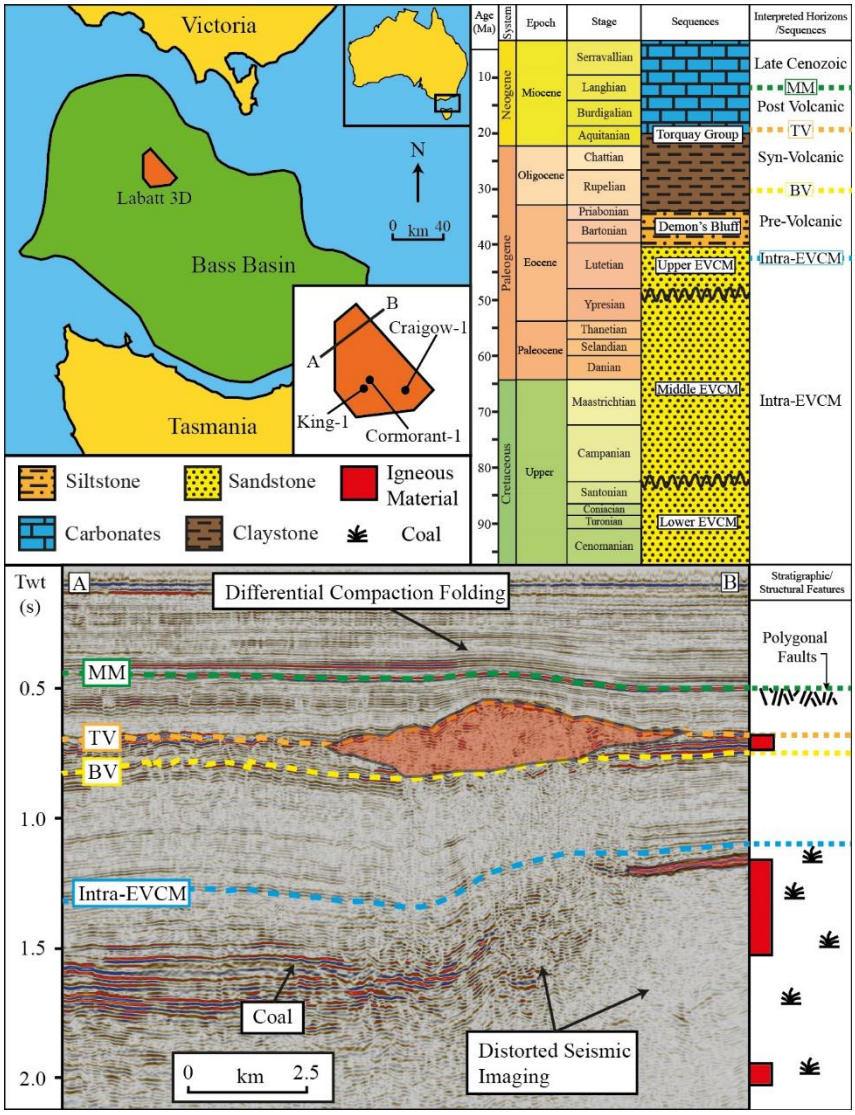

Figure 1*: Location of the Labatt 3D seismic survey within the Bass Basin, along with a representative stratigraphic column and seismic cross-section. Also defined are the interpreted horizons and seismic sequences.*

Intrusive and extrusive igneous rocks are prevalent within the sedimentary sequences of the Bass Basin with evidence of multiple phases of magmatic activity (Blevin et al., 2003; Holford et al., 2012). Igneous rocks encountered within the Bass Basin can be broadly grouped into three categories based on their methods of emplacement; submarine volcanic rocks, igneous intrusions, and subaerial volcanic rocks (Watson et al., 2019). The oldest volcanic rocks encountered within the basin are Early Cretaceous volcaniclastic rocks within the Otway Group sequence (Holford et al., 2012). These volcanoclastic rocks are interpreted to have been sourced from basaltic volcanism near the Hawkesdale area of Western Victoria or ignimbritic volcanoes along the Lord Howe Rise to the east of the Bass Basin (Blevin et al., 2003; Watson et al., 2019). Upper crustal extension associated with rifting in the Tasman Basin to the east of the Bass Basin during the Mid Cretaceous resulted in the deposition of igneous flows, mounds and cones within the Bass Basin, predominantly within the

Durroon Sub-basin (Blevin et al., 2003). The Durroon-1 well within the Durroon Sub-basin encountered a thick (>100 m) succession of highly altered olivine basalt with interbedded clastic sediments overlying the Mid Cretaceous Otway Group sequence (Blevin et al., 2003). A subsequent phase of igneous activity occurred during the Late Cretaceous to Early Paleogene which resulted in deposition of extrusive volcanic material as well as the emplacement of igneous intrusions in the central and northern parts of the Bass Basin, synchronous with deposition of the Middle EVCM sequence (Holford et al., 2012). Fourteen exploration and appraisal wells in the Bass Basin, including Bass-1, Yolla-1 and Cormorant-1, have intersected extrusive basaltic flows and igneous sills within the EVCM formation (Blevin et al., 2005; Holford et al., 2012; Watson et al., 2019). The Aroo-1 well located on the northern flank of the Yolla Trough encountered over 500 m of stacked subaerial lava flows and volcanoclastic rocks with interbedded thin (< 1 m) siltstones and sandstones within the Middle EVCM whereas the Flinders-1 well encountered a 64 m thick dolerite intrusion within the same stratigraphic sequence (Watson et al., 2019). The latest and most recent phase of igneous activity within the Bass Basin occurred during the Oligocene to Miocene (Blevin et al., 2003). This phase saw widespread formation of intrusive and extrusive volcanic features, including submarine volcanos, volcanoclastic deposits, lava flows, dykes and sills, across the basin at varying stratigraphic levels (Holford et al., 2012; Reynolds et al., 2018; Watson et al., 2019). Extrusive volcanic mounds and vents that developed during this phase of magmatic activity can be observed on seismic data within the central and north-western regions of the Bass Basin. Miocene volcanic rocks encountered by Bass-1, Tilana-1 and Yolla-1 wells within the central part of the basin consist of balastic flows and weathered pyroclasts (Blevin et al., 2003; Reynolds et al., 2018; Watson et al., 2019). Miocene aged igneous intrusions, with thicknesses up to 150 m, have also been identified within the Late Cretaceous to Early Eocene sections of the EVCM sequence (Blevin et al., 2003).

The Bass Basin is a moderately explored basin with 45 wells (36 exploration wells) drilled since 1965, by which there have been four commercial fields discovered; the Yolla, White Ibis, Pelican, and Treefoil fields with Yolla being the only producing field at present (Blevin et al., 2005; Watson et al., 2019). Numerous other wells across the basin have identified gas shows within the Late Cretaceous to early Cenozoic EVCM succession, indicating the presence of a working petroleum system (Blevin et al., 2005). Regionally, fluvio-deltaic sediments of the Upper EVCM succession are recognized as a hydrocarbon reservoir unit with Paleocene to Early Eocene coals from the underlying Middle EVCM succession as source rocks (Boreham et al., 2003; Cummings et al., 2002). The Demon's Bluff formation that overlies the EVCM sequence acts as a regional seal (Boreham et al., 2003; Cummings et al., 2002).

4. Data and Methodology

This study uses the Labatt 3D seismic survey which was acquired in 2008 and is located in the Cormorant Trough to the northeast of the Bass Basin. The data is time-migrated with in-line and cross-line spacings of 12.5 and 25 m respectively, and has a record length of 6 seconds two-way travel time (TWT). The quality of seismic data however, deteriorates rapidly below 2 s TWT and does not allow for data interpretation below this depth. The seismic data has a reverse SEG ("European") polarity, where an increase in acoustic impedance is represented by a trough. The intervals of interest to this study are the EVCM, Demon's Bluff and Torquay sequences. These sequences are between 0.4 to 1.5 s TWT, with dominant frequencies ranging from approximately 50 to 35 Hz respectively. Wireline log data from three wells within the study area (King-1, Comorant-1, and Craigow-1), were used to constrain stratigraphic interpretations, calculate seismic resolution and perform time to depth conversions. Using velocities from wells within the study area and the quarter-wavelength criterion, vertical seismic resolution is estimated to range between 10 to 25 m within the interval of interest.

Five seismic horizons, including the seafloor, were interpreted in this study (Fig 1). After the seafloor, the shallowest surface interpreted is a peak reflection within the Torquay succession which is referred to as the Mid Miocene (MM) horizon. Reynolds et al. (2018) had identified two surfaces that bound a stratigraphic sequence within which igneous vents are identified in the Labatt 3D survey. These two surfaces occur within the Torquay Group and two horizons were interpreted in this study based on the surfaces identified by Reynolds et al. (2018). The two horizons are referred to as the Top Volcanic (TV) and Base Volcanic (BV) horizons. The deepest interpreted horizon is a peak reflector within the upper EVCM and is referred to as the Intra-EVCM horizon.

We define a number of seismic sequences that are bounded by the interpreted seismic horizons. The shallowest sequence, bound by the seafloor and MM horizon, is referred to as the 'Late Cenozoic' sequence. The seismic facies of this sequence consists of relatively flat-lying, parallel reflectors with low to moderate amplitudes. The sequence bound by the MM and TV horizons is referred to as the 'Post-Volcanic' sequence. Similar to the Late Cenozoic sequence, the seismic facies of this sequence consists of flat-lying, parallel reflectors with low to moderate amplitudes. The upper half of this sequence contains polygonal faults that do not extend above the MM horizon (Fig 1). While the seismic reflectors within the upper half of this sequence are clearly imaged, imaging quality of the lower half is poor, making reflector interpretation within this zone difficult (Fig 1). The sequence bound by the TV and BV horizons is referred to as the 'Syn-Volcanic' sequence. The seismic expression of this sequence is of moderate amplitude parallel reflectors that also contains volcanic mounds and vents as identified by Reynolds et al. (2018). The seismic sequence bound by the BV and Intra-EVCM horizons is referred to as the 'Pre-Volcanic' sequence. This sequence consists of the Lower Torquay Group, the Demon's Bluff Formation, and the upper part of the EVCM sequence.

Seismic amplitudes of reflectors within the Pre-Volcanic sequence vary. Seismic reflectors at the top of the Lower Torquay Group are laterally continuous and have moderate amplitudes; however the seismic signal-to-noise ratio deteriorates with depth. A laterally continuous and high amplitude seismic reflector (relative to the overlying and underlying seismic reflectors) at the base of the Lower Torquay Group marks the top of the Demon's Bluff Formation. Seismic reflectors of the Demons Bluff Formation and the upper part of the EVCM sequence within the Pre-Volcanic sequence are laterally continuous with low seismic amplitudes. The sequence underlying the Intra-EVCM horizon is referred to as the 'Intra Eastern View Coal Measure (Intra-EVCM)' sequence. This sequence comprises parallel reflectors of moderate amplitude strength with anomalous high amplitude reflection events across the survey area.

Several seismic attributes were used to highlight features of interest in this study. Structural features in the seismic data are accentuated and identified using a variance attribute which highlights and quantifies lateral discontinuities along a seismic reflector within a time window (Marfurt et al., 1998). Root-mean-square (RMS) amplitudes were calculated to highlight lateral variation in seismic reflector amplitudes (Chopra and Marfurt, 2007). It should be noted that this attribute quantifies both troughs and peaks as a positive number, which means it does not differentiate between increases and decreases of a similar scale in acoustic impedance. The nature of RMS amplitude anomalies should be verified by interpreting the polarity of the reflection events causing them on 'raw' amplitude seismic cross-sections. We also use isochron mapping that measures the time thickness of a seismic sequence bound by two selected horizons. Spectral decomposition, an imaging method that isolates and combines discrete frequency bands of seismic time series data, was used to highlight stratigraphic features (Partyka et al., 1999).

5. Overburden Deformation Features

Extrusive volcanic features, such as volcanic mounds and lava flows, are prevalent within the Syn-Volcanic sequence of the Labatt 3D seismic survey, particularly along the north-eastern edge of the survey area. Reynolds et al. (2018) has documented these submarine volcanic features in detail, thus we do not discuss these features in study.

We identify and categorize four predominant types of feature in this study; sub-vertical linear columns with overlying conjugate faults, radial faults, surficial depressions and concentric faults.

5.1. Sub-Vertical Linear Columns with Overlying Conjugate Faults

Variance time slices between 1.2 to 1.8 s TWT reveal thirteen sub-vertical linear columns within the Intra-EVCM sequence (L1-13) (Fig 2). These features have higher variance values (~0.3-0.8) relative to the surrounding host rock (~0.05). The length of these features range from 2.7 to 16 km with orientations between NNW-SSE to NE-SW. On seismic cross sections, they are imaged as columns of upward deflected seismic reflectors with thicknesses between 100 to 200 m and seismic amplitudes similar to those of the surrounding seismic reflectors (Fig 2 b,d). The upper tips of these columns terminate along the Intra-EVCM horizon while the depth at which their bases terminate could not be determined due to the deterioration of both seismic data quality and resolution with depth. Four of the sub-vertical linear columns (L1, L2, L9, L10) are overlain by volcanic vents as identified by Reynolds et al. (2018) (Fig 2c).

The uppermost tips of each sub-vertical linear column are overlain by broadly symmetrical pairs of conjugate normal faults, i.e. two normal faults that dip toward each other (Fig 2 b,d). The conjugate faults have maximum throws that range between 10 to 60 m and dips that range between 34° and 53° with an average dip of 48°. The strike orientation and length of each conjugate fault pair is similar to those of the sub-vertical linear columns that underlie them.. The basal tips of each conjugate fault pair appear to intersect and terminate along the Intra-EVCM horizon at the top of the columnar features. Upper tips of the conjugate faults appear to terminate either along the TV or MM horizons.

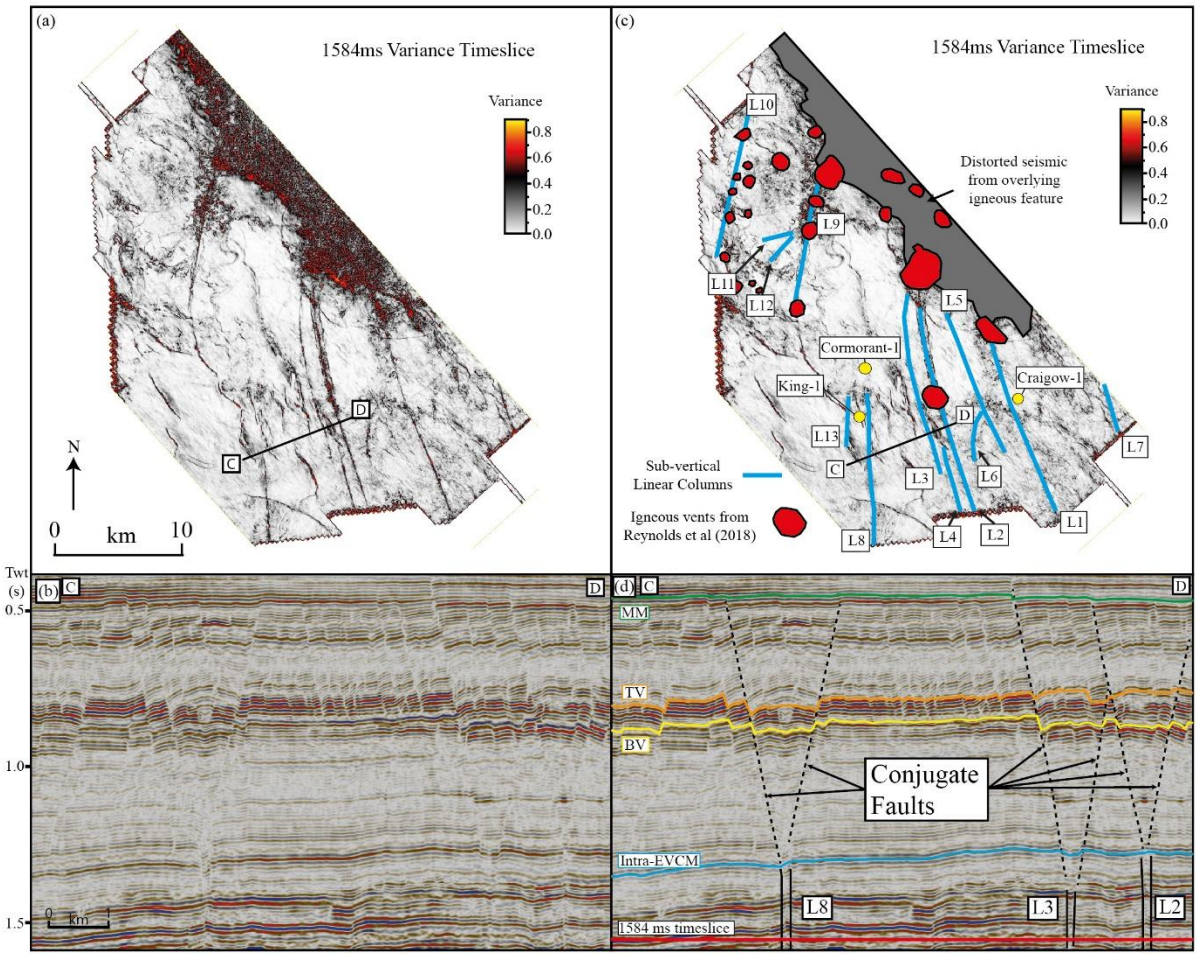

***Figure 2**: Variance attribute time-slice within the EVCM sequence (a) with and (c) without interpretations highlighting linear features. (b) Seismic cross section identifying the linear features and highlighting conjugate faults (b) and (d) without interpretations.*

5.2. Radial Faults Associated With Localised Structural Highs

Four areas of radial faulting, referred to as R1-4 respectively, were identified within the Syn-Volcanic sequence (Fig 3). Each area of radial faulting is geometrically spherical with diameters ranging from approximately 5 to 9 km. Within each area of radial faulting, the radial faults are imaged as an array of faults with strike orientations that are radially symmetrical along a central axis, and thus appear to 'radiate out' from a central point. On seismic cross-sections, all four radial fault sets consist of normal faults forming horsts and grabens (Fig 3c).

The upper tips of the radial faults terminate along the TV horizon whereas the basal tips extend down to ~150 m below the BV horizon (Fig 3c). R1 appears unique however, in that several (~4) radial faults appear to extend above the TV horizon and terminate within the zone of polygonal faulting within the Post-Volcanic sequence. Also unique to R1 is the presence of a concentric fault along the periphery of the R1 fault set (referred to as the "RC fault") (Fig 3b). This concentric fault cross-cuts

several radial faults and has a strike perpendicular to those of the radial faults it intersects. The RC fault extends from the polygonally faulted section within the Post-Volcanic sequence down to ~220 m below the BV horizon.

Detailed mapping of the BV surface shows that areas of radial faulting all coincide with local structural highs. Relative to areas on the BV surface not affected by radial faulting, TWT values along the BV surface are approximately 120 ms shallower at R1, 65 ms at R2, 80 ms at R3 and 55 ms at R4. A similar trend of localized structural highs associated with areas of radial faulting is seen for TWT values along the Intra-EVCM and TV horizons as well. Relative to areas not affected by radial faults along their surfaces, TWT values at radially faulted areas along the TV surface are between 30 to 130 ms less, whereas TWT values at radially faulted areas along the Intra-EVCM surface are between 40 to 120 ms less. Along both the TV and Intra-EVCM surfaces, the largest magnitude of structural highs are located at R1.

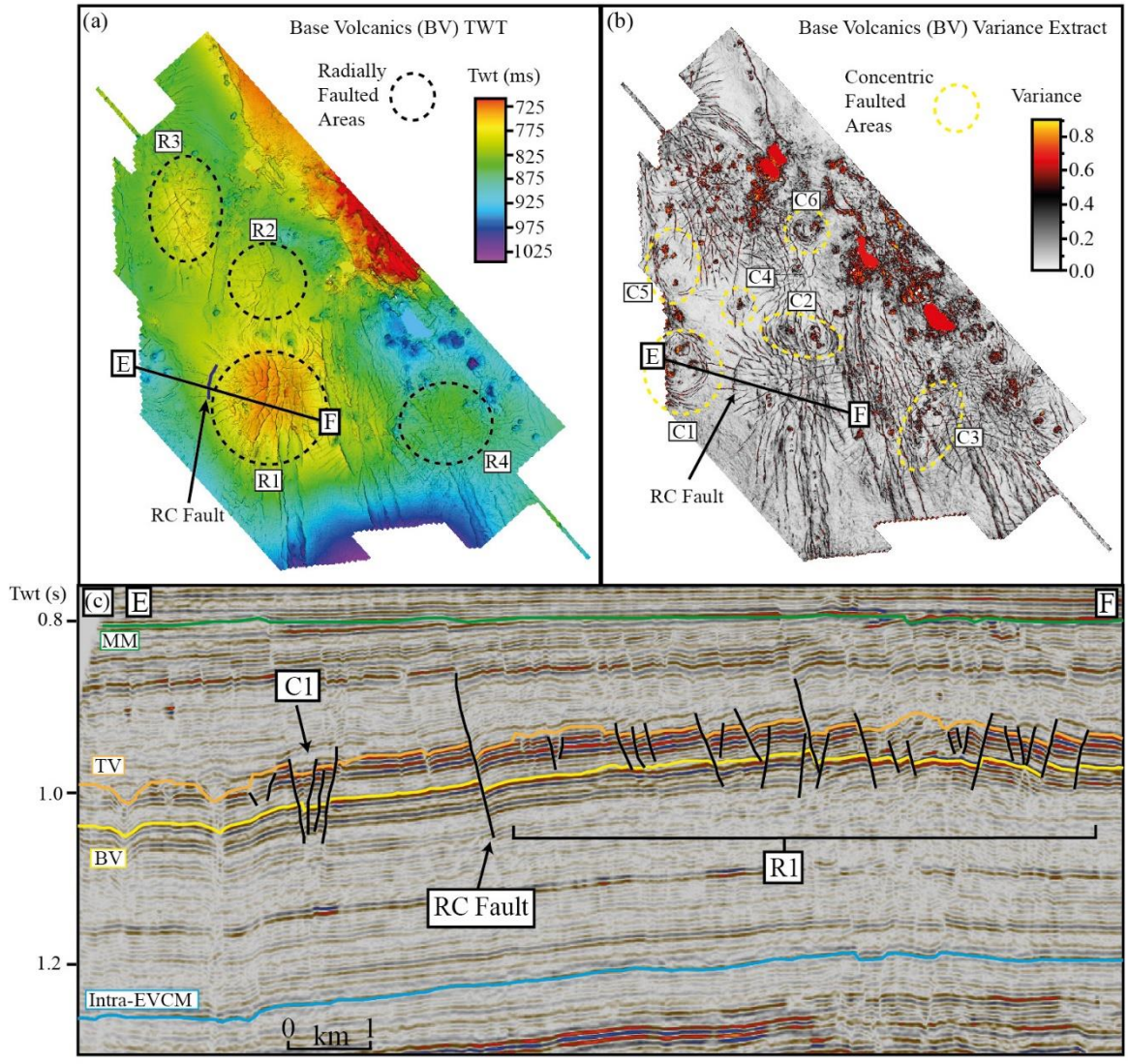

Figure 3: *(a) Interpreted TWT Base Volcanics (BV) horizon that highlights areas with interpreted radial faults (R1-4) and (b) variance attribute extract along Base Volcanics (BV) horizon that highlights areas with interpreted concentric faults (C1-6). (c) Seismic cross section representation of interpreted radial and concentric faults (R1 and C1).*

5.3. Surficial Depressions and Infilling Seismic Reflector Morphologies

A total of 101 surficial depressions were identified within the Syn-Volcanic sequence, with 32 identified along the BV horizon and 69 along the TV horizon, with no clear observable pattern to their spatial distributions (Fig 4c). The lateral dimensions of the depressions range from 60 to 1500 m. The depressions can be categorized into three groups on the basis of their morphology; pipes, craters, and unclassified (Fig 4, 7c). On seismic cross sections, crater depressions are interpreted to have a conical shape whereas pipe depressions are columnar in shape. Unclassified depressions are those that are poorly resolved on seismic cross-sections and thus could not be classified into either crater or pipe categories. A total of 35 craters, 33, pipes, and 33 unclassified depressions were documented.

The surficial depressions were further categorized according to the character of seismic reflectors that infill the depressions. Four categories were identified; parallel, convex, pinnacle, and unclassified. Parallel infill reflectors are those that are flat-lying and parallel, or sub-parallel, to seismic reflectors of the overlying Post-Volcanic or Syn-Volcanic sequences; convex infills are seismic reflectors within depressions that are concave downward/convex upward, and pinnacles are infill reflectors that have a pinnacle-like morphology with seismic reflectors from the overlying Post-Volcanic sequence onlapping onto them (Fig 4 d,e,f). A total of 11 pinnacle, 31 convex, and 52 parallel depression infills were identified while 7 are unclassified due to poor seismic imaging of infill reflectors (Fig 7c). There is no observed correlation between the morphology of depressions and the character of the infill reflectors.

Each depression is underlain by vertical columns of disrupted or discontinuous seismic reflectors that have a lower seismic amplitude relative to the surrounding reflectors (Fig 4a). These columns extend down from the base of the depressions and either terminate or fall below the seismic resolution threshold within the Pre-Volcanic or EVCM sequences. The tallest column is approximately 840 m.

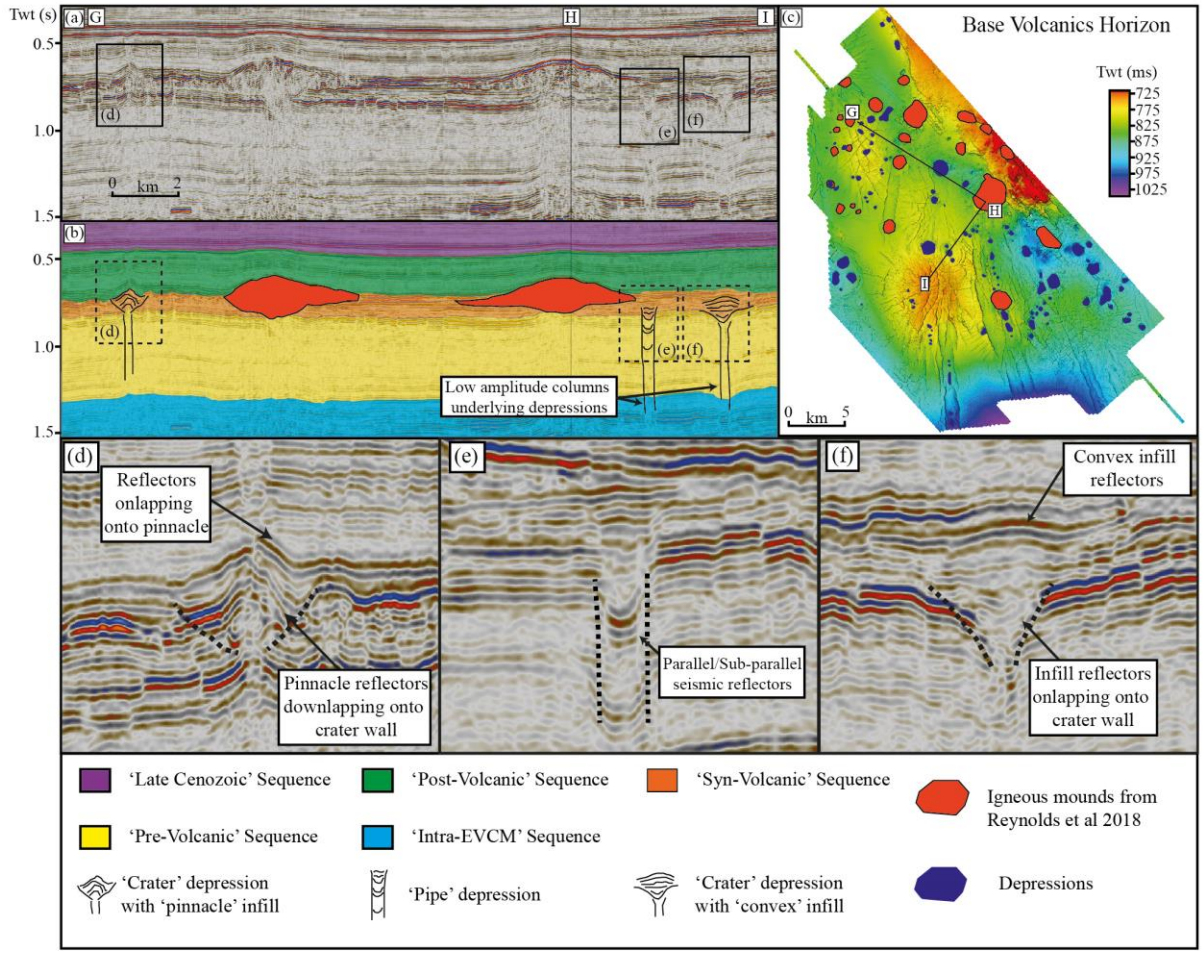

Figure 4: *Seismic cross section (a) without and (b) with identified seismic sequences, igneous features and surficial depressions. (c) Location of the surficial depression features within the survey area along the interpreted Base Volcanic horizon. Zoom-in cross section views highlight reflector characteristics of a (d) crater depression with pinnacle infill, (e) pipe depression with parallel infill and (f) crater depression with convex infill.*

5.4. Concentric Faults

Six areas of concentric faults (C1-6) were identified along the TV surface and on variance time-slices (0.7 – 1.0 s TWT) through the Syn-Volcanic sequence (Fig 3b). On a plan view, the concentric faults form discontinuous, circular or elliptical ring-like patterns around a central locus. The diameter of 'concentric rings' range between 1.5 and 5.7 km. At C1, three surficial depressions are observed within the locus of the concentric faults.

Of the six concentric fault sets, only one (C1) was resolved clearly enough on seismic cross-sections for detailed quantitative and qualitative analysis. On seismic cross-sections, the concentric faults of C1 are normal faults that predominantly dip towards the center of the concentric locus and have a graben-like geometry (Fig 3c). These normal faults have throws of up to 30 m and extend from the

TV horizon down into the Pre-Volcanic sequence, up to 80 m below the BV horizon. Closer to the surficial depressions, we observe steeply dipping, near-vertical reverse faults that dip away from the depressions. These reverse faults appear to be constrained within the Syn-Volcanic sequence, i.e. they extend from the TV to BV horizons, and have throws that are at the limits of the seismic resolution threshold (~10-15 m). Seismic reflectors within the Syn-Volcanic and Pre-Volcanic sequences in the area 'enclosed' by the concentric faults are have a downward sag of up to 80 m relative to the surrounding undeformed seismic reflectors.

6. Discussion

We document four types of structural deformation feature within the Labatt 3D seismic survey; linear features with overlying conjugate faults, radial faults, surficial depressions and concentric faults. Here we discuss the potential origins of these features and their possible association with contemporaneous magmatic activity.

6.1. Sub-vertical Linear Columns and Overlying Conjugate Faults

We document 13 sub-vertical linear columns (L1-13) within the Intra-EVCM sequence. The upper tip of each column is overlain by broadly symmetrical pairs of conjugate normal faults that have strike orientations and lengths similar to those of the underlying sub-vertical linear columns. Within the EVCM sequence of the Yolla 3D survey (south-east adjacent to Labatt 3D), Cummings et al. (2004) interpreted analogous linear column-like features strike-slip zones. Cummings et al. (2004) also interpreted negative flower structures to overlie the strike-slip zones (analogous to the conjugate faults identified in this study) and the negative flower structures are in turn overlain by volcanic mounds. The strike-slip zones and negative flower structures were interpreted to have been magma conduits for the overlying volcanic mounds. Interpretation of the analogous sub-vertical linear columns as strike-slip zones by Cummings et al. (2004) was supported by indications that Late Cretaceous to Eocene NW-SE normal faults within the EVCM sequence have been segmented by strike-slip movement (Fig 5a). Conversely, Holford et al. (2017) interpreted the same analogous linear features in the Yolla 3D survey to be near-vertical igneous dykes that supplied magma to the overlying volcanic mounds. We compare our observations and interpretations of the sub-vertical linear columns and overlying conjugate faults with the interpretations of Cummings et al. (2004) and Holford et al. (2017). We utilize spectral decomposition within the Intra-EVCM to identify potential structural or stratigraphic features that can provide evidence of strike-slip movement across the sub-vertical linear columns. Within the Intra-EVCM sequence, we identified and interpreted three channels that cross-cut the sub-vertical linear columns and NW-SE normal faults. These channels show no evidence of having undergone lateral displacement, suggesting that the sub-vertical linear columns were not loci of lateral movement (Fig 5 b,c). Based on this observation, we agree with the interpretation of Holford et al

(2017) and similarly interpret the sub-vertical linear columns of this study to be igneous dykes. The apparent segmentation of the NW-SE faults may therefore be attributed to the nature of fault development.

The Intra-EVCM sequence was analysed using the RMS amplitude attribute to identify potential amplitude anomalies associated with the interpeted igneous dykes. Coal deposits are prevalent within this sequence and are highlighted by the attribute as bright amplitude bodies (Fig 5d) (Boreham et al., 2003). On seismic cross-sections of the study area, the coal deposits manifest as either individual or vertical stacks of high seismic amplitude reflectors (up to 6 times higher than surrounding reflectors) capped by a strong peak reflection event (Fig 1, 5e). In the eastern section of the study area, a sub-vertical linear column cuts across an interpreted body of coal and we observe a zone of lower RMS amplitudes, parallel to and centered on the columnar feature (Fig 5d, e). This zone of lower RMS amplitude is approximately 780 m wide and is interpreted to be an alteration zone around a dyke that is approximately 140 m in width. The alteration zone is likely due to thermal metamorphism of the coal, resulting in coke formation. Coke has a higher density than coal which would result in a lower acoustic impedance contrast with the surrounding rock relative to coal, thus manifesting as a zone of lower RMS amplitude (McFarlane, 1929). Analogous metamorphism of coals to coke around dyke intrusions has been documented and quantified in South Africa and the United States of America (McFarlane, 1929; Saghafi et al., 2008).

The conjugate faults that overlie the dykes are interpreted to be dyke-related grabens. Similar structures have been documented at volcanic regions in Hawaii, Italy, Iceland and mid-ocean ridges (Chadwick and Embley, 1998; Rubin, 1992; Rubin and Pollard, 1988). Detailed geodetic and seismic monitoring of dyke-related grabens has demonstrated that dyke intrusions trigger the formation of overlying grabens (Chadwick and Embley, 1998). Modelling studies suggest that during dyke intrusion, horizontal compressive stress within the host rock is increased along the sides of the dyke, but horizontal stress in a broad region above the dyke is reduced, thereby inducing a tensional stress regime (Rubin and Pollard, 1988). The induced tensional stress is greatest away from the dyke and minimal along the plane of the dyke, resulting in two zones of maximum horizontal tensional stress which leads to the development of two parallel fissure zones and normal faulting that are the dyke-induced faults (Chadwick and Embley, 1998).

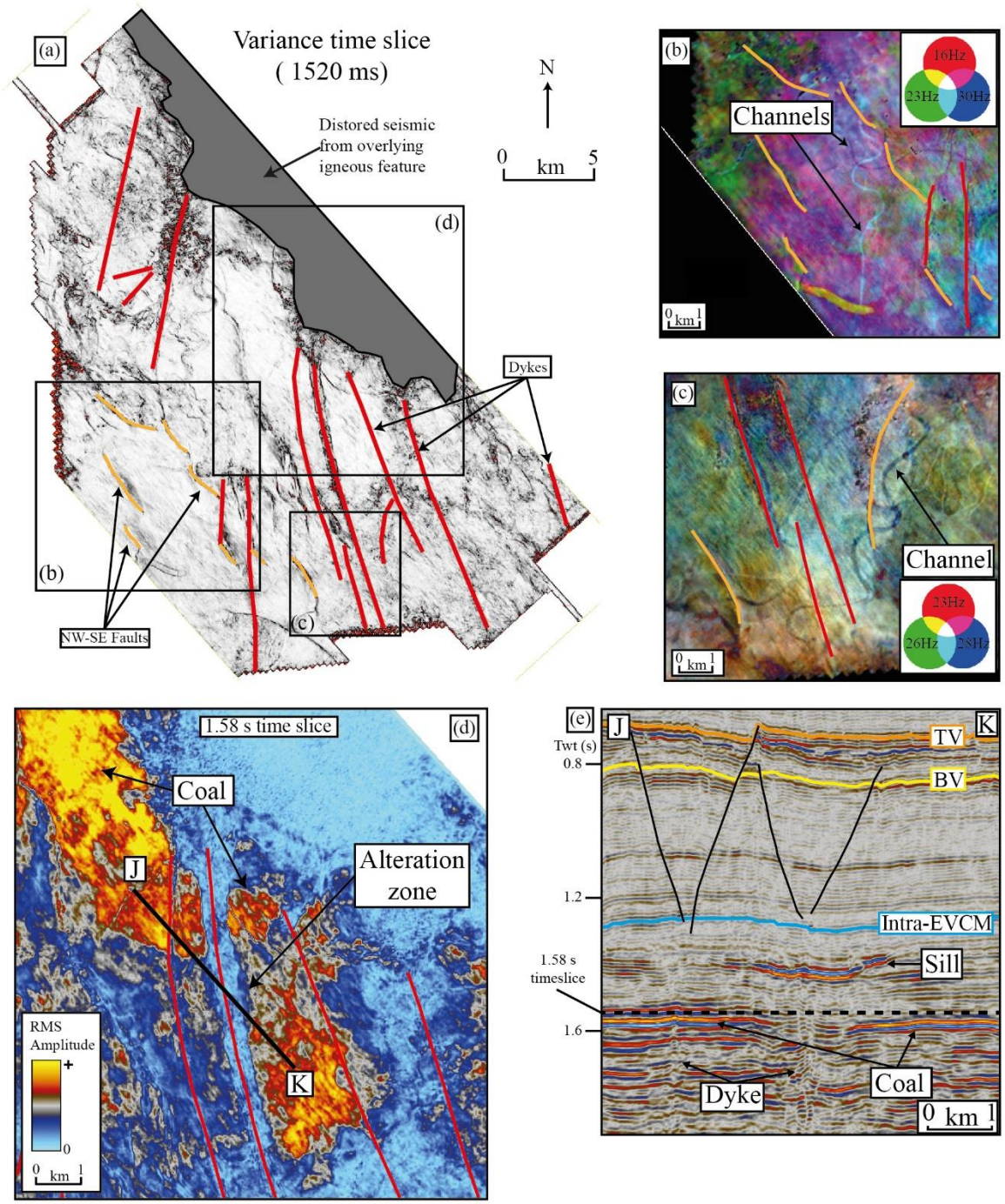

Figure 5: *(a) Variance time-slice within the EVCM sequence with interpreted igneous intrusions, dykes, and NW-SE faults. (b), (c) Spectral decomposition of the EVCM sequence with channels (highlighted by black arrows) that cross-cut the the dykes and NW-SE faults. (d) RMS amplitude time-slice showing an interpreted alteration zone around a dyke through a coal body along with (e) a seismic cross-section of the alteration zone.*

The upper tips of conjugate faults appear to terminate either along the TV horizon, or extend through the polygonal faulted rocks of the Post Volcanic sequence to terminate within this sequence or along

the MM horizon. Interpreting termination depths of the upper tips of conjugate faults can be misleading as there is a potential for dip-linkage between the conjugate faults and polygonal faults of the Post Volcanic sequence. The possibility of conjugate and polygonal fault dip-linkage introduces an uncertainty to determining the 'true' termination depth of the upper tips of conjugate faults, which in turn adds uncertainty in constraining the timing of fault development based on fault termination depths. To test the hypothesis of potential dip linkage between polygonal and conjugate faults, we analyse the growth history of the conjugate faults by measuring depth-displacement profiles along their fault planes. Depth-displacement profiles allow assessment of dip linkage along a fault plane and thus, identification of vertical segmentation (Magee and Jackson, 2018; Mansfield and Cartwright, 1996; Robson et al., 2016). Displacement measurements were taken along seismic cross-sections perpendicular to the conjugate fault planes (Fig 6a). We note that there is an apparent variation in vertical seismic resolution within the seismic sequences that the conjugate faults propagate through (Post-Volcanic, Syn-Volcanic and Pre-Volcanic) that could introduce artificial trends in the displacement depth profiles that area a function of the seismic resolution variation as opposed to the conjugate fault's growth profile. We compensate for this variation by normalizing TWT displacement measurements with the period of the dominant frequency centred on the point of measurement (Fig 6a). The resulting measurement value is dimensionless and quantifies the variation of displacement along the seismically resolvable fault plane. We also note that the Post-Volcanic sequence that immediately overlies the TV horizon has very poor seismic resolution from which displacement measurements could not be made. We refer to this region as the "blank zone".

A total of 784 displacement measurements were taken along the planes of seven pairs of conjugate faults that overlie dykes (i.e. 14 faults in total). From the 784 points, a total of 61 depth-displacement profiles were generated (20 for L1, 7 for L2, 9 for L3, 3 for L4, 3 for L5, 17 for L8, 2 for L9). Displacement profiles of conjugate fault pairs were found to be similar to each other. Representative displacement profiles for conjugate fault pairs were selected (3 for L1, 3 for L2, 4 for L3, 3 for L4, 2 for L5, 4 for L8, 2 for L9) and plot in Figure 6. The profiles in Figure 6 show two identifiable local peaks of displacement, one within the polygonal faults of the Post-Volcanic sequence, and the other within the Syn-Volcanic sequence. The two peaks are resolvable outside the "blank zone", suggesting that they are not an artificial result due to the lack of measurements within the "blank zone" sequence. These results suggest that the conjugate faults that appear to extend upwards to the MM horizon are likely to be two sets of faults (polygonal and conjugate faults) that are dip-linked. Similar displacement profiles and dip-link interaction between faults were observed in the Ceduna Sub-basin of the Great Australian Bight by Robson et al. (2016). It is thus likely that the conjugate faults formed prior to deposition of the Post-Volcanic sequence, terminating along the TV horizon and had subsequently dip-linked to overlying polygonal faults.

The depth displacement profiles of conjugate faults may also provide insight into how dyke-induced faults nucleate. While it is broadly agreed that dyke-induced faults form as a response to an induced tensional stress regime in sedimentary rocks overlying the dyke intrusion, the location of fault nucleation is still poorly understood (Magee and Jackson, 2018). At present, there are five hypotheses for the nucleation of dyke induced faults; (i) nucleating along a surface and extending downwards to the dyke (Acocella et al., 2003), (ii) nucleating at the upper tip of the dyke and extending upwards to the surface (Xu et al., 2016), (iii) a combination of (i) and (ii) with both segments linking (Tentler, 2005), (iv) nucleating between the dyke and surface then extending upwards and downwards (Mastin and Pollard, 1988), or (v) nucleating in front of a laterally propagating dyke that is eventually cross-cut by the dyke (Rubin and Pollard, 1988). Magee and Jackson (2018) hypothesize the displacement-depth trends for the five modes of dyke-induced fault nucleation, as shown in Figure 6b-f. Displacement depth profiles (within the Syn-Volcanic and Pre-Volcanic sequences) of conjugate faults identified in this study most closely resemble that of Figure 6e, whereby the dyke-induced faults are interpreted to have nucleated between the surface and upper tip of the dyke. Magee and Jackson (2018) interpreted similar nucleation patterns for dyke-induced faults interpreted within Jurassic and Triassic sequences on the Exmouth Plateau in the North West Shelf of Australia.

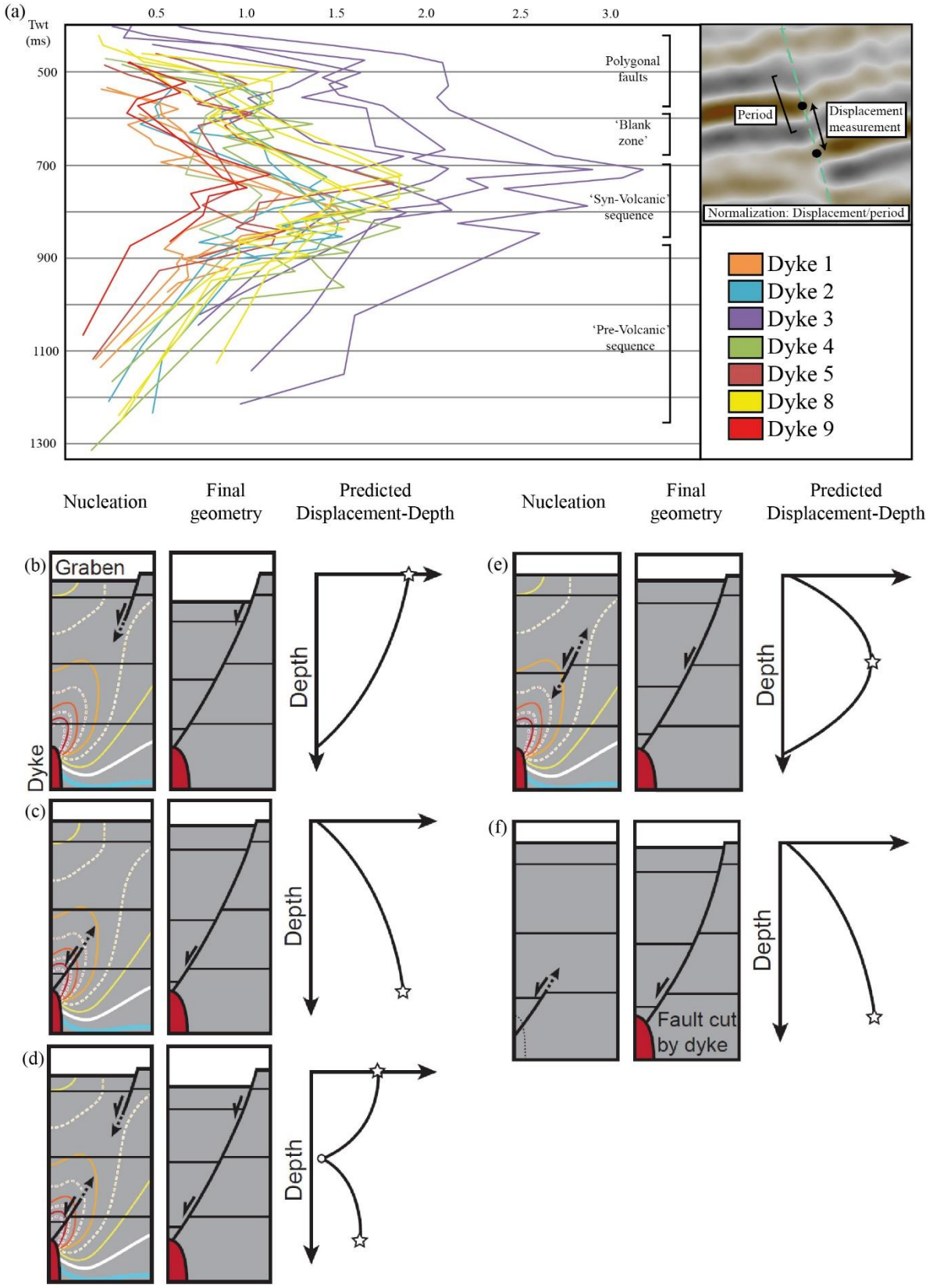

***Figure 6**: (a) 21 Normalized displacement profiles of seven pairs of conjugate fault planes.(b-f) Predicted displacement-depth profiles for five hypothesized modes of nucleation for dyke-induced fault (Modified from Magee and Jackson (2018)).*

6.2. Radial Faults and Localized Structural Highs

Four areas of radial faults (R1-4) were identified within the Syn-Volcanic sequence of the Labatt 3D survey. The areas of radial faults are associated with structural highs as observed along the TV, BV and MM surfaces. Radial faults are commonly associated with subsurface doming events such as the inflation of a magma chamber or salt diapirism (Stewart, 2006; Troll et al., 2002). Several scaled physical modelling studies have been undertaken to better understand the complex fault patterns within radial fault sets (Komuro, 1987; Komuro et al., 1984; Marti et al., 1994). The fault patterns generated in these studies are similar to the ones observed in our study area in that the fault strikes from the modelling studies and radial faults of this study have a radial symmetry around a central axis when observed on plan view. As mentioned in section 4.2, the faults forming R2, R3 and R4 have similar vertical extents, i.e. they extend from the TV horizon to just below the BV horizon. While most faults of R1 have similar vertical ranges as those in the other radial fault sets, several are of greater vertical extent with upper tips observed to extend into the overlying Post-Volcanic sequence that overlies the TV horizon. Furthermore, R1 is the only radial fault set that has a concentric fault (RC Fault) associated with it. While radial faults are associated with doming, concentric faults are commonly associated with subsurface collapse mechanisms (Komuro, 1987; Komuro et al., 1984; Marti et al., 1994). In the aforementioned modelling studies, concentric faults along the periphery of radial faults were observed in scenarios of subsurface collapse that follow a doming event.

Isochron maps were generated for the Late Cenozoic, Post-Volcanic, and Pre-Volcanic sequences to constrain the timing of potential doming events that resulted in radial fault formation (Fig 7). In the Pre-Volcanic isochron map, there is an increase in sequence thickness at radial fault locations, however, this is interpreted to be due to a regional increase in sequence thickness from the NE to SW. No anomalous thickness variations associated with the radial faults are observed on the Post-Volcanic sequence isochron map. On the Late Cenozoic isochron map however, the regions of the sequence associated with R1 and R3 are up to 78 ms (20%) thinner than regions without radial faults. Doming associated with radial faults along the TV horizon and the absence of isochron thickness variation in sequences overlying R2 and R4 suggest that these radial fault sets had formed prior to deposition of the Post-Volcanic sequence whereas R1 and R3 formed subsequently.

We verify this interpretation by analysing the vertical extent of the radial faults. The upper tips of all radial faults associated with R 2, 3, and 4 terminate along the TV horizon, indicating they had formed prior to deposition of the Post-Volcanic sequence. Most faults at R1 have similar vertical extents, however, several of them and the RC fault extend into the overlying Post-Volcanic sequence, suggesting a later time of formation and supporting observations from the isochron maps.

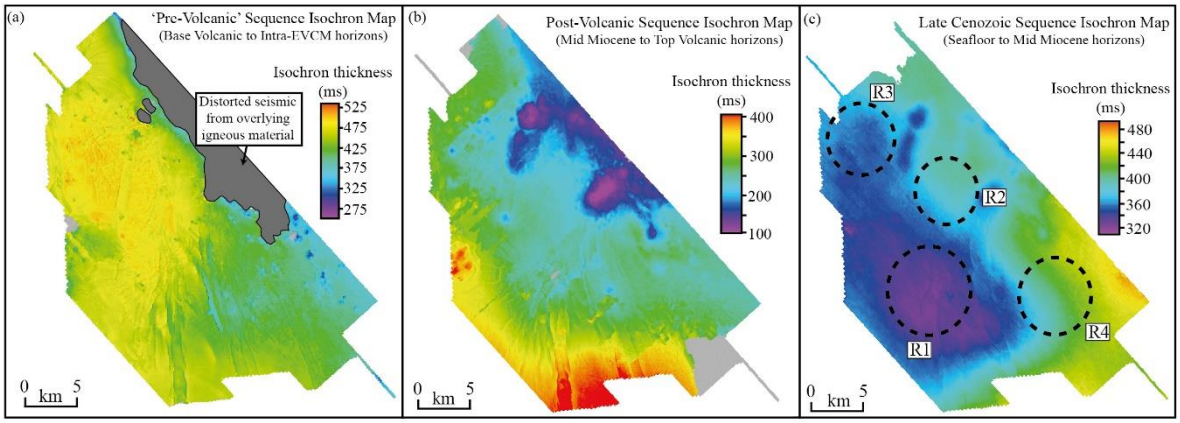

***Figure 7**: Isochron maps of the (a) Pre-Volcanic, (b) Volcanic, and (c) Late Cenozoic sequences.*

Based on these results, the radial faults are interpreted to have formed as a result of episodic, structural deformation of the Syn-Volcanic sequence through domal uplifting by an underlying source of 'inflation'. The radial faults and doming along the interpreted horizons at R2 and R4 had likely formed after deposition of the Syn-Volcanic sequence and prior to deposition of the Post-Volcanic sequence which would account for the termination of radial faults along the TV horizon. A subsequent episode of deformation occurred after deposition of the Post-Volcanic sequence at R1 and R3, which resulted in a second phase of doming and isochron thinning in the Late Cenozoic sequence that would account for the smaller isochron thickness values within the Late Cenozoic sequence. A phase of subsurface subsidence then occurred at R1 which led to formation of the concentric fault associated with the periphery of the radial fault set.

The Bass Basin has experienced multiple episodes of igneous activity during the Cretaceous and Cenozoic with igneous and volcanic features identified within stratigraphic sequences of Mid–Cretaceous to Miocene ages (Blevin et al., 2003; Holford et al., 2012; Reynolds et al., 2018). The radial faults and the surficial doming associated with them could be interpreted as a result of igneous intrusion within the Pre-Volcanic sequence. The broad morphology of the radially faulted domal regions is reminiscent of forced folds that develop above sill intrusions. Hansen and Cartwright (2006) interpreted radial and concentric fault patterns, similar to those identified at R1 of this study, within Cenozoic sequences in the Rockall Basin offshore United Kingdom. The radial and concentric faults of that study were identified to have formed over and around a forced fold that had developed as a result of emplacement of a sill intrusion approximately 300 m below the forced fold. Igneous intrusions often result in uplift of the overburden and while the extent of uplift is often equal to the thickness of the intrusion, it is also possible to have overburden uplift that is significantly less than the thickness of the intrusion (Jackson et al., 2013). A study by Jackson et al. (2013) measured the thickness of 33 igneous intrusions in the Ceduna Sub-basin and compared intrusion thicknesses with the extent of overburden uplift that resulted from emplacement of the intrusions. The study showed

that the amplitude of overburden uplift from emplacement of an underlying igneous intrusion can be as low as a quarter of the intrusion thickness. Furthermore, they discuss a conceptual model that quantifies the trade-off between the extent of overburden uplift with the depth and thickness of an intrusion; i.e. the deeper an intrusion is, the thicker it would have to be to produce a similar amount of uplift as a thinner, shallower intrusion. Magee et al. (2019) expands on the relationship between igneous intrusions and overlying forced fold amplitudes quantified by Jackson et al. (2013) by suggesting that amplitudes of forced folds that overlie igneous intrusions can decrease with time as the uplifted sedimentary rocks are subjected to burial related compaction. The implication of Magee et al. (2019) study is that while the ratio of forced fold amplitude to intrusion thickness can be as low as 1:4 as indicated by Jackson et al. (2013), this ratio could decrease further for forced fold structures that are buried and sedimentary rocks of the forced fold subsequently undergo compaction.

An investigation of seismic data in our study area reveals no indications of igneous intrusions underlying the domed regions; however, the limit of seismic interpretation within the Labatt 3D seismic data is effectively up to 2 s TWT due to the rapid decrease of seismic signal-to-noise ratio below this depth. We interpret regional 2D seismic lines that cross R1 to investigate the potential presence of igneous intrusions in seismic sequences below 2 s TWT; however, no indication of igneous intrusion presence is observed (Blevin et al., 2003). Following the study of Jackson et al. (2013), the shallower an intrusion is, the thinner it would have to be to cause a similar amount of overburden uplift as a deeper, thicker intrusion. At R1, the TV horizon is approximately 100 m shallower than outside the domed region. Using a ratio of 1:1 for uplift amplitude to intrusion thickness (a conservative ratio in terms of inferable intrusion thickness), we would expect to see an intrusion of 100 m underlying R1, which is well above the seismic resolution threshold of 20m at this depth. Seeing as how the radial faults are identified within the Syn-Volcanic sequence, the shallowest depth this hypothesized intrusion would be at is approximately 220 m below the BV horizon, which is within the top of the Pre-Volcanic sequence where the deepest extent of the RC fault is identified in this study. No indications of igneous intrusions were observed on seismic cross-sections within the stratigraphic sequences that underlie the Syn-Volcanic sequence at R1. The Cormorant-1 well is located in the middle of R1, targeting an anticlinal structure within the upper EVCM sequence that had formed as a result of tectonic inversion during the Late Cenozoic (Blevin et al., 2003). The well encountered an igneous intrusion, approximately ~150 m thick, within the Upper EVCM sequence; however, this intrusion is approximately 1800 m below the TV horizon (Reynolds et al., 2018). The 150 m thickness of the aforementioned intrusion at this depth does not sufficiently account for the 100 m uplift at R1. It could be argued however that the igneous intrusion associated with the localized uplift at R1 is not clearly imaged in this seismic data set. A study by Watson et al. (2019) analysed the factors that influence predictability of the presence of igneous intrusions prior to drilling in the Bass Basin. In their study, mineralogical and geophysical analysis of igneous intrusions in the Bass Basin

were undertaken using well site cutting descriptions, thin section micrographs from side-wall cores, geophysical logs from wells in the basin that intersected intrusions, and two 3D seismic surveys (Shearwater Marine and Yolla 3D). Geochemical analysis of igneous intrusions in the Bass Basin by Watson et al. (2019) indicate that rafts of less dense silicic intrusive materials occur within igneous intrusions of the basin. The study suggests that occurrence of the felsic material within the igneous intrusions could result in the deterioration of seismic response along and intrusion boundary, making the intrusion boundary difficult to define and resolve. Furthermore, Watson et al. (2019) goes on to suggest that the abundant presence of coal within the EVCM sequence can act as a seismic signal transmission filter that can mask imaging of the igneous intrusions below them due to the high reflectivity coefficient nature of coals. Based on these two factors, the felsic inclusions in intrusions and seismic signal masking by overlying coals, it is plausible that the domal uplift associated with the R1 (and by extension, R2-4) had formed as a result of emplacement of underlying igneous intrusions that could not be detected or resolved clearly within the limits of the seismic data used in this study.

An alternate interpretation for the formation of radial faults with localized structural highs is that they had formed as a result of tectonic inversion. The Bass Basin is interpreted to have undergone tectonic inversion during the Late Cenozoic (Blevin et al., 2003; Blevin et al., 2005; Holford et al., 2011a; Holford et al., 2011b). Horizontal compression during this time, oriented approximately northwest to southeast, is interpreted to have reverse-reactivated normal faults within the Otway Group, EVCM and Demon's Bluff sequences to result in broadly northeast to southwest striking anticlinal structures within the Torquay sequence (Blevin et al., 2005; Holford et al., 2011b). The plan view geometry of domal structures/structural highs associated with the four areas of radial faults of this study however are circular and show no observable orientation of elongation to suggest a preferred orientation of formation. While the interpreted timing of radial fault and associated structural high formation is coeval with the timing of tectonic inversion across the Bass Basin, we do not interpret these structural overburden deformation features to have formed as a result of Late Cenozoic tectonic inversion.

6.3. Surficial Depressions and Infilling Reflectors

A total of 101 surficial depressions were identified within the Syn-Volcanic sequence of this study; 32 along the BV horizon and 69 along the TV horizon. Underlying each of the depressions are columns of disrupted or discontinuous seismic reflectors with amplitudes lower than those of the surrounding stratigraphy. The surficial depressions and columns of disrupted seismic reflectors that underlie them are interpreted to be fluid escape features. The columns represent fluid migration pathways commonly referred to as fluid escape pipes and the depressions are the surficial manifestations of fluid expulsion along the paleo-surface. Seismic reflectors within the depressions represent 'infill' sediments that were deposited after the depressions had formed. Fluid escape features have been documented and studied in various regions globally including the Northwest Shelf of Australia, the Lower Congo

Basin and offshore Namibia (Gay et al., 2007; Moss and Cartwright, 2010; Velayatham et al., 2018). While fluid escape features are commonly associated with dewatering from rapid sediment deposition, or hydrocarbon generation and expulsion, they have also been documented in igneous provinces (Cartwright et al., 2007; Judd and Hovland, 2007; Svensen et al., 2004). Igneous intrusions can superheat host rock pore fluids or even induce hydrocarbon generation and expulsion from source rocks in petroleum prone sequences, driving rapid fluid displacement resulting in the formation of fluid escape features in overlying strata (Jamtveit et al., 2004; Judd, 2003; Othman et al., 2001).

As described in section 5.3, the fluid escape features in this study are categorized according to the morphology of surficial depressions (pipes, craters and unclassified) and the character of the infill seismic reflectors (parallel, convex, pinnacle and unclassified). We observe no correlation between depression and infill reflector morphologies (Fig 8c). There is also no discernible trend to the spatial distribution of the fluid escape features based on depression morphology (Fig 8a). When analysed based on reflector infill morphology however, we find that occurrence of depressions with convex and pinnacle infills are focused at areas that are adjacent to extrusive volcanic features identified by Reynolds et al. (2018) or overlie the igneous dykes we have interpreted in this study (Fig 8b). Of the 20 convex and 3 pinnacle infill reflector morphologies associated with crater or pipe depressions, 15 convex (75%) and 2 pinnacle (66.7%) infill reflector morphologies are associated with crater depressions.

Reynolds et al. (2018) identified igneous vent structures, interpreted to be submarine volcanoes within Miocene Torquay group sequence (Syn-Volcanic equivalent sequences of this study) in the Labatt 3D and Yolla 3D seismic survey. The vent structures identified in the study were categorized as crater or cone type vents based on their seismic morphology. The crater type vents were described as sub-circular excavations along a paleo-surface that were filled with low amplitude, sub-horizontal reflections that onlap with crater margins. The cone type vents were described as having a conical morphology with seismic reflections within the vent downlapping the underlying horizon and seismic reflections of overlying sedimentary rocks onlapping onto the vents. The seismic morphology of the crater vents in Reynolds et al. (2018) are similar to the crater depressions of this study while the morphology of cone vents of Reynolds et al. (2018) is similar to depressions with convex or pinnacle infill reflectors of this study. The crater depressions of this study have infilling seismic reflectors that onlap onto the crater margins whereas seismic reflectors of the convex and pinnacle infill morphologies of this study downlap onto the underlying seismic horizon and have seismic reflectors of the overlying Post Volcanic sequence onlapping onto them (Fig 4d,f).

Reynolds et al. (2018) infer that the variation of crater and cone type vents represent different stages of volcano evolution. The crater vents represent maar-diatreme complexes that mark the early stage of volcano formation whereas the cone vents represent late stage vent construction. Maar structures are

craters that form as a result of near surface phreatomagmatic eruption in which magma interacts with water in the near surface (Schulz et al., 2005). This interaction generates vapour and creates an explosion chamber due to hyperbaric pressure, which then fractures the surrounding host rock and ejects the contents of the chamber towards the surface, resulting in an explosion cavity along a surface (Schulz et al., 2005). Based on the similarities of seismic expressions between the crater and cone vents identified in Reynolds et al. (2018) with the crater depressions, mound and pinnacle infill reflector morphologies of this study, we similarly interpret the crater depressions to be maar complexes whereby the mound and pinnacle infill reflectors represent volcanic vent constructions at varying stages of development. Our interpretation of the volcanic vents is also supported by the observation that 14 (45%) depressions with convex infill morphologies and 8 (72%) depressions with pinnacle infill morphologies are observed to occur within 300 m (laterally offset) of underlying igneous dykes identified in this study, which could be a potential source of magma for vent formation (Fig8b).

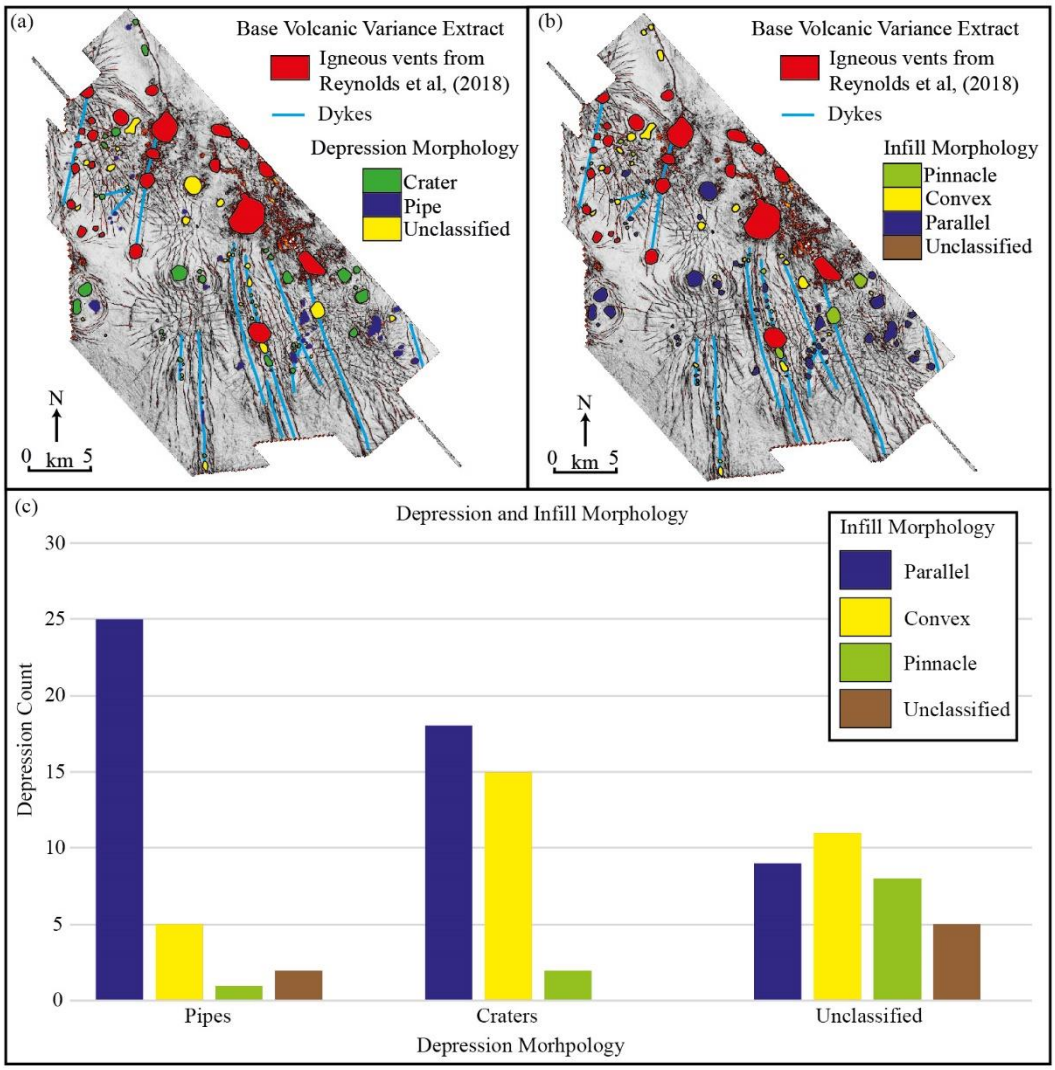

Figure 8: *Spatial distribution of surficial depressions based on (a) depression and (b) infill morphology. (c) Bar chart of depressions categorized by infill morphology.*

Eighteen (18) of the crater depressions have parallel infills, indicating the absence of a volcanic vent. It is plausible that these depressions are also maar structures that did not develop volcanic vents due to a lack of magma supply and/or that the igneous source that formed the maars fall below seismic resolution. An alternative interpretation is that these crater depressions with parallel infills are hydrothermal vents. A study by Jamtveit et al. (2004) identified fluid escape features in South Africa that resemble the crater depressions with parallel infill reflectors of this study. In their proposed model for hydrothermal vent formation, igneous intrusions in the subsurface superheated pore fluids of the surrounding host rock, resulting in overpressure generation that then led to fluid venting. The pipe depressions are similarly interpreted to have formed as a result of hydrothermal venting. The column like structure of these depressions could be attributed to a less catastrophic expulsion event than those forming crater depressions. Though Reynolds et al. (2018) and Jamtveit et al. (2004) provide different models for similar structural features, we believe that both interpretations are applicable in this study and can be used to explain the variation in depression and infill morphologies.

The depressions interpreted in this study formed within the Syn-Volcanic sequence, either along the TV or BV horizons, suggesting that they formed synchronously with its deposition. While the convex and pinnacle infill craters are interpreted to have been formed by an igneous source, the nature of the hydrothermal fluids that formed parallel infill crater and pipe depressions could not be determined. Eighty (79%) of the fluid escape pipes have seismically resolvable bases that terminate within the EVCM sequence. The Middle and Lower sections of the EVCM sequence are identified as hydrocarbon source rocks within the Bass Basin (Boreham et al., 2003). It is thus plausible for underlying igneous intrusions to have induced hydrocarbon generation or heated up pore fluids, which resulted in fluid migration to form fluid escape pipes and associated surficial depressions.

6.4. Concentric Faults

Concentric faults are commonly associated with evacuation of subsurface sediments (Bertoni and Cartwright, 2005; McDonnell et al., 2007; Ward et al., 2016). They have been documented in regions with salt withdrawal, caldera formation, evaporate dissolution, and even around sunken clastic pipes, however there has been little to no documentation of them being associated with fluid escape features (McDonnell et al., 2007; Netoff and Shroba, 2001; Ward et al., 2016).

The concentric faults of C1 form a ring-like feature around three surficial depressions (two crater depressions and one pipe depression). Seismic reflectors within the Syn-Volcanic and Pre-Volcanic sequences that underlie the area encompassed by the concentric faults have a downward sag of up to 80 ms which could be interpreted as a result of localised subsidence of the sedimentary rocks in the

Syn-Volcanic and Pre-Volcanic sequences (Fig 9c). A study by McDonnell et al. (2007) similarly identified circular sag structures in the Fort Worth Basin of Texas. These structures were quantified by measuring the width of a 'sag column' (the "sag width", S.W.), defined as the distance between points of inflection along the sagging seismic reflectors (Fig 9a). According to McDonnell et al. (2007), a S.W. that broadens with depth correlates to a scenario of subsurface subsidence. Where seismically resolvable on seismic cross-sections, we define and measure three S.W. profiles as per McDonnell et al. (2007). The measurements show narrowing upward S.W. trends, which support an interpretation of subsurface subsidence (Fig 9 c, d).

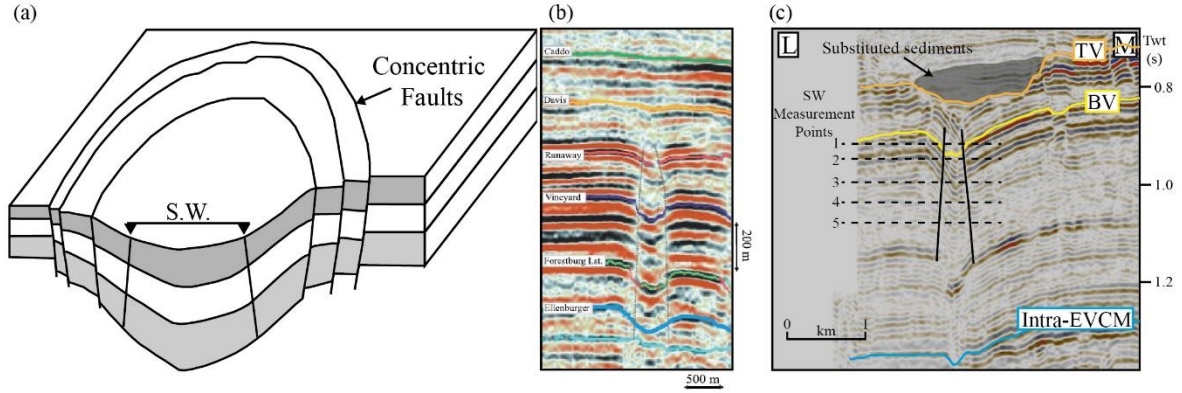

(e)

Measurement Point	S.W. location 1	S.W. location 2	S.W. location 3
1	323	239	148
2	351	263	160
3	406	293	184
4	453	300	208
5	500	-	228

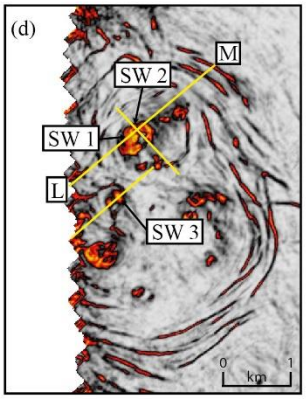

Figure 9: *(a), (b) Schematic on how the Sag Width (S.W.) is defined based on McDonnell (2007). (c) Seismic cross-section from Labatt 3D along which one set of S.W. measurements were taken. (d) Variance extract along the BV horizon defining locations where S.W. measurements were taken. (e) Three sets of S.W. measurements taken.*

An alternative interpretation of sagging reflectors is that they could represent a seismic imaging artefact. Wireline log data and lithological descriptions from interpreted well completion reports of Craigow-1 and King-1 wells indicate that sedimentary rocks within the Syn-Volcanic sequence have a higher velocity than sedimentary rocks of the Post-Volcanic sequence. The area 'enclosed' by the concentric faults has a thicker Post-Volcanic sequence compared to its surroundings, due to the presence of surficial depression (Fig 9c). This thicker sequence of comparatively lower acoustic

velocity sedimentary rocks could result in an artificial pushdown of underlying seismic reflectors in TWT. To test this hypothesis, we calculate the variation of TWT values for the sagging Pre-Volcanic sequence reflectors if the overlying Post-Volcanic sequence sediments were substituted with those of the Syn-Volcanic sequence (Fig 9c). Based on sonic velocity logs from Craigow-1, the acoustic velocity of the Post-Volcanic sequence is approximately 1966 ms^{-1} while the velocity of the Syn-Volcanic sequence is 2345 ms^{-1}. At the measurement location, the TWT thickness of substituted Post-Volcanic sediments is 123 ms. We find that TWT values of the sagging reflectors would be 20 ms shallower if sediments of the Post-Volcanic sequence were replaced with sediments of the Syn-Volcanic sequence. This amount of variation is insufficient to explain the apparent degree of sag in reflectors, supporting the interpretation that the observed sag is caused by subsidence.

As discussed in section 5.3, the crater depressions within the sag region could be interpreted as either maar structures or hydrothermal vents. The indication of subsurface subsidence suggests that depressions associated with the concentric fault set are more likely to be maar structures. Following the formation of a phreatomagmatic explosion crater, the surrounding and overlying rocks are likely to collapse into the space that was created, resulting in the formation of concentric faults (Schulz, 2000). Concentric faults within the Bass Basin have been identified to be associated with maar-diatreme and volcano formation by Reynolds et al. (2018). Boyce (2013) mapped distributions of and classified 416 volcanic eruption centers in the Newer Volcanics Province of Western Victoria in Australia. Of the 416 eruption centers, 27 were categorized as complex maar associated structures of which the plan view for one such structure (Red Rock maar-cone volcanic complex) is shown in Figure 10 (b). Boyce (2013) suggests that the complex maar structures can consist of a coalescence of smaller maar craters. This description of complex maar structure formation is analogous to our interpretation for the formation of the crater depressions and encompassing concentric faults identified in this study. In a plan view comparison of the Red Rock complex maar-cone structure identified by Boyce (2013) with the crater depressions and concentric faults of the TV horizon of this study, we see similar morphological characteristics in surficial expressions (Fig 10). The surficial expression of maar associated depressions of the Red Rock structure are analogous to the surficial expression of crater depressions encompassed by concentric faults along the TV horizon of this study. It is unclear if the lack of surficial expressions of potential concentric faults at the Red Rock complex is due to the absence of concentric faults or whether they are blind faults. Nevertheless, the quantitative analysis of sagging reflectors within C1, along with similarities in qualitative comparison between the surficial expression of C1 and the Red Rock maar-cone volcanic complex identified by Boyce (2013), supports our interpretation that C1 (and C2-6 by extension), had likely formed as a result of subsurface sediment subsidence.

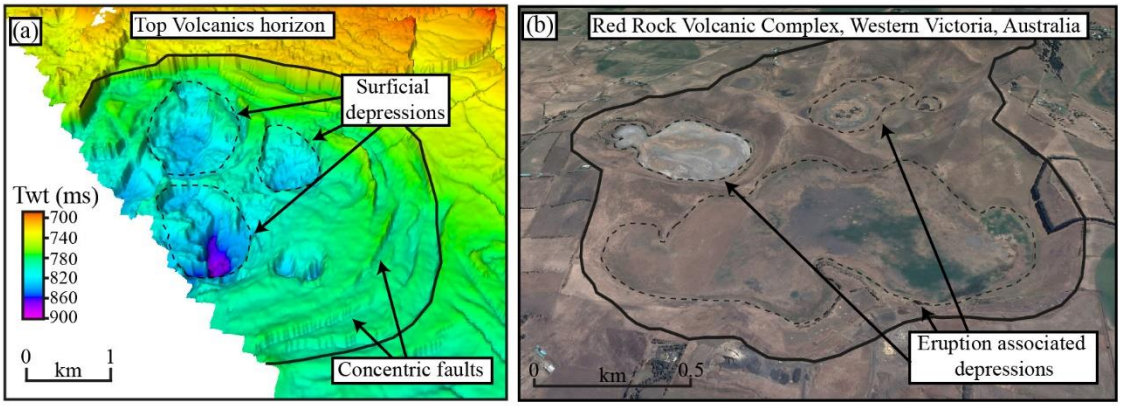

***Figure 10**: (a) Concentric fault set and depressions along the TV horizon with morphological similarities to complex maar craters in the Newer Volcanic Province of Victoria (Boyce, 2013).*

7. Impact of igneous deformation on hydrocarbon prospectivity and exploration

There has been growing interest and increasing hydrocarbon exploration in basins where igneous activity has occurred. As such, the impact of igneous intrusions in hydrocarbon bearing basins have been studied extensively, with a focus on issues such as the impact of intrusions on maturation of hydrocarbon source rocks, or how igneous sills and dykes can act as barriers or conduits to fluid migration (Cartwright et al., 2007; Holford et al., 2012; Othman et al., 2001; Rateau et al., 2013; Schofield et al., 2017). While there have also been extensive studies on intrusion associated deformation features, these focus on the potential of intrusion associated forced folds to act as hydrocarbon traps (Hansen and Cartwright, 2006; Magee et al., 2017; Senger et al., 2017). There is less focus on the potential impact of igneous intrusion associated fault and collapse structures on petroleum systems. Our study highlights four types of deformation structures that are interpreted to be the result of igneous intrusions; conjugate faults (Fig 2), radial faults (Fig 3a), fluid escape features (Fig 4) and concentric faults (Fig 3b). In this section, we briefly discuss the possible impacts of these deformation structures on petroleum systems within the study area.

In the Bass Basin, the fluvio-deltaic sandstones within upper EVCM is identified as the key reservoir-bearing sequence, with hydrocarbons being sourced primarily from the coaly sequences of the Middle EVCM that are particularly abundant in the Cormorant, Yolla and Pelican Troughs (Boreham et al., 2003; Cummings et al., 2002; Lennon et al., 1999). The overlying Demon's Bluff formation (part of the Pre-Volcanic Sequence) acts as a regional top seal for the upper EVCM sequence (Lennon et al., 1999). The conjugate faults in this study extend from the Syn-Volcanic to Intra-EVCM sequence, providing a potential secondary migration pathway for accumulated hydrocarbons within the upper EVCM. Craigow-1 was drilled targeting a reservoir within the upper EVCM sequence but did not

encounter hydrocarbons. In the well's post-drilling interpretative completion report, the lack of hydrocarbons was attributed to dykes having acted as fluid migration barriers that laterally compartmentalized reservoirs within the upper EVCM sequence and prevented charge of the targeted reservoir. In this study, we interpret the presence of a NW trending dyke approximately 200 m to the east of the Craigow-1 well location (Fig 2c). The well did however encounter minor gas shows within the overlying Torquay and Demon's Bluff formations. While dykes may have compartmentalized EVCM reservoirs, gas shows in the base of the Torquay sequence that overlies the Demon's Bluff formation may indicate that the conjugate faults compromised seal integrity and acted as fluid migration pathways for residual volumes of hydrocarbon. Cormorant-1 was similarly drilled targeting a sandstone reservoir within the uppermost EVCM sequence. The targeted structure was a northwest-southeast trending anticline that formed as a result of Miocene compression (Blevin et al., 2003). The well did not encounter commercial hydrocarbon accumulations within the reservoir but found oil and gas shows within the EVCM sequence. The lack of economic accumulation was attributed to an ineffective seal and late development of the trapping structure relative to hydrocarbon migration (Blevin et al., 2003). Though the Cormorant-1 well was drilled within 1 km of seismically resolvable igneous dykes interpreted in this study (Fig 2c), the presence of hydrocarbon shows at the EVCM sequence at suggest that these dykes may not have played a role in hydrocarbon migration at this location.

We also document numerous fluid escape features that are interpreted to have formed as a result of igneous intrusions. The fluid escape features are often interpreted as hydrothermal vents whereby pore fluids were superheated by an intrusion, thereby generating overpressure that led to fluid migration and expulsion (Jamtveit et al., 2004). If emplaced within an organic-rich source rock unit, the intrusion may also have generated overpressure by inducing hydrocarbon generation. While the fluid escape pipes documented in this study are observed to extend down to the EVCM sequence, the nature of fluids that formed the pipes and depressions could not be determined. If the expelled fluids were hydrocarbons from source rocks of the EVCM sequence, this would have increased the source risk for hydrocarbon exploration as the source rocks would have a lower hydrocarbon generation potential than otherwise considered.

Igneous rocks and intrusions are prevalent across the Early Cretaceous to Miocene sediments of the Bass Basin; however, they have proven to be difficult to predict pre-drill (Watson et al., 2019). Of the 20 exploration wells in the basin that encountered igneous rocks, 13 (65%) were not predicted pre-drill (Watson et al., 2019). While the igneous rocks can be difficult to identify and predict on seismic data (for reasons discussed in section 6.2), identification and interpretation of igneous intrusion associated deformation features can be used to infer the presence of underlying igneous intrusions. Detailed mapping of intrusion associated deformation features, such as the radial, conjugate, and concentric faults identified in this study, can be used to delineate the distribution of underlying

intrusions. For instance, in this study, we identified 13 pairs of conjugate faults within the Pre-Volcanic and Syn-Volcanic sequences. By focusing variance attribute and spectral decomposition analysis of the Intra-EVCM sequence at locations underlying the conjugate faults (Fig 2, 5), we identified and interpreted the occurrence of igneous dykes that may not be immediately apparent for interpretation on seismic cross-sections.

8. Conclusions

We have documented a series of structural deformation features that are interpreted to be associated with igneous intrusions; conjugate faults, radial faults, fluid escape pipes, surficial depressions and concentric faults. Thirteen igneous dykes, along with pairs of overlying conjugate faults, were identified in the study area. While previous studies identified these features to be strike-slip faults, we observe no evidence of lateral strain movement along them within the sequence. The occurrence of volcanic vents overlying these features support the interpretation of these features as igneous dykes. Four sets of radial faults were documented within the Syn-Volcanic sequence and are interpreted to be the result of doming events for which the source of overburden uplift could not be concluded in this study. One hundred and one (101) surficial depressions with underlying fluid escape pipes were also identified in the study area with variations in the depression morphology and the morphology of infilling seismic reflectors. Pipe depressions are interpreted to be hydrothermal vents whereas crater depressions are interpreted as either maars or more typically hydrothermal vents. Convex and pinnacle infill reflector morphologies are interpreted to represent volcanic vents at varying stages of evolution. A set of concentric faults in the west of the study area is interpreted to be the result of subsurface subsidence. Although igneous intrusions in sedimentary basins are often the focus of increased risk in hydrocarbon exploration, the structural deformation features they form can also have a significant impact on elements of a petroleum system. In particular, their role as possible fluid migration pathways should be considered when assessing exploration risk.

9. References

Acocella, V., Korme, T., Salvini, F., 2003. Formation of normal faults along the axial zone of the Ethiopian Rift. Journal of Structural Geology 25, 503-513.

Bertoni, C., Cartwright, J.A., 2005. 3D seismic analysis of circular evaporite dissolution structures, Eastern Mediterranean. Journal of the Geological Society, London 162, 909-926.

Blevin, J.E., Boreham, C.J., Trigg, K.R., Cummings, A., Daniel, R., Kaldi, J., Lang, S., Lemon, N., Root, R., Tingate, P., Partridge, A.D., 2003. Petroleum Geology of the Bass Basin - Interpretation Report. Geoscience Australia, Canberra Australia.

Blevin, J.E., Trigg, K.R., Partridge, A.D., Boreham, C.J., Lang, S.C., 2005. Tectonostratigraphy and potential source rocks of the Bass Basin. APPEA Journal 45, 601-622.

Boreham, C.J., Blevin, J.E., Radlinski, A.P., Trigg, K.R., 2003. Coal as a source of oil and gas: A case study from the Bass Basin, Australia. APPEA Journal 43, 117-148.

Boyce, J., 2013. The Newer Volcanics Province of southeastern Australia: a new classification scheme and distribution map for eruption centres. Australian Journal of Earth Sciences 60, 449-462.

Cartwright, J., Huuse, M., Aplin, A., 2007. Seal bypass systems. AAPG Bulletin 91, 1141-1166.

Chadwick Jr, W.W., Embley, R.W., 1998. Graben formation associated with recent dike intrusions and volcanic eruptions on the mid-ocean ridge. Journal of Geophysical Research 103, 9807-9825.

Chopra, S., Marfurt, K.J., 2007. Seismic attributes for prospect identification and reservoir characterization. Society of Exploration Geophysicists and European Association of Geoscientists and Engineers, 464 pp.

Cummings, A.M., Hillis, R.R., Tingate, P.R., 2002. Structural evolution and thermal maturation modelling of the Bass Basin. APPEA Journal 42, 175-191.

Cummings, A.M., Hillis, R.R., Tingate, P.R., 2004. New perspectives on the structural evolution of the Bass Basin: Implications for petroleum prospectivity, in: Boult, P.J., Johns, D.R., S.C.Lang (Eds.), Eastern Australian Basins Symposium II. Petroleum Exploration Society of Australia, Adelaide, Australia, 133-149.

Gay, A., Lopez, M., Brendt, C., Séranne, M., 2007. Geological controls on focused fluid flow associated with seafloor seeps in the Lower Congo Basin. Marine Geology 244, 68-92.

Hansen, D.M., Cartwright, J., 2006. The three-dimensional geometry and growth of forced folds above saucer-shaped igneous sills. Journal of Structural Geology 28, 1520-1535.

Hill, K.C., Hill, K.A., Cooper, G.T., O'Sullivan, A.J., O'Sullivan, P.B., Richardson, M.J., 1995. Inversion around the Bass Basin, SE Australia. Geological Society of London, Special Publications 88, 525-547.

Holford, S.P., Hillis, R.R., Duddy, I.R., Green, P.F., Stoker, M.S., Tuitt, A.K., Backé, G., Tassone, D.R., MacDonald, J.D., 2011a. Cenozoic post-breakup compressional deformation and exhumation of the Southern Australian Margin. APPEA Journal 51, 613-638.

Holford, S.P., Hillis, R.R., Duddy, I.R., Green, P.F., Tassone, D.R., Stoker, M.S., 2011b. Paleothermal and seismic constraints on late Miocene–Pliocene uplift and deformation in the Torquay sub-basin, southern Australian margin. Australian Journal of Earth Sciences 58, 543-562.

Holford, S.P., Schofield, N., MacDonald, J.D., Duddy, I.R., Green, P.F., 2012. Seismic analysis of igneous systems in sedimentary basins and their impacts on hydrocarbon prospectivity: Examples from the soutern Australian Margin, The APPEA Journal 52, 229-252.

Holford, S.P., Schofield, N., Reynolds, P., 2017. Subsurface fluid flow focused by buried volcanoes in sedimentary basins: Evidence from 3D seismic data, Bass Basin, offshore southeastern Australia. Interpretatoin 5, SK39-SK50.

Jackson, C.A., Schofield, N., Golenkov, B., 2013. Geometry and controls on the development of igneous sill-related forced folds: A 2-D seismic reflection case study from offshore southern Australia. GSA Bulletin 125, 1874-1890.

Jamtveit, B., Svensen, H., Podladchikov, Y.Y., Planke, S., 2004. Hydrothermal vent complexes associated with sill intrusions in sedimentary basins. Physical Geology of High-Level Magmatic Systems. Geological Society, London Special Publications, 233-241.

Judd, A.G., 2003. The global importance and context of methane escape from the seabed. Geo-Marine Letters 23, 147-154.

Judd, A.G., Hovland, M., 2007. Seabed Fluid Flow: The Impact on Geology, Biology and the Marine Environment. Cambridge University Press, United Kingdom, 408 pp.

Komuro, H., 1987. Experiments on cauldron formation: A polygonal cauldron and ring fractures. Journal of Volcanology and Geothermal Research 31, 139-149.

Komuro, H., Fujita, Y., Kodama, K., 1984. Numerical and Experimental Models on the Formation Mechanism of Collapse Basins during the Green Tuff Orogenesis of Japan. Bulletin Volcanologique 47, 649-666.

Lennon, R.G., Suttill, R.J., Guthrie, D.A., Waldron, A.R., 1999. The renewed search for oil and gas in the Bass Basin: Results of Yolla-2 and White Ibis-1. APPEA Journal 39, 248-262.

Magee, C., Hoggett, M., Jackson, C.A., Jones, S.M., 2019. Burial-Related Compaction Modifies Intrusion-Induced Forced Folds Implications for Reconciling Roof Uplift Mechanisms Using Seismic Reflection Data. Frontiers in Earth Science 7, 16 pp.

Magee, C., Jackson, C.A., 2018. How do normal faults grow above dykes?, https://doi.org/10.31223/osf.io/ahxn5.

Magee, C., Jackson, C.A.., Hardman, J.P., Reeve, M.T., 2017. Decoding sill emplacement and forced fold growth in the Exmouth Sub-basin, offshore northwest Australia: Implications for hydrocarbon exploration. Interpretation 5, SK11-SK22.

Mansfield, C.S., Cartwright, J.A., 1996. High resolution fault displacement mapping from three-dimensional seismic data: evidence for dip linkage during fault growth. Journal of Structural Geology 18, 249-263.

Marfurt, K.J., Kirlin, R.L., Farmer, S.L., Bahorich, M.S., 1998. 3-D seismic attributes using a semblance-based coherency algorithm. Geophysics 63, 1150-1165.

Marti, J., Ablay, G.J., Redshaw, L.T., Sparks, R.S.J., 1994. Experimental studies of collapse calderas. Journal of the Geological Society, London 151, 919-929.

Mastin, L.G., Pollard, D.D., 1988. Surface Deformation and Shallow Dike Intrusion Processes at Inyo Craters, Long Valley, California. Journal of Geophysical Research 93, 13221-13235.

McDonnell, A., Loucks, R.G., Dooley, T., 2007. Quantifying the origin and geometry of circular sag structures in northern Fort Worth Basin, Texas: Paleocave collapse, pull-apart fault systems, or hydrothermal alteration? AAPG Bulletin 91, 1295-1318.

McFarlane, G.C., 1929. Igneous Metamorphism of Coal Beds. Economic Geology 24, 1-14.

Moss, J.L., Cartwright, J., 2010. The spatial and temporal distribution of pipe formation, offshore Namibia. Marine and Petroleum Geology 27, 1216-1234.

Netoff, D.I., Shroba, R.R., 2001. Conical sandstone landforms cored with clastic pipes in Glen Canyon National Recreation Area, southeastern Utah. Geomorphology 39, 99-110.

Othman, R., Arouri, K.R., Ward, C.R., McKirdy, D.M., 2001. Oil generation by igneous intrusions in the northern Gunnedah Basin, Australia. Organic Geochemistry 32, 1219-1232.

Parnell, J., Green, P.F., Watt, G., Middleton, D., 2005. Thermal history and oil charge on the UK Atlantic margin. Petroleum Geoscience 11, 99-112.

Partyka, G., Gridley, J., Lopez, J., 1999. Interpretational applications of spectral decomposition in reservoir characterization. The Leading Edge 18, 353-360.

Rateau, R., Schofield, N., Smith, M., 2013. The potential role of igneous intrusions on hydrocarbon migration, West of Shetland. Petroleum Geoscience 19, 259-272.

Reynolds, P., Schofield, N., Brown, R.J., Holford, S.P., 2018. The architecture of submarine monogenetic volcanoes – insights from 3D seismic data. Basin Research 30, 437-451.

Robson, A.G., King, R.C., Holford, S.P., 2016. Structural evolution of a gravitationally detached normal fault array: analysis of 3D seismic data from the Ceduna Sub-Basin,Great Australian Bight. Basin Research 29, 605-624.

Rubin, A.M., 1992. Dike-Induced Faulting and Graben Subsidencein Volcanic Rift Zones. Journal of Geophysical Research 97, 1839-1858.

Rubin, A.M., Pollard, D.D., 1988. Dike-induced faulting in rift zones of Iceland and Afar. Geology 16, 413-417.

Saghafi, A., Pinetown, K.L., Grobler, P.G., 2008. CO2 storage potential of South African coals and gas entrapment enhancement due to igneous intrusions. International Journal of Coal Geology 73, 74-87.

Schmiedel, T., Kjoberg, S., Planke, S., Magee, C., Galland, O., Schofield, N., Jackson, C.A., Jerram, D.A., 2017. Mechanisms of overburden deformation associated with the emplacement of the Tulipan sill, mid-Norwegian margin. Interpretation 5, SK23-SK38.

Schofield, A., Totterdell, J., 2008. Distribution, timing and origin of magmatism in the Bight and Eucla basins. Geoscience Australia, Record 2008/24, 19 pp.

Schofield, N., Holford, S., Millett, J., Brown, D., Jolley, D., Passey, S.R., Muirhead, D., Grove, C., Magee, C., Murray, J., Hole, M., Jackson, C.A., Stevenson, C., 2017. Regional magma plumbing and emplacement mechanisms of the Faroe-Shetland Sill Complex: implications formagma transport and petroleum systemswithin sedimentary basins. Basin Research 29, 41-63.

Schofield, N., Jolley, D., Holford, S., Archer, S., Watson, D., Hartley, A., Howell, J., Muirhead, D., Underhill, J., Green, P., 2018. Challenges of Future Exploration within the UK Rockall Basin. Geological Society, London, Petroleum Geology Conference Series 8, 211-229.

Schulz, H.D., 2000. Quantification of early diagenesis: dissolved constituents in marine pore water. In Marine Geochemistry (pp. 85-128). Springer, Berlin, Heidelberg.

Schulz, R., Buness, H., Gabriel, G., Pucher, R., Rolf, C., Wiederhold, H., Wonik, T., 2005. Detailed investigation of preserved maar structures by combined geophysical surveys. Bulletin of Volcanology 68, 95-106.

Schutter, S.R., 2003. Hydrocarbon occurence and exploration in and around igneous rocks, in: Petford, N., McCaffrey, K.J.W. (Eds.), Hydrocarbons in Crustalline Rocks. Geological Society of London, London, pp. 7-33.

Senger, K., Millett, J., Planke, S., Ogata, K., Eide, C.H., Festøy, M., Galland, O., Jerram, D.A., 2017. Effects of igneous intrusions on the petroleum system: a review. First Break 35, 47-56.

Stagg, H.M.J., Willcox, J.B., Symonds, P.A., O'Brien, G.W., Colwell, J.B., Hill, P.J., Lee, C., Moore, A.M.G., Struckmeyer, H.I.M., 1999. Architecture and evolution of the Australian continental margin. AGSO Journal of Australian Geology & Geophysics 17, 17-33.

Stewart, S.A., 2006. Implications of passive salt diapir kinematics for reservoir segmentation by radial and concentric faults. Marine and Petroleum Geology 23, 843-853.

Sun, Q., Wu, S., Cartwright, J., Lüdmann, T., Yao, G., 2013. Focused fluid flow systems of the Zhongjiannan Basin and Guangle Uplift, South China Sea. Basin Research 25, 97-111.

Svensen, H., Planke, S., Malthe-Sørenssen, A., Jamtveit, B., Myklebust, R., Eidem, T.R., Rey, S.S., 2004. Release of methane from a volcanic basin as a mechanism for initial Eocene global warming. Nature 429, 542-545.

Tentler, T., 2005. Propagation of brittle failure triggered by magma in Iceland. Tectonophysics 406, 17-38.

Troll, V.R., Walter, T.R., Schmincke, H.U., 2002. Cyclic caldera collapse: Piston or piecemeal subsidence? Field and experimental evidence. Geology 30, 135-138.

Velayatham, T., Holford, S.P., Bunch, M.A., 2018. Ancient fluid flow recorded by remarkably long, buried pockmark trains observed in 3D seismic data, Exmouth Plateau, Northern Carnarvon Basin. Marine and Petroleum Geology 95, 303-313.

Ward, N.I.P., Alves, T.M., Blenkinsop, T.G., 2016. Reservoir leakage along concentric faults in the Southern North Sea: Implications for the deployment of CCS and EOR techniques. Tectonophysics 690, 97-116.

Watson, D., Holford, S., Schofield, N., Mark, N., 2019. Failure to predict igneous rocks encountered during exploration of sedimentary basins: A case study of the Bass Basin, Southeastern Australia. Marine and Petroleum Geology 9, 526-547.

Xu, W., Jónsson, S., Corbi, F., Rivalta, E., 2016. Graben formation and dike arrest during the 2009 Harrat Lunayyir dike intrusion in Saudi Arabia: Insights from InSAR, stress calculations and analog experiments. Journal of Geophysical Research: Solid Earth 121, 2837-2851.

Chapter 6

Summary and Conclusions

Summary and Conclusions

The overarching objective of this project was to document the character, distribution and origin of focused fluid flow phenomena in offshore basins of Australia. The study concentrates on three offshore sedimentary basins where focused fluid flow features have previously been documented; the Northern Carnarvon Basin of the North West Shelf, the Ceduna Sub-Basin of the Great Australian Bight, and the Bass Basin, offshore Southeastern Australia. The aims of this project are two-fold:

1. To improve understanding of active and ancient subsurface fluid dynamics by developing models for the genesis of focussed fluid flow features in offshore basins of Australia.
2. To assess and evaluate the implications of focused fluid flow occurrences on petroleum systems elements in the respective regions of study.

Chapters 2 and 3 - A geological model for the genesis of a Late Jurassic fluid expulsion event in the Exmouth Plateau of the Northern Carnarvon Basin

Chapters 2 and 3 establish a geological model for the formation of focused fluid flow features in the Exmouth Plateau of the Northern Carnarvon Basin. Three 3D seismic surveys from across the plateau were interpreted; Io-Jansz 3D, Thebe 3D and Claudius 3D. Across the three surveys, 315 paleo-pockmarks were identified; these occur in linear trends developed on a major unconformity that represents the top of the Jurassic sequence. Each paleo-pockmark was underlain by a fluid escape pipe that extends into the Triassic Mungaroo Formation. Focused fluid flow features occur in linear spatial tracks that collectively exhibit a radial trend across the three surveys; striking 167°/347° in Claudius 3D (the westernmost survey studied), 176°/356° in Thebe 3D, and 15°/195° in Io-Jansz 3D (the easternmost survey).

The focused fluid flow features occur parallel to, but are laterally offset from, the upper tips of normal faults that extend through the Jurassic and Triassic sequences. Furthermore, bases of fluid escape pipes appear to intersect the normal fault planes within the Triassic Mungaroo Formation. These observations indicate that the faults did not act as fluid migration pathways themselves, but act as a control on spatial distribution of focused fluid flow features. The faults are interpreted to have formed during the Late Jurassic and intersected an overpressured sequence within the Triassic Mungaroo formation. At the point of intersection between the fault and overpressured sequence, the overburden stress was reduced, which induced vertical fluid migration. Based on fluid escape pipe termination

depths on seismic cross-sections, along with interpretation of Jurassic and Triassic sequence isochron maps, the timing of fluid expulsion was constrained to be at the end of the Jurassic and the fluids are likely sourced from the Triassic Mungaroo formation, though the nature of the fluid has not been determined to this point.

Present day overpressure generation within the Triassic sequences of the Northern Carnarvon Basin are often attributed to either disequilibrium compaction or fluid expansion from hydrocarbon generation. Overpressure generation from disequilibrium compaction commonly occurs in basins with high sedimentation rates (>100 m/ Ma). Though the Triassic Mungaroo Formation of the Exmouth Plateau is documented to have been characterised sedimentation rates that are low for generating disequilibrium compaction overpressures (~50 m/Ma), the lithological composition of the Mungaroo Formation (predominantly claystone or sandstones with interbedded claystones) could be a contributing factor for overpressure generation by this mechanism. Relative to coarse-grained sedimentary rock, fine-grained sedimentary rock such as shales or claystones, have low permeabilities that can impede fluid migration or expulsion from within a formation or from/to neighbouring formations. Thus, the lengthier time needed for fluids to be expelled from fine grained sedimentary rocks of the Mungaroo Formation may have compensated for the relatively lower sedimentation rates across the Exmouth Plateau during the Triassic in order for disequilibrium compaction overpressure to have been developed. The Mungaroo Formation is a regionally recognized hydrocarbon source and reservoir unit (Longley et al 2002). Thermal maturity modelling results indicate that at the time of formation, focused fluid flow features could have been formed by hydrocarbons migrating from parts of the Mungaroo Formation that had entered the hydrocarbon generation window. Though the specific overpressure generation mechanism could not be determined in this study, both disequilibrium compaction and fluid expansion from hydrocarbon generation are plausible causes of overpressure that resulted in fluid migration events and formed associated focused fluid flow features.

The occurrence of paleo-pockmarks with underlying fluid escape pipes that have an observably consistent generational mechanism and timing of formation in a radial trend across the Exmouth Plateau suggests that the fluid expulsion was a coeval basin-wide event. The timing of paleo-pockmark formation in the Late Jurassic coincides chronologically with interpreted mantle plume activity along the southern margin of the Exmouth Plateau. Linear features (that are poorly resolved in the seismic data sets used in this study) are identified to underlie the normal faults associated with fluid flow pipes and pockmarks. The linear features have orientations that mirror the radial trend of the overlying normal faults and fluid escape features across the three seismic surveys. These linear features are interpreted to be igneous dykes sourced from the magmatism along the southern margin plateau, and may be responsible for the nucleation of normal faults that triggered formation of the Late Jurassic focused fluid flow event(s).

Chapter 4 - Focused fluid flows in the Ceduna Sub-basin of the Great Australian Bight: A potential indicator of a working petroleum system

Chapter 4 builds on the results of Chapters 2 and 3 by expanding on the previously developed model to understand the genesis of fault-associated focused fluid flows in the Ceduna Sub-Basin. Fluid escape pipes were identified within both the Cenozoic sedimentary sequence and the shallowest 400 m of the Late Cretaceous Hammerhead Supersequence along the south-western edge of the Ceduna 3D survey. These focused fluid flow features overlie upper tips of normal faults within the Hammerhead Supersequence. The spatial distribution of fluid escape pipes varies across the study area, as does the predominant fault type within the Hammerhead Supersequence. Fluid escape pipes occur with apparently random spatial distribution when overlying polygonal faults in the north-west, whereas they occur in linear clusters with underlying normal faults in the south-east that show listric-like characteristics.

In contrast to the model developed for focused fluid flow features in the Northern Carnarvon Basin, an alternative model for fault-fluid interaction is proposed whereby faults were utilized as fluid migration pathways, resulting in the development of fluid escape pipes that overlie their upper tips. The normal and polygonal faults within the study area are interpreted to have developed in the Late Cretaceous and are dip-linked with underlying, Mid Cretaceous-age listric faults that intersect the Tiger, White Pointer and Blue Whale Supersequences. The upper terminus of fluid escape features occur at varying stratigraphic levels within the Late Cretaceous Hammerhead and Cenozoic sequences. Furthermore, some fluid escape pipes are observed to breach the sea floor on seismic data. These two observations on fluid escape pipe termination level suggest that the focused fluid flow system was an event that occurred from the Late Cretaceous through to the Cenozoic. Mid Cretaceous-age Tiger, White Pointer and Blue Whale supersequences have been identified as potential source rock units and regional basin modelling studies indicate that the(se) sequence(s) generated and expelled hydrocarbons from the Late Cretaceous onwards. It is thus inferred that the identified focused fluid flow features were potentially formed by the generation of hydrocarbons within Mid Cretaceous Supersequences and migrated to shallower depths through the dip-linked Mid to Late Cretaceous listric, normal and polygonal fault systems.

Chapter 5 - Igneous intrusion associated focused fluid flows and overburden deformation features

While chapters 2, 3 and 4 developed our understanding of hydrocarbon-associated focused fluid flow features, Chapter 5 expands on the focused fluid flow feature development models hypothesised so far by investigating focused fluid flow features associated with igneous intrusions in the Bass Basin, offshore Southeast Australia. A total of 101 surficial depressions with underlying fluid escape pipes were identified within the Oligocene to Miocene-age Torquay Group and were categorized on the basis of seismic morphology of surficial depression (pipe-like and crater-like) and infilling seismic reflectors (parallel, convex and pinnacle). Alongside the surficial depressions, a variety of overburden deformation structures induced by underlying igneous bodies were also documented within the Eocene to Miocene Torquay Group and Demon's Bluff sequences, manifesting as radial, conjugate, and concentric faults. Localized structural highs are associated with areas of radial faulting and 13 sub-vertical column-like features were identified within the Early Cenozoic Eastern View Coal Measures (EVCM) sequence. These sub-vertical column-like features underlie the conjugate faults with, and have length and orientations that mirror, those of the overlying conjugate faults. No spatial link was observed between the aforementioned complex fault systems (conjugate radial, concentric faults) and surficial depressions.

The surficial depressions and complex fault systems (radial, concentric and conjugate faults) are interpreted to be associated with the emplacement of underlying igneous intrusions. The surficial depressions are interpreted to be hydrothermal vents or maar craters based on their seismic morphologies with the convex and pinnacle infilling seismic reflectors representing varying stages of volcanic vent evolution. Utilizing spectral decomposition methods, the sub-vertical column-like features identified within the EVCM sequence are evidenced to be igneous dykes and the conjugate faults that overlie them are dyke-induced normal faults. Sandbox modelling studies suggest that radial faults form in response to elastic deformation during sediment doming, whereas concentric faults form as a result of subsurface sediment evacuation. The source of doming that resulted in four areas of radial fault formation could not be identified definitively in this study, but is inferred to be a number of underlying igneous intrusions that could not be clearly imaged within the study dataset or a deeper source of 'inflation' that is beyond the imaging limits of the 3D seismic survey data. Six areas of identified concentric faulting are associated with the presence of maars or hydrothermal vents. Quantitative analysis of seismic reflector sag within the locus of one concentric fault set indicate that the concentric faults had formed as a result of subsurface sediment evacuation. It is likely that subsurface sediment evacuation event occurred when the surficial depressions within the concentric fault locus were formed.

Subsurface volcanic material in the Bass Basin has historically been difficult to predict prior to drilling or to image on seismic data. Chapter 5 develops an interpretation framework that uses the analysis of both fluid flow and overburden deformation features to delineate the presence of igneous intrusions in the subsurface.

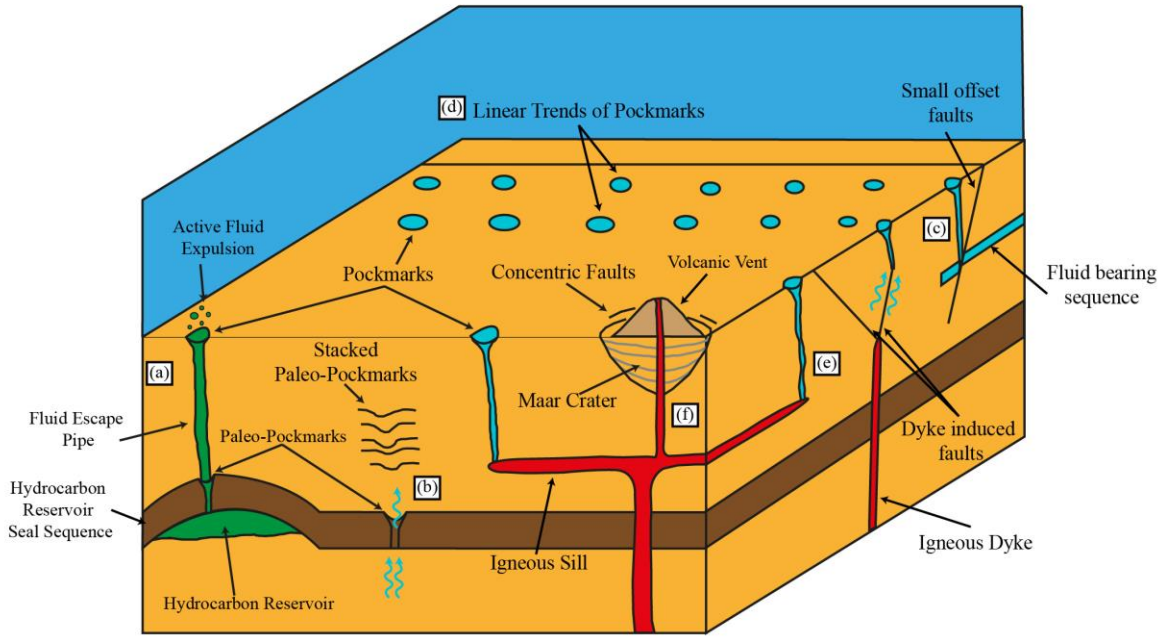

Figure 1: *Schematic illustration that summarizes key findings on focused fluid flow systems within this thesis. (a) and (b) illustrate how the integrity of a sealing sequence can be compromised by the presence of paleo-focused fluid flow features. In (a), accumulated hydrocarbons leak through the paleo-fluid flow features to form fluid escape pipes (or gas chimneys) and potentially seep through an active pockmark on the seafloor. At (b) the paleo-fluid escape features act as a migration pathway for fluid subsequent to their formation. Episodic fluid expulsion along paleo-surfaces can result in a vertical succession of pockmarks referred to as stacked paleo-pockmarks. Structural features, such as faults at (c), are able to act as controls on spatial distribution of fluid escape features. Faults can act as fluid migration pathways, or triggers for focused fluid migration. Underlying geological control on the spatial distribution of focused fluid features can result in organized distribution of fluid escape features. At (d), underlying faults controlling the spatial distribution of overlying fluid escape features result in linear trains of pockmarks parallel to the orientation of fault strike. Focused fluid flow systems are also associated with igneous intrusions. (e) Igneous intrusions are able to superheat pore fluids in the host rock to induce focused fluid migration. (f) Alongside fluid escape features, emplacement of igneous intrusions can result in overburden deformation structures such as dyke induced faults, maar craters and concentric faults. Mapping these features can help delineate the distribution of underlying intrusions.*

Implications of focused fluid flow systems on petroleum system elements and hydrocarbon exploration efforts

This project has developed three models for the formation of focused fluid flow features in the Northern Carnarvon Basin, the Ceduna Sub-basin and the Bass Basin of offshore Australia; three basins that represent currently producing, frontier and mature hydrocarbon basins respectively. This thesis highlights varying interactions between subsurface fluid migration systems and geological structures that can lead to the formation of focused fluid flows. As such, the different models for genesis of focused fluid flow features developed in Chapters 2-5 can have varying implications for the assessment of petroleum systems elements during hydrocarbon exploration.

1. In the Exmouth Plateau, normal faults acted as a trigger for the formation of focused fluid flow features. While the faults do not appear to have been utilized as fluid migration pathways, the fluid escape pipes themselves can act as such pathways once buried and preserved. The observation that normal faults within the Triassic Mungaroo Formation are not fluid migration pathways can lead to re-evaluation of play types that rely on faults as hydrocarbon migration pathways. For instance, the Tiberius -1 well was drilled into a Late Triassic carbonate reef along the western edge of the Exmouth Plateau to test a new exploration play in 2010. In this play, the carbonate reefs are reservoirs that are charged by hydrocarbons that had migrated along normal faults developed within the underlying Triassic Mungaroo Formation source rock. The well did not encounter hydrocarbons; the failure was attributed to a lack of fluid migration pathways into the carbonate reservoirs. The findings from chapters 2 and 3 of this thesis suggest that normal faults within the Mungaroo Formation act as a control on the spatial distribution of focused fluid migration but not as fluid migration pathways. With this revised understanding of the role of the aforementioned faults on subsurface fluid dynamics, a reassessment of this carbonate reef play type should reflect a different risk profile regarding fluid migration and associated petroleum systems elements. Alongside their potential impact on hydrocarbon charge, the presence of fluid escape pipes within a sealing unit may indicate compromised seal integrity and increased risk that hydrocarbon accumulations were evacuated from reservoirs within the Mungaroo Formation.
2. The Ceduna Sub-basin is a frontier hydrocarbon exploration region where the lack of direct evidence for the existence hydrocarbon prone source rocks within distal parts of the sub-basin is a key exploration risk. The identification of fluid escape pipes that are potentially associated with hydrocarbon generation, expulsion and migration indicates the possible

presence of productive Mid Cretaceous source rocks and establishes Late Cretaceous faults as viable fluid migration pathways. These results could enhance hydrocarbon prospectivity by reducing the source risk and encouraging a re-evaluation of exploration targets in the region.

3. Fluid flow and overburden deformation features in the Bass Basin developed as a result of subsurface igneous intrusions. The igneous dykes identified in this study may impact petroleum systems elements by acting as fluid migration barriers that compartmentalize hydrocarbon reservoirs or sequences otherwise viable as secondary or tertiary migration pathways. Igneous intrusion-associated complex fault systems (radial, conjugate, concentric faults) may compromise seal rock integrity and provide fluid migration pathways for subsequently generated hydrocarbons.

Recommendations for future work

This thesis represents a pioneering attempt to document and develop geological models for the occurrence of ancient focussed fluid flow systems in offshore basins of Australia. The findings established in this study provide a basis for future research on focused fluid flow systems in offshore Australian basins. Several recommendations for future work are described below:

- This study utilized seismic interpretation workflows that revolve around seismic reflection or individual seismic attribute analysis. Advances in seismic imaging technology, compounded by rapidly improving computer processing power, has led to the development of simultaneous multi-attribute seismic analysis methods such as the chimney cube or neural-network analysis in recent years. Utilizing advanced workflows and methods such as these, semi-automated seismic interpretation workflows can be developed to detect focused fluid flow features that may not be identifiable with conventional seismic interpretation techniques.
- Chapters 2 and 3 utilized three 3D seismic surveys from the eastern, central and western regions of the Exmouth Plateau in the Northern Carnarvon Basin to reveal a potential basin-wide fluid expulsion event that occurred during the Late Jurassic. The spatial distribution of these fluid flow features is controlled by Late Jurassic normal faults that are potentially igneous dyke-associated faults, though the igneous intrusions could not be identified in this study. While a radial trend in linear trains of paleo-fluid escape features is observed within this study, further interpretation of 3D seismic surveys from across the plateau would better define the spatial distribution of paleo-focused fluid flow features across the Exmouth Plateau. Comprehensive mapping of Late Jurassic fluid flow features across the plateau will enable identification of potential basin-wide spatial distribution trends of focussed fluid flow systems. This information can then be integrated with the spatial distribution of igneous

intrusions across the Exmouth Plateau to identify correlations between the occurrence of focused fluid flow features and the presence of igneous intrusions. Potential correlations between the two features could then lead to utilizing the occurrence of Late Jurassic fluid escape features as a predictive feature for identifying underlying igneous intrusions.

- As highlighted in Chapter 3, a plausible source of overpressure generation within the Triassic Mungaroo formation of the Exmouth Plateau, that led to formation of the Late Jurassic focused fluid flow features, is fluid expansion from hydrocarbon generation. One-dimensional burial history modelling of the Mungaroo Formation show that organic matter within the formation could have entered the hydrocarbon generation window when the overburden thickness reached approximately 500 m or more. The varying overburden thicknesses used in this modelling study represent hypothetical values of Jurassic sedimentary rocks that had been eroded across the Exmouth Plateau at the end of the Jurassic (prior to formation of the focused fluid flow features). If the amount of erosion that Jurassic sedimentary rocks had undergone in the Late Jurassic could be better constrained, more realistic burial history modelling parameters could be defined to test the hypothesis of fluid expansion from hydrocarbon generation as a source of overpressure generation in the Mungaroo Formation. Furthermore, 2D or 3D basin modelling studies that generated overpressure as an output could also be undertaken to develop a clearer understanding of the paleo-pressure regime across the Exmouth Plateau during the Late Jurassic.
- Chapter 4 documents hydrocarbon-based focused fluid flow features within the Cenozoic sequence and shallowest ~400 m of the Upper Cretaceous Hammerhead Supersequence in the Ceduna Sub-basin of the Great Australian Bight. Some of these features appear to breach the seafloor on seismic cross-sections. In 2009, Geoscience Australia acquired seabed sediment cores across the Ceduna Sub-basin utilizing gravity corers to identify and characterise potential natural hydrocarbon seeps. Sampling sites and locations were selected based on 2D seismic profile data, bathymetry and Synthetic Aperture Radar (SAR) data, though the gravity core sampling sites do not coincide with regions of the Ceduna Sub-basin where focused fluid flow features were identified in this study. The location and spatial distribution of focused fluid flow features within the Ceduna Sub-basin identified in Chapter 3 can be used as a basis for selecting future seabed sampling or shallow drilling sites to obtain direct sediment sample measurements of the aforementioned focused fluid flow features. Geochemical analysis of such sediment samples could test the hypothesis of whether the identified focused fluid flow features had formed as a result of hydrocarbon generation.
- Chapters 2, 3, and 5 highlight the potential role of igneous intrusions in the formation or spatial control of focused fluid flow features. In Chapters 2 and 3, potential igneous dykes may have formed focused fluid flow associated normal faults within the Triassic Mungaroo

Formation of the Exmouth Plateau in the Northern Carnarvon Basin. In Chapter 5, hydrothermal vents, maar crater depressions and overburden deformation structures (manifesting as conjugate, radial and concentric faults) within Eocene to Miocene Torquay and Demon's Bluff formations are interpreted to have developed due to emplacement of underlying igneous intrusions. In all three chapters, the igneous intrusions are poorly imaged on seismic data. Potential field data, such as magnetic or controlled source electromagnetic (CSEM) data, measure subsurface conductivity/resistivity and are sensitive to the presence of igneous material that tends to have higher electrical conductivity relative to the surrounding sedimentary rocks. Existing potential field data in the Northern Carnarvon and Bass Basins have predominantly been acquired for basement or crustal studies and as such, the parameters of these data sets are not optimized for identifying smaller, localized igneous features. Acquiring a denser grid of potential field data over areas of interest, with acquisition parameters that are tuned for detecting localized igneous intrusions, will enable more accurate interpretations of their spatial distributions within the Northern Carnarvon and Bass Basins. With a clearer delineation on the location of igneous intrusions in the two basins, spatial correlations between the focused fluid flows and igneous intrusions can be identified and geological models for the genesis of focused fluid flow features developed in chapters 2, 3 and 5 can be further refined.

Appendix 1

Dimensions and spatial measurements of paleo-pockmarks from the Exmouth Plateau, Northern Carnarvon Basin

Dimensions and spatial measurements of Claudius Paleo-pockmarks (Chapter 2)

Paleo-pockmark	X coordinate	Y coordinate	Paleo-pockmark Width (m)	Paleo-pockmark Length (m)	Pipe length (twt ms)	Paleo-pockmark distance from minor fault (m)	Pipe reflector sag (ms)	Amplitude anomaly overlying paleo-pockmark
1	610780.94	7759910	261	322	381	424		n
2	610763.15	7760412.84	228	249	360	476		n
3	610687.54	7760821.97	134	256	342	529		n
4	610496.32	7761337.84	173	195	423	544		n
5	610385.15	7762102.76	351	691	308	764	43	n
6	610251.73	7762769.82	391	311	285	829	41	n
7	610073.85	7764272.95	367	737	384	808	62	n
8	609864.83	7765389.17	225	253	295	796	36	n
9	609624.68	7765918.38	184	213	165	742	17	n
10	609357.86	7766834.49	228	295	181	819	34	n
11	609139.95	7767554.93	193	202	248	845		n
12	608886.46	7768106.38	349	414	275	593	30	n
13	608704.13	7768528.86	269	274	377	542	43	n
14	608287.95	7769729.64	83	101	177	698	10	n
15	608193.79	7769960.18	170	182	253	612	16	n
16	607989.24	7770255.65	300	300	334	569	50	n
17	607304.13	7771577.18	377	634	411	760	51	n
18	606888.51	7772310.98	224	285	361	777	30	n
19	606739.15	7772489.57	65	99	92	786		n
20	606472.9	7773840.3	182	242	379	784		n
21	606245.61	7774116.3	268	297	392	748	40	n
22	605953.39	7774622.83	193	284	238	794	23	
23	605320.23	7775337.16	449	522	457	632	67	n
24	603959.75	7776814.53	540	582	359	648	14	n
25	615461.65	7759151.62						
26	616978.51	7762965.99	71	76	271	780		n
27	616843.03	7765096	98	165	167	645		n
28	616927.22	7765472.65	326	413	293	644	29	n
29	617006.98	7766150.62	316	611	236	694	21	n
30	613568.38	7766088.58	350	833	204	879		
31	617095.61	7767072.3	272	275	159	729	26	n
32	618318.9	7768390.76	347	739	252	794		n
33	616891.77	7768676.39	177	233	320	638	13	n
34	617967.22	7769146.62	290	293	157	763		n
35	617641.79	7769886.72	296	455	315	782		n
36	616487.01	7769897.22	138	163	398	536	8.6	n
37	617290.1	7770616.33	373	450	336	773		n
38	616250.81	7770458.86	304	391	303	716	45	n
39	615972.61	7770815.79	268	567	335	835	17	n

40	615736.41	7771697.62	107	146	207	798		n
41	616466.01	7772143.78	363	397	303	1685		n
42	616298.04	7772490.21	130	220	310	1423		n
43	616166.83	7772847.14	219	284	312	1323		n
44	616025.1	7773571.5	295	589	265	584		n
45	615355.72	7773656.43	102	107	173	769		n
46	615196.1	7773859	85	98	180	724	20	n
47	615074.43	7774730.94	268	445	355	994	18	n
48	615046.3	7775164.12	228	330	290	388	28	n
49	614849.4	7775715.44	346	595	368	904	41	n
50	614534.36	7776373.65	326	606	438	826	28	n
51	614269.95	7777127.5	394	539	400	773	51	n
52	614112.44	7777583.18	220	280	412	779	35	n
53	613831.15	7778292.02	138	143	255	708	19	n
54	613639.87	7778865.85	398	399	435	789	63	n
55	613465.47	7779169.64	144	214	176	861		n
56	612942.28	7779557.81	319	398	317	750	40	n
57	613111.04	7780193.52	288	325	362	769	23	n
58	612970.4	7780598.57	295	329	377	747	35	n
59	612902.9	7780891.11	117	152	195	732		n
60	612846.65	7781099.26	114	122	201	725		n
61	611867.76	7781599.19	171	175	205		26	n
62	612447.21	7782173.77	155	210	203	788		n
63	611676.49	7781875.61	209	238	244		22	n
64	611502.09	7782061.25	125	131	174		12	n
65	611445.83	7782280.66	138	164	180			n
66	611372.7	7782646.33	264	308	219		28	n
67	612165.92	7782905.11	340	426	450	778	23	n
68	611923.97	7783972.27	324	346	471	895		n
69	611693.69	7784545.02	289	323	258	948	15	n
70	611563.78	7785058.73	152	171	206	863		n
71	611457.51	7785289.01	300	302	259	902	28	y
72	611321.7	7785749.57	282	357	208	948	41	y
73	610648.57	7787243.44	294	386	197	993	39	n
74	609136.99	7787550.48	336	371	229	81		n
75	612649.71	7768821.11	416	450	373	316	42	n
76	612394.86	7769158.61	308	312	215	243	33	n
77	611644.1	7770921.86	460	602	275	978		n
78	603469.75	7759126.57	164	167	171	558		n
79	604096.9	7761542.07	408	415	224	560	36	n
80	603711.38	7764531.93	303	314	344	1074		n
81	603664.17	7764878.13	231	270	209	1036		n
82	603011.12	7764091.32	454	618	227	642		n
83	602806.55	7764649.96	223	242	257	544		n
84	602814.42	7765082.7	433	454	176	490		n
85	603278.63	7766396.66	180	227	244	474		n

86	602961.46	7766848.43	163	258	243	830		n
87	602535.99	7767073.86	262	327	396	816	62	n
88	602675.91	7767796.79	157	168	217	551		n
89	602411.61	7767928.94	94	130	181	416		n
90	602046.26	7768791.79	177	245	308	443		n
91	601813.06	7769211.55	455	548	330	842	50	n
92	602201.73	7769483.62	278	293	291	738		n
93	601898.57	7769950.03	110	165	358	594	20	n
94	601478.8	7770082.18	207	353	251	297	24	n
95	601486.58	7770424.21	183	231	199	408	24	n
96	601323.33	7770626.32	128	246	199	363		n
97	601237.83	7770945.03	180	223	126	440		n
98	601175.64	7771613.55	404	753	344	486	61	n
99	600746.96	7773474.81	152	172	247	330		n
100	600702.52	7773911.78	349	545	406	496	48	n
101	599591.36	7777640.5	327	363	397	466	50	n
102	599631.75	7778149.32	135	166	217	477	25	n
103	599639.83	7778561.23	277	392	256	523	27	n
104	598872.55	7778835.83	282	348	291	382	31	n
105	602716.99	7780402.68	141	179	244	585		
106	599276.38	7780895.35	417	856	541	527	33	n
107	599139.08	7781993.77	198	221	283	229		n
108	598299.11	7782567.22	271	330	519	480	25	n
109	596901.86	7784497.5	353	358	567	552		n
110	602033.71	7782527.2	110	121	238	812		n
111	601987.3	7783176.93	495	567	482	957		n
112	601694.55	7783726.7	288	309	230	934	31	n
113	601455.37	7784115.83	317	344	393	880		n
114	601223.32	7784558.5	117	161	202	835		n
115	601051.96	7784886.94	109	119	195	811		n
116	597479.97	7793494.44	385	487	454	820	55	n
117	601005.55	7785129.7	112	135	476	830		n
118	600791.35	7785515.25	92	135	232	637		n
119	600711.34	7786191.48	361	371	511	765	25	n
120	600490.01	7786698.42	394	616	433	621	69	n
121	600183.62	7787343.75	252	282	347	675	50	n
122	597909.92	7788707.41	266	349	322	704	37	n
123	599569.54	7788947.31	258	345	357	756	20	n
124	597794.41	7789446.77	578	676	419	869		n
125	599392.57	7789403.51	268	289	441	781	42	n
126	599227.39	7789678.8	264	298	360	785		n
127	601449.4	7790241.18	481	526	442	438		n
128	602959.58	7790193.99	241	384	325	589		n
129	603046.1	7790551.87	425	462	383	856	51	n
130	595807.51	7785858.12	266	674	554	883		y
131	595489.83	7786857.1	368	373	336	894	28	y

132	594732.04	7788942.51	265	266	510	940	40	y
133	597457.96	7790534.38	290	355	360	1143	32	n
134	598799.06	7790589.49	178	236	229	636		n
135	598648.42	7791034.08	246	450	378	644	21	n
136	598387.55	7791607.26	286	373	281	660		n
137	593476.67	7791746.04	378	1082	471	703		n
138	595050.51	7792444.2	283	313	339	532		n
139	596930.41	7792068.22	125	157	175	625		n
140	597782.84	7792698.73	188	186	153	757		n
141	597708.83	7793083.07	373	380	420	796	40	n
142	596463.14	7793439.4	276	407	370	738		n
143	597164.2	7794175.23	301	381	393	776	28	n
144	596935.35	7794719.85	317	388	403			n
145	596022.8	7794722.75	409	448	434	814		y
146	596225.35	7796173.69	330	460	484	823	40	y
147	596349.28	7795826.68	174	180	192	795		y
148	595960.14	7796835.48	375	533	392	726	42	y
149	595894.41	7796146.28	313	395	395	789	28	n
150	595831.97	7798451.55	110	149	217	813		n
151	595868.97	7798624.99	149	151	196	966		n
152	595690.89	7799027.39	179	263	416	888	21	n
153	595452.69	7800091.2	238	340	397	794		n
154	592063.81	7795963.05	288	303	510	840	45	y
155	592587.28	7797687.42	129	154	201	981		y
156	591181.1	7798318.66	334	409	376	944		n
157	604792.77	7796738.33	282	357	256	404	31	n
158	599916.46	7798320.2	309	570	556	638		y
159	599007.88	7800816.2	726	727	616	785		y
160	609207.44	7790149.29	430	719	391	880	35	n
161	607167.24	7792019.47	258	409	400	556		n
162	608373.3	7792471.08	173	180	289	759		n
163	606970.66	7792577.34	225	286	225	551	32	n
164	607831.37	7793639.95	162	172	370	743		n
165	607931.36	7793831.21	122	141	244	805		n
166	606062.13	7794601.6	453	480	351	432		n
167	607804.8	7794187.18	290	296	320	864		n
168	607353.2	7795903.29	134	170	388	651		n
169	607209.75	7796184.88	329	348	464	669		n
170	607156.61	7796487.72	196	304	233	578		n
171	604978.16	7799823.46	328	566	412	939		y
172	605647.6	7800673.54	296	358	395	597	25	y
173	605387.25	7801056.07	335	429	543	602	25	y
174	605137.54	7801624.56	211	349	196	714	6	y
175	604914.39	7802347.14	304	319	271		23	y
176	604760.31	7802703.11	122	207	213	845	17	y
177	615593.7	7803233.56	250	360	305	654	22	n

178	614835.26	7804533.74	338	445	418	846		y
179	616975.13	7805089.02	446	486	433	756		y
180	604539.24	7803782.49	256	417	437	721	32	y
181	604544.37	7804177.66	274	225	205	830		y
182	602399.18	7804023.7	165	225	181	260		n
183	602168.24	7804598.49	110	130	196	258		n
184	601439.49	7806204.81	160	248	198	400		y
185	602989.37	7808206.3	169	181	180	285		n
186	603235.71	7808350	239	292	383	544		n
187	612645.39	7811158.84	139	235	432	612		n
188	610728.17	7816544.95	295	558	203	598		n
189	610199.22	7817322.8	213	382	205			n
190	610370.35	7818236.81	323	372	220	469		y
191	609898.78	7820123.92	480	601	320			y
192	609134.13	7822911.56	301	383	346	589	32	n
193	611017.62	7825235.09	145	220	194	349		n
194	611102.33	7826265.75	202	242	230	842	24	y
195	607876.18	7827177.76	191	233	152			n
196	607899.88	7827966.68	310	339	234	378	58	n
198	601078.29	7815385.22	198	201	248	760		y
199	600912.3	7816145.27	544	645	388	889		n
200	599037.98	7821470.81	530	1028	549	890	80	y
201	598412.23	7822925.1	370	609	433	733	58	n
202	598168.88	7823689.91	235	301	449	889		n
203	598058.8	7824170.81	278	279	493	1069	19	n
204	597977.69	7824559	187	278	341	1083		y
205	590015.32	7802323.53	163	172	183	410		n
206	590097.82	7802637.06	316	409	456	627	54	y
207	593191.52	7803597.06	231	241	332	483		n
208	592969.72	7804513.16	199	417	313	544		n
209	593297.59	7805397.13	214	286	304	531	24	n
210	593024.36	7805512.85	340	398	381	368		n
211	592943.87	7806907.45	369	451	410	841		y
212	589034.72	7806866.75	432	466	412	436	33	y
213	588997.2	7807562.9	487	660	503	617	55	n
214	597143.85	7808252.65	347	455	211			n
215	592535.38	7808576.31	231	272	387	807		y
216	592471.88	7808832.37	266	272	365	824		y
217	592375.61	7809211.33	215	265	202	738		n
218	591746.85	7811419.37	241	320	349	656		y
219	591517.49	7812290.92	194	267	361	702	27	n
220	587452.62	7812624.78	182	334	306	884	42	n
221	586798.77	7814598.37	336	401	362	791	36	n
222	586312.25	7815583.84	298	372	230	767	35	y
223	591167.26	7814458.08	298	325	427	854	33	n
224	593713.35	7815728.9	473	561	441	590	28	y

225	590837.29	7814846.01	102	126	205	574		n
226	590709.63	7816750.23	202	264	396	739	24	n
227	590709.63	7816750.23	430	661	226	772	25	n
228	585820.41	7817756.95	250	393	229	526	31	n
229	585297.01	7819635.97	275	336	388	632		n
230	595744.07	7818406.77	173	298	217	367		y
231	595649.07	7819429.87	295	311	218	431		y
232	589819.63	7819440.57	130	228	363	861		n
233	589485.2	7819475.51						
234	590995.82	7821212.36	450	452	449	695		y
235	594293.75	7824672.3	255	297	357	574		y
236	596577.88	7824937.63	339	357	330	984		n
237	596945.81	7826267.07	435	663	353	818		n
238	587570.5	7826137.34	289	307	205			n
239	587174.01	7828003.89						
240	583013.3	7824588.76						
241	582856.27	7824667.28	97	143	243	590		n
242	582294.59	7826328.16						
243	582415.38	7825983.91	266	301	229	332		n
275	582463.7	7825802	103	140	180	326		n
244	583670.04	7823236.85	197	202	205	697		n
245	575635	7812993.55	297	581	398			y
246	573564.63	7807660.89	260	342	415	911		n
247	572828.34	7806039.38	129	180	218	506		n
248	577003.45	7796922						
249	576407.3	7796098.93	138	144	176			n
250	573580.44	7791301.67	302	338	185	554		n
251	570438.21	7786846.79	640	636	291	770		n
252	561279.3	7772828.88	219	296	352			n
253	569318.74	7785401.5	356	273	271			n
254	567167.76	7796062.28	251	308	282	390		y
255	563803.67	7805009.47	182	280	192	261		y
256	556399.05	7789364.64	146	203	217	591		n
257	566097.87	7789027.14	155	158	200	366		n
258	555866.14	7788539.64	131	181	344	204		y
259	561131.51	7784639.66	334	535	266	454		y
260	559283.11	7781876.1	200	209	249	489		y
261	559077	7781557						
262	558555.38	7780865.11	236	329	195	404		y
263	555747	7776904.18	320	444	310	447		y
264	556007.67	7776202.19	401	446	296	667		n
265	555203.55	7769412.18	359	445	315	599		n
266	554981	7769827						
267	556091.54	7762102.24	185	266	275	534		n
268	609499.77	7766340.86						
269	609503.59	7766354.41	165	230	278	776		n

270	617565.17	7759364.75	265	303	246	584	n
271	617618.9	7759815.83	269	329	351	642	n
272	617488.7	7760714.74	107	119	141	596	n
273	591593.95	7811994.67	181	189	251	674	n
274	591589.54	7811978.79	194	202	353	634	n
275	582461.06	7825807.12	140	151	160	309	n

Dimensions and spatial measurements of Io-Jansz 3D Paleo-pockmarks (Chapter 3)

Pockmark Number	Pockmark Width (m)	Pockmark Length (m)	Pipe height (twt)	Pipe height (m)
1	150	180	166	282.2
2	400	800	370	629
3	307	490	298	506.6
4	312	314	258	438.6
5	133	140	234	397.8
6	356	390	247	419.9
7	125	180	142	241.4
8	156	214	250	425
9	208	335	134	227.8
10	590	644	378	642.6
11	376	480	220	374
12	260	327	60	102
13	251	454	210	357
14	357	387	158	268.6
15	205	318	187	317.9
16	331	463	260	442
17	288	431	102	173.4
18	155	179	126	214.2
19	378	395	315	535.5
20	189	236	175	297.5
21	367	431	255	433.5
22	171	179	194	329.8
23	150	160	161	273.7

Dimensions and spatial measurements of Thebe 3D Paleo-pockmarks (Chapter 3)

Pockmark Number	Type	Pockmark Width (m)	Pockmark Length (m)	Pipe height (twt)	Pipe height (m)
1	D	238	404	135	168.75
2	A	184	280	80	100
3	A	230	300	107	133.75
4	A	213	230	122	152.5
5	A	376	455	182	227.5
6	D	143	150	126	157.5
7	D	472	616	328	410
8	B	456	463	347	433.75
9	B	297	351	86	107.5
10	B	186	214	51	63.75
11	B	146	148	47	58.75
12	D	290	350	189	236.25
13	D	125	274	262	327.5
14	B	182	217	97	121.25
15	A	323	383	95	118.75
16	D	115	154	93	116.25
17	D	152	197	81	101.25

Appendix 2

Throw measurements of conjugate fault pairs from the Labatt 3D, Bass Basin (Chapter 5)

Conjugate Fault Throw Measurement (Chapter 5)

Conjugate Fault	Seismic Crossline	TWT depth (ms)	Fault throw (ms)	Period(ms)	Normalized throw
1.1	4202	680	10	26	0.384615385
		725	10.2	22	0.463636364
		914	23.4	18	1.3
		950	19.6	22	0.890909091
		1030	14	24	0.583333333
		1216	4.7	22	0.213636364
	4140	617	11.9	23	0.517391304
		693	16.8	26.5	0.633962264
		891	24	24.7	0.971659919
		918	16.3	19.7	0.827411168
		961	14	29	0.482758621
		1012	12.4	22.9	0.541484716
		1209	4	25	0.16
	4074	604	14.4	22	0.654545455
		684	22.6	25	0.904
		864	7.3	20.6	0.354368932
		893	14.1	17	0.829411765
		921	13.18	22.9	0.575545852
		951	17.6	17.9	0.983240223
		1001	13.8	22.4	0.616071429
		1198	4	22.9	0.174672489
	3952	590	8.6	21	0.40952381
		629	12.5	19	0.657894737
		679	17.8	24	0.741666667
		694	14.2	27	0.525925926
		790	28.3	19	1.489473684
		821	29.2	18.7	1.561497326
		852	23.5	24.2	0.97107438
		881	21.1	23.8	0.886554622
		902	17.2	26.7	0.644194757
		924	14.8	16.5	0.896969697
		953	13.4	21.6	0.62037037
		974	13.4	23.8	0.56302521
	3890	556	4.3	25.7	0.167315175
		579	12	23.8	0.504201681
		611	14.4	19.7	0.730964467
		659	21.5	27	0.796296296
		670	21.5	26.6	0.808270677
		807	30.6	22.4	1.366071429
		829	28	25.2	1.111111111
		843	31	22.4	1.383928571

	864	23.4	16.6	1.409638554
	906	20.5	16	1.28125
	928	16.2	19.7	0.822335025
	947	15.3	20	0.765
	959	14.8	22	0.672727273
	1153	3.5	22	0.159090909
3840	534	5.7	24.9	0.228915663
	570	12.2	23.4	0.521367521
	592	11.1	20.9	0.531100478
	622	14.8	23.2	0.637931034
	660	19.6	27	0.725925926
	672	19.1	27	0.707407407
	771	30.1	20.5	1.468292683
	794	29.9	20.5	1.458536585
	815	28.7	22	1.304545455
	847	26.8	23	1.165217391
	872	22.6	27	0.837037037
	909	18	27	0.666666667
	942	14.9	22	0.677272727
	1135	4.5	23	0.195652174
3770	537	4.4	22	0.2
	560	9.4	20	0.47
	580	12	19.3	0.621761658
	613	9	26	0.346153846
	643	13.4	28.7	0.466898955
	656	12.5	25.5	0.490196078
	758	22.7	19	1.194736842
	791	21.1	19	1.110526316
	812	23.2	27	0.859259259
	841	18.7	28.4	0.658450704
	881	11.3	20.8	0.543269231
	893	13.1	20.2	0.648514851
	912	11.3	18.4	0.614130435
	923	13.8	22	0.627272727
	1117	4	24	0.166666667
3668	511	7.3	21	0.347619048
	533	12.3	23.4	0.525641026
	571	17.7	19.3	0.917098446
	593	16.2	24	0.675
	616	19.6	23	0.852173913
	640	18.7	26	0.719230769
	766	16.5	22	0.75
	776	18.1	22	0.822727273
	818	16.4	21.5	0.762790698
	861	12.5	19	0.657894737
	870	12.5	22.6	0.553097345

		888	12.7	22	0.577272727
		912	11.05	24	0.460416667
		1092	5.2	24	0.216666667
	3594	505	6.7	22.3	0.30044843
		537	10.1	20.5	0.492682927
		557	12	19.9	0.603015075
		589	12.9	25.2	0.511904762
		627	14.9	25.5	0.584313725
		655	10.4	28	0.371428571
		745	18	26.7	0.674157303
		765	17.7	20.2	0.876237624
		810	12.9	27.9	0.462365591
		839	11.9	22.5	0.528888889
		870	13.4	21.3	0.629107981
		893	10	23.4	0.427350427
		1090	5.2	22.3	0.233183857
1.2	4202	608	9.3	20.6	0.451456311
		878	22	18	1.222222222
		959	20	27	0.740740741
		1003	21	21	1
		1201	9.2	21	0.438095238
	4140	600	6.2	22	0.281818182
		666	13.7	27.5	0.498181818
		702	18.8	26	0.723076923
		834	17.5	19.2	0.911458333
		872	27	18.3	1.475409836
		937	22.1	30.7	0.719869707
		986	18.4	23.8	0.773109244
		1193	5	24	0.208333333
	4074	594	8.4	21	0.4
		633	8	20.6	0.388349515
		675	14.6	24	0.608333333
		795	26.4	17.9	1.474860335
		840	28.7	19.4	1.479381443
		867	37.2	17	2.188235294
		935	22.9	27	0.848148148
		982	20.7	24.7	0.83805668
		1201	5.5	26.1	0.210727969
	3952	668	7.2	27	0.266666667
		789	11.5	21	0.547619048
		823	41.7	22	1.895454545
		866	21.5	24.2	0.888429752
		910	15.1	31	0.487096774
		946	15.3	21.3	0.718309859
		959	12.9	22	0.586363636
		1175	4.6	22	0.209090909

3890	662	5.7	22.4	0.254464286
	674	7.2	25.7	0.280155642
	811	25.9	20	1.295
	847	23.4	29.2	0.801369863
	874	22.54	33.3	0.676876877
	910	21.1	22	0.959090909
	929	22	22	1
	943	17.2	22.3	0.771300448
	1158	5.9	23.1	0.255411255
3840	541	4.2	24.9	0.168674699
	577	7.3	22	0.331818182
	599	7.3	20.5	0.356097561
	660	3	24.5	0.12244898
	831	20.24	24.2	0.836363636
	877	14.8	28	0.528571429
	909	16.26	20.5	0.793170732
	930	15	23	0.652173913
3770	598	13	22.6	0.575221239
	625	14.7	28	0.525
	649	18.9	24	0.7875
	662	15.7	28.4	0.552816901
	745	17.2	19	0.905263158
	773	18.1	19	0.952631579
	792	16.9	18	0.938888889
	811	19.6	23	0.852173913
	866	19.2	27	0.711111111
	880	16.4	22.3	0.735426009
	899	15.5	21.5	0.720930233
	911	14.3	21.5	0.665116279
	1120	10.7	23	0.465217391
3668	533	5.2	22.9	0.227074236
	556	7.9	20.6	0.383495146
	574	11.06	20.2	0.547524752
	607	12.3	27	0.455555556
	621	12.6	24	0.525
	633	14.12	23	0.613913043
	657	13.2	25.2	0.523809524
	716	16.57	19.7	0.841116751
	730	22.1	20	1.105
	755	16.9	27	0.625925926
	777	15.3	18	0.85
	810	15.1	27	0.559259259
	859	14.84	24	0.618333333
	891	12.8	22.9	0.558951965
	1094	4.5	22	0.204545455
3594	521	5.3	26.9	0.197026022

		553	8	19.9	0.40201005
		576	6.5	20.5	0.317073171
		596	5.3	21.7	0.244239631
		607	8	24	0.333333333
		630	13	24.9	0.522088353
		641	14.9	24.6	0.605691057
		748	8.8	23	0.382608696
		769	9.5	20	0.475
		792	10.3	27.8	0.370503597
		823	8.8	28.7	0.306620209
		856	8.8	24	0.366666667
		877	6.1	21.4	0.285046729
		888	5.7	24	0.2375
2.1	3768	530	10.7	15	0.713333333
		575	19.7	20.6	0.95631068
		585	17.8	20.6	0.86407767
		596	17.3	20	0.865
		629	16.1	23.4	0.688034188
		648	26.3	24.4	1.077868852
		691	33.6	30	1.12
		826	32.3	21.5	1.502325581
		846	32.9	22.08	1.490036232
		862	30.5	21.6	1.412037037
		881	26.3	19	1.384210526
		901	22.8	23.45	0.97228145
	3644	496	13.8	19.7	0.700507614
		529	18.5	20.9	0.885167464
		538	20.3	18.7	1.085561497
		576	18.5	21.3	0.868544601
		595	28.1	22.7	1.237885463
		609	28.1	29.1	0.965635739
		639	28.7	33.59	0.854420959
		759	17.9	20.4	0.87745098
		789	22.2	16.9	1.313609467
		804	21.5	19.5	1.102564103
		824	17.9	21.4	0.836448598
		847	13.7	24.2	0.566115702
		875	12	36.6	0.327868852
		893	17.3	20.9	0.827751196
		915	18.2	23	0.791304348
		1117	5.9	22.5	0.262222222
	3588	469	14.2	23.4	0.606837607
		512	18.7	20.2	0.925742574
		522	18.7	19.9	0.939698492
		555	26.9	24.9	1.080321285
		578	26.9	25.2	1.067460317

		603	30.7	34	0.902941176
		621	32.2	34	0.947058824
		726	30.5	21.2	1.438679245
		748	27.5	20.5	1.341463415
		773	25.7	18	1.427777778
		793	23.9	20.8	1.149038462
		815	22.2	22	1.009090909
		846	24.4	26.7	0.913857678
		866	22.1	30	0.736666667
		876	21.6	22.9	0.943231441
		899	19.1	24	0.795833333
		1089	9.5	22.6	0.420353982
		1208	5.3	22.2	0.238738739
	3524	455	14.3	19.9	0.718592965
		477	18.5	20.6	0.898058252
		493	23.4	20.4	1.147058824
		503	23.3	20.1	1.15920398
		538	29.3	24.9	1.176706827
		560	32.3	26.3	1.228136882
		572	31.7	27.7	1.144404332
		604	30.5	38	0.802631579
		717	17.9	18.3	0.978142077
		727	18.5	22.3	0.829596413
		770	11.4	20.1	0.567164179
		826	21.3	16	1.33125
		849	21.5	22.5	0.955555556
		872	19.7	21	0.938095238
		1068	7.1	21	0.338095238
		1173	4.1	22.5	0.182222222
2.2	3768	558	13.1	20.1	0.651741294
		588	11.4	18.3	0.62295082
		607	19.7	24	0.820833333
		633	21.9	27	0.811111111
		647	18.6	26.7	0.696629213
		790	12.5	18.1	0.690607735
		808	15.6	20.2	0.772277228
		848	28.7	18.7	1.534759358
		867	26.9	17.4	1.545977011
		890	24	23.7	1.012658228
		922	24.9	27	0.922222222
		941	25.1	27	0.92962963
		966	20.3	24.4	0.831967213
		979	17.9	24	0.745833333
		1184	6.5	20.9	0.311004785
	3644	515	9.1	20.1	0.452736318
		536	11	18.8	0.585106383

		575	11	22.3	0.493273543
		598	12.9	24.9	0.518072289
		612	11.5	28	0.410714286
		646	16.7	26	0.642307692
		795	29.75	18	1.652777778
		830	31	26	1.192307692
		854	25.8	16.9	1.526627219
		880	23	24.6	0.93495935
		902	23	21.4	1.074766355
		915	20.6	21.3	0.96713615
		1113	11.5	21.4	0.537383178
		1233	9.1	19	0.478947368
3.1	3599	460	8.3	20.7	0.400966184
		483	14.3	25.7	0.556420233
		517	18	19.7	0.913705584
		534	19.1	18.7	1.021390374
		580	26.9	26.5	1.01509434
		592	26.3	29.3	0.897610922
		621	31.1	30	1.036666667
		742	18.6	19.4	0.958762887
		760	16.7	20.5	0.814634146
		777	17.3	19.4	0.891752577
		798	15.2	18.7	0.812834225
		819	15	24.4	0.614754098
		830	13.7	24.2	0.566115702
		897	4.1	20.2	0.202970297
		1095	6.6	19.2	0.34375
	3501	454	10.2	22	0.463636364
		484	21.6	20	1.08
		502	25.19	19.7	1.278680203
		539	22.7	23.8	0.953781513
		557	25.7	24.3	1.057613169
		571	25.1	29	0.865517241
		708	34.7	20.6	1.684466019
		728	34.1	19.3	1.766839378
		752	32.9	18.4	1.788043478
		770	32.9	20.8	1.581730769
		794	29.3	23.6	1.241525424
		827	25.4	23.4	1.085470085
		858	19.7	22.2	0.887387387
		883	16.1	23.1	0.696969697
		949	18.2	26.3	0.692015209
		1063	19.6	22.9	0.855895197
		1185	13.9	23.1	0.601731602
		1238	6.2	28	0.221428571
	3423	381	11.2	21.4	0.523364486

	403	12.7	19.9	0.638190955
	412	16.4	21.9	0.748858447
	443	27.7	18.9	1.465608466
	462	34.4	18.4	1.869565217
	480	37.4	18	2.077777778
	530	50.2	23.8	2.109243697
	554	57.7	28.2	2.046099291
	582	50.9	24.1	2.112033195
	679	54.7	20.3	2.694581281
	710	59.2	18.6	3.182795699
	727	61.4	20	3.07
	751	57.7	23.9	2.414225941
	788	54.1	18.8	2.877659574
	826	47.9	22.2	2.157657658
	847	50.2	19.23	2.61050442
	1024	35.9	22.5	1.595555556
	1149	34.4	22.4	1.535714286
	1213	30.51	31.7	0.962460568
3293	379	7.4	21.4	0.345794393
	411	10.2	24.2	0.421487603
	436	19.6	22.5	0.871111111
	510	31.1	22.9	1.358078603
	525	29.9	24.2	1.23553719
	549	34.7	29.3	1.184300341
	660	37.1	24.4	1.520491803
	682	35.9	22.7	1.581497797
	716	40.1	16.7	2.401197605
	726	40.1	19.7	2.035532995
	747	41.3	22.7	1.81938326
	780	40.9	24.4	1.676229508
	795	39.4	26.5	1.486792453
	829	37.1	24.9	1.489959839
	1013	24.5	20.2	1.212871287
	1131	32.9	22.35	1.472035794
	1193	32.9	20.4	1.612745098
3217	383	8.4	21.3	0.394366197
	427	7.2	22.5	0.32
	440	20.3	23	0.882608696
	475	28.7	17.4	1.649425287
	511	26.3	18.6	1.413978495
	532	32.3	20.8	1.552884615
	554	38.9	29.9	1.301003344
	578	43	25.9	1.66023166
	659	35.9	21	1.70952381
	678	39.5	20	1.975
	709	48.5	16.7	2.904191617

	729	49.75	22.5	2.211111111
	749	49.1	21.1	2.327014218
	776	44.6	21.8	2.04587156
	797	44.3	20.8	2.129807692
	819	40.7	23.9	1.70292887
	1016	30	22.3	1.34529148
	1143	24	23.4	1.025641026
3133	401	6	23.3	0.25751073
	421	8.9	19.3	0.461139896
	443	21.6	24	0.9
	502	31.7	19.5	1.625641026
	526	36.5	25.1	1.454183267
	549	37.1	24.6	1.508130081
	573	43.7	25	1.748
	667	42.5	20.3	2.093596059
	687	43.1	22.5	1.915555556
	708	56.3	26.7	2.108614232
	732	51.5	25.6	2.01171875
	777	43.9	27	1.625925926
	802	41.9	22.3	1.878923767
	824	38.9	22.3	1.744394619
	1022	16.7	22.6	0.738938053
3003	426	12	21.3	0.563380282
	447	13.5	23.2	0.581896552
	483	23.2	16.4	1.414634146
	518	27.7	20.4	1.357843137
	551	29.9	30.2	0.990066225
	583	27	28	0.964285714
	658	31.4	22	1.427272727
	686	33.7	23.2	1.452586207
	715	42.7	24.8	1.721774194
	791	36.7	22.5	1.631111111
	812	37.4	22.7	1.647577093
	1048	20.3	23.8	0.852941176
2903	440	9.6	19.9	0.48241206
	499	25.7	18.4	1.39673913
	532	31.7	25.7	1.233463035
	557	29.9	29.8	1.003355705
	651	29.3	21.3	1.375586854
	681	36.5	19.6	1.862244898
	711	41.3	26	1.588461538
	783	36.4	17.5	2.08
	809	32.9	23	1.430434783
	830	30.5	22.6	1.349557522
	1044	17.9	24.4	0.733606557
2859	448	8.6	18.4	0.467391304

		508	17.2	19.5	0.882051282
		532	17.9	21.9	0.817351598
		553	18.7	26.1	0.716475096
		661	17.9	23.1	0.774891775
		695	22.4	26.3	0.851711027
		747	26.2	26.6	0.984962406
		791	21.9	20.3	1.078817734
		828	17.2	21.8	0.788990826
		849	17.9	22.5	0.795555556
		1062	12	25.5	0.470588235
4.1	3729	503	8.9	20.7	0.429951691
		526	14.9	16.1	0.925465839
		569	23.9	21.4	1.11682243
		590	22.8	22	1.036363636
		640	30.5	26.6	1.146616541
		664	29.9	34.4	0.869186047
		815	37.7	24.3	1.551440329
		834	38.9	21.1	1.843601896
		863	34.1	21.2	1.608490566
		892	32.3	24.3	1.329218107
		939	30.7	21.3	1.441314554
		963	29.9	19.5	1.533333333
		987	25.19	26	0.968846154
		1314	3	21	0.142857143
	3701	496	8.1	20.2	0.400990099
		517	12.4	16.7	0.74251497
		567	16.2	22.5	0.72
		589	12	19.9	0.603015075
		632	28.2	27.5	1.025454545
		660	24.9	28.2	0.882978723
		773	41.2	18.7	2.203208556
		815	31.1	23	1.352173913
		842	30.6	17.4	1.75862069
		859	32.5	16.6	1.957831325
		878	34	23.4	1.452991453
		899	32.1	20.75	1.546987952
		924	29.4	19.8	1.484848485
		957	27.8	23.4	1.188034188
		984	21.5	24.5	0.87755102
		1177	8.1	21.5	0.376744186
	3667	483	7.8	24.9	0.313253012
		510	13.8	26	0.530769231
		545	20.3	18.4	1.10326087
		562	21.6	18.8	1.14893617
		589	24.5	26.6	0.921052632
		612	32.9	24.2	1.359504132

		638	28.7	33.08	0.867593712
		755	35	17.7	1.97740113
		784	33.58	23	1.46
		804	29.7	18	1.65
		829	27.3	19.2	1.421875
		849	23.9	19.6	1.219387755
		887	23.9	15.3	1.562091503
		904	24.1	20.7	1.164251208
		928	24.4	19.3	1.264248705
		950	21.3	24.9	0.855421687
		1166	6	23.3	0.25751073
5.1	3719	486	4.5	20.7	0.217391304
		507	8.2	23.3	0.35193133
		541	13.9	20.6	0.674757282
		562	13.9	19.3	0.720207254
		588	18.2	17.6	1.034090909
		615	24.2	27.6	0.876811594
		642	21.6	22.7	0.95154185
		740	34.9	19.3	1.808290155
		780	24.7	23.1	1.069264069
		817	19.1	18.4	1.038043478
		834	19.6	20.8	0.942307692
		854	20.6	17.8	1.157303371
		871	23.7	20.8	1.139423077
		905	15.8	20.4	0.774509804
		927	12	23.1	0.519480519
		1118	4.7	31	0.151612903
	3617	460	8.5	17	0.5
		477	11.5	17.6	0.653409091
		517	19.5	20.5	0.951219512
		526	19.9	19.9	1
		568	18.3	25.2	0.726190476
		591	23.5	23.4	1.004273504
		615	20.9	28.5	0.733333333
		750	22.4	23.6	0.949152542
		787	15	19.84	0.756048387
		824	18.5	19.2	0.963541667
		841	22.3	18.4	1.211956522
		899	19.6	26.6	0.736842105
	3249	470	5.08	23.2	0.218965517
		510	15.8	19.2	0.822916667
		527	16.7	17.1	0.976608187
		547	17.2	21.8	0.788990826
		570	20.6	23.9	0.861924686
		594	20.6	26.7	0.771535581
		629	22.03	29.3	0.751877133

		721	18.6	28	0.664285714
		743	18.2	18	1.011111111
		764	22.5	20.8	1.081730769
		795	22	21.9	1.00456621
		837	21.1	28.4	0.742957746
		863	22.5	24.4	0.922131148
		895	20	22.7	0.881057269
		1100	8	22.3	0.358744395
8.1	3553	500	10.2	16.2	0.62962963
		549	20.4	18	1.133333333
		612	31.7	26.5	1.196226415
		639	28.1	29.3	0.959044369
		792	48.5	25.8	1.879844961
		837	47.9	21.3	2.248826291
		855	50.3	21.8	2.30733945
		903	43.1	17.2	2.505813953
		920	43.4	22.7	1.911894273
		946	35.4	22.2	1.594594595
		977	31.7	22.1	1.43438914
		988	31.7	24.5	1.293877551
		1192	14.3	20.4	0.700980392
		1315	14	21.3	0.657276995
	3507	542	10.1	17.9	0.56424581
		551	11.4	19	0.6
		591	19.1	26.4	0.723484848
		618	18	32.6	0.552147239
		654	19.7	35.6	0.553370787
		789	24.6	24.2	1.016528926
		824	29.3	25.3	1.158102767
		844	35.9	20.4	1.759803922
		865	32.3	22.7	1.422907489
		889	25.7	21.8	1.178899083
		914	23.5	23.2	1.012931034
		940	17.9	22.3	0.802690583
		957	22.2	19.9	1.115577889
		979	20.9	21.3	0.981220657
		1052	17.9	24.4	0.733606557
		1179	7.2	21.7	0.331797235
	3461	480	7.2	26.4	0.272727273
		526	15.5	19.4	0.798969072
		568	22.7	23.7	0.957805907
		593	22.2	28.7	0.773519164
		628	23.3	30.7	0.758957655
		751	39.5	19.9	1.984924623
		799	44.3	21.3	2.079812207
		817	46.1	21.8	2.114678899

	843	35.3	24.18	1.459884202
	861	34.7	16.4	2.115853659
	879	34.3	24.2	1.417355372
	905	35.1	21.8	1.610091743
	936	28.7	23	1.247826087
	948	25.8	25.3	1.019762846
3405	461	10.4	24.6	0.422764228
	494	21.7	17.1	1.269005848
	549	19.4	23.3	0.832618026
	571	24.7	27	0.914814815
	602	29.2	29.5	0.989830508
	727	37.4	20.3	1.842364532
	770	38.9	21.2	1.83490566
	790	35.1	20.7	1.695652174
	814	32.9	25.2	1.305555556
	848	30.7	22.5	1.364444444
	873	28.5	21.9	1.301369863
	903	26.2	21	1.247619048
	927	22.4	19.9	1.125628141
	1127	15	18	0.833333333
3379	447	8.3	21.7	0.382488479
	497	16.7	20.8	0.802884615
	527	16.1	29.1	0.553264605
	560	24.5	27	0.907407407
	591	31.1	30	1.036666667
	718	37.1	21.8	1.701834862
	763	34.1	21.9	1.557077626
	783	31.1	20.5	1.517073171
	804	33.5	21.5	1.558139535
	839	30.7	22.4	1.370535714
	865	28.7	22.1	1.298642534
	902	25.7	23.9	1.075313808
	1107	13.5	19.6	0.68877551
3317	437	6.5	19.2	0.338541667
	472	7.8	18.3	0.426229508
	522	13.7	23.4	0.585470085
	541.9	21.6	21.3	1.014084507
	581	28.7	30.2	0.950331126
	692	31.7	21.2	1.495283019
	733	34.7	19.9	1.743718593
	751	35.9	21.2	1.693396226
	774	34.8	23.3	1.493562232
	811	34.5	21.7	1.589861751
	832	37.1	22.5	1.648888889
	854	32.3	18.9	1.708994709
	874	30.5	22.3	1.367713004

		1069	24.5	21.1	1.161137441
	3223	423	12.5	27.6	0.452898551
		446	16.1	16.7	0.964071856
		504	18.5	23.7	0.780590717
		527	21.5	22.6	0.951327434
		553	27.5	29.6	0.929054054
		669	28.7	19.9	1.442211055
		707	29.3	17.3	1.693641618
		723	28.1	21.4	1.313084112
		758	25.19	17	1.481764706
		777	32.15	23.1	1.391774892
		809	28.1	19	1.478947368
		828	26.3	20.8	1.264423077
		849	25.1	24	1.045833333
		1031	17.3	23.4	0.739316239
		1154	15	23.2	0.646551724
	3163	437	11.2	23.6	0.474576271
		474	20.3	17.9	1.134078212
		515	22.7	22	1.031818182
		539	23.9	28.6	0.835664336
		567	30.5	28.9	1.055363322
		610	29.3	17.9	1.636871508
		659	39.5	19.1	2.068062827
		698	41.3	19	2.173684211
		734	37.1	23.48	1.580068143
		764	32.3	18.4	1.755434783
		785	33.5	18.16	1.844713656
		812	30.2	24	1.258333333
		839	27.8	27	1.02962963
		1020	11.48	20	0.574
8.2	3553	524	14.4	17.2	0.837209302
		563	23.4	15.7	1.49044586
		600	22.1	20.7	1.06763285
		620	34.1	21.8	1.564220183
		644	30.5	31.2	0.977564103
		813	35.3	23.1	1.528138528
		852	34.7	17.3	2.005780347
		871	32.9	20.9	1.574162679
		894	33.5	23.8	1.407563025
		913	34.1	16.9	2.017751479
		927	35.5	22.9	1.550218341
		955	31.1	22.7	1.370044053
		976	26.3	19.4	1.355670103
		997	25.8	23.2	1.112068966
		1197	13.2	19.3	0.683937824
	3507	501	17.3	16.6	1.042168675

	555	28.1	16.6	1.692771084
	579	29.9	25.3	1.181818182
	605	35.9	23.9	1.50209205
	617	35.3	25.6	1.37890625
	781	36.5	20.4	1.789215686
	828	38.3	20.6	1.859223301
	845	40.1	20.2	1.985148515
	869	38.9	23.7	1.641350211
	890	38.3	17.1	2.239766082
	905	38	23.02	1.650738488
	934	32.9	18.6	1.768817204
	954	29.9	19.4	1.541237113
	976	27.5	21.9	1.255707763
	1175	11.9	19.1	0.623036649
3461	500	16.6	24.5	0.67755102
	532	29.9	18.9	1.582010582
	551	33.5	25.9	1.293436293
	591	40.1	22.1	1.814479638
	616	39.5	25.9	1.525096525
	769	45.5	23.1	1.96969697
	815	32.3	21.9	1.474885845
	833	37.7	21	1.795238095
	859	33.5	24	1.395833333
	877	37.1	21.8	1.701834862
	908	31.7	28.3	1.120141343
	931	28.7	19.5	1.471794872
	953	25.7	22.3	1.152466368
	978	19.7	20.6	0.95631068
3405	486	11.2	25.9	0.432432432
	534	12	20.1	0.597014925
	582	20.9	24.5	0.853061224
	601	24.7	31.5	0.784126984
	754	28.5	18.7	1.524064171
	791	29.9	20.8	1.4375
	810	27.7	20.1	1.378109453
	830	27	23.3	1.158798283
	850	25.4	19.3	1.316062176
	868	27.4	22.3	1.228699552
	896	28.45	24.6	1.156504065
	925	24.7	22.9	1.07860262
	948	22.4	27.8	0.805755396
	1254	6	20.2	0.297029703
3379	451	7.8	23.26	0.335339639
	478	11.9	27.6	0.43115942
	521	20.4	17.9	1.139664804
	569	25.7	22.6	1.137168142

	593	26.2	32.3	0.811145511
	743	30.7	20.4	1.504901961
	779	31.4	17.8	1.764044944
	794	34.4	19.2	1.791666667
	816	32.9	24.9	1.321285141
	837	30.6	19.9	1.537688442
	866	28.45	29.5	0.96440678
	893	27	20.2	1.336633663
	922	23.2	25.3	0.916996047
	1238	6.7	22.7	0.295154185
3317	421	3.6	19.6	0.183673469
	442	4.5	21.9	0.205479452
	465	8.4	22.2	0.378378378
	505	17.3	20.8	0.831730769
	550	22.7	24.9	0.911646586
	587	34.7	32.5	1.067692308
	722	36.5	19.7	1.852791878
	759	26.3	19.3	1.362694301
	776	26.9	21.1	1.274881517
	798	26.3	22.3	1.179372197
	833	27.4	21.8	1.256880734
	861	22.7	23.7	0.957805907
	895	20.3	21.2	0.95754717
	1089	7.8	25.1	0.310756972
3223	429	10.5	17.7	0.593220339
	474	18.7	17.6	1.0625
	490	20.9	16.7	1.251497006
	520	27	20.5	1.317073171
	541	26.2	21.1	1.241706161
	566	26.9	24.9	1.080321285
	685	39.7	19.5	2.035897436
	726	43.4	18	2.411111111
	746	41.9	20.9	2.004784689
	769	38.9	25.8	1.507751938
	804	37.5	21.1	1.777251185
	832	31.4	23.9	1.313807531
	871	22.5	21.8	1.032110092
	1060	12.7	21.1	0.601895735
3163	405	12.5	19.8	0.631313131
	426	23.9	17.6	1.357954545
	473	33.6	19.8	1.696969697
	512	33.5	24.9	1.345381526
	558	44.3	24.2	1.830578512
	659	56.9	22.3	2.551569507
	692	61.75	19.5	3.166666667
	724	56.3	25.8	2.182170543

		748	54.5	22.5	2.422222222
		771	56.6	21.8	2.596330275
		795	55.1	25.3	2.177865613
		839	44.9	21.8	2.059633028
		1021	36.5	24.9	1.465863454
		1147	38.4	23.9	1.606694561
	3063	399	9.7	22.7	0.427312775
		495	27.7	18.3	1.513661202
		533	41.9	28.6	1.465034965
		645	42	22.3	1.883408072
		678	38.9	17.6	2.210227273
		703	41.9	23.5	1.782978723
		747	36	20.4	1.764705882
		774	23.9	23.9	1
		812	17.9	24.6	0.727642276
		1002	14.2	22	0.645454545
9.1	2265	478	7.4	20.9	0.354066986
		522	12.7	23.4	0.542735043
		544	14.9	23.5	0.634042553
		573	12.7	31.9	0.398119122
		677	19.4	26.5	0.732075472
		727	18.7	21.6	0.865740741
		748	20.9	20.9	1
		766	15.7	19.9	0.788944724
		808	18.5	24.4	0.758196721
		864	14.2	24.6	0.577235772
	2248	480	7.6	22	0.345454545
		523	14.6	22	0.663636364
		558	11.3	28.6	0.395104895
		589	8	23.5	0.340425532
		686	17.5	20.5	0.853658537
		720	20.18	17.9	1.127374302
		761	14.6	21.2	0.688679245
		792	15.7	21.2	0.740566038
		825	16.8	28.5	0.589473684
		873	10.2	28.6	0.356643357
		1066	2.3	23.7	0.097046414

Appendix 3

Dimensions and categorization surficial depressions and their infilling seismic reflectors from the Labatt 3D in the Bass Basin (Chapter 5)

Dimensions and categorization of surficial depressions in Labatt 3D (Chapter 5)

Depression Number	Crater-like or Pipe-like Depression	Parallel, Convex or Pinnacle reflectors	Inline	Xline	Depression Width (m)	Depression Length (m)	Pipe height (ms)	Pipe base Formation
1	C	C	1774	1516	357	753	434	EVCM
2	C	C	1808	1352	314	367	483	Uncertain
3	P	C	1774	1357	292	320	480	Uncertain
4	P	Pa	1406	1658	84	101	363	EVCM
5	P	Unclassified	1362	1716	90	121	771	EVCM
6	Unclassified	C	1392	1730	149	152	485	Uncertain
7	C	C	1482	1772	204	522	765	EVCM
8	C	C	1536	1772	536	581	665	EVCM
9	C	Pin	1503	1750	236	348	700	EVCM
10	Unclassified	C	1407	1799	320	351	665	EVCM
11	Unclassified	C	1575	1815	349	1281	702	EVCM
12	Unclassified	Pin	1506	1857	272	330	627	Uncertain
13	P	C	1485	1899	274	284	659	Demons Bluff
14	Unclassified	C	1296	1963	184	447	639	EVCM
15	Unclassified	Pa	1450	1923	375	615	554	EVCM
16	C	Pa	1361	1983	165	175	278	Uncertain
17	C	C	1369	2015	361	386	647	EVCM
18	P	Pa	1484	2043	235	261	657	EVCM
19	Unclassified	C	1449	2071	128	248	540	EVCM
20	Unclassified	Pin	1445	2095	137	175	724	EVCM
21	P	Pa	1347	2135	163	174	742	EVCM
22	P	Pa	1369	2135	310	370	751	EVCM
23	P	C	1346	2169	97	125	613	EVCM
24	P	Pa	1346	2229	194	202	692	EVCM
25	Unclassified	Pa	1593	2291	1122	1361	676	EVCM
26	C	Pa	1144	2355	778	1053	525	EVCM
27	C	Pa	1082	2427	447	1089	548	EVCM
28	P	Pa	1129	2461	667	780	635	EVCM
29	Unclassified	Pa	1083	2483	185	173	420	Uncertain
30	P	Pa	1529	2417	291	309	651	EVCM
31	Unclassified	C	1523	2455	503	577	665	Uncertain
32	Unclassified	C	1624	2527	550	384	722	EVCM
33	Unclassified	Unclassified	1527	2531	74	127	412	EVCM
34	Unclassified	Pa	1098	2643	92	117	736	EVCM
35	C	Pa	1398	2665	1057	1357	735	EVCM
36	C	C	1442	2747	199	244	676	EVCM
37	C	Pa	1429	2787	457	489	832	EVCM
38	P	Pa	1423	2843	249	302	758	EVCM

39	C	Pa	1246	2797	71	106	454	EVCM
40	P	Pa	1516	2765	281	322	578	EVCM
41	Unclassified	Pa	1524	2801	179	220	507	EVCM
42	Unclassified	C	1541	2781	222	316	669	EVCM
43	Unclassified	C	1549	2807	237	243	517	EVCM
44	Unclassified	Pin	1564	2787	152	163	609	EVCM
45	C	Pa	1230	2861	249	270	578	EVCM
46	C	C	1230	2881	84	151	665	EVCM
47	C	Pa	1220	2899	152	259	753	EVCM
48	Unclassified	Pin	1561	2915	321	365	538	EVCM
49	C	C	1630	2923	247	345	581	EVCM
50	C	C	1628	2971	352	393	629	EVCM
51	Unclassified	Pa	1531	2995	246	642	Unclear	EVCM
52	P	Pa	1617	3017	81	96	702	EVCM
53	Unclassified	Pa	1467	3055	143	201	373	Uncertain
54	C	Pa	1509	3064	122	160	314	EVCM
55	C	Pa	1496	3095	130	244	477	EVCM
56	Unclassified	Pin	1496	3131	171	185	532	EVCM
57	Unclassified	C	1481	3104	101	111	Unclear	Uncertain
58	C	C	1217	3064	211	339	425	Uncertain
59	Unclassified	Unclassified	1217	3097	107	172	374	Uncertain
60	P	Pa	1199	3113	177	295	659	EVCM
61	Unclassified	Unclassified	1189	3141	124	216	402	Uncertain
62	Unclassified	Unclassified	1180	3159	120	262	294	Uncertain
63	C	C	1625	3137	649	939	555	EVCM
64	Unclassified	Pin	1463	3171	140	190	Unclear	Uncertain
65	P	Pin	1471	3201	114	120	491	EVCM
66	C	Pa	1227	3261	171	185	590	EVCM
67	P	Pa	1611	3305	166	513	600	EVCM
68	C	Pin	1756	3333	730	872	596	EVCM
69	C	Pa	1801	3375	403	427	316	Uncertain
70	P	Pa	1347	3335	397	575	587	EVCM
71	Unclassified	Pin	1427	3367	490	808	681	EVCM
72	C	C	1416	3417	269	781	580	EVCM
73	Unclassified	Pa	1399	3482	58	76	514	EVCM
74	Unclassified	Pin	1645	3384	948	1034	491	EVCM
75	P	Pa	1580	3384	482	991	498	EVCM
76	P	C	1582	3465	183	212	482	EVCM
77	P	Pa	1556	3465	161	258	463	EVCM
78	P	Pa	1529	3482	356	459	488	EVCM
79	P	Pa	1529	3527	272	457	463	EVCM
80	P	Pa	1529	3456	130	188	399	EVCM
81	Unclassified	Unclassified	1517	3584	113	218	Unclear	Uncertain
82	C	Pa	1511	3483	248	302	488	Uncertain
83	C	Pa	1503	3466	220	302	564	EVCM
84	C	Pa	1492	3487	191	246	279	EVCM

85	P	Pa	1479	3507	447	886	596	EVCM
86	C	Pa	1448	3570	335	410	431	EVCM
87	C	C	1186	3325	110	140	Unclear	Uncertain
88	P	C	1178	3347	117	154	383	EVCM
89	P	Unclassified	1164-1138	3441-3387	171	1042	Unclear	EVCM
90	C	C	1075	3597	180	244	260	Uncertain
91	Unclassified	C	1048-1063	3633-3661	278	736	Unclear	Uncertain
92	C	C	1759	3455	193	200	482	EVCM
93	C	Pa	1752	3513	786	1065	551	EVCM
94	C	Pa	1666	3651	537	633	596	EVCM
95	P	Pa	1689-1754	3674-3745	718	1490	440	EVCM
96	P	Pa	1805	3713	286	506	533	EVCM
97	Unclassified	Pa	1781	3741	356	421	323	EVCM
98	P	Pa	1714	3785	270	359	421	EVCM
99	P	Pa	1742	3908	172	319	434	EVCM
100	P	Pa	1723	3922	377	595	618	EVCM
101	P	Pa	1742	4025	382	466	460	EVCM